# APPENDIX B[a]
# DATA TRACKING NUMBERS FOR THE TSPA-LA MODEL

# B1[a] INTRODUCTION

Appendix B of the parent document describes the interrelationships among the Total System Performance Assessment for the License Application (TSPA-LA) Model output data tracking numbers (DTNs) for the TSPA-LA Model. Additional output generated as a result of the analysis presented in this addendum is described in Appendix B[a]. Figure B-3[a] shows the information flow among the output DTNs submitted to the Technical Data Management System for the analyses documented in this addendum.

The following sections contain brief descriptions of the contents of the DTNs. The respective ReadMe.doc file located in each DTN provides more detailed information on the contents of each DTN. Figure B-3[a] provides an overview of the relationships between the DTNs.

# B2[a] DESCRIPTIONS OF THE DATA TRACKING NUMBERS

The following text supports Figure B-3[a]. Figures B-1 and B-2 in the parent document remain unchanged and are documented in Appendix B, Section B.2, of the parent document.

## B2.1[a] MODEL DEVELOPMENT RECORDS PACKAGE

This records package documents each of the model changes that were generated since v5.000 of the Model. This records package contains v5.001 through v5.005 of the Groundwater Model. All model versions generally follow the same folder content. For example, the content for a typical folder would contain a Master Folder and the specific case folders that were appropriate at that stage of model development. Each Master Folder generally contains the following:

- One or more change approval forms
- Change checklist
- Implementation checklist
- Conceptual checklist
- Conceptual description
- GoldSim model file
- GoldSim version report
- Additional information directory (optional).

This records package feeds output DTN: MO0710ADTSPAWO.000_R0 [DIRS 183752], which utilizes the final version of the Groundwater Model (v5.005).

## B2.2[a] PLOTS AND FIGURES FOR THE TSPA-LA ADDENDUM (V5.005): OUTPUT DTN: MO0710PLOTSFIG.000_R1 [DIRS 185207]

**Reference Figure B-3[a], Block 4**—This DTN contains electronic copies of the plots and any post-processing files for all of the plots generated for this document. The plots were generated using SigmaPlot 2002 for Windows Version 8.0, (www.sigmaplot.com). Each figure generated for this document includes header information listing the file name(s) which contain the output data used in the plot (generally a GoldSim file with the file extension .gsm) which can be found in the source DTN listed for the plot. The plot header information contains the file name(s) of the SigmaPlot (file extension .JNB) and any post-processing files used to generate the plot which

can be found in this DTN. In addition, any checklists used for checking of the plots are also included.

**B2.3[a] TSPA-LA ADDENDUM PARAMETER SENSITIVITY ANALYSIS: OUTPUT DTN: MO0801TSPAPRSA.000_R0 [DIRS 184620]**

**Reference Figure B-3[a], Block 6**—This DTN contains analyses to evaluate the significant uncertain parameters in the TSPA-LA Groundwater Models that are documented in output DTN: MO0710ADTSPAWO.000_R0 [DIRS 183752].

**B2.4[a] TSPA-LA ADDENDUM, REPRESENTATION OF (GW V5.005) NAVAL SPENT NUCLEAR FUEL: OUTPUT DTN: MO0801TSPANSNF.000_R0 [DIRS 184619]**

**Reference Figure B-3[a], Block 5—**This DTN contains the TSPA-LA Model cases, including checking documentation, that were run to evaluate the representation of naval spent nuclear fuel in the TSPA-LA Model as discussed in Section 7.5.3[a].

**B2.5[a] TSPA-LA ADDENDUM GROUNDWATER MODEL (V5.005) AND ERUPTIVE MODEL (V1.004) WITH FINAL DOCUMENTATION: OUTPUT DTN: MO0710ADTSPAWI.000_R0 [DIRS 183751]**

**Reference Figure B-3[a], Block 10—**This is the version of the TSPA-LA Groundwater Model (v5.005) and Eruptive Model (v1.004) that is used to generate the GoldSim Player Files that support the TSPA-LA. The difference between the GoldSim files in this DTN versus output DTN: MO0710ADTSPAWO.000_R0 [DIRS 183752] is that this DTN contains the master file for v5.005 and for v1.004. These master files have been modified to update the explanatory text. The explanatory text that is in output DTN: MO0710ADTSPAWO.000_R0 [DIRS 183752] is not as detailed as the explanatory text included in this DTN. The enclosed master files have not been run; therefore, there are no results in this DTN. The value in providing an input file without the output is that the files can be opened on most current model personal computers. The value in adding the documentation is that an interested party can read the embedded text to obtain an overview of how the model is constructed. Also included is a data only copy of the TSPA Input Database. The value of the data-only version of the TSPA Input Database is that an interested party can review the input parameters to quickly determine the numerical value of a parameter as well as the product that the value is documented within. In most cases, the product is an output DTN from a model and/or analysis report.

**B2.6[a] TSPA GENERATED INPUTS AND POST-PROCESSED INPUTS: OUTPUT DTN: MO0711GENERINP.000_R0 [DIRS 183937]**

**Reference Figure B-3[a], Block 2—**This DTN contains inputs that fall into two categories: (1) TSPA-LA Model-generated inputs and (2) post-processed inputs. The TSPA-LA Model generated inputs do not have any external inputs used to create the input values. Post-processed inputs have external inputs supplied by supporting analysis and/or model reports. These external inputs must be post-processed for use in the TSPA-LA Model.

**B2.7[a] TSPA-LA ADDENDUM GROUNDWATER MODELING CASES (V5.005) WITHOUT FINAL DOCUMENTATION (USED FOR REGULATORY COMPLIANCE): OUTPUT DTN: MO0710ADTSPAWO.000_R0 [DIRS 183752]**

**Reference Figure B-3[a], Block 3—**This is the version of the Groundwater Model (v5.005) that is used for Regulatory Compliance presented in Section 8[a]. This DTN contains all the modeling cases and supporting checking documentation.

**B2.8[a] TSPA-LA ADDENDUM, WASTE PACKAGE AND DRIP SHIELD DEGRADATION ANALYSIS: OUTPUT DTN: MO0801TSPAWPDS.000_R1 [DIRS 185077]**

**Reference Figure B-3[a], Block 9—**This DTN contains the TSPA-LA Waste Package (WP) and Drip Shield (DS) degradation stand alone analysis documented in Section 8.3[a].

**B2.9[a] TSPA-LA MODEL (GROUNDWATER) USED FOR REGULATORY COMPLIANCE STABILITY ANALYSIS: OUTPUT DTN: MO0801TSPAADSA.000_R1 [DIRS 185078]**

**Reference Figure B-3[a], Block 7—**This DTN contains the GoldSim runs confirming that the TSPA-LA Model is statistically stable as discussed in Section 7.3.1[a].

**B2.10[a] TSPA-LA ADDENDUM, MODEL VALIDATION AND ANALYSES CASES: OUTPUT DTN: MO0801TSPAMVAC.000_R1 [DIRS 185080]**

**Reference Figure B-3[a], Block 8—**This DTN contains GoldSim files addressing the following subjects that support model validation:

- Single Realizations (discussed in Section 7.7.1[a])
- Accuracy of Expected Dose (discussed in Section 7.3.2[a])
- Validation of the Number of Human Intrusion Scenario Timesteps (discussed in Section 7.3.3[a]).

**B2.11[a] TSPA-LA ADDENDUM, SEEPAGE RESULTS FROM THE TSPA-LA MODEL: OUTPUT DTN: MO0705TSPASEEP.000_R1 [DIRS 183008]**

**Reference Figure B-3[a], Block 11**—This DTN contains the extracted seepage rates and seepage fractions. The results are taken from model development v5.005_GS_9.60.300 of the TSPA-LA Model for one-million years for the Seismic Fault Displacement and Igneous Intrusion Modeling Cases.

INTENTIONALLY LEFT BLANK

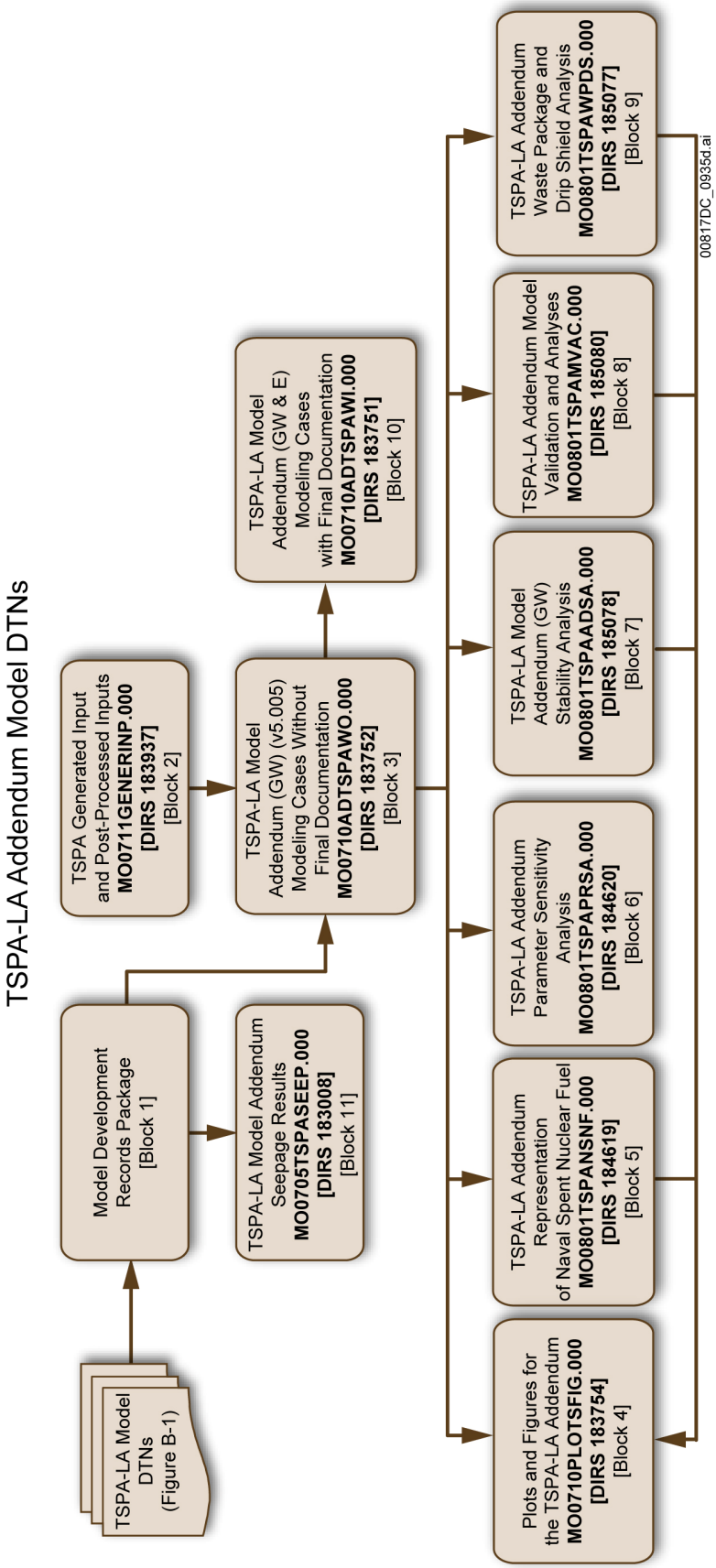


Figure B-3[a]. Road Map of TSPA-LA Model v5.005 Data Tracking Numbers

INTENTIONALLY LEFT BLANK

# APPENDIX C[a]
# PERFORMANCE MARGIN ANALYSIS

## C1[a] PURPOSE AND OBJECTIVE

Appendix C of the parent document includes the analyses and results supporting the Performance Margin Analysis (PMA). This addendum documents an additional impact analysis of a single issue identified in the performance margin model implementation that was not previously documented in Section C9 of the parent document. Table C9-1 of the parent document is included as Table C9-1[a] of this addendum. The items numbered 1 through 14 in the table are repeated from the parent document, only the last item (item #15) has been added in this addendum.

## C2[a] QUALITY ASSURANCE

No change.

## C3[a] USE OF SOFTWARE

No change.

## C4[a] INPUTS

No change.

## C5[a] ASSUMPTIONS

No change.

## C6[a] PERFORMANCE MARGIN ANALYSIS DESCRIPTION

No change, except for the following subsection, C6.3.1[a].

### C6.1[a] METHODOLOGY

No change.

### C6.2[a] DRIFT-SCALE UNSATURATED ZONE FLOW

No change.

### C6.3[a] WASTE PACKAGE AND DRIP SHIELD DEGRADATION

No change.

### C6.3.1[a] CONCEPTUAL MODEL

The following paragraphs are edited to correct the value for the WP surface area, and replace the corresponding paragraphs in the parent document.

**Localized Corrosion WP Failure Area**

Localized corrosion is a phenomenon in which corrosion progresses at discrete sites or in a non-uniform manner (SNL 2007 [DIRS 178519], Section 6.4.4). The area of the Alloy 22 WP outer barrier that is contacted by seepage is potentially subject to localized corrosion (SNL 2007 [DIRS 178519], Sections 6.3.5 and 6.4.4.8.3). In the TSPA-LA Model, it is assumed the maximum available area for localized corrosion (i.e., the area of the WP wetted by seepage) is the area of the WP damaged by localized corrosion (SNL 2007 [DIRS 178519], Section 6.3.5.2.2). Therefore, the entire surface area of the WP is removed as a barrier to water inflow and transport of radionuclides from a localized corrosion damaged WP.

In the PMA, the results of an ACM are used to establish a minimum WP area subject to crevice corrosion processes from localized corrosion (SNL 2007 [DIRS 178519], Section 6.4.4.8.3). The ACM considers a minimum WP creviced surface area based on the WP-to-emplacement pallet contact area (SNL 2007 [DIRS 178519], Sections 6.4.4.8.3). The calculated minimum WP-pallet contact area is $1.924 \times 104$ $mm^2$ (SNL 2007 [DIRS 178519], Section 6.4.4.8.3). Therefore, the minimum creviced area is about 0.05 percent of the cylindrical WP surface area of 33 $m^2$ for the transportation, aging, and disposal (TAD) canister-bearing WP configuration. The maximum available area for localized corrosion is the area of the WP wetted by seepage. In the absence of specific information regarding local environments on the WP, for the PMA the area of the WP failed by localized corrosion was assumed to have a log-uniform distribution that was sampled between the range of the entire WP surface area that is exposed to seepage (100 percent) and the calculated ACM minimum of 0.05 percent of the WP surface area (SNL 2007 [DIRS 178519], Section 6.4.4.8.3).

## C7[a] RESULTS

No change.

### C7.1[a] PERFORMANCE MARGIN IN TOTAL ANNUAL DOSE PREDICTIONS

No change.

### C7.2[a] PERFORMANCE MARGIN ANALYSIS—MODELING CASE RESULTS

No change.

### C7.3[a] KEY FACTORS AFFECTING THE PERFORMANCE MARGIN

No change.

## C8[a] SUMMARY

No change.

## C9[a] IMPACT ANALYSIS

Table C9-1 has been updated to include one additional issue (#15) identified during completion of the addendum.

Table C9-1[a]. Impact Assessment Summary Table

| | ISSUE DESCRIPTION | IMPACT ASSESSMENT |
|---|---|---|
| 1 | Fifteen of the sixteen UZ_Params_Multi_PMA tables, input files to FEHM DLL (version 2.25), need to be populated at run time according to the model simulation specific settings. | This issue does not impact the TSPA-LA PMA dose calculation which uses the appropriate updated UZ_Params file for 300 epistemic realizations. The UZ_Params_Multi files, tables of sampled values of epistemically uncertain parameters, are only used when the PMA model is run with the compliance implementation of the unsaturated zone. |
| 2 | The 4 external FEHM .mptr input files for the EF 10k and 1Myr cases need to be updated to point to the correct UZ_Params_Multi_PMA file to use. | This modification only impacts EF EXDOC PMA simulations that turn the PMA UZ implementation off (i.e., compliance UZ implementation is used). This feature was not used for the PMA dose calculations, but was intended for future sensitivity analyses. This change needs to occur in conjunction with populating the UZ_Params_Mult files identified in issue #1.<br>This issue does not have any impact on dose results. |
| 3 | The selector containing the logic for the determination of the CDSP WP Seismic first damage time is incorrectly set. | The first switch in the selector element, Seismic_1st_Dam_Time_CDSP is incorrectly set to suppress any seismic events. The correct setting should select the EXDOC table, Seismic_Time_A1_Spec, which specifies the sampling configuration for the Seismic GM 10,000-year simulation.<br>This issue, which only applies to the 10,000-year Seismic GM simulation, was corrected prior to running the model, and therefore has no impact on dose. |
| 4 | UZ tortuosity parameters, UZ_Tortuosity_RG2_a and UZ_Tortuosity_RG3_a were incorrectly set (v10.002)<br>(err#-case# 001-10.002 needs to change to 002-10.002) | The UZ tortuosity parameters should Correct settings:<br>min(1.0,(10^(UZDC_Mean_RG2+UZDC_STN_RG2*UZDC_SD_RG2)))<br>The expression for UZ_Tortuosity_RG3_a should be min(1.0,(10^(UZDC_Mean_RG3+UZDC_STN_RG3*UZDC_SD_RG3)))<br>This error should have negligible or no impact in all modeling cases. |
| 5 | The IWPD submodel selector elements for the timing of the first Igneous or Seismic event are incorrectly set to supress events until 400,000 years. To correct this, the first two switches in the selector elements, Event_Time_Feed_IWPD_CDSP and Event_Time_Feed_IWPD_CSNF need to be deleted.<br>(err#-case# 002-10.016) | This issue is scenario specific to the Igneous, Seismic FD, and Seismic GM 10,000-year simulations, as well as the Seismic FD 1, 000,000 year simulations. The model file for each of the affected cases was corrected prior to running the file, and therefore does not impact the dose calculations. |
| 6 | ExDoc type runs for both 1Myr EF cases are run with the PMA cladding failure submodel calculations turned on.<br>(err#-case# 003-10.016) | This is not an error and is not applicable to the impact evaluation. |
| 7 | The RH threshold for the fluoride ion calculation is incorrect in nineteen of the tables. | Most of these incorrect values were not used in the actual simulations because these values, both the incorrect and the corrected ones, are low (<0.65). At such low RH, the temperatures in the drift will be still high (> 96$^{o}$C) and there will be no seepage water dripping. For the other incorrect values, the differences between the incorrect and the correct ones are small (<0.012). Therefore, the impact on dose is expected to be negligible. |

Table C9-1[a]. Impact Assessment Summary Table (Continued)

| | ISSUE DESCRIPTION | IMPACT ASSESSMENT |
|---|---|---|
| 8 | The PMA early failure scenarios distribute the EBS mass released to the UZ nodes unevenly within a given percolation subregion. | Although the EBS mass released to the UZ nodes is distributed unevenly within a given percolation subregion in each realization, the even distribution is captured by calculating the annual mean dose from 300 realizations sampling uncertainty uniformly. Therefore no dose impact is expected. |
| 9 | Certain parameters within the model were not connected to the PMA database. | The PMA simulations use the correct values for the parameters listed below, and therefore this issue does not affect the dose calculations. The parameters that need to be linked to the PMA database include,<br>FPLRZN, FPLRZS, FPLRZE, FPVO_PMA, Rf1-Rf10, Kd_Np_RZ, Kd_Np_RZ, SZ_Block_Length, SZ_Block_Thickness, Viscosity_water_T, Sat_Vap_Density_Outside_WP, Water_Vap_Diff_Coeff, Water_Vap_Diff_Cond, Air_Entry_Potential, Sat_Vap_Density_Inside_WP, Osmotic_Coeff, pH_eq |
| 10 | Certain parameters within the model were not locked on to the PMA database. GoldSim allows you to “lock onto” the file that is being referenced by a file element. When you lock onto a file (by checking the Lock onto this file option in the File element dialog), the following additional information regarding the referenced file is saved with the element: File and path name; Date the file was created; Date the file was last modified; File size; and CRC signature. Once you have locked onto a file, this information is displayed in a tool-tip when you hold your cursor over the filename in the dialog. | The PMA simulations used the correct files because they were downloaded from the controlled PMA database when the model was run, and therefore this issue does not affect the dose calculations. |
| 11 | The pH regression equation contains incorrect coefficients. | The coefficients in the regression for pH_eq need to be corrected. The value of 7.2625 should be rounded to 7.3. The value of 0.00185 has an extra zero and should also be rounded to 0.02. pH_eq is the pH where the acid and the alkaline dissolution rates cross over, and this pH weakly depends on temperature. For the most part of repository time period, the resulting difference in pH_eq due to the error is less than one unit, which is within the uncertainty range of predicted in-package pH values. Therefore, the impact on annual dose is expected to be negligible. |

Table C9-1[a]. Impact Assessment Summary Table (Continued)

| | ISSUE DESCRIPTION | IMPACT ASSESSMENT |
|---|---|---|
| 12 | There are incorrect values in some of the tables used in the in-package chemistry calculations. | Some of the inputs in the PMA database for the lookup tables named: IPC_XXX_pH_Rsw_YY_Z_LUT (where XXX = CSNF, DHLW, or MCO; YY = 15, 2, 3, or 4; and Z = A-I) has some rows with erroneous data.<br>The DTN that supplied the tables had some independent variables that were duplicated in multiple rows. GoldSim could not read tables with these duplicate independent variables. The DTN supplier indicated that it was acceptable to average these rows together. The error occurred because the analyst who averaged these rows failed to expand out each cell to display the maximum number of significant figures. Therefore some rows were rounded together that did not need to be. No impacts to the dose results are expected.<br>More information is provided in PEF 500. The PEF has a Roadmap to the TSPA-produced DTN that holds the modified lookup tables. This DTN now has two file sets: Uncorrected and Corrected. To correct this error, replace the PMA database entries with the tables in the Corrected folder. |
| 13 | The parameter specifying the value of Np Carbonate Eps is incorrect. | The input in the PMA database for parameter "Np_Carbonate_PMA_Eps" is not correct. It should be a triangular distribution with a=-0.5 and b=0 and c=0.5 rather than a truncated normal distribution. The truncated normal distribution is equally well justified. No impacts to the dose results are expected. |
| 14 | In determining whether the drift chemical environment is benign or aggressive for drip shield general corrosion, 5 mM dissolved fluoride concentration is used instead of 0.5 mM as suggested in C6.3.1. | The value of 5 mM is justifiable because this value is close to the middle point of the fluoride concentration interval within which the corrosion rate starts to increase at the lower bound (0.5 mM) and then levels off at the upper bound (5 mM). Furthermore, this error only affects one out four initial seepage waters used in the model and this effect will diminish as the seepage water composition returns to the ambient conditions after the thermal event. Therefore, the impact of this error is negligible. |

Table C9-1[a]. Impact Assessment Summary Table (Continued)

| | ISSUE DESCRIPTION | IMPACT ASSESSMENT |
|---|---|---|
| 15 | The Water Balance submodel incorrectly calculates:<br>1) the stainless steel degradation rate for Co-disposed (CDSP) WPs .<br>2) the average stainless steel degradation rate<br>3) the stainless steel degradation rate by treating all corrosion products as degraded stainless steel | 1) The expression for the degradation rate in the CDSP portion of the model should be divided by the number of packages failed to obtain a per-package degradation rate. Otherwise, the rate is too high which keeps the water saturation low and ionic strength high until the steel is gone. Low water saturation may reduce the diffusive release from the waste form. High ionic strength tends to increase radionuclide solubility because of out-of-bound conditions. The overall effect is anticipated to be small because CSNF WPs usually dominate the dose. The early failed scenarios are not affected because they fail only one WP.<br>2) The stainless steel degradation rate is based on the difference between the volume of corrosion products times the number of failed packages at the current timestep and the previous timestep. However, the corrosion products volume is already an average so this technique is unnecessary. This results in small overestimation of the stainless steel degradation rate when the number of failed WPs increases with time, such as in the Nominal Modeling Case run for the 1,000,000 year duration. The overall effect on dose is anticipated to be small because the water saturation inside the WP would not be greatly affected by this overestimation.<br>3) The stainless steel degradation rate uses a conversion factor for calculating the volume of corrosion products per kilogram of stainless steel. However, some of the corrosion products in the CDSP WPs are formed from the degradation of carbon steel, which should use a different conversion factor. The effect is anticipated to be small because the conversion factors would be approximately the same. |

# APPENDIX D[a]
# PARAMETER LISTING

# D1[a] INTRODUCTION

The Total System Performance Assessment (TSPA) Input Database was updated and includes the parameters used in both TSPA-LA Model v5.000 (documented in the parent document) and TSPA-LA Model v5.005 (documented in this addendum). The details of this database are described in Section 4.7 of the parent document and Section 4[a] of this addendum. Parameter Entry Form series 200 numbers, listed in Tables 4-1[a] and 4-2[a], contain the additional TSPA-LA Model v5.005 parameters. Additionally, Appendix K of the parent report contains two tables that describe the significant uncertain parameters (Tables K.3-1 and K.3-2).

INTENTIONALLY LEFT BLANK

# APPENDIX H[a]
# YUCCA MOUNTAIN REVIEW PLAN ACCEPTANCE CRITERIA

# H1[a] EVALUATION OF THE TOTAL SYSTEM PERFORMANCE ASSESSMENT FOR THE LICENSE APPLICATION MODEL DOCUMENT AGAINST REGULATORY REQUIREMENTS

Appendix H[a] includes minor editorial changes from the text included in the parent document when referencing the proposed rule. The supplemental information presented in this addendum should be used to clarify these issues.

## H1.1[a] EVALUATION AGAINST 10 CFR 63.113(a); 10 CFR 63.115(a); AND 10 CFR 63.115(b)

No change.

## H1.2[a] EVALUATION AGAINST 10 CFR 63.113(b)

No change.

## H1.3[a] EVALUATION AGAINST 10 CFR 63.113(c)

Acceptance Criterion 1 and 2 below have been revised slightly from the parent document with some minor updates to the references. The bulk of the information presented is the same as in the parent document.

**Acceptance Criterion 1–An Adequate Demonstration is Provided that the Expected Concentration of Combined $^{226}$Ra and $^{228}$Ra, Expected Concentration of Specified Alpha-Emitting Radionuclides, and Expected Whole Body or Organ–Specific Doses from any Photon– or Beta–Emitting Radionuclides at Any Year During the Compliance Period Do Not Exceed the Separate Standards for Protection of Groundwater—**Section 8.1.2 presents the results of analyses addressing the separate standards for protection of groundwater in 10 CFR 63.331 [DIRS 180319], Table 1. In particular, Section 8.1.2 shows the estimate of groundwater radioactivity for the representative volume of groundwater that includes combined $^{226}$Ra and $^{228}$Ra, gross alpha activity (including due to $^{226}$Ra, but excluding that due to radon and uranium), and combined beta- and photon-emitting radionuclides. Sections 6.3 and 8.1.2 discuss the methods, assumptions, models, and data used in calculating these estimates. Sections 6.3 and 8.1.2 show that these estimates are consistent with the repository performance assessment calculations for likely processes and events that may occur after disposal, and that the calculations are supported by an adequate technical basis. Therefore, the material in Sections 6.3 and 8.1.2 provides information useful in evaluating Acceptance Criterion 1.

**Acceptance Criterion 2–The Methods and Assumptions Used to Determine the Position of the Representative Volume of Groundwater are Credible and Consistent, and the Representative Volume of Groundwater Includes the Highest Concentration Level in the Plume of Contamination in the Accessible Environment—**Section 6.3.10 discusses the methods and assumptions for determination of groundwater concentrations in the representative volume that is located along the radionuclide migration path from the repository at Yucca Mountain to the accessible environment. Section 8.1.2 provides results and a detailed evaluation of the concentrations in the context of the groundwater concentration standards (10 CFR 63.331 [DIRS 180319], Table 1). In the TSPA-LA Model, a conservative approach is used in which

radionuclide concentrations are estimated by assuming the entire annual release from the repository system is discharged into the representative volume, located 18 km from the repository (66 FR 55732 [DIRS 156671], III Public Comments and Responses, 3.5, p. 55750). Therefore, the estimated radionuclide concentrations provide an upper bound to the groundwater concentrations needed to assess the groundwater protection requirements. This approach eliminates the need to specify the dimensions of the representative volume or the water usage by the reasonably maximally exposed individual (RMEI) (Section 1.1.1) (10 CFR 63.332(a)(3) [DIRS 180319]). The information provided in Sections 6.3.10 and 8.1.2 therefore, supports evaluation of Acceptance Criterion 2 by the U.S. Nuclear Regulatory Commission (NRC).

**Acceptance Criterion 3–The Methods and Assumptions Used to Calculate the Physical Dimensions of the Representative Volume of Groundwater are Credible and Consistent**—No changes.

## H1.4[a] EVALUATION AGAINST 10 CFR 63.113(d)

**Acceptance Criterion 1–Evaluation of the Time of an Intrusion Event**—No change.

**Acceptance Criterion 2–Evaluation of an Intrusion Event Demonstrates That the Annual Dose to the Reasonably Maximally Exposed Individual in Any Year During the Compliance Period Is Acceptable—**Sections 6.7 and 8.1.3 discuss how the TSPA-LA Model addresses the Human Intrusion Scenario, the implementation, and how the resultant RMEI dose complies with the requirement of this acceptance criterion. Section 6.7.3 specifically discusses implementation of the TSPA-LA Model for human intrusion separately from the overall TSPA, and is consistent with the requirements for performance assessments, as specified in NRC Proposed rule 10 CFR 63.114 [DIRS 178394]. Section 6.7 analyzes a postulated human intrusion event with characteristics as defined in 10 CFR 63.322 [DIRS 180319], and excludes the consideration of unlikely natural features, events, or processes (10 CFR 63.342(b) [DIRS 178394]) (Section 6.7.2.2). Sections 6.7.3 and 6.7.4 show that many of the nominal abstractions, process models, and parameters values are used in the analysis of the TSPA-LA Human Intrusion Scenario, and therefore, many of the implementation provisions in Section 6.3 apply to the Human Intrusion Modeling Case. In addition, the numerical values in the Individual Protection Standard in NRC Proposed Rule 10 CFR 63.311(a) [DIRS 178394] are identical to the numerical values of the Individual Protection Standard for Human Intrusion in NRC Proposed Rule 10 CFR 63.321(b) [DIRS 178394]. Section 7.3 provides information regarding the fact that a sufficient number of realizations have been run using the TSPA-LA Model, to ensure that the results of the calculations are statistically stable. Section 8.1.3 discusses the overall system performance analyses and presents the resulting annual dose curves for the Human Intrusion Scenario. The information provided in Sections 6.7 and 8.1 supports confirmation that the repository system meets performance objectives specified in 10 CFR 63.321 [DIRS 178394] for a human intrusion into the repository.

**Acceptance Criterion 3—The Total System Performance Assessment Code Provides a Credible Representation of the Intrusion Event**—No change.

Table H-1[a]. Applicable Regulatory Requirements of 10 CFR Part 63 and NUREG-1804 Acceptance Criteria Addressed in this Document

| Applicable Sections of 10 CFR Part 63 | Associated Section of NUREG-1804 Acceptance Criterion | NUREG-1804 Acceptance Criterion | | Section of Report Addressing NUREG-1804 Acceptance Subcriterion |
|---|---|---|---|---|
| | | Criterion | Subcriterion | |
| 10 CFR 63.113(b) [DIRS 180319] and 10 CFR 63.311 [DIRS 178394] | 2.2.1.4.1.3 Demonstration of Compliance with Postclosure Individual Protection Standard | 1. Scenario Classes | 1. Scenario class screening | 6.1.2 |
| | | | 2. Combining mean annual dose from scenario classes | 6.1.2 and 8.1.1.1 |
| | | 2. Mean Annual Doses | 1. Number of realizations | 7.3 |
| | | | 2. Uncertainty in mean annual dose | 6.1.3 and 8.1.1.2 |
| | | | 3. Performance of components and subsystems | 8.2 – 8.4 |
| | | | 4. Comparison with individual protection standard (10 CFR 63.311 [DIRS 178394]) | 8.1.1.2 |
| | | 3. Credible TSPA-LA Model | 1. Consistency of assumptions | 5, 6.3 to 6.6 |
| | | | 2. Model verification | 7.2 |
| | | | 3. Uncertainty analysis | 6.1.3 and 7.4 |
| | | | 4. Parameter sampling | 6.1.3 |
| 10 CFR 63.113(c) [DIRS 180319], 10 CFR 63.331 [DIRS 180319], Table 1, and 10 CFR 63.332 [DIRS 180319] | 2.2.1.4.3.3 Demonstration of Compliance with Groundwater Protection Standards | 1. Groundwater Protection Standards | 1. Compliance with concentration and dose standards | 8.1.2.1 to 8.1.2.2, and 8.1.2.3 |
| | | | 2. Methods and assumptions | 8.1.2 |
| | | | 3. Comparison with groundwater protection standards (10 CFR 63.331 [DIRS 180319], Table 1) | 8.1.2 |
| | | 2. Position of Representative Volume | 1. Along radionuclide migration path | 6.3.10 |
| | | | 2. Method of locating position | 6.3.10 |
| | | | 3. Highest concentration | 6.3.10 |
| | | 3. Dimensions of Representative Volume | 1. Specifications on representative volume | 8.1.2 |
| | | | 2. Method to determine dimensions | 6.3.10 and 8.1.2 |
| | | | 3. Consistency with water usage | 8.1.2 and 6.3.11 |

Table H-1[a]. Applicable Regulatory Requirements of 10 CFR Part 63 and NUREG-1804 Acceptance Criteria Addressed in this Document (Continued)

| Applicable Sections of 10 CFR Part 63 | Associated Section of NUREG-1804 Acceptance Criterion | NUREG-1804 Acceptance Criterion | | Section of Report Addressing NUREG-1804 Acceptance Subcriterion |
|---|---|---|---|---|
| | | Criterion | Subcriterion | |
| 10 CFR 63.113(d) [DIRS 180319], 10 CFR 63.321 [DIRS 178394], and 10 CFR 63.322 [DIRS 180319] | 2.2.1.4.2 Demonstration of Compliance with the Human Intrusion Standard | 1. Evaluation of the Time of a Human Intrusion Event | 1. The technical basis and associated analyses adequately support the selection of the time of occurrence of a human intrusion, as specified in 10 CFR 63.321 [DIRS 178394]. | 6.7.2 |
| | | 2. Evaluation of an Intrusion Event Demonstrates That the Annual Dose to the RMEI in Any Year During the Compliance Period Is Acceptable | 1. The TSPA for the Human Intrusion Scenario is performed separately from the overall TSPA, and meets the requirements for performance assessments, specified in 10 CFR 63.114 [DIRS 178394]. | 6.7.3 and 6.7.4 |
| | | | 2. The TSPA for the Human Intrusion Scenario is identical to the TSPA for individual protection, except that it assumes the occurrence of a postulated human intrusion event with characteristics, as defined in 10 CFR 63.322 [DIRS 180319] and excludes the consideration of unlikely natural features, events, or processes in 10 CFR 63.342(b) [DIRS 178394]. | 6.7.2.2, 6.7.3, and 6.7.4 |
| | | | 3. A sufficient number of realizations have been run using the TSPA code, to ensure that the results of the calculations are statistically stable. | 8.1.1.2 and 7.3 |
| | | | 4. The estimated repository performance is reasonable and consistent with the analysis of overall repository performance, and with the characteristics of the postulated Human Intrusion Scenario. | 8.1.3.2 |
| | | | 5. The annual dose curve for limited human intrusion confirms that the repository system meets performance objectives, specified in 10 CFR 63.321 [DIRS 178394], for limited human intrusion events. | 8.1.3.2 |

Table H-1[a]. Applicable Regulatory Requirements of 10 CFR Part 63 and NUREG-1804 Acceptance Criteria Addressed in this Document (Continued)

| Applicable Sections of 10 CFR Part 63 | Associated Section of NUREG-1804 Acceptance Criterion | NUREG-1804 Acceptance Criterion | | Section of Report Addressing NUREG-1804 Acceptance Subcriterion |
|---|---|---|---|---|
| | | Criterion | Subcriterion | |
| | | 3. The TSPA Code Provides a Credible Representation of a Human Intrusion Event. | 1. Assumptions made on the method of transport from a breached waste package within the TSPA for evaluating the postulated intrusion event are consistent among different modules of the code. The use of assumptions and parameter values that differ among modules of the code is adequately documented. | 5, 6.7.1 to 6.7.5, and 7.7 |
| | | | 2. The TSPA code for evaluating human intrusion is properly verified, such that there is confidence that the code is modeling the physical processes in the repository system in a manner that is consistent with the characteristics of the postulated intrusion event. The transfer of data between modules of the code is conducted properly. | 7.2 |
| | | | 3. The estimate of uncertainty in the performance assessment results is consistent with the uncertainties considered in the characteristics of the postulated intrusion event, and with model and parameter uncertainty. | 8.1.3, 6.7.3 ,6.1.3, and 7.4 |
| | | | 4. The sampling method used in the TSPA ensures that sampled parameters of the postulated intrusion event have been sampled across their ranges of uncertainty. | 6.1.3, 6.7, and 7.4 |

Sources: 10 CFR Part 63 [DIRS 178394 and DIRS 180319]; NUREG-1804 (NRC 2003 [DIRS 163274]).

INTENTIONALLY LEFT BLANK

# APPENDIX I[a]
# FEATURES, EVENTS, AND PROCESSES MAPPED TO TSPA-LA MODEL

# I1[a] INTRODUCTION

Appendix I[a] contains a revision to selected descriptions listed in Table I-2 of the parent document. One new description for the EBS Thermal Hydrologic Environment Submodel is included in Table I-2[a]. Only the table entries that have been revised are included in the updated Table I-2[a] included in this addendum. The corrected table entries should be substituted into the original table presented in Appendix I of the parent document.

INTENTIONALLY LEFT BLANK

Table I-2[a]. Model Implementation for Included Features, Events, and Processes

| Submodel Implemented in the TSPA-LA Model and Section Number | Path in GoldSim Model File | FEPs Included in the Submodel | TSPA Inclusion Explanation | Performance Assessment Standard[a] | TSPA-LA Model Implementation |
|---|---|---|---|---|---|
| EBS TH Environment Submodel<br><br>6.3.2 | Epistemic: \Input_Params_Epistemic\Epistemic_Params_EBS_Environ\Uncertain_Params_TH<br>EBS: \Global_Inputs_and_Calcs\Global_EBS_Environ\EBS_Environment\ThermoHydrology | 2.1.06.06.0A<br><br>Effects of drip shield on flow | The effects of a drip shield on flow is included in the Multiscale Thermohydrologic Model (MSTHM) by predicting the temperature of the in-drift environment both inside and outside the intact drip shield. Water fluxes in the invert are influenced by temperature and capillary pressure processes. The thermal effects on flow are assessed by multiple MSTHM process model simulations. These simulations are used to develop the MSTHM Abstraction implemented in the TSPA-LA Model. | 10 CFR 63.311<br>10 CFR 63.331<br>10 CFR 63.321 | MA |
| WP and DS Degradation Submodel<br><br>6.3.5 | Epistemic: \Input_Params_Epistemic\Epistemic_Params_WP_DS_Deg\<br><br>Aleatory: \Model_Calcs_Aleatory\Aleatory_Calcs_WP_DS_Deg<br><br>EBS: \Time_Zero\EBS_PS_Loop\Static_Calcs_PS_Loop\Static_Calcs_WP_DS_Deg<br><br>\Global_Inputs_and_Calcs\Global_WP_DS_Deg\Global_IWPD | 2.1.03.05.0A<br><br>Microbially influenced corrosion of waste packages | Microbially influenced corrosion is modeled in the TSPA-LA Model as an enhancement factor uniformly distributed between 1 and 2 due to uncertainty. The factor is applied to the entire waste package outer barrier general corrosion rate when the relative humidity at the waste package outer corrosion barrier surface is above a threshold value represented by, and sampled from, a uniform distribution ranging from 75 percent to 90 percent. | 10 CFR 63.311<br>10 CFR 63.331 | DLL |

Table I-2[a] Model Implementation for Included Features, Events, and Processes (Continued)

| Submodel Implemented in the TSPA-LA Model and Section Number | Path in GoldSim Model File | FEPs Included in the Submodel | TSPA Inclusion Explanation | Performance Assessment Standard[a] | TSPA-LA Model Implementation |
|---|---|---|---|---|---|
| Biosphere Submodel<br><br>6.3.11 | Epistemic: \Input_Params_Epistemic\Epistemic_Params_Biosphere<br><br>Other: \TSPA_Model\Biosphere | 2.4.01.00.0A<br><br>Human characteristics (physiology, metabolism) | Metabolic and physiologic considerations consistent with present knowledge of adults, as per 10 CFR 63.312(e) [DIRS 180319], were used in the development of parameter distributions for the external exposure, inhalation, and ingestion submodels. Therefore, this feature, event, or process (FEP) is included in the biosphere component of the TSPA-LA Model through the use of groundwater exposure scenario biosphere dose conversion factors (BDCFs) that are direct inputs to the TSPA-LA for the scenario classes involving radionuclide release to the groundwater, and through the use of the conversion factors for demonstrating compliance with the groundwater protection standards. The annual doses are calculated as the product of radionuclide concentration in groundwater and the BDCFs or conversion factors. | 10 CFR 63.311<br>10 CFR 63.321<br>10 CFR 63.331 | MA |

[a] 10 CFR 63.311 Individual Protection (70 FR 53313 [DIRS 178394]).
10 CFR 63.331 Groundwater Protection (10 CFR 63 [DIRS 180319]).
10 CFR 63.321 Human Intrusion (70 FR 53313 [DIRS 178394]).

# APPENDIX J[a]
# CONCEPTUAL STRUCTURE OF TSPA-LA

# J1[a] INTRODUCTION

Appendix J of the parent document includes detailed documentation of the TSPA-LA Model conceptual structure. This addendum includes additional supplemental material in Section J3[a] that presents an overview of the underlying concepts used in the TSPA-LA Model, which are described in Appendix J of the parent document. The supplemental material provided in Section J3[a] of this addendum should be reviewed in conjunction with Appendix J included with the parent document.

# J2[a] REQUIREMENTS UNDERLYING CONCEPTUAL STRUCTURE OF TSPA-LA

No change.

# J3[a] TUTORIAL ON PROBABILITY, UNCERTAINTY AND THE STRUCTURE OF PERFORMANCE ASSESSMENTS

The conceptual and computational design of the TSPA-LA is based on standard concepts underlying risk assessments for complex systems. An overview of the evolution and development of these concepts is provided in Rechard (1999 [DIRS 145383]).

A natural starting place in a discussion of the antecedents to the TSPA-LA conceptual and computational design is the Reactor Safety Study, which was initiated by the Atomic Energy Commission to study the risk from commercial nuclear power plants and completed by the NRC (1975 [DIRS 107799]). This was a landmark study and constituted the largest systematic risk analysis ever performed at the time of its completion. The primary emphasis of this study was on aleatory uncertainty in the sense of the universe of possible accidents that could occur at a commercial nuclear power plant.

After the completion of the Reactor Safety Study, the NRC commissioned a review of the study that is now commonly referred to as the Lewis Report (Lewis et al. 1978 [DIRS 107800]). This report was highly complimentary of the Reactor Safety Study but had one notable criticism. This criticism was that the Reactor Safety Study had not appropriately assessed and presented the uncertainty in its results. Here, the uncertainty being referred to was of a state of knowledge or epistemic character.

The Reactor Safety Study was highly influential and set the stage for a number of the following risk assessments (e.g., PLG 1983 [DIRS 185063]; PLG 1982 [DIRS 107812]). It was out of this work that the Kaplan/Garrick ordered triple representation for risk emerged (Kaplan and Garrick 1981 [DIRS 100557]). Conceptually, the TSPA-LA can be cast in the context of this representation for risk. However, for computational reasons the TSPA-LA uses a continuous integral-based version of the original ordered triple representation for risk. It was also during this period that Latin hypercube sampling was introduced for use in uncertainty and sensitivity analyses for computationally demanding models (McKay et al. 1979 [DIRS 127905]).

After the publication of the Reactor Safety Study, the NRC initiated the development of a risk assessment methodology at Sandia National Laboratories for the disposal of radioactive waste (Campbell et al. 1978 [DIRS 185064]; Cranwell et al. 1987 [DIRS 185066]). As a result of the

Lewis Committee's report on the importance of the treatment of (epistemic) uncertainty, the appropriate treatment of such uncertainty was given high importance in the methodology development at Sandia (Iman and Conover 1982 [DIRS 165064]; Iman et al. 1980 [DIRS 124198]; and Iman et al. 1978 [DIRS 159559]).

The early work on uncertainty and sensitivity analysis in the preceding project significantly influenced later analyses for complex systems. In particular, it formed the basis for the treatment of uncertainty in the NRC's MELCOR project to develop a new suite of models for reactor accidents (Iman and Helton 1985 [DIRS 185067]), the NRC's reassessment of the risk from commercial nuclear power plants (i.e., the NUREG-1150 analyses) (Breeding et al. 1992 [DIRS 107727]; Breeding et al. 1992 [DIRS 185068]; Brown et al. 1992 [DIRS 185069]; Gregory et al. 1992 [DIRS 185070]; Helton and Breeding 1993 [DIRS 184402]; Payne et al. 1992 [DIRS 185071]; and NRC 1990 [DIRS 107798]), the NRC's Risk Methods Integration and Evaluation Program (Payne 1992 [DIRS 107814]), and the U.S. Department of Energy's (DOE's) successful compliance certification application to the U.S. Environmental Protection Agency (EPA) for the Waste Isolation Pilot Plant (Helton and Marietta 2000 [DIRS 171759]; and DOE 1996 [DIRS 100975]). The basic ideas underlying the treatment of uncertainty and the performance of associated sensitivity analyses in the preceding analyses are summarized in a number of review articles (Helton 1993 [DIRS 100452]; Helton 1994 [DIRS 107739]; Helton 1997 [DIRS 107496]; Helton 2003 [DIRS 170558]; Helton and Davis 2003 [DIRS 170518]; and Helton et al. 2006 [DIRS 183873]).

The conceptual organization of the TSPA-LA is the same as the conceptual organization of the NRC's NUREG-1150 analyses and the DOE's analysis for the Waste Isolation Pilot Plant. Of course, the details of the analyses are different because different facilities, and hence different processes and models, are involved. However, the analyses are the same conceptually and have a structure of the form described in Helton (2003 [DIRS 170558]). Further, all of these analyses use uncertainty and sensitivity analysis procedures of the form described in Helton and Davis (2003 [DIRS 170518]) and Helton et al. (2006 [DIRS 183873]). Thus, the TSPA-LA has an overall conceptual structure that has been successfully used in several preceding and important analyses. A detailed illustration of the conceptual ideas that underlie the calculation of expected dose to the reasonably RMEI in the TSPA-LA is presented in Helton and Sallaberry (2007 [DIRS 185072]).

## J4[a] CONCEPTUAL STRUCTURE OF TSPA-LA

No change.

## J5[a] NOMINAL SCENARIO CLASS

No change.

## J6[a] EARLY FAILURE SCENARIO CLASSES

No change.

## J7[a] IGNEOUS SCENARIO CLASSES

No change.

## J8[a] SEISMIC SCENARIO CLASSES

No change.

## J9[a] EXPECTED DOSE FROM ALL SCENARIO CLASSES

No change.

## J10[a] JUSTIFICATION FOR ANALYSIS DECOMPOSITION

No change.

## J11[a] HUMAN INTRUSION SCENARIO

No change.

INTENTIONALLY LEFT BLANK

# APPENDIX K[a]
# UNCERTAINTY AND SENSITIVITY ANALYSIS RESULTS

# K1[a] INTRODUCTION

No change.

# K2[a] UNCERTAINTY AND SENSITIVITY ANALYSIS PROCEDURES

No change.

# K3[a] INDEPENDENT AND DEPENDENT VARIABLES

No change.

# K4[a] NOMINAL SCENARIO CLASS

No change.

## K4.1[a] Nominal Scenario Class: Summary

No change.

## K4.2[a] Nominal Scenario Class: Drip Shield (DS) and Waste Package (WP) Failure

No change.

## K4.3[a] Nominal Scenario Class: Engineered Barrier System (EBS) Conditions

No change.

## K4.4[a] Nominal Scenario Class: Release Results Engineered Barrier System (EBS), Unsaturated Zone (UZ) and Saturated Zone (SZ)

No change.

## K4.5[a] Nominal Scenario Class: Dose to Reasonably Maximally Exposed Individual (RMEI)

No substantive changes in the uncertainty and sensitivity analyses for dose to the RMEI (*DOSTOT*, mrem/yr) over the time interval [0, 1,000,000 yr] resulting from nominal conditions were observed (i.e., compare the results in Figures K4.5-1 and K4.5-2 with the results in Figures K4.5-1[a] and K4.5-2[a]). Additional comparisons are presented in Figures 7.3.1-18[a] and 7.3.1-19[a] and are discussed in Section 7.3.1.5.1[a].

For reader convenience, the following discussion of the expected dose results in Figures K4.5-1[a] and K4.5-2[a] is provided. This discussion updates Section K4.5 from the parent report.

The uncertainty and sensitivity analyses for total dose to the RMEI (*DOSTOT*, mrem/yr) are summarized in Figures K4.5-1[a] and K4.5-2[a]. Nonzero values for *DOSTOT* begin as early as 20,000 yr as a result of WP failure and then show a general tendency to increase

(Figure K4.5-1a,b[a]). However, some dose curves and especially some of the curves with the largest values for *DOSTOT*, change from increasing to decreasing at some point in time. This change results from inventory depletion, and hence decreasing or terminating releases, for highly mobile species such as $^{99}$Tc and $^{129}$I. All curves remain below 10 mrem/yr.

The PRCCs in Figure K4.5-1c[a] indicate that the uncertainty in *DOSTOT* is dominated by *WDGCA22* (temperature dependence coefficient associated with the general corrosion rate for Alloy 22, K), with *DOSTOT* tending to decrease as *WDGCA22* increases. This effect results because the general corrosion rate for Alloy 22 decreases as *WDGCA22* increases. Smaller effects are indicated for *SCCTHR* (stress corrosion cracking threshold, MPa), *WDZOLID* (scale factor used to incorporate uncertainty into the stress intensity factor for closure-lid weld), *THERMCON* (host rock thermal conductivity level), *WDNSCC* (stress corrosion cracking growth rate exponent), and *CPUCOLWF* (concentration of irreversibly attached plutonium on stable glass/waste form colloids, mol/L). The variables *SCCTHR*, *WDZOLID*, *THERMCON* and *WDNSCC* affect *DOSTOT* through their effects on WP failure. Specifically, increasing *SCCTHR* increases the stress level at which stress corrosion cracking initiates and thus reduces failures at the closure-lid weld; increasing *WDZOLID* increases the stress at the closure lid and thus increases failures at the closure-lid weld; increasing *THERMCON* tends to lower WP temperatures and thus reduce the rate of corrosion; and increasing *WDNSCC* tends to increase the threshold stress intensity factor, which determines the threshold stress at which stress corrosion cracks propagate, and thus reduces failures at the closure-lid weld. The indicated effects of *CPUCOLWF* are small and possibly spurious.

The PRCCs in Figure K4.5-1d[a] are for [200,000; 1,000,000 years] rather than for [0; 1,000,000 years] as is the case for the PRCCs in Figure K4.5-1c[a]. The only substantive difference is the selection of *INFRCTC* (initial release fraction for $^{99}$Tc in a CSNF WP) as the last variable in the analysis for [200,000; 1,000,000 years]; in contrast *CPUCOLWF* is selected as the last variable in the analysis for [0; 1,000,000 years]. The PRCCs presented originally in Figure K4.5-1c are for [0; 1,000,000 years]; however, the written discussion of the PRCC results in Section K4.5 is for PRCCs obtained for [200,000; 1,000,000 years]. As a result, the effects of *INFRCTC* are discussed in Section K4.5 although a PRCC for *INFRCTC* does not appear in Figure K4.5-1c. The effects for *INFRCTC* discussed in Section K4.5 can be seen in Figure K4.5-1d[a].

More detailed sensitivity analysis results for *DOSTOT* are provided by the regression results in Figure K4.5-2a[a]. Specifically, *WDGCA22* is the dominant variable with $R^2$ values of 0.78, 0.85 and 0.63 at 400,000 yr, 600,000 yr and 800,000 yr, respectively. Actually, the indicated $R^2$ values tend to under represent the effect of *WDGCA22* because of the nonlinear relationship between *WDGCA22* and *DOSTOT* that can be seen in Figure K4.5-2b,c,d of Appendix K and is more apparent in Figure K4.5-3 of Appendix K. Specifically, large values of *WDGCA22* result in small values for *DOSTOT* at late times because of limited WP failure and hence limited radionuclide releases, and small values of *WDGCA22* also result in small values for *DOSTOT* at late times because of extensive, early WP failure and the resultant reduction in radionuclide inventory by late times.

In addition to *WDGCA22*, the regressions in Figure K4.5-2a[a] indicate small effects for the following variables that affect WP failure: *WDZOLID*, *THERMCON*, *INFIL* (infiltration level), *SCCTHR*, *WDNSCC*, and *WDGCUA22* (pointer variable used to select the distribution of base

corrosion rates of Alloy 22 at 60ºC over the patches on the WPs). The effects of *WDZOLID*, *THERMCON*, *SCCTHR* and *WDNSCC* have already been discussed in conjunction with Figure K4.5-1c[a]. Like *THERMCON*, the negative effect associated with *INFIL* probably results because increased values for *INFIL* result in lower WP temperatures and thus lower rates of corrosion. The variable *WDGCUA22* has a small positive effect on the uncertainty in *DOSTOT*. Specifically, *WDGCUA22* is a pointer variable used to select from three uncertain distributions that derive from both the uncertainty in a base corrosion rate for Alloy 22 at 60ºC and the uncertainty that exists in the prediction of small scale variability in chemical and physical conditions across patches used in the modeling of WP degradation. Increasing *WDGCUA22* results in higher overall corrosion rates and thus higher values for *DOSTOT*. The dominance of *WDGCA22* with respect to the uncertainty associated with *DOSTOT* can be seen in the scatterplot in Figure K4.5-2b[a].

The regressions in Figure K4.5-2a[a] also indicate very small effects of several variables related to physical processes. However, the effects of these variables are minor given the much larger effects of variables related to WP failure and, in particular, the dominant effect of *WDGCA22* on WP failure.

## K5[a] EARLY FAILURE SCENARIO CLASSES

No change.

### K5.1[a] Early Failure Scenario Classes: Summary

No change.

### K5.2[a] Early Failure Scenario Classes: Engineered Barrier System (EBS) Conditions

No change.

### K5.3[a] Early Failure Scenario Classes: Release from Engineered Barrier System (EBS)

No change.

### K5.4[a] Early Failure Scenario Classes: Release from Unsaturated Zone (UZ)

No change.

### K5.5[a] Early Failure Scenario Classes: Release from Saturated Zone (SZ)

No change.

### K5.6[a] Early Failure Scenario Classes: Dose to Reasonably Maximally Exposed Individual (RMEI)

No change.

## K5.7[a] Early Failure Scenario Classes: Expected Dose to Reasonably Maximally Exposed Individual (RMEI)

No change.

## K5.7.1[a] Early Failure Scenario Classes: Expected Dose to Reasonably Maximally Exposed Individual (RMEI) from Early Drip Shield (DS) Failure

**Expected Dose to RMEI over [0, 20,000 yr]: *EXPDOSE*.** The uncertainty and sensitivity analyses for expected dose to the RMEI (*EXPDOSE*, mrem/yr) over the time interval [0, 20,000 yr] resulting from early DS failure are summarized in Figures K5.7.1-1[a] and K5.7.1-2[a]. Specifically, Figures K5.7.1-1[a] and K5.7.1-2[a] have the same structure as Figures K5.7.1-1 and K5.7.1-2 but present results calculated with version 5.005 of the TSPA-LA Model rather than with version 5.000 used in the calculation of the results in Figures K5.7.1-1 and K5.7.1-2. A comparison of the results in Figures K5.7.1-1a[a] and K5.7.1-1a obtained with the two versions of the TSPA-LA Model is provided in Figures 7.3.1-20[a] and 7.3.1-22[a]; discussion of the differences in the results is provided in Section 7.3.1.5.2[a]. As examination of Figures 7.3.1-20[a] and 7.3.1-22[a] shows, there is little difference in the values for *EXPDOSE* obtained with the two versions of the TSPA-LA Model. Consistent with this comparison, there is also little difference in the sensitivity analysis results presented in Figures K5.7.1-1c and K5.7.1-2 for version 5.000 and the corresponding results presented in Figures K5.7.1-1c[a] and K5.7.1-2[a] for version 5.005. As a result, the discussion presented in Section K5.7.1 for *EXPDOSE* over the time interval [0, 20,000 yr] resulting from early DS failure for results obtained with version 5.000 of the TSPA-LA Model also applies to the results obtained with version 5.005 of the TSPA-LA Model. For this reason, no additional discussion is provided.

For reader convenience, the following discussion of the expected dose results in Figures K5.7.1-1[a] and K5.7.1-2[a] is provided. This discussion updates the corresponding material in Section K5.7.1 from the parent report.

The uncertainty and sensitivity analyses for expected dose to the RMEI (*EXPDOSE*, mrem/yr) over the time interval [0, 20,000 years] resulting from early DS failure are summarized in Figures K5.7.1-1[a] and K5.7.1-2[a]. There are sharp peaks in *EXPDOSE* prior to 1000 yr resulting from the release of $^{99}$Tc. At the time of these peaks, maximum values for *EXPDOSE* are in the vicinity of 0.01 mrem/yr, although the values for most sample elements are considerably smaller (Figure K5.7.1-1a,b[a]). After the early peaks, *EXPDOSE* has values in a range from $10^{-7}$ to $10^{-3}$ mrem/yr.

The PRCCs in Figure K5.7.1-1c[a] indicate that the uncertainty in *EXPDOSE* is dominated by *PROBDSEF* (probability that a randomly selected DS will experience an early failure), with the value for *EXPDOSE* increasing as *PROBDSEF* increases. This effect results because increasing *PROBDSEF* increases the expected number of DSs that experience early failure and hence increases *EXPDOSE.*

In addition to *PROBDSEF*, smaller effects are indicated for *SZFIPOVO* (flowing interval porosity in the volcanic unit of the SZ), *SZGWSPDM* (groundwater specific discharge multiplier*;* as sampled, *SZGWSPDM* is actually the logarithm of the indicated multiplier), *SEEPUNC*

(pointer variable used to determine local seepage rates), *INFIL* (infiltration level), and *THERMCON* (host rock thermal conductivity level) (Figure K5.7.1-1c[a]). A negative effect is indicated for *SZFIPOVO* at early times (i.e., prior to 3000 yr), with this effect then going to zero. This effect results because increasing *SZFIPOVO* increases the time required for the initial releases of mobile species such as $^{99}$Tc to reach the location of the RMEI. The positive effect associated with *SZGWSPDM* results from increasing the flow velocity in the SZ, which in turn moves radioactive species more rapidly to the location of the RMEI. This effect is especially pronounced at early times (i.e., prior to 2000 yr) because increasing *SZGWSPDM* decreases the time of first arrival of radioactive species at the location of the RMEI. Both *INFIL* and *THERMCON* have small positive effects on *EXPDOSE* at early times (i.e., prior to 3000 yr). These effects are possibly related to the influence of these variables on repository temperature and hence the time at which release from the EBS can begin. Specifically, increasing *INFIL* and *THERMCON* tends to reduce EBS temperatures and thus reduce the time at which releases from the EBS can begin. After 3000 yr, *THERMCON* has no effect on *EXPDOSE*; however, *INFIL* continues to have a small effect, probably resulting from increased water flow through the EBS and UZ that results as *INFIL* increases in value.

More detailed sensitivity analyses for *EXPDOSE* are provided by the regression analyses in Figure K5.7.1-2a[a]. The dominant effect of *PROBDSEF* on the uncertainty in *EXPDOSE* is indicated by $R^2$ values of 0.70, 0.71 and 0.63 for the regressions containing only *PROBDSEF* at 3000, 5000 and 10,000 yr. After *PROBDSEF*, the most important variable is *SEEPUNC*. However the incremental effect associated with *SEEPUNC* is small as the $R^2$ values for the regression models containing both *PROBDSEF* and *SEEPUNC* are 0.77 and 0.78 at 3000 and 5000 yr, respectively.

After *PROBDSEF* and *SEEPUNC*, smaller effects are indicated for a number of variables (Figure K5.7.1-2a[a]). For example, the following additional variables are indicated as affecting *EXPDOSE* at 10,000 yr: *INFIL*, *SEEPPRM* (mean fracture permeability in lithophysal rock units, $m^2$; as sampled, *SEEPPRM* is actually the logarithm of the indicated permeability), *ALPHAL* (capillary strength parameter in lithophysal rock units), *SZCOLRAL* (colloid retardation factor in alluvial unit of SZ, dimensionless*;* as sampled, *SZCOLRAL* is actually the logarithm of the indicated retardation factor), *MICPU239* (dose conversion factor for $^{239}$Pu for modern interglacial climate, (rem/yr)/(pCi/L)), *CPUCOLWF* (concentration of irreversibly attached plutonium on stable glass/waste form colloids*,* mol/L), *SEEPPRMN* (mean fracture permeability in nonlithophysal rock units, $m^2$; as sampled, *SEEPPRMN* is actually the logarithm of the indicated permeability), *RHMU0* (scale factor used to represent uncertainty in chloride concentration in drift waters for relative humidities in the range [0, 0.2]; as sampled, *RHMU0* is actually the logarithm of the indicated scale factor), *SMECSA* (specific surfaces area for smectite colloids, $m^2/g$), *SZGWSPDM* (groundwater specific discharge multiplier*;* as sampled, *SZGWSPDM* is actually the logarithm of the indicated multiplier), *UZFAG4* (fracture aperture for Group 4 rock units in UZ), and *EP1LOWPU* (scale factor used to incorporate uncertainty into plutonium solubility under low ionic strength conditions; as sampled, *EP1LOWPU* is actually the logarithm of the indicated scale factor). Specifically, the positive effects associated with *INFIL* and *SEEPUNC* result from increasing water flux through the EBS; the negative effects associated with *SEEPPRM*, *SEEPPRMN* and *ALPHAL* result from increasing water diversion around the EBS; the negative effect associated with *SZCOLRAL* results from increasing colloid

retardation in the SZ; the positive effect associated with *MICPU239* results from increasing the received dose for a given exposure to $^{239}$Pu (and possibly other radionuclides due to positive correlations that exist between uncertain dose factors); the positive effect associated with *CPUCOLWF* results from increasing the amount of plutonium attached to colloids; and the remaining variables have very small effects that may be real or may be spurious.

The dominant effect of *PROBDSEF* is readily apparent in the scatterplot in Figure K5.7.1-2b[a]. Further, the smaller effects of *INFIL* and *SEEPUNC* can be seen in the scatterplots in Figure K5.7.1-2b,c[a].

Two of the variables identified in the analysis with PRCCs (i.e., *SZFIPOVO*, *THERMCON*) in Figure K5.7.1-1c[a] do not appear in the regressions in Figure K5.7.1-2a[a]. However, the times at which these variables have identifiable effects on *EXPDOSE* in Figure K5.7.1-1c[a] are not the times at which the regressions in Figure K5.7.1-2a[a] are performed.

**Expected Dose to RMEI over [0, 1,000,000 yr]: *EXPDOSE*.** The uncertainty and sensitivity analyses for expected dose to the RMEI (*EXPDOSE*, mrem/yr) over the time interval [0, 1,000,000 yr] resulting from early DS failure are summarized in Figures K5.7.1-3[a] and K5.7.1-4[a]. Specifically, Figures K5.7.1-3[a] and K5.7.1-4[a] have the same structure as Figures K5.7.1-3 and K5.7.1-4 but present results calculated with version 5.005 of the TSPA-LA Model rather than with version 5.000 used in the calculation of the results in Figures K5.7.1-3 and K5.7.1-4. A comparison of the results in Figures K5.7.1-3a[a] and K5.7.1-3a obtained with the two versions of the TSPA-LA Model is provided in Figures 7.3.1-21[a] and 7.3.1-23[a]; discussion of the differences in the results is provided in Section 7.3.1.5.2[a]. As examination of Figures 7.3.1-21[a] and 7.3.1-23[a] shows, there is little difference in the values for *EXPDOSE* obtained with the two versions of the TSPA-LA Model. Consistent with this comparison, there is also little difference in the sensitivity analysis results presented in Figures K5.7.1-3c and K5.7.1-4 for version 5.000 and the corresponding results presented in Figures K5.7.1-3c[a] and K5.7.1-4[a] for version 5.005. As a result, the discussion presented in Section K5.7.1 for *EXPDOSE* over the time interval [0, 1,000,000 yr] resulting from early DS failure for results obtained with version 5.000 of the TSPA-LA Model also applies to the results obtained with version 5.005 of the TSPA-LA Model. For this reason, no additional discussion is provided.

For reader convenience, the following discussion of the expected dose results in Figures K5.7.1-3[a] and K5.7.1-4[a] is provided. This discussion updates the corresponding material in Section K5.7.1 from the parent report.

The uncertainty and sensitivity analyses for expected dose to the RMEI (*EXPDOSE*, mrem/yr) over the time interval [0, 1,000,000 years] resulting from early DS failure are summarized in Figures K5.7.1-3[a] and K5.7.1-4[a]. The time dependent results for *EXPDOSE* tend to decrease until about 200,000 yr and then level off (Figure K5.7.1-3-a,b[a]). This decrease is due to the decay of $^{239}$Pu, which has a half life of 24,100 yr, and is the largest contributor to expected dose before 200,000 yr (Figure 8.2-4[a]). The values for *EXPDOSE* are bounded above by 0.01 mrem/yr and, after 200,000 yr, by 0.001 mrem/yr.

The sensitivity analyses for the time interval [0, 1,000,000 yr] are similar to those for the time interval [0, 20,000 yr]. Specifically, the sensitivity analysis with PRCCs for [0, 1,000,000 yr] in

Figure K5.7.1-3c[a] identifies the following variables as influencing the uncertainty in *EXPDOSE*: *PROBDSEF* (probability that a randomly selected DS will experience an early failure), *SEEPPRM* (mean fracture permeability in lithophysal rock units, $m^2$; as sampled, *SEEPPRM* is actually the logarithm of the indicated permeability), *INFIL* (infiltration level), *SZFIPOVO* (flowing interval porosity in the volcanic unit of the SZ), *SZGWSPDM* (groundwater specific discharge multiplier; as sampled, *SZGWSPDM* is actually the logarithm of the indicated multiplier), and *SEEPUNC* (pointer variable used to determine local seepage rates). Similarly, the sensitivity analysis with PRCCs for [0, 20,000 yr] in Figure K5.7.1-1c[a] identifies the following variables as influencing the uncertainty in *EXPDOSE*: *PROBDSEF*, *SZFIPOVO*, *SZGWSPDM*, *SEEPUNC*, *INFIL*, and *THERMCON* (host rock thermal conductivity level). For both time periods, *PROBDSEF* is the dominant contributor to the uncertainty in *EXPDOSE*, with the other variables making much smaller contributions to the uncertainty in *EXPDOSE*. The PRCC plots are constrained to contain a maximum of 6 variables. As a result, the slight differences in the variables shown in Figures K5.7.1-1c[a] and K5.7.1-3c[a] result from slight variations in the importance of individual variables over the time intervals under consideration.

More detailed sensitivity analyses for the time interval [0, 1,000,000 yr] are provided by the regressions in Figure K5.7.1-4a[a]. Similar to the regressions for [0, 20,000 yr] in Figure K5.7.1-2a[a], the dominant variable is *PROBDSEF*. Specifically, the dominant effect of *PROBDSEF* on the uncertainty in *EXPDOSE* is indicated by $R^2$ values of 0.47, 0.55 and 0.52 for the regressions containing only *PROBDSEF* at 50,000, 200,000 and 500,000 yr. These values are lower than the corresponding $R^2$ values of 0.70, 0.71 and 0.63 obtained in the analyses in Figure K5.7.1-2a[a] at 3000, 5000 and 10,000 yr, which suggests that more variables are having small effects on the uncertainty in *EXPDOSE* at later times than is the case for the first 20,000 yr. This is borne out by the large number of variables indicated as having small effects on *EXPDOSE* in the regression analyses in Figure K5.7.1-4a[a]. After *PROBDSEF*, the next most important variable in the three regressions is either *SZGWSPDM* or *INFIL*, with *EXPDOSE* tending to increase as *INFIL* increases as a result of increased water flow through the EBS and UZ and also to increase as *SZGWSPDM* increases as a result of increased water flow in the SZ. Together, the first two selected variables result in regressions with $R^2$ values of 0.55, 0.63 and 0.63 at 50,000, 200,000 and 500,000 yr.

After the first two variables, the three regressions select a subset of *INFIL*, *SEEPPRM*, *SZGWSPDM*, *EP1LOWPU* (scale factor used to incorporate uncertainty into plutonium solubility under low ionic strength conditions; as sampled, *EP1LOWPU* is actually the logarithm of the indicated scale factor), and *SEEPUNC* as the next three variables to add to the regression models (Figure K5.7.1-4a[a]). Addition of these three variables brings the $R^2$ values up to 0.73, 0.77 and 0.75 at 50,000, 200,000 and 500,000 yr. As previously discussed, *INFIL* has positive effect on *EXPDOSE* as a result of increasing water flow through the EBS and UZ; *SEEPPRM* has a negative effect on *EXPDOSE* as a result of increasing water flow around the EBS and thus reducing water flow through the EBS; *EP1LOWPU* has a positive effect on *EXPDOSE* as a result of increasing the solubility of plutonium in the EBS; *SZGWSPDM* has a positive effect on *EXPDOSE* as a result of speeding up flow in the SZ; and *SEEPUNC* has a positive effect on *EXPDOSE* as a result of increasing water flow through the EBS.

After the first five variables, the regressions at 50,000, 200,000 and 500,000 yr add 8, 11 and 11 additional variables, respectively, and produce models with $R^2$ values of 0.82, 0.86 and 0.87 (Figure K5.7.1-4a[a]). Thus, as noted earlier, a large number of variables are having small effects on the uncertainty in *EXPDOSE* at later times.

The dominant effect of *PROBDSEF* on the uncertainty in *EXPDOSE* can also been seen in the scatterplot in Figure K5.7.1-4b[a]. In contrast, the much smaller effects of *INFIL* and *SEEPPRM* on the uncertainty in *EXPDOSE* can been in the scatterplots in Figure K5.7.1-4c,d[a].

### K5.7.2[a] Early Failure Scenario Classes: Expected Dose to Reasonably Maximally Exposed Individual (RMEI) from Early Waste Package (WP) Failure

**Expected Dose to RMEI over [0, 20,000 yr]: *EXPDOSE*.** The uncertainty and sensitivity analyses for expected dose to the RMEI (*EXPDOSE*, mrem/yr) over the time interval [0, 20,000 yr] resulting from early WP failure are summarized in Figures K5.7.2-1[a] and K5.7.2-2[a]. Specifically, Figures K5.7.2-1[a] and K5.7.2-2[a] have the same structure as Figures K5.7.2-1 and K5.7.2-2 but present results calculated with version 5.005 of the TSPA-LA Model rather than with version 5.000 used in the calculation of the results in Figures K5.7.2-1 and K5.7.2-2. A comparison of the results in Figures K5.7.2-1a[a] and K5.7.2-1a obtained with the two versions of the TSPA-LA Model is provided in Figures 7.3.1-24[a] and 7.3.1-26[a]; discussion of the differences in the results is provided in Section 7.3.1.5.3[a]. As examination of Figures 7.3.1-24[a] and 7.3.1-26[a] shows, there is little difference in the values for *EXPDOSE* obtained with the two versions of the TSPA-LA Model. Consistent with this comparison, there is also little difference in the sensitivity analysis results presented in Figures K5.7.2-1c and K5.7.2-2 for version 5.000 and the corresponding results presented in Figures K5.7.2-1c[a] and K5.7.2-2[a] for version 5.005. As a result, the discussion presented in Section K5.7.2 for *EXPDOSE* over the time interval [0, 20,000 yr] resulting from early WP failure for results obtained with version 5.000 of the TSPA-LA Model also applies to the results obtained with version 5.005 of the TSPA-LA Model. For this reason, no additional discussion is provided.

For reader convenience, the following discussion of the expected dose results in Figures K5.7.2-1[a] and K5.7.2-2[a] is provided. This discussion updates the corresponding material in Section K5.7.2 from the parent report.

The uncertainty and sensitivity analyses for expected dose to the RMEI (*EXPDOSE*, mrem/yr) over the time interval [0, 20,000 yr] resulting from early WP failure are summarized in Figures K5.7.2-1[a] and K5.7.2-2[a]. There are sharp peaks in *EXPDOSE* between 1000 and 2000 yr resulting from the release of $^{99}$Tc from the failure of CDSP WPs (Figure K5.7.2-1a,b[a]). At the time of these peaks, maximum values for *EXPDOSE* are in the vicinity of 0.1 mrem/yr, although the values for most sample elements are considerably smaller. After these initial early peaks, *EXPDOSE* has values in a range from approximately $10^{-5}$ to $10^{-2}$ mrem/yr until a time of about 10,000 yr.

Between approximately 9000 and 14,000 yr, there are sharp jumps in the values for *EXPDOSE* (Figure K5.7.2-1a,b[a]). These jumps result from the arrival of radionuclide releases at the location of the RMEI that result from the failure of CSNF WPs. The CSNF WPs are hotter than the CDSP WPs, with the result that releases from CSNF WPs are delayed until both the WP

temperature falls below 100ºC and the relative humidity interior to these packages reaches 95 percent, at which time diffusive transport begins. The jumps in *EXPDOSE* correspond to the arrival of $^{99}$Tc at the location of the RMEI (Figure 8.2-6a[a]). After these jumps, the values for *EXPDOSE* again decrease as the pulse of $^{99}$Tc passes.

This bimodal behavior of *EXPDOSE* with different peaks for the two waste types does not occur for early DS failure (compare Figures K5.7.1-1a,b[a] and K5.7.2-1a,b[a]). Early DS failure is assumed to result in WP failure only if the failed DS is experiencing seepage; otherwise, there is no WP failure and hence no radionuclide release. Because all failed WPs are in seepage environments, water flows into every failed WP as soon as WP temperature falls below 100ºC and advective transport occurs immediately, with the result that there is little temporal variability in the start of radionuclide releases from the EBS for different WP types.

The PRCCs in Figure K5.7.2-1c[a] indicate that the uncertainty in *EXPDOSE* is dominated by *PROBWPEF* (probability that a randomly selected WP will experience an early failure), with the value for *EXPDOSE* increasing as *PROBWPEF* increases. This effect results because increasing *PROBWPEF* increases the expected number of WPs that experience early failure and hence increases *EXPDOSE*. The PRCCs for *PROBWPEF* decrease in value over the period from approximately 9000 to 14,000 yr because of the noise introduced into the analysis as a result of the pulse releases arriving from the failed CSNF WPs.

In addition to *PROBWPEF*, smaller effects are indicated for *SZFIPOVO* (flowing interval porosity in the volcanic unit of the SZ), *THERMCON* (host rock thermal conductivity level), *INFIL* (infiltration level), *SZGWSPDM* (groundwater specific discharge multiplier; as sampled, *SZGWSPDM* is actually the logarithm of the indicated multiplier), and *DSNFMASS* (scale factor used to characterize uncertainty in the amount of DSNF contained in CDSP WPs) (Figure K5.7.2-1c[a]). The effects of *SZFIPOVO*, *INFIL*, and *SZGWSPDM* are the same as previously discussed in conjunction with Figure K5.7.1-1c[a]. The effect of *THERMCON* is similar, although more pronounced. Increasing *THERMCON* leads to lower drift temperatures and earlier arrival of seepage waters, and thus to earlier beginning of diffusive transport. This effect is evident in the positive correlation between *THERMCON* and *EXPDOSE* between 0 yr and 1500 yr. However, between 2500 yr and 9500 yr, the correlation becomes negative. This change in correlation results from the effect of temperature on waste form degradation. Increasing temperature increases the dissolution rate of the HLW in CDSP WPs (BSC 2004 [DIRS 169988], Section 6.5.2.1). Consequently, as *THERMCON* increases, temperatures decrease and HLW degradation slows, resulting in less radionuclides available for mobilization and transport, and in turn reducing *EXPDOSE*. This pattern repeats for the CSNF waste, which starts diffusive transport at about 9500 yr. The positive effect associated with *DSNFMASS* results from increasing the amount of $^{99}$Tc in CDSP WPs and hence the dose from $^{99}$Tc that results from the failure of these WPs.

More detailed sensitivity analyses for *EXPDOSE* are provided by the regression analyses in Figure K5.7.2-2a[a]. The dominant effect of *PROBWPEF* on the uncertainty in *EXPDOSE* is indicated by $R^2$ values of 0.62, 0.77 and 0.47 for the regressions containing only *PROBWPEF* at 3000, 5000 and 10,000 yr.

As for the PRCCs for *PROBWPEF* in Figure K5.7.2-1c[a], the $R^2$ value for the regression at 10,000 years decreases in value as a result of the noise introduced into the analysis by the pulse releases arriving from the failed CSNF WPs over the period from approximately 9000 to 14,000 yr. Because of this noise, the final regression model at 10,000 has an $R^2$ value of 0.71; in contrast, the analyses at 3000 and 5000 yr have final $R^2$ values of 0.80 and 0.89. However, a clearer view of what is driving the uncertainty in *EXPDOSE* at 10,000 yr is provided by the scatterplots in Figure K5.7.2-2b,c,d[a]. Specifically, the uncertainty in *EXPDOSE* is still clearly dominated by *PROBWPEF* (Figure K5.7.2-2b[a]), with smaller contributions to this uncertainty from *INFIL* (Figure K5.7.2-2c[a]) and *THERMCON* (Figure K5.7.2-2d[a]). The scatterplot for *PROBWPEF* (Figure K5.7-2b[a]) shows an interesting pattern in that it contains two separate populations of points that each increase monotonically with *PROBWPEF*. The upper population of points consists of realizations in which the CSNF WPs in one or more percolation bins have begun diffusive transport (relative humidity interior to the WP exceeds 95 percent) by 10,000 yr. Because infiltration rates and temperatures vary between percolation bins, the time at which diffusive transport begins also varies, with most CSNF WPs beginning diffusive transport between 9000 yr and 14,000 yr, whereas CDSP WPs begin diffusive transport between 500 yr and 3000 yr. The differences are also apparent in Figure K5.7.2-1a[a] as two jumps in expected dose corresponding to the occurrence of dose from each of the two WP types.

Figure K5.7.2-2c[a] indicates that the expected dose at 10,000 yr decreases as *INFIL* increases. As *INFIL* increases, percolation rates tend to increase in most percolation bins, leading to earlier arrival of seepage into a drift. Because increased infiltration also leads to lower temperatures, and at lower drift temperatures, the difference in relative humidity on WPs of different temperatures becomes more pronounced, increasing infiltration results in the counter-intuitive effect that the warmer WPs (CSNF WPs) have lower relative humidity at higher values of infiltration. These lower values of relative humidity are less likely to permit diffusive transport, which in turn yields a negative relationship between *INFIL* and expected dose at 10,000 years. The relationship between infiltration, temperature and relative humidity is described and documented in Multiscale Thermohydrologic Model (SNL 2007 [DIRS 181383]).

Figure K5.7.2-2c[a] indicates that expected dose at 10,000 yr slightly increases as *THERMCON* increases. This correlation is valid at 10,000 yr because at this time CSNF WPs are just beginning diffusive transport, so the correlation indicates the positive relationship between *THERMCON* and *EXPDOSE* described above. If the correlation were to be performed at later times, after transport has begun, the relationship between *THERMCON* and *EXPDOSE* would be reversed, because at these times *THERMCON* is affecting waste degradation rates, as described above.

In contrast, more informative results are given by the regression analyses at 3000 and 5000 years without the added need to examine scatterplots (Figure K5.7.2-2a[a]). Specifically, both indicated regressions select the following four variables after *PROBWPEF*: *MICTC99* (dose conversion factor for $^{99}$Tc for modern interglacial climate, (rem/yr)/(pCi/L)), *MICC14* (dose conversion factor for $^{14}$C for modern interglacial climate, (rem/yr)/(pCi/L)), *DSNFMASS*, and *UZFAG8* (fracture aperture for Group 8 rock units in UZ). Increasing *MICTC99* and *MICC14* has a positive effect on *EXPDOSE* that results from increasing the received dose for a given exposure level; increasing *DSNFMASS* has a positive effect on *EXPDOSE* that results from increasing the amount of radionuclides in CDSP WPs and hence the dose that results from the

failure of these WPs; and increasing *UZFAG8* has a negative effect on *EXPDOSE* that results from decreasing the proportion of radionuclides moving through fractures in the UZ. Specifically, increasing *UZFAG8* increases the proportion of the interface area between the EBS and the UZ that consists of fractures, which increases the mass of radionuclides that diffuse into fractures in the UZ, where radionuclide movement is relatively rapid, and decreases the mass of radionuclides that diffuse into the surrounding rock matrix, where radionuclide movement is slower. Collectively, the inclusion of *MICTC99*, *MICC14*, *DSNFMASS* and *UZFAG8* increases the $R^2$ values for the two regressions to 0.74 and 0.86. After *MICTC99*, *MICC14*, *DSNFMASS* and *UZFAG8*, the regressions add an additional six and eight variables, respectively, that have small effects and result in final models that have $R^2$ values of 0.80 and 0.89. The regression models at 3000 yr tend to have smaller $R^2$ values than the regression models at 5000 yr because of the noise introduced by the arrival of the $^{99}$Tc releases (i.e., compare the smoothness of the time-dependent releases at 3000 and 5000 yr in Figure K5.7.2-2a,b[a]).

**Expected Dose to RMEI over [0, 1,000,000 yr]: *EXPDOSE*.** The uncertainty and sensitivity analyses for expected dose to the RMEI (*EXPDOSE*, mrem/yr) over the time interval [0, 1,000,000 yr] resulting from early WP failure are summarized in Figures K5.7.2-3[a] and K5.7.2-4[a]. Specifically, Figures K5.7.2-3[a] and K5.7.2-4[a] have the same structure as Figures K5.7.2-3 and K5.7.2-4 but present results calculated with version 5.005 of the TSPA-LA Model rather than with version 5.000 used in the calculation of the results in Figures K5.7.2-3 and K5.7.2-4. A comparison of the results in Figures K5.7.2-3a[a] and K5.7.2-3[a] obtained with the two versions of the TSPA-LA Model is provided in Figures 7.3.1-25[a] and 7.3.1-27[a]; discussion of the differences in the results is provided in Section 7.3.1.5.3[a]. As examination of Figures 7.3.1-25[a] and 7.3.1-27[a] shows, there is little difference in the values for *EXPDOSE* obtained with the two versions of the TSPA-LA Model. Consistent with this comparison, there is also little difference in the sensitivity analysis results presented in Figures K5.7.2-3c and K5.7.2-4 for version 5.000 and the corresponding results presented in Figures K5.7.2-3c[a] and K5.7.2-4[a] for version 5.005. As a result, the discussion presented in Section K5.7.2 for *EXPDOSE* over the time interval [0, 1,000,000 yr] resulting from early WP failure for results obtained with version 5.000 of the TSPA-LA Model also applies to the results obtained with version 5.005 of the TSPA-LA Model. For this reason, no additional discussion is provided.

For reader convenience, the following discussion of the expected dose results in Figures K5.7.2-3[a] and K5.7.2-4[a] is provided. This discussion updates the corresponding material in Section K5.7.2 from the parent report.

The uncertainty and sensitivity analyses for expected dose to the RMEI (*EXPDOSE*, mrem/yr) over the time interval [0, 1,000,000 yr] resulting from early WP failure are summarized in Figures K5.7.2-3[a] and K5.7.2-4[a].

Except for a few sample elements, the values for *EXPDOSE* fall between $10^{-6}$ and 0.1 mrem/yr for the 0 to 1,000,000 yr time interval (Figure K5.7.2-3a[a]). For most sample elements, the values for *EXPDOSE* monotonically decrease until about 300,000 yr, at which time they show a sharp increase in value as the result of the failure of the DSs from general corrosion (Figure 8.1-4[a]). This failure allows seeping water to directly contact the failed WPs, and as a consequence, produces larger radionuclide releases from the failed WPs.

The single most important variable with respect to the uncertainty in *EXPDOSE* is *PROBWPEF* (probability that a randomly selected WP will experience an early failure), with the value for *EXPDOSE* increasing as *PROBWPEF* increases. This effect results because increasing *PROBWPEF* increases the expected number of WPs that experience early failure and hence increases *EXPDOSE* (Figures K5.7.2-3c[a] and K5.7.2-4a[a]). The positive effect of *PROBWPEF* can be seen in the scatterplot in Figure K5.7.2-4b[a].

Prior to 300,000 yr, *ISCSNS* (pointer variable used to determine ionic strength in CSNF cell under vapor influx conditions) and *SZGWSPDM* (groundwater specific discharge multiplier*;* as sampled, *SZGWSPDM* is actually the logarithm of the indicated multiplier) also have significant positive effects on the uncertainty in *EXPDOSE* (Figures K5.7.2-3c[a] and K5.7.2-4a[a]). These effects result because increasing *ISCSNS* increases plutonium solubility, and increasing *SZGWSPDM* increases water flow in the SZ. After 300,000 yr, *INFIL* (infiltration level) is indicated as having a positive effect on *EXPDOSE* (Figures K5.7.2-3c[a] and K5.7.2-4a[a]). This effect results because increasing *INFIL* increases water flow in the EBS and UZ. After *PROBWPEF*, *ISCSNS*, *SZGWSPDM* and *INFIL*, the analyses identify a number of additional variables that have small effects on *EXPDOSE*.

**K5.7.3[a] Early Failure Scenario Classes: Expected Dose to Reasonably Maximally Exposed Individual (RMEI) from Both Early Drip Shield (DS) Failure and Early Waste Package (WP) Failure**

No change.

**K5.7.4[a] Early Failure Scenario Classes: Expected Dose to Reasonably Maximally Exposed Individual (RMEI) from Early Drip Shield (DS) Failure, Early Waste Package (WP) Failure, and Nominal Processes**

No change.

## K6[a] IGNEOUS SCENARIO CLASSES

No change.

**K6.1[a] Igneous Scenario Classes: Summary**

No change.

**K6.2[a] Igneous Intrusive Scenario Classes: Engineered Barrier System (EBS) Conditions over the Time Interval [0, 1,000,000 yr] for an Event at 250 years**

No change.

**K6.3[a] Igneous Intrusive Scenario Classes: Release from Engineered Barrier System (EBS)**

No change.

### K6.3.1[a] Igneous Intrusive Scenario Classes: Release from Engineered Barrier System (EBS) over the Time Interval [0, 20,000 yr] for an Event at 10 years

No change.

### K6.3.2[a] Igneous Intrusive Scenario Classes: Release from Engineered Barrier System (EBS) over the Time Interval [0, 1,000,000 yr] for an Event at 250 years

Results from TSPA-LA Model v5.000 determined that $^{226}$Ra was the dominant contributor to the expected (mean) dose to the RMEI for the Igneous Intrusive Scenario Class (Figure 8.2-8). However, analysis determined that the contribution to expected (mean) dose from $^{226}$Ra was due to an unconstrained distribution describing the uncertainty in longitudinal dispersivity (LDISP in Table K3-1), (see Appendix P, Section P15). For TSPA-LA Model v5.005, the uncertainty distribution for longitudinal dispersivity was constrained so that values sampled from this distribution would be physically meaningful (Section 6.3.10.2[a]). Because of this change, and because of the importance of $^{226}$Ra to expected (mean) dose, additional sensitivity analyses are presented for the transport of radionuclides in the decay chain for $^{226}$Ra, namely $^{234}$U, $^{230}$Th and $^{226}$Ra, for the Igneous Intrusive Scenario Class.

**Movement of Dissolved $^{234}$U: *ESU234* and *ESU234C*.** The uncertainty and sensitivity analyses for the time-dependent release rates (*ESU234*, g/yr) and cumulative releases (*ESU234C*, g) over the time interval [0, 1,000,000 yr] for the movement of dissolved $^{234}$U from the EBS to the UZ resulting from an igneous intrusive event at 250 years that destroys all WPs in the repository are summarized in Figures K6.3.2-5[a] and K6.3.2-6[a].

The dominant contributors to the uncertainty in *ESU234* and *ESU234C* are *EP1LOWOU* (scale factor used to incorporate uncertainty into uranium solubility under low ionic strength conditions after an igneous intrusive event; as sampled, *EP1LOWOU* is actually the logarithm of the indicated scale factor), *GOESITED* (density of sorption sites on goethite, sites/nm$^2$), and *INFIL* (infiltration level) (Figures K6.3.2-5e,f[a] and K6.3.2-6a,b[a]). The variables *EP1LOWOU* and *INFIL* have positive effects on *ESU234* and *ESU234C* because increasing *EP1LOWOU* increases uranium solubility and increasing *INFIL* increases water flow through the EBS. In contrast, increasing *GOESITED* has a negative effect on *ESU234* and *ESU234C* as a result of increasing the sorption of uranium onto corrosion products**.** All the regression models select *EP1LOWOU* and *INFIL* as the first two variables and have $R^2$ values between 0.48 and 0.64 with the inclusion of these two variables (Figure K6.3.2-6a,b[a]).

In addition to *EP1LOWOU, GOESITED* and *INFIL*, generally smaller but significant effects are also indicated for *PHCSS* (pointer variable used to determine pH in CSNF cell 1 under liquid influx conditions), *CORRATSS* (corrosion rate for stainless steel, μm/yr), and *HFOSA* (surface area for hydrous ferrous oxide, m$^2$/g) (Figures K6.3.2-5e,f[a] and K6.3.2-6a,b[a]). The positive effect associated with *PHCSS* results because increasing *PHCSS* increases uranium solubility**,** and the negative effects associated with *CORRATSS* and *HFOSA* result because increasing these variables increases uranium sorption on corrosion products. The effect on *ESU234* associated with *CORRATSS* varies with time, because while stainless steel is corroding, corrosion products are increasing and the sorption of uranium on the corrosion products reduces the release rate of uranium. However, once corrosion of stainless steel has ceased (roughly at 200,000 yr),

additional corrosion materials are not subsequently produced, so the release rate of uranium is controlled by factors other than the rate at which the corrosion products are generated.

The effects of *EP1LOWOU, GOESITED*, *INFIL* and *PHCSS* on *ESU234* and *ESU234C* can be seen in the scatterplots in Figure K6.3.2-6 c,d,e,f,g,h[a]. In particular, the dominant positive effect of *EP1LOWPU* is apparent in Figure K6.3.2-6 c,f[a].

A number of additional variables that have small effects on *ESU234* and *ESU234C* are also identified at the latter stages of the stepwise regressions in Figure K6.3.2-6a,b[a]. The final regression models in Figure K6.3.2-6a,b[a] have $R^2$ values between 0.75 and 0.81. Thus, most of the uncertainty in *ESU234* and *ESU234C* is being accounted for.

**Movement of $^{230}$Th: *ESTH230* and *ESTH230C*.** The uncertainty and sensitivity analyses for the time-dependent release rates (*ESTH230*, g/yr) and cumulative releases (*ESTH230C*, g) over the time interval [0, 1,000,000 yr] for the movement of dissolved and reversible attached $^{230}$Th from the EBS to the UZ resulting from an igneous intrusive event at 250 years that destroys all WPs in the repository are summarized in Figures K6.3.2-7[a] and K6.3.2-8[a].

The dominant contributors to the uncertainty in *ESTH230* and *ESTH230C* are *INFIL* (infiltration level), *COLGW* (concentration of groundwater colloids when colloids are stable, mg/L), *KDTHSMEC* (distribution coefficient for reversible sorption of thorium to waste form, i.e., smectite, colloids, mL/g), *PHCSS* (pointer variable used to determine pH in CSNF cell 1 under liquid influx conditions), *EP1LOWTH* (scale factor used to incorporate uncertainty into thorium solubility at an ionic strength below 1 molal; as sampled, *EP1LOWTH* is actually the logarithm of the indicated scale factor), and *UZKDTHDT* (sorption coefficient for thorium in devitrified tuff units of UZ, mL/g; also used as sorption coefficient for thorium in ballast in EBS) (Figures K6.3.2-7e,f[a] and K6.3.2-8a,b[a]). The variables *INFIL, COLGW, KDTHSMEC, PHCSS* and *EP1LOWTH* have positive effects on *ESTH230* and *ESTH230C* because (1) increasing *INFIL* increases water flow through the EBS, (2) increasing *COLGW* and *KDTHSMEC* increases the amount of thorium sorbed to colloids, and (3) increasing *PHCSS* and *EP1LOWTH* increases the solubility of thorium. In contrast, increasing *UZKDTHDT* has a negative effect on *ESTH230* and *ESTH230C* as a result of increasing the sorption of uranium onto the ballast used in the EBS.

In addition to *INFIL, COLGW, KDTHSMEC, PHCSS*, *EP1LOWTH* and *UZKDTHDT*, the stepwise regression analyses identify several additional variables that have small effects on *ESTH230* and *ESTH230C* (Figure K6.3.2-8a,b[a]). The final regression models contain from 9 to 12 variables and have $R^2$ values between 0.64 and 0.72. To some extent, the regression models are probably being challenged by the difficulty of capturing effects that derive from the decay of $^{234}$U to $^{230}$Th, as well as relationships between concentrations of radionuclides proscribed by the regression model for surface complexation and sorption onto corrosion products (SNL 2007 [DIRS 177407], Section 6.5.2.4). In particular, the positive influence of *EP1LOWOU* (scale factor used to incorporate uncertainty into uranium solubility under low ionic strength conditions after an igneous intrusive event; as sampled, *EP1LOWOU* is actually the logarithm of the indicated scale factor) on *ESTH230* and *ESTH230C* (Figure K6.3.2-8a,b[a]) results from both the decay of $^{234}$U to $^{230}$Th, as well as the negative relationship between the

concentration of dissolved uranium and the concentration of thorium sorbed to corrosion products (SNL 2007 [DIRS 177407], Table 6.5-14).

Overall, the three dominant variables are *INFIL, COLGW* and *KDTHSMEC*. The positive effects associated with these variables can be seen in the scatterplots in Figure K6.3.2-8c,d,e,f,g,h[a]).

The PRCCs for *COLGW* are somewhat larger than the PRCCs for *INFIL*. In contrast, all the stepwise regression analyses except one select *INFIL* first and then *COLGW*. This slight inconsistency possibly results because there is a rank correlation of 0.078 between *INFIL* and *COLGW* in the sample in use. In addition, both *INFIL* and *COLGW* have rank correlations with other variables that are as high as 0.18 in absolute value. It is possible that some of these correlations could also be affecting the PRCCs in Figure K6.3.2-7e,f[a]; also, the fact that *INFIL* is a discrete variable with only four levels could be affecting the analysis. However, as is evident from the scatterplots in Figure K6.3.2-8ac,d,f,g[a]), both *ESTH230* and *ESTH230C* tend to increase as *INFIL* and *COLGW* increase.

**Movement of Dissolved $^{226}$Ra: *ESRA226* and *ESRA226C*.** The uncertainty and sensitivity analyses for the time-dependent release rates (*ESRA226*, g/yr) and cumulative releases (*ESRA226C*, g) over the time interval [0, 1,000,000 yr] for the movement of dissolved $^{226}$Ra from the EBS to the UZ resulting from an igneous intrusive event at 250 years that destroys all WPs in the repository are summarized in Figures K6.3.2-9[a] and K6.3.2-10[a].

The dominant contributors to the uncertainty in *ESRA226* and *ESRA226C* are *UZKDCSDT* (sorption coefficient for cesium and radium in devitrified tuff units of UZ, mL/g; also used as sorption coefficient for cesium and radium in ballast in EBS), *INFIL* (infiltration level), and *COLGW* (concentration of groundwater colloids when colloids are stable, mg/L) (Figures K6.3.2-9e,f[a] and K6.3.2-10a,b[a]). The negative effects associated with *UZKDCSDT* and *COLGW* result because (i) increasing *UZKDCSDT* increases the sorption of $^{226}$Ra to ballast material in the EBS and thus increases the loss of $^{226}$Ra in the EBS as the result of decay and (ii) increasing *COLGW* increases the removal of $^{230}$Th attached to colloids from the EBS and thus reduces the production of $^{226}$Ra from the decay of $^{230}$Th. The positive effect associated with *INFIL* results from increasing water flow through the EBS.

Similarly to *COLGW*, the negative effects on *ESRA226* and *ESRA226C* associated with *KDTHSMEC* (distribution coefficient for reversible sorption of thorium to waste form, i.e., smectite, colloids, mL/g), *PHCSS* (pointer variable used to determine pH in CSNF cell 1 under liquid influx conditions), and *EP1LOWOU* (scale factor used to incorporate uncertainty into uranium solubility under low ionic strength conditions after an igneous intrusive event; as sampled, *EP1LOWOU* is actually the logarithm of the indicated scale factor) result from increasing the removal of the parent and grandparent of $^{226}$Ra from the EBS. Specifically, increasing *KDTHSMEC* increases the removal of $^{230}$Th attached to waste form colloids; increasing *PHCSS* increases the solubility of uranium, thorium and radium; and increasing *EP1LOWOU* increases the solubility of uranium. In contrast, *CSNFMASS* (scale factor used to characterize uncertainty in amount of CSNF in CSNF WPs), *DSNFMASS* (scale factor used to characterize uncertainty in amount of DSNF in DSNF WPs), and *GOESITED* (density of sorption sites on goethite, sites/nm$^2$) have positive effects on *ESRA226* and *ESRA226C* because

(i) increasing *CSNFMASS* and *DSNFMASS* increases the amount of waste in the repository and (ii) increasing *GOESITED* increases the amount of $^{234}$U and $^{230}$Th retained in the EBS.

Overall, the three dominant variables are *UZKDCSDT*, *INFIL* and *COLGW*. The effects associated with these variables can be seen in the scatterplots in Figure K6.3.2-10c,d,e,f,g,h[a]. Of the three, *UZKDCSDT* is clearly the most influential variable.

## K6.4[a] Igneous Intrusive Scenario Classes: Release from Unsaturated Zone (UZ)

No change.

### K6.4.1[a] Igneous Intrusive Scenario Classes: Release from Unsaturated Zone (UZ) over the Time Interval [0, 20,000 yr] for an Event at 10 years

No change.

### K6.4.2[a] Igneous Intrusive Scenario Classes: Release from Unsaturated Zone (UZ) over the Time Interval [0, 1,000,000 yr] for an Event at 250 years

**Movement of Dissolved $^{234}$U: *UZU234* and *UZU234C*.** The uncertainty and sensitivity analyses for the time-dependent release rates (*UZU234*, g/yr) and cumulative releases (*UZU234C*, g) over the time interval [0, 1,000,000 yr] for the movement of dissolved $^{234}$U from the UZ to the SZ resulting from an igneous intrusive event at 250 years that destroys all WPs in the repository are summarized in Figures K6.4.2-1[a] and K6.4.2-2[a]. Further, a comparison of the movement of $^{234}$U into and out of the UZ is presented in Figure K6.4.2-3[a]. As shown by the results in Figure K6.4.2-3[a], the movement of $^{234}$U into the UZ (i.e., *ESU234C*) is effectively the same as the movement of $^{234}$U out of the UZ (i.e., *UZU234C*) for the time scales under consideration. Because of this behavior, the uncertainty and sensitivity analysis results in Figures K6.4.2-1[a] and K6.4.2-2[a] for the release of $^{234}$U from the UZ to the SZ are essentially the same as the results in Figures K6.3.2-5[a] and K6.3.2-6[a] for the release of $^{234}$U from the EBS to the UZ. As a result, the discussion of the results in Figures K6.3.2-5[a] and K6.3.2-6[a] also applies to the results in Figures K6.4.2-1[a] and K6.4.2-2[a].

**Movement of Dissolved $^{230}$Th: *UZTH230* and *UZTH230C*.** The uncertainty and sensitivity analyses for the time-dependent release rates (*UZTH230*, g/yr) and cumulative releases (*UZTH230C*, g) over the time interval [0, 1,000,000 yr] for the movement of dissolved $^{230}$Th from the UZ to the SZ resulting from an igneous intrusive event at 250 years that destroys all WPs in the repository are summarized in Figures K6.4.2-4[a] and K6.4.2-5[a]. Further, a comparison of the movement of $^{230}$Th into and out of the UZ is presented in Figure K6.4.2-6[a]. As shown by the results in Figure K6.4.2-6[a], the movement of $^{230}$Th into the UZ (i.e., *ESU234C*) is related to the movement of $^{230}$Th out of the UZ (i.e., *UZU234C*) by a constant fractional shift for the time scales under consideration; specifically, the ratio *UZTH230C* to *ESTH230C* is approximately 0.5 for the results in Figure K6.4.2-6[a]. The reduction occurs primarily because of the spatial variability in UZ transport, specifically, $^{230}$Th released into the UZ under the northern part of the repository transits through the UZ relatively rapidly, whereas $^{230}$Th released into the UZ under the southern part of the repository is very unlikely to ever leave the UZ (SNL 2008 [DIRS 184748], Figure 6.6.2-7[b]). Because the ratio of *UZTH230C* to

*ESTH230C* is essentially constant, the uncertainty and sensitivity analysis results in Figures K6.4.2-4[a] and K6.4.2-5[a] for the release of $^{230}$Th from the UZ to the SZ are essentially the same as the results in Figures K6.3.2-7[a] and K6.3.2-8[a] for the release of $^{230}$Th from the EBS to the UZ. This similarity is particularly evident when the stepwise regression analyses in Figures K6.3.2-8a,b[a] and K6.4.2-5[a] are compared. As a result, the discussion of the results in Figures K6.3.2-7[a] and K6.3.2-8[a] also applies to the results in Figures K6.4.2-4[a] and K6.4.2-5[a].

**Movement of Dissolved $^{226}$Ra: *UZRA226* and *UZRA226C*.** The uncertainty and sensitivity analyses for the time-dependent release rates (*UZRA226*, g/yr) and cumulative releases (*UZRA226C*, g) over the time interval [0, 1,000,000 yr] for the movement of dissolved $^{226}$Ra from the UZ to the SZ resulting from an igneous intrusive event at 250 years that destroys all WPs in the repository are summarized in Figures K6.4.2-7[a] and K6.4.2-8[a]. Further, a comparison of the movement of $^{226}$Ra into and out of the UZ is presented in Figure K6.4.2-9[a]. As shown by the results in Figure K6.4.2-9[a], the UZ has noticeable effect on the movement of $^{226}$Ra from the EBS to the SZ; specifically, the releases of $^{226}$Ra out of the UZ are smaller than the releases into the UZ for most sample elements.

The dominant variables affecting the uncertainty in *UZRA226* and *UZRA226C* are *UZKDCSDT* (sorption coefficient for cesium and radium in devitrified tuff units of UZ, mL/g; also used as sorption coefficient for cesium and radium in ballast in EBS), *INFIL* (infiltration level), *UZFAG8* (fracture aperture for Group 8 rock unit in UZ, m), and *UZTORRG3* (tortuosity for Group 3 rock unit in UZ) (Figures K6.4.2-7e,f[a] and K6.4.2-8a,b[a]). The negative effects associated with *UZKDCSDT* and *UZTORRG3* result because (1) increasing *UZKDCSDT* increases the retardation of $^{226}$Ra in the EBS and the UZ and (2) increasing *UZTORRG3* increases the complexity of the transport path in the UZ. The positive effects associated with *INFIL* and *UZFAG8* result because (1) increasing *INFIL* increases water flow in both the EBS and UZ and (2) increasing *UZFAG8* increases the amount of $^{226}$Ra transported by flow in fractures.

After *UZKDCSDT*, *INFIL*, *UZFAG8* and *UZTORRG3*, the regression analyses identify several additional variables that have small effects on *UZRA226* and *UZRA226C* (Figure K6.4.2-8a,b[a]). Specifically, positive effects are identified for *CSNFMASS* (scale factor used to characterize uncertainty in amount of CSNF in CSNF WPs), *COLGW* (concentration of groundwater colloids when colloids are stable, mg/L), *KDTHSMEC* (distribution coefficient for reversible sorption of thorium to waste form, i.e., smectite, colloids, mL/g), and *UZKDTHDT* (sorption coefficient for thorium in devitrified tuff units of UZ, mL/g; also used as sorption coefficient for thorium in ballast in EBS). These effects result because (1) increasing *CSNFMASS* increases the amount of waste in the repository, (2) increasing *COLGW* and *KDTHSMEC* increases the amount of $^{230}$Th that enters the UZ and thus increases the amount of $^{226}$Ra that can be produced by decay in the UZ, and (3) increasing *UZKDTHDT* increases the retention of $^{230}$Th in the UZ and thus increases the amount of $^{226}$Ra that can be produced by decay in the UZ. A negative effect is indicated for *EP1LOWOU* (scale factor used to incorporate uncertainty into uranium solubility under low ionic strength conditions after an igneous intrusive event; as sampled, *EP1LOWOU* is actually the logarithm of the indicated scale factor) and results from the role of *EP1LOWOU* in mobilizing $^{234}$U in the EBS and thus reducing the

production of $^{226}$Ra by the decay of $^{230}$Th in the EBS and UZ. Very small effects are indicated for several additional variables.

Scatterplots showing the negative effect of *UZKDCSDT* and the positive effects of *INFIL* and *UZFAG8* are presented in Figure K6.4.2-8c,d,e,f,g,h[a].

### K6.5[a] Igneous Intrusive Scenario Classes: Release from Saturated Zone (SZ)

No change.

### K6.5.1[a] Igneous Intrusive Scenario Classes: Release from Saturated Zone (SZ) over the Time Interval [0, 20,000 yr] for an Event at 10 years

No change.

### K6.5.2[a] Igneous Intrusive Scenario Classes: Release from Saturated Zone (SZ) over the Time Interval [0, 1,000,000 yr] for an Event at 250 years

**Movement of Dissolved $^{234}$U: *SZU234* and *SZU234C*.** The uncertainty and sensitivity analyses for the time-dependent release rates (*SZU234*, g/yr) and cumulative releases (*SZU234C*, g) over the time interval [0, 1,000,000 yr] for the movement of dissolved $^{234}$U across a subsurface plane at the location of the RMEI resulting from an igneous intrusive event at 250 years that destroys all WPs in the repository are summarized in Figures K6.5.2-5[a] and K6.5.2-6[a]. Further, a comparison of the movement of $^{234}$U into and out of the SZ is presented in Figure K6.5.2-7[a]. As shown by the results in Figure K6.5.2-7[a], the SZ has a noticeable effect on the movement of $^{234}$U in the SZ over the 50,000-yr time period (Figure K6.5.2-7a[a]). However, with increasing time, much of the $^{234}$U released into the SZ exits the SZ at the location of the RMEI (Figure K6.5.2-7b,c,d[a]). Also, decay of $^{238}$U produces $^{234}$U within the SZ as can be observed in Figure K6.5.2-7d[a]. Although the half-life of $^{238}$U is very long ($4.47 \times 10^9$ yr), the mass of $^{238}$U in the inventory is thousands of times greater than the mass of $^{234}$U (SNL 2007 [DIRS 180472], Table 7-2[a]), thus decay of $^{238}$U over 600,000 yr can produce enough $^{234}$U that the additional mass of $^{234}$U can be observed in Figure K6.5.2-7d[a].

The dominant variables affecting *SZU234* and *SZU234C* are *EP1LOWOU* (scale factor used to incorporate uncertainty into uranium solubility under low ionic strength conditions after an igneous intrusive event; as sampled, *EP1LOWOU* is actually the logarithm of the indicated scale factor), *INFIL* (infiltration level), *GOESITED* (density of sorption sites on goethite, sites/nm$^2$), *PHCSS* (pointer variable used to determine pH in CSNF cell 1 under liquid influx conditions), and *SZGWSPDM* (groundwater specific discharge multiplier*;* as sampled, *SZGWSPDM* is actually the logarithm of the indicated multiplier) (Figures K6.5.2-5e,f[a] and K6.5.2-6a,b[a]). The positive effects associated with *EP1LOWOU*, *INFIL* and *PHCSS* and the negative effect associated with *GOESITED* result from the previously discussed effects of these variables on the release of $^{234}$U from the EBS. The positive effect associated with *SZGWSPDM* results from increasing water flow in the SZ. Smaller effects are indicated for a number of additional variables.

The dominant effect of *EP1LOWOU* and the lesser effects of *INFIL* and *GOESITED* can be seen in the scatterplots in Figure K6.5.2-6c,d,e,f,g,h[a].

**Movement of Dissolved $^{230}$Th: *SZTH230* and *SZTH230C*.** The uncertainty and sensitivity analyses for the time-dependent release rates (*SZTH230*, g/yr) and cumulative releases (*SZTH230C*, g) over the time interval [0, 1,000,000 yr] for the movement of dissolved $^{230}$Th across a subsurface plane at the location of the RMEI resulting from an igneous intrusive event at 250 years that destroys all WPs in the repository are summarized in Figures K6.5.2-8[a] and K6.5.2-9[a]. Further, a comparison of the movement of $^{234}$U into and out of the SZ is presented in Figure K6.5.2-10[a]. As shown by the results in Figure K6.5.2-10[a], the SZ has a noticeable effect on the movement of $^{230}$Th from the UZ to the location of the RMEI; specifically, the releases of $^{230}$Th out of the SZ at the location of the RMEI are much smaller than the releases into the SZ for most sample elements.

The dominant variables affecting *SZTH230* and *SZTH230C* are *SZCONCOL* (concentration of colloids in ground water, g/mL; as sampled, *SZCONCOL* is actually the logarithm of the indicated concentration), *EP1LOWOU* (scale factor used to incorporate uncertainty into uranium solubility under low ionic strength conditions after an igneous intrusive event; as sampled, *EP1LOWOU* is actually the logarithm of the indicated scale factor), *SZKDAMCO* (sorption coefficient for reversible sorption of americium, thorium and protactinium onto ground water colloids, mL/g), *INFIL* (infiltration level), *SZGWSPDM* (groundwater specific discharge multiplier*;* as sampled, *SZGWSPDM* is actually the logarithm of the indicated multiplier), and *GOESITED* (density of sorption sites on goethite, sites/nm$^2$) (Figures K6.5.2-8e,f[a] and K6.5.2-9a,b[a]).

The positive effects associated with *SZCONCOL* and *SZKDAMCO* result from increasing the amount of $^{230}$Th transported on colloids. The interaction of *SZCONCOL* and *SZKDAMCO* in affecting *SZTH230* and *SZTH230C* can be seen in the scatterplots in Figure K6.5.2-9c,e,f,h[a]. The positive effects associated with *EP1LOWOU* and *INFIL* result from increasing the release of $^{234}$U from the EBS and increasing water flow in the EBS and UZ, respectively. The positive effect associated with *SZGWSPDM* results from increasing water flow in the SZ. The negative effect associated with *GOESITED* results from reducing the release of $^{234}$U and $^{230}$Th from the EBS. Smaller effects are indicated for a number of additional variables.

**Movement of Dissolved $^{226}$Ra: *SZRA226* and *SZRA226C*.** The uncertainty and sensitivity analyses for the time-dependent release rates (*SZRA226*, g/yr) and cumulative releases (*SZRA226C*, g) over the time interval [0, 1,000,000 yr] for the movement of dissolved $^{226}$Ra across a subsurface plane at the location of the RMEI resulting from an igneous intrusive event at 250 years that destroys all WPs in the repository are summarized in Figures K6.5.2-11[a] and K6.5.2-12[a]. Further, a comparison of the movement of $^{226}$Ra into and out of the SZ is presented in Figure K6.5.2-13[a]. As shown by the results in Figure K6.5.2-13[a], the SZ has a large effect on the movement of $^{226}$Ra from the UZ to the location of the RMEI.

Overall, the two most important variables affecting *SZRA226* and *SZRA226C* are *EP1LOWOU* (scale factor used to incorporate uncertainty into uranium solubility under low ionic strength conditions after an igneous intrusive event; as sampled, *EP1LOWOU* is actually the logarithm of the indicated scale factor) and *SZGWSPDM* (groundwater specific discharge multiplier*;* as sampled, *SZGWSPDM* is actually the logarithm of the indicated multiplier) (Figures K6.5.2-11e,f[a] and K6.5.2-12a,b[a]). The positive effects associated with *EP1LOWOU* and *SZGWSPDM* result because increasing *EP1LOWOU* increases the release of $^{234}$U from the

EBS and increasing *SZGWSPDM* increases water flow in the SZ. The positive effects of *EP1LOWOU* and *SZGWSPDM* can be seen in the scatterplots in Figure K6.5.2-12c,d,f,g[a]. In addition to *EP1LOWOU* and *SZGWSPDM*, a number of additional variables have smaller effects on *SZRA226* and *SZRA226C* (Figures K6.5.2-11e,f[a] and K6.5.2-12a,b[a]).

## K6.6[a] Igneous Intrusive Scenario Classes: Dose to Reasonably Maximally Exposed Individual (RMEI)

No change.

### K6.6.1[a] Igneous Intrusive Scenario Classes: Dose to Reasonably Maximally Exposed Individual (RMEI) over the Time Interval [0, 20,000 yr] for an Event at 10 years

No change.

### K6.6.2[a] Igneous Intrusive Scenario Classes: Dose to Reasonably Maximally Exposed Individual (RMEI) over the Time Interval [0, 1,000,000 yr] for an Event at 250 years

**Dose to RMEI from Dissolved $^{234}$U: *DOU234*.** The uncertainty and sensitivity analyses for dose to the RMEI (*DOU234*, mrem/yr) over the time interval [0, 1,000,000 yr] for the movement of dissolved $^{234}$U across a subsurface plane at the location of the RMEI resulting from an igneous intrusive event at 250 years that destroys all WPs in the repository are summarized in Figures K6.6.2-5[a] and K6.6.2-6[a].

The uncertainty in *DOU234* is determined primarily by the uncertainty in *SZU234* (Figure K6.6.2-6e[a]). As a result, the analyses in Figures K6.6.2-5[a] and K6.6.2-6[a] for *DOU234* are essentially the same as the analyses in Figures K6.5.2-5[a] and K6.5.2-6[a] for *SZU234*. The only substantive difference is the appearance of *MICU234* (dose conversion factor for $^{234}$U for modern interglacial climate (rem/yr)/(pCi/L)) in the analyses for *DOU234* in Figures K6.6.2-5[a] and K6.6.2-6[a]. The positive effect associated with *MICU234* results from increasing the dose that derives from a unit intake of $^{234}$U.

**Dose to RMEI from Dissolved $^{230}$Th: *DOTH230*.** The uncertainty and sensitivity analyses for dose to the RMEI (*DOTH230*, mrem/yr) over the time interval [0, 1,000,000 yr] for the movement of dissolved $^{230}$Th across a subsurface plane at the location of the RMEI resulting from an igneous intrusive event at 250 years that destroys all WPs in the repository are summarized in Figures K6.6.2-7[a] and K6.6.2-8[a].

The uncertainty in *DOTH230* is determined primarily by the uncertainty in *SZTH230* (Figure K6.6.2-8e[a]). As a result, the analyses in Figures K6.6.2-7[a] and K6.6.2-8[a] for *DOTH230* are essentially the same as the analyses in Figures K6.5.2-8[a] and K6.5.2-9[a] for *SZTH230*. The only minor difference is the appearance of *MICTH229* (dose conversion factor for $^{229}$Th for modern interglacial climate (rem/yr)/(pCi/L)) in the analyses for *DOTH230* in Figure K6.6.2-8a[a]. The positive effect associated with *MICTH229* results from increasing the dose that derives from a unit intake of $^{230}$Th.

**Dose to RMEI from Dissolved $^{226}$Ra: *DORA226*.** The uncertainty and sensitivity analyses for dose to the RMEI (*DORA226*, mrem/yr) over the time interval [0, 1,000,000 yr] for the movement of dissolved $^{226}$Ra across a subsurface plane at the location of the RMEI resulting from an igneous intrusive event at 250 years that destroys all WPs in the repository are summarized in Figures K6.6.2-9[a] and K6.6.2-10[a].

The uncertainty in *DORA226* is determined primarily by the uncertainty in *SZRA226* (Figure K6.6.2-10e[a]). As a result, the analyses in Figures K6.6.2-9[a] and K6.6.2-10[a] for *DORA226* are essentially the same as the analyses in Figures K6.5.2-11[a] and K6.5.2-12[a] for *SZRA226*. The only minor difference is the appearance of *MICRA226* (dose conversion factor for $^{226}$Ra for modern interglacial climate (rem/yr)/(pCi/L)) in the analyses for *DORA226* in Figure K6.6.2-10a[a]. The positive effect associated with *MICRA229* results from increasing the dose that derives from a unit intake of $^{226}$Ra.

### K6.7[a] Igneous Intrusive Scenario Classes: Expected Dose (*EXPDOSE*) to Reasonably Maximally Exposed Individual (RMEI)

No change.

### K6.7.1[a] Igneous Intrusive Scenario Classes: Expected Dose (*EXPDOSE*) to Reasonably Maximally Exposed Individual (RMEI) over [0, 20,000 yr]

No substantive changes in the uncertainty and sensitivity analyses for expected dose to the RMEI (*EXPDOSE*, mrem/yr) over the time interval [0, 20,000 yr] resulting from igneous intrusion were observed (i.e., compare the results in Figures K6.7.1-1 and K6.7.1-2 with the results in Figures K6.7.1-1[a] and K6.7.1-2[a]). Additional comparisons are presented in Figures 7.3.1-28[a] and 7.3.1-30[a]; discussion of the differences in the results is provided in Section 7.3.1.5.4[a].

### K6.7.2[a] Igneous Intrusive Scenario Classes: Expected Dose (*EXPDOSE*) to Reasonably Maximally Exposed Individual (RMEI) over [0, 1,000,000 yr]

No substantive changes in the uncertainty and sensitivity analyses for expected dose to the RMEI (*EXPDOSE*, mrem/yr) over the time interval [0, 1,000,000 yr] resulting from igneous intrusion were observed (i.e., compare the results in Figures K6.7.2-1 and K6.7.2-2 with the results in Figures K6.7.2-1[a] and K6.7.2-2[a]. Additional comparisons are presented in Figures 7.3.1-29[a] and 7.3.1-31[a]; discussion of the differences in the results is provided in Section 7.3.1.5.4[a].

### K6.8[a] Igneous Eruptive Scenario Classes: Expected Dose (*EXPDOSE*) to Reasonably Maximally Exposed Individual (RMEI)

No change.

### K6.8.1[a] Igneous Eruptive Scenario Classes: Expected Dose (*EXPDOSE*) to Reasonably Maximally Exposed Individual (RMEI) over [0, 20,000 yr]

No change.

**K6.8.2[a] Igneous Eruptive Scenario Classes: Expected Dose (*EXPDOSE*) to Reasonably Maximally Exposed Individual (RMEI) over [0, 1,000,000 yr]**

No change.

## K7[a] SEISMIC SCENARIO CLASSES

No change.

**K7.1[a] Seismic Scenario Classes: Summary**

No change.

**K7.2[a] Seismic Ground Motion Scenario Classes: Engineered Barrier System (EBS) Conditions over the Time Interval [0, 20,000 yr]**

No change.

**K7.3[a] Seismic Ground Motion Scenario Classes: Release from Engineered Barrier System (EBS) over the Time Interval [0, 20,000 yr]**

No change.

**K7.4[a] Seismic Ground Motion Scenario Classes: Release from Unsaturated Zone (UZ) over the Time Interval [0, 20,000 yr]**

No change.

**K7.5[a] Seismic Ground Motion Scenario Classes: Release from Saturated Zone (SZ) over the Time Interval [0, 20,000 yr]**

No change.

**K7.6[a] Seismic Ground Motion Scenario Classes: Dose to Reasonably Maximally Exposed Individual (RMEI) over the Time Interval [0, 20,000 yr]**

No change.

**K7.7[a] Seismic Ground Motion Scenario Classes: Expected Dose to Reasonably Maximally Exposed Individual (RMEI)**

**K7.7.1[a] Seismic Ground Motion Scenario Classes: Expected Dose (*EXPDOSE*) to Reasonably Maximally Exposed Individual (RMEI) over the Time Interval [0, 20,000 yr]**

No substantive changes in the uncertainty and sensitivity analyses for expected dose to the RMEI (*EXPDOSE*, mrem/yr) over the time interval [0, 20,000 yr] resulting from seismic ground motion were observed (i.e., compare the results in Figures K7.7.1-1 and K7.7.1-2 with the results in Figures K7.7.1-1[a] and K7.7.1-2[a]). Additional comparisons are presented in

Figures 7.3.1-32[a] and 7.3.1-33[a]; discussion of these comparisons is provided in Section 7.3.1.5.6[a].

For reader convenience, the following discussion of the expected dose results in Figures K7.7.1-1[a] and K7.7.1-2[a] is provided. This discussion updates the corresponding material in Section K7.7.1 from the parent report.

The uncertainty and sensitivity analyses for expected dose to the RMEI (*EXPDOSE*, mrem/yr) over the time interval [0, 20,000 yr] resulting from seismic ground motion events are summarized in Figures K7.7.1-1[a] and K7.7.1-2[a]. After the earliest arrival of released radionuclides at the location of the RMEI, *EXPDOSE* increases monotonically with time (Figure K7.7-1a,b[a]). At 10,000 yr, the value for *EXPDOSE* falls between $10^{-4}$ and 1 mrem/yr for most sample elements, with a few sample elements having values for *EXPDOSE* between 1 and 10 mrem/yr. Due to the use of the quadrature-based methods rather than Monte Carlo methods to evaluate expected dose to the RMEI over the time interval [0, 20,000 yr] (see Equations J8.3-8 and J8.3-13), the expected dose results in Figure 7.7.1-1a,b[a] are relatively smooth.

The PRCCs in Figure K7.7.1-1c[a] indicate that the uncertainty in *EXPDOSE* is dominated by residual stress threshold *SCCTHRP* (as sampled, *SCCTHRP* is a percent of a base value of 351 MPa and is related to the stress corrosion cracking threshold, *SCCTHR*, by *SCCTHRP* = (*SCCTHR* × 100)/(351 MPa)). The value for *EXPDOSE* decreases as *SCCTHRP* increases. This effect occurs because increasing *SCCTHRP* increases the stress required to initiate stress corrosion cracking and thus decreases the probability that a given seismic ground motion event will cause WP damage.

In addition to *SCCTHRP*, smaller effects are indicated for *SZGWSPDM* (groundwater specific discharge multiplier; as sampled, *SZGWSPDM* is actually the logarithm of the indicated multiplier), *SZFIPOVO* (flowing interval porosity in the volcanic unit of the SZ), *INFIL* (infiltration level), *DSNFMASS* (scale factor used to characterize uncertainty in the radionuclide content of DSNF contained in CDSP WPs), and *MICC14* (dose conversion factor for $^{14}C$ for modern interglacial climate, (rem/yr)/(pCi/L)) (Figure K7.7.1-1c[a]). The variables *SZGWSPDM*, *DSNFMASS* and *MICC14* have positive effects on *EXPDOSE*, with these effects resulting because (1) increasing *SZGWSPDM* increases water flow in the SZ, (2) increasing *DSNFMASS* increases the amount of radionuclides in CDSP WPs and hence the dose from the failure of these WPs, and (3) increasing *MICC14* increases the received dose from $^{14}C$ for a given exposure level. The variables *SZFIPOVO* and *INFIL* have effects at early times, but limited effects at later times. The negative effect for *SZFIPOVO* results from slowing water flow in the SZ and thus delaying the initial arrival of radionuclides at the location of the RMEI. In contrast, the positive effect for *INFIL* results from accelerating the initial arrival of radionuclides at the location of the RMEI; specifically, increased values for *INFIL* result (1) in cooler conditions in the EBS, which contributes to earlier radionuclide releases, and (2) in more water flux in the EBS and UZ, which contributes to more rapid radionuclide movement. Owing to the nature of the integration process that defines *EXPDOSE*, the indicated effects associated with *SZFIPOVO* and *INFIL* decrease with increasing time.

More detailed sensitivity analyses for *EXPDOSE* are provided by the regression analyses in Figure K7.7.1-2a[a]. The dominant effect of *SCCTHRP* on the uncertainty in *EXPDOSE* is indicated by $R^2$ values of 0.81, 0.86 and 0.88 for the regressions containing only *SCCTHRP* at 3000, 5000 and 10,000 yr. After *SCCTHRP*, the regressions select a large number of variables that have small effects on *EXPDOSE*. For example, the regression at 3000 yr then selects *SZGWSPDM*, *INFIL* and *MICTC99* (dose conversion factor for $^{99}$Tc for modern interglacial climate, (rem/yr)/(pCi/L)) and produces a model with an $R^2$ value of 0.87; the regression at 5,000 yr then selects *MICTC99*, *DSNFMASS* and *MICC14* and produces a model with an $R^2$ value of 0.90; and the regression at 10,000 yr then selects *MICTC99*, *DSNFMASS* and *HLWDRACD* (rate term for dissolution of HLW glass in CDSP WPs under low pH conditions, g/m$^2$/d) and produces a model with an $R^2$ value of 0.91. After the first four variables, the regressions at 3000, 5000 and 10,000 yr select an additional 12, 11 and 12 variables, respectively, and produce final models with $R^2$ values of 0.92, 0.94 and 0.95. Thus, the uncertainty in *EXPDOSE* is dominated by *SCCTHRP*, with small contributions to this uncertainty by many additional variables.

The doses that are integrated to obtain *EXPDOSE* arise primarily from $^{99}$Tc (Figure 8.2-12(a) and Figure J8.3-8). The importance of $^{99}$Tc to *EXPDOSE* is also evident in the regression results at 10,000 yr (Figure K7.7.1-2a[a]). Specifically, the three variables selected immediately after *SCCTHRP* (i.e., *MICTC99*, *DSNFMASS* and *HLWDRACD*) are variables that affect the dose received from $^{99}$Tc. Specifically, increasing *MICTC99* increases the dose received from a fixed concentration of $^{99}$Tc in groundwater; increasing *DSNFMASS* increases the mass of $^{99}$Tc present to be released from the CDSP WPs; and increasing *HLWDRACD* increases the rate at which $^{99}$Tc is released from the glass waste form.

The dominant effect of *SCCTHRP* on the uncertainty in *EXPDOSE* can be seen in the scatterplot in Figure K7.7.1-2b[a]. The much smaller effects associated with *MICTC99* and *DSNFMASS* can be seen in the scatterplots in Figure K7.7.1-2c,d[a].

It is important to recognize that the results in Figures K7.7.1-1[a] and K7.7.1-2[a] reflect the sensitivity of *EXPDOSE* to the parameters that are treated as being uncertain in the TSPA-LA Model. Some important parameters and model inputs are not treated as being uncertain, but are instead represented by conservative, fixed values or by assumptions. The sensitivity of *EXPDOSE* to these parameters can be discussed qualitatively but cannot be quantified. For example, the results in Figures K7.7.1-1[a] and K7.7.1-2[a] were generated with a fixed value for the seismic hazard curve, estimated as the mean of a distribution of possible seismic hazard curves. This mean seismic hazard curve underlies the probabilistic weightings of the seismic events that give rise to *EXPDOSE* through an integration process (Section 6.1.2.4.4). Significant uncertainty is associated with the definition of the mean seismic hazard curve (SNL 2007 [DIRS 176828], Section 6.4.1). If the uncertainty associated with the seismic hazard curve was incorporated into the analysis, it is likely that this uncertainty would have a significant effect on the uncertainty associated with *EXPDOSE*. Including this uncertainty in the TSPA-LA Model would likely improve the estimated repository performance, because the mean seismic hazard curve typically lies above the 80th percentile of the distribution of seismic hazard curves. Including the uncertainty in the seismic hazard curve would reduce the frequency of damaging seismic events in most realizations, which would reduce releases from the repository and

improve repository performance. Thus, the use of the mean seismic hazard curve results in conservative estimates of repository performance.

### K7.7.2[a] Seismic Ground Motion Scenario Classes: Expected Dose (*EXPDOSE*) to Reasonably Maximally Exposed Individual (RMEI) over the Time Interval [0, 1,000,000 yr]

The results obtained with version 5.005 of the TSPA-LA Model in the uncertainty analyses for expected dose to the RMEI (*EXPDOSE*, mrem/yr) over the time interval [0, 1,000,000 yr] resulting from seismic ground motion tend to be somewhat smaller than the results obtained with version 5.000 of the TSPA-LA Model (i.e., compare the results in Figures K7.7.2-1 and K7.7.2-2 with the results in Figures K7.7.2-1[a] and K7.7.2-2[a]. Additional comparisons are presented in Figures 7.3.1-35[a] and 7.3.1-36[a]; discussion of the differences in the results is provided in Section 7.3.1.5.6[a]. However, there is a large amount of variability in the comparisons across sample elements, with (1) version 5.005 producing smaller results for some sample elements, (2) version 5.000 producing smaller results for some sample elements, and (3) both versions producing similar results for some sample elements (Figures K7.3.1-35[a] and 7.3.1-36[a]). The major cause for the difference in the results from both model versions is the change to the models for estimating damage from seismic events, as described in Appendix P, Section P3, with other minor effects from the other errors described in Appendix P. To some extent, this variability is also influenced by the use of only 30 futures in the estimation of *EXPDOSE* for each sample element. The sensitivity analyses tended to agree on the two most important variables but showed considerable disagreement on less important variables. The differences in sensitivity analysis results are due to the differences between the model versions, primarily to the time and extent of seismic damage (Appendix P, Section P3), and secondarily to the processes by which radionuclide transport occurs.

For reader convenience, the following discussion of the expected dose results in Figures K7.7.2-1[a] and K7.7.2-2[a] is provided. This discussion updates the corresponding material in Section K7.7.2 from the parent report.

The uncertainty and sensitivity analyses for expected dose to the RMEI (*EXPDOSE*, mrem/yr) over the time interval [0, 1,000,000 yr] resulting from seismic ground motion are summarized in Figures K7.7.2-1[a] and K7.7.2-2[a].

The time-dependent values for *EXPDOSE* for the 1,000,000-yr period in Figure K7.7.2-1a,b[a] are much choppier than the values for the 20,000 yr time period in Figure K7.7.1-1a,b[a]. This difference results from the numerical procedures used over 20,000-yr and 1,000,000-yr, respectively, to evaluate the integrals that define *EXPDOSE*. Because the effects of the seismic ground motion events are relatively well behaved for the 20,000-yr time period, it is possible to use a quadrature procedure to evaluate *EXPDOSE* for this time period. This results in the relatively smooth time-dependent values for *EXPDOSE* in Figure K7.7.1-1a,b[a]. In contrast, the effects of seismic ground motion events are much more complex for the 1,000,000-yr time period. As a result of this complexity, it is not possible to use a quadrature procedure to evaluate the defining integral for *EXPDOSE* over this longer time period. Instead, it was necessary to use a sampling-based (i.e., Monte Carlo) integration procedure to evaluate the defining integral for *EXPDOSE*. Specifically, thirty 1,000,000-yr futures involving seismic ground motion events

were randomly sampled for each LHS element and then the 30 time-dependent dose results associated with these futures were vertically averaged at each point in time to produce the estimated time-dependent value for *EXPDOSE* for each sample element (Appendix J, Figures J8.4-1 and J8.4-2). Because individual seismic ground motion events are discrete occurrences that initiate radionuclide releases that ultimately lead to doses to the RMEI, the time dependent doses associated with individual futures and their vertical averages to produce expected doses for individual LHS elements tend to be choppy. In addition, the progression of nominal processes and the occurrence of resultant DS and WP failures contribute to the complexity of the 1,000,000-yr dose calculations. The individual curves in Figure K7.7.2-1a,b would eventually converge to smooth curves if a sufficiently large number of futures was sampled for each LHS element, or if an appropriate kernel smoother was used on the time-dependent results for each LHS element. However, despite the lack of smoothness in the results presented in Figure 7.7.2-1a,b[a], the distribution of expected annual doses (*EXPDOSE*) is shown to be statistically stable (Section 7.3.1) by means of a replicated sampling procedure (Section J4.10). In addition, confidence intervals are computed that show that the mean annual dose is estimated with sufficient accuracy (Section 7.3.1). The stability of the results from TSPA-LA Model v5.005 is discussed in Section 7.3.1.5[a].

Most values for *EXPDOSE* in Figure K7.7.2-1a,b[a] are less than 10 mrem/yr, with a few values between 10 and 100 mrem/yr. The sharp peaks in *EXPDOSE* in Figure K7.7.2-1a,b[a] are associated with peaks that derive from single seismic ground motion events sampled in a single future. The peaks in *EXPDOSE* would be reduced if the sampling-based approximations to the integrals defining *EXPDOSE* were more fully converged.

Although the results in Figure K7.7.2-1a,b[a] are choppy, insights can be gained from a careful examination. In particular, Figure K7.7.2-1b[a] is more informative than Figure K7.7.2-1a[a] because the time-dependent values for *EXPDOSE* for individual LHS elements are more distinct. Overall, after an initial peak, there is a tendency for *EXPDOSE* to decrease up to about 200,000 yr, with this decrease resulting from the depletion of soluble radionuclides (i.e. $^{99}$Tc and $^{129}$I) in WPs with seismic damage (Figure 8.2-12[a]. In this time period, the values of *EXPDOSE* derive from the occurrence of seismic ground motion events as the failure of WPs from nominal processes does not begin until about 200,000 yr. The dominance of seismic ground motion events is indicated by the importance of the residual stress threshold *SCCTHRP* (as sampled, *SCCTHRP* is a percent of a base value of 351 MPa and is related to the stress corrosion cracking threshold, *SCCTHR*, by *SCCTHRP* = (*SCCTHR* × 100)/(351 MPa)); specifically, the PRCCs in Figure K7.7.2-1c[a] indicate that *SCCTHRP* dominates the uncertainty in *EXPDOSE* out to approximately 200,000 yr. This result is also indicated by the regression for *EXPDOSE* at 50,000 yr in Figure K7.7.2-2a [a], where *SCCTHRP* is the first variable selected in the analysis with an $R^2$ value of 0.71.

Beyond 200,000 years, corrosion processes become important to *EXPDOSE* as WPs that have not been damaged by seismic events begin to fail by SCC of lid welds (Section 8.2.1[a]). Consistent with this, the PRCCs in Figure K7.7.2-1c[a] indicate that the uncertainty in *EXPDOSE* becomes dominated by *WDGCA22* (temperature dependence coefficient associated with the general corrosion rate for Alloy 22, K). Specifically, *WDGCA22* corresponds to a coefficient used to alter the general corrosion rate for Alloy 22 as function of temperature, with the Alloy 22 corrosion rate decreasing as *WDGCA22* increases. As indicated in

Figures K4.2-2e,f and K4.5-1c[a], *WDGCA22* is the dominant variable with respect to the uncertainty associated with the failure of WPs from nominal processes. After 400,000 yr, the values for *EXPDOSE* tend to increase and beyond 700,000 years are somewhat smoother than at earlier times (Figure K7.7.2-1a,b[a]). This smoothness results from an increasing dominance of nominal corrosion processes in the values for *EXPDOSE*.

In addition to *SCCTHRP* and *WDGCA22*, the PRCCs in Figure K7.7.2-1c[a] indicate effects for several additional variables. However, the effects are small and the PRCCs are very choppy as a result of the choppiness in the values for *EXPDOSE*. Smoother results for *EXPDOSE* would result in smoother values for the PRCCs in Figure K7.7.2-1c[a].

More detailed sensitivity analyses for *EXPDOSE* are provided by the regression analyses in Figure K7.7.2-2a[a]. Specifically, *SCCTHRP* is the dominant contributor to the uncertainty in *EXPDOSE* at 50,000 yr; *SCCTHRP* is the dominant contributor to the uncertainty in *EXPDOSE* at 200,000 yr with a contribution from *WDGCA22*; and *WDGCA22* is the dominant contributor to the uncertainty in *EXPDOSE* at 500,000 yr with a contribution from *SCCTHRP*. The individual regressions then add several additional variables that have small effects on *EXPDOSE*. The final regression models 50,000, 200,000 and 500,000 yr have $R^2$ values of 0.77, 0.62 and 0.76, which are not particularly high due in part to the choppiness of the values for *EXPDOSE* (Figure K7.7.2-1a,b[a]) and in part to the large number of processes that affect *EXPDOSE* for the 1,000,000 yr seismic ground motion calculation.

For perspective, the scatterplots in Figure K7.7.2-2b,c,d[a] show the effects of *WDGCA22*, *SCCTHRP* and *WDNSCC* (stress corrosion cracking growth rate exponent) at 500,000 yr. The negative effects of *WDGCA22* and *SCCTHRP* can be easily seen in the scatterplots in Figure K7.7.2-2b,c[a]. The negative effect for *WDNSCC* is more subtle but still discernable in the scatterplot in Figure K7.7.2-2d[a].

As previously indicated in conjunction with Figures K7.7.1-1[a] and K7.7.1-2[a] for the 20,000-year time period, it is important to recognize that the results in Figures K7.7.2-1[a] and K7.7.2-2[a] reflect the sensitivity of *EXPDOSE* for the 1,000,000-yr time period to those parameters that are treated as being uncertain in the TSPA-LA Model. Some important parameters and model inputs are not treated as being uncertain, but are instead represented by conservative, fixed values or by assumptions. The sensitivity of *EXPDOSE* to these parameters can be discussed qualitatively but cannot be quantified. In particular, significant uncertainty is associated with the definition of the seismic hazard curve that underlies the occurrence of seismic events and the effects of seismic events. If the uncertainty associated with the seismic hazard curve was incorporated into the analysis, it is likely that this uncertainty would have a significant effect on the uncertainty associated with *EXPDOSE*.

### K7.8[a] Seismic Fault Displacement Scenario Classes: Expected Dose (*EXPDOSE*) to Reasonably Maximally Exposed Individual (RMEI)

No change.

### K7.8.1[a] Seismic Fault Displacement Scenario Classes: Expected Dose (*EXPDOSE*) to Reasonably Maximally Exposed Individual (RMEI) over the Time Interval [0, 20,000 yr]

No substantive changes in the uncertainty and sensitivity analyses for expected dose to the RMEI (*EXPDOSE*, mrem/yr) over the time interval [0, 20,000 yr] resulting from fault displacement were observed (i.e., compare the results in Figures K7.8.1-1 and K7.8.1-2 with the results in Figures K7.8.1-1[a] and K7.8.1-2[a]). Additional comparisons are presented in Figures 7.3.1-37[a] and 7.3.1-39[a]; discussion of the differences in the results is provided in Section 7.3.1.5.7[a].

### K7.8.2[a] Seismic Fault Displacement Scenario Classes: Expected Dose (*EXPDOSE*) to Reasonably Maximally Exposed Individual (RMEI) over the Time Interval [0, 1,000,000 yr]

No substantive changes in the uncertainty and sensitivity analyses for expected dose to the RMEI (*EXPDOSE*, mrem/yr) over the time interval [0, 1,000,000 yr] resulting from fault displacement were observed (i.e., compare the results in Figures K7.8.2-1 and K7.8.2-2 with the results in Figures K7.8.2-1[a] and K7.8.2-2[a]). Additional comparisons are presented in Figures 7.3.1-38[a] and 7.3.1-40[a]; discussion of the differences in the results is provided in Section 7.3.1.5.7[a].

## K8[a] ALL SCENARIO CLASSES: EXPECTED DOSE (*EXPDOSE*) TO REASONABLY MAXIMALLY EXPOSED INDIVIDUAL (RMEI)

No change.

### K8.1[a] All Scenario Classes: Expected Dose (*EXPDOSE*) to Reasonably Maximally Exposed Individual (RMEI) over the Time Interval [0, 20,000 yr]

No substantive changes in the uncertainty and sensitivity analyses for expected dose to the RMEI (*EXPDOSE*, mrem/yr) over the time interval [0, 20,000 yr] resulting from all scenario classes were observed (i.e., compare the results in Figures K8.1-1 and K8.1-2 with the results in Figures K8.1-1[a] and K8.1-2[a]). The similarity in expected dose to the RMEI results from the similarity in the results of the Seismic Ground Motion Scenario Class. Additional comparisons are presented in Figures 7.3.1-42[a] and 7.3.1-43[a] and discussed in Section 7.3.1.5.8[a].

For reader convenience, the following discussion of the expected dose results in Figures K8.1-1[a] and K8.1-2[a] is provided. This discussion updates the corresponding material in Section K8.1 from the parent report.

The uncertainty and sensitivity analyses for expected dose to the RMEI (*EXPDOSE*, mrem/yr) over the time interval [0, 20,000 yr] resulting from all scenario classes are summarized in Figures K8.1-1[a] and K8.1-2[a]. Initial transport to the location of the RMEI takes up to 2000 yr; after the earliest possible arrival time for released radionuclides at the location of the RMEI, *EXPDOSE* increases monotonically with time (Figure K8.1-1a,b[a]). At 10,000 yr, the value for *EXPDOSE* falls between $10^{-3}$ and 4 mrem/yr. As indicated by Figure 8.1-3a[a], the expected dose to the RMEI from all scenario classes is predominantly determined by the

expected dose to the RMEI resulting from seismic ground motion and igneous intrusion. However, for some sample elements, minor effects from early WP failures can be observed in Figure K8.1-1b[a], where the initiation of transport from CNSF WPs after 9000 yr produces spikes in the expected dose. In turn, these spikes result in minor variability in the PRCCs (Figure K8.1-1c[a]).

The PRCCs in Figure K8.1-1c[a] indicate that the four most important variables with respect to the uncertainty in *EXPDOSE* over the time interval [0, 20,000 yr] are *SCCTHRP* (residual stress threshold; as sampled, *SCCTHRP* is a percent of a base value of 351 MPa and is related to the stress corrosion cracking threshold, *SCCTHR*, by *SCCTHRP* = (*SCCTHR* × 100)/(351 MPa)), *IGRATE* (rate of occurrence of igneous intrusive events, $yr^{-1}$), *SZGWSPDM* (groundwater specific discharge multiplier; as sampled, *SZGWSPDM* is actually the logarithm of the indicated multiplier), and *MICC14* (dose conversion factor for $^{14}C$ for modern interglacial climate, (rem/yr)/(pCi/L)). The negative effect associated with *SCCTHRP* results because increasing *SCCTHRP* results in WPs being more resistant to seismic ground motion damage; the positive effect associated with *IGRATE* results because increasing *IGRATE* increases the probability of occurrence for igneous events; the positive effect associated with *SZGWSPDM* results because increasing *SZGWSPDM* increases water flow in the SZ; and the positive effect associated with *MICC14* results from increasing the dose that results from a given exposure to $^{14}C$ (and probably other radionuclides as a result of positive correlations involving dose factors). As indicated by the size of the PRCCs, *SCCTHRP* is the most important of these four variables.

After *SCCTHRP*, *IGRATE*, *SZGWSPDM* and *MICC14*, smaller effects are indicated for *SZFIPOVO* (flowing interval porosity in the volcanic unit of the SZ) and *INFIL* (infiltration level) (Figure K8.1-1c[a]) before about 5,000 years. The negative effect associated with *SZFIPOVO* at early times results from initially slowing the movement of radioactive species in the SZ, and the positive effect associated with *INFIL* results from its role in both speeding the cooling of the repository and increasing water flow in the EBS and UZ.

More detailed sensitivity analyses for *EXPDOSE* are provided by the regression analyses and associated scatterplots in Figure K8.1-2[a]. Overall, the dominant variable with respect to the uncertainty in *EXPDOSE* is *SCCTHRP*. Specifically, the regressions containing only *SCCTHRP* have $R^2$ values of 0.55, 0.66 and 0.69 at 3000, 5000 and 10,000 yr, respectively (Figure K8.1-2a[a]). After *SCCTHRP*, the next variable selected in all regressions is *IGRATE*, with the inclusion of *IGRATE* raising the cumulative $R^2$ values to 0.62, 0.71 and 0.73. Thus, the effect of *IGRATE* on *EXPDOSE* is not as great as the effect of *SCCTHRP*. In consistency with the analysis with PRCCs, *SZGWSPDM* is then the third variable selected in the three regressions analyses. The negative effect associated with *SCCTHRP* and the positive effects associated with *IGRATE* and *SZGWSPDM* can be seen in the scatterplots in Figure K8.1-2a,b,c[a]. After *SCCTHRP*, *IGRATE* and *SZGWSPDM*, the regressions select a number of additional variables that have small effects on *EXPDOSE*. The final regression models have $R^2$ values of 0.81, 0.85 and 0.82, which indicates that they are reasonably successful in accounting for the uncertainty in *EXPDOSE*. However, as is always the case, some of the variables selected at the ends of individual regression analyses that have very small effects on cumulative $R^2$ values may be spurious.

It is important to recognize that the results in Figures K8.1-1[a] and K8.1-2[a] reflect the sensitivity of *EXPDOSE* for the 20,000-yr time period to those parameters that are treated as being uncertain in the TSPA-LA Model. Where parameters and model inputs are not treated as being uncertain, but are instead represented by conservative, fixed values or by assumptions, the sensitivity of *EXPDOSE* to these parameters can be discussed qualitatively but cannot be quantified. For example, significant uncertainty is associated with the definition of the seismic hazard curve that underlies the occurrence of seismic events and the effects of seismic events. If the uncertainty associated with the seismic hazard curve was incorporated into the analysis, it is likely that this uncertainty would have an effect on the uncertainty associated with *EXPDOSE*.

### K8.2[a] All Scenario Classes: Expected Dose (*EXPDOSE*) to Reasonably Maximally Exposed Individual (RMEI) over the Time Interval [0, 1,000,000 yr]

Because of the changes to the Seismic Ground Motion Scenario Class (Appendix P, Section P3), and the importance of this scenario class to the total expected dose (Figure 8.1-3[a]), the changes to the Seismic Ground Motion Scenario Class affect the uncertainty and sensitivity analyses for expected dose to the RMEI (*EXPDOSE*, mrem/yr) over the time interval [0, 1,000,000 yr]. As discussed in Section K7.7.2[a], the change to the models for estimating damage from seismic events, as described in Appendix P, Section P3, alters the relationships between input and output variables. The most significant effect of the model changes is to flatten the peak in the expected (mean) dose that occurs around 230,000 years (compare Figure 8.1-2 and Figure 8.1-2[a]). As a consequence, the input variables identified as important at 200,000 yr and at 252,000 yr are different for the two model versions. However, at earlier and at later times, the sensitivity analyses for both model versions agree on the three most important variables but showed considerable disagreement on less important variables (i.e., compare the results in Figures K8.2-1 and K8.2-2 with the results in Figures K8.2-1[a] and K8.2-2[a]). Additional comparisons are presented in Figures 7.3.1-45[a] and 7.3.1-46[a] and discussed in Section 7.3.1.5.9[a].

For reader convenience, the following discussion of the expected dose results in Figures K8.2-1[a] and K8.2-2[a] is provided. This discussion updates the corresponding material in Section K8.2 from the parent report.

The uncertainty and sensitivity analyses for expected dose to the RMEI (*EXPDOSE*, mrem/yr) over the time interval [0, 1,000,000 yr] resulting from all scenario classes are summarized in Figures K8.2-1[a] and K8.2-2[a]. As indicated by Figure 8.1-3b[a], the expected dose to the RMEI from all scenario classes is predominantly determined by the expected dose to the RMEI resulting from seismic ground motion and from igneous intrusion.

The time-dependent values for *EXPDOSE* appear somewhat choppy as a result of the sampling-based effects of nominal processes and seismic ground motion events (Figure K7.7.2-1[a]). Smoother results could be obtained by using a larger sample of aleatory futures for seismic ground motion events or possibly a more sophisticated integration procedure for the incorporation of such events. However, because the distribution of *EXPDOSE* has been shown to be statistically stable (Section 7.3.1.3 and Section 7.3.1.5.9[a]), improved convergence or use of a better integration procedure would produce smoother estimates of expected dose, but

would not produce results that differ substantially from those shown in Figure K8.2-1[a]. The values for *EXPDOSE* fall in a range from $10^{-4}$ to 40 mrem/yr.

The PRCCs in Figure K8.2-1c[a] indicate that the three most important variables with respect to the uncertainty in *EXPDOSE* are *SCCTHRP* (residual stress threshold; as sampled, *SCCTHRP* is a percent of a base value of 351 MPa and is related to the stress corrosion cracking threshold, *SCCTHR*, by *SCCTHRP* = (*SCCTHR* × 100)/(351 MPa)), *IGRATE* (rate of occurrence of igneous intrusive events, $yr^{-1}$), *SZGWSPDM* (groundwater specific discharge multiplier; as sampled, *SZGWSPDM* is actually the logarithm of the indicated multiplier), and *WDGCA22* (temperature dependence coefficient associated with the general corrosion rate for Alloy 22, K). The negative effect associated with *SCCTHRP* results because increasing *SCCTHRP* increases the resistance of WPs to seismic ground motion damage; the positive effect associated with *IGRATE* results because increasing *IGRATE* increases the probability of occurrence for igneous events; the positive effect associated with *SZGWSPDM* results because increasing *SZGWSPDM* increases water flow in the SZ; and the negative effect associated with *WDGCA22* results from its role in slowing the rate of general corrosion of Alloy 22, which in turn delays and reduces WP failures due to both seismic ground motion events and general corrosion.

Smaller effects are indicated for *SZFIPOVO* (flowing interval porosity in the volcanic unit of the SZ) and *EP1LOWPU* (scale factor used to incorporate uncertainty into plutonium solubility under low ionic strength conditions; as sampled, *EP1LOWPU* is actually the logarithm of the indicated scale factor). The negative effect of *SZFIPOVO* only occurs at very early times (Figure K8.1-1c[a]) and results from increasing the time required for an initial radionuclide release into the SZ to reach the RMEI. The positive effect of *EP1LOWPU* results from increasing the amount of dissolved plutonium that is released from the EBS.

More detailed sensitivity analysis results are provided by the regression analyses and associated scatterplots in Figure K8.2-2[a]. At 50,000 yr, the most important variable is *SCCTHRP*, which results in a single-variable regression model with an $R^2$ value of 0.27. At 200,000 and 500,000 yr, the most important variable is *IGRATE*, which results in single-variable regression models with $R^2$ values of 0.38 and 0.29. Further, *IGRATE* is the second variable selected at 50,000 yr. After these initial selections, the stepwise analyses continue and construct models with 9, 16 and 13 variables and corresponding $R^2$ values of 0.67, 0.74 and 0.70. Thus, a large number of variables are affecting uncertainty in *EXPDOSE* over 1,000,000 yr with no single variable dominating this uncertainty. For perspective, the effects of *IGRATE*, *WDGCA22* and *SZGWSPDM* on *EXPDOSE* at 500,000 yr can be seen in the scatterplots in Figure K8.2-2b,c,d[a].

As previously indicated in conjunction with Figures K8.1-1[a] and K8.1-2[a] for the 20,000-yr time period, it is important to recognize that the results in Figures K8.2-1[a] and K8.2-2[a] reflect the sensitivity of *EXPDOSE* for the 1,000,000 yr time period to those parameters that are treated as being uncertain in the TSPA-LA Model. Some important parameters and model inputs are not treated as being uncertain, but are instead represented by conservative, fixed values or by assumptions. In particular, if the uncertainty associated with the seismic hazard curve was incorporated into the analysis, it is likely that this uncertainty would have an effect on the uncertainty associated with *EXPDOSE*.

## K9[a] SUMMARY

This addendum updates uncertainty and sensitivity analyses for expected dose to the RMEI reported in Appendix K with results obtained from TSPA-LA Model v5.005. In addition, for the Igneous Intrusion Scenario Classes, this addendum reports new uncertainty and sensitivity analyses for the movement of $^{234}U$, $^{230}Th$, and $^{226}Ra$ out of the EBS, UZ and SZ, as well as dose to the RMEI for these radionuclides. Comparison of the results of the uncertainty and sensitivity analyses for the two TSPA-LA Model versions shows that the two models produce similar results, although some differences in results can be observed for the Seismic Ground Motion Scenario Class, and for a few sample elements in most scenario classes. Due to the similarity evident in the results from the two models, the analyses presented in Appendix K for the movement of representative radionuclides ($^{239}Pu$, $^{237}Np$, and $^{99}Tc$) are not repeated; conclusions from these analyses apply equally to TSPA-LA Model v5.005.

Table K9-1[a] summarizes sensitivity analysis results for total expected dose and expected dose by scenario class by listing the key uncertain inputs identified by the analysis, using results from TSPA-LA Model v5.005. The key uncertain inputs in Table K9-1[a] are listed in decreasing order of importance with the first listed input having the most effect on the output quantity. The key uncertain inputs are identified on the basis of sensitivity analysis results at roughly the time the mean of the output variable achieves its maximum value. Table K9-1[a] and Table K9-1 generally show the same key uncertain inputs for each scenario class, but there are exceptions. The changes to the Seismic Ground Motion Scenario Class for TSPA-LA Model v5.005 caused the maximum of the expected (mean) dose for this scenario class as well as for total expected (mean) dose to move from 230,000 yr to 1,000,000 yr. Consequently, the key uncertain inputs for these two output variables are different. Additionally, the third or fourth uncertain inputs for some scenario classes have changed due to other corrections to the TSPA-LA Model.

Generally, the uncertain inputs that predominantly determine uncertainty in expected dose for each scenario class are those inputs that describe the occurrence and extent of failure of EBS components. This conclusion is the same for both model versions. For the Seismic Ground Motion Scenario Class, the key uncertain input at early times is *SCCTHRP* (residual stress threshold; as sampled, *SCCTHRP* is a percent of a base value of 351 MPa and is related to the stress corrosion cracking threshold, *SCCTHR*, by $SCCTHRP = (SCCTHR \times 100)/(351\ \text{MPa})$), which essentially determines the probability of damage to CDSP or CSNF WPs for each seismic event. At later times, because the Seismic Ground Motion Scenario Class is combined with the Nominal Scenario Class, the key uncertain input is *WDGCA22* (temperature dependence coefficient associated with general corrosion rate for Alloy 22, K), which essentially determines the uncertainty in the time and extent of general corrosion failures (both by stress-corrosion cracking and by patches). For the Igneous Intrusive Scenario Class, the key uncertain input is *IGRATE* (rate of occurrence of igneous intrusive events, $yr^{-1}$). For the Nominal Scenario Class the key uncertain input is *WDGCA22* (temperature dependence coefficient associated with general corrosion rate for Alloy 22, K), which essentially determines the uncertainty in the time and extent of general corrosion failures (both by SCC and by patches). For the Early Failure Scenario Classes key uncertain inputs are *PROBWPEF* (probability that a randomly selected WP will experience an early failure) and *PROBDSEF* (probability that a randomly selected DS will experience an early failure). For the Igneous Eruptive Scenario Class the key uncertain input is *IGERATE* (rate of occurrence of volcanic eruption events, $yr^{-1}$). For the Seismic Fault

Displacement Modeling Case, no single input emerged as predominant. Rather, the analysis identified several uncertain inputs with moderately monotonic effects on the expected dose for the scenario class.

INTENTIONALLY LEFT BLANK

Table K9-1[a]. Summary of Selected Sensitivity Analysis Results

| Scenario Class | TSPA-LA Model Output (time of maximum mean value) | Key Uncertain Inputs[a] |
|---|---|---|
| Total System | Total expected dose 0 to 10,000 years (10,000 years) | • Residual stress threshold for SCC (*SCCTHRP*)<br>• Frequency of occurrence of igneous events (*IGRATE*)<br>• Logarithm of scale factor in ground water specific discharge (*SZGWSPDM*) |
| | Total expected dose 10,000 to 1,000,000 years (1,000,000 years) | • Frequency of occurrence of igneous events (*IGRATE*)<br>• General corrosion rate (Alloy 22) temperature dependence (*WDGCA22*)<br>• Logarithm of scale factor in ground water specific discharge (*SZGWSPDM*) |
| Nominal | Expected dose resulting from corrosion processes (720,000 years) | • General corrosion rate (Alloy 22) temperature dependence (*WDGCA22*)<br>• Deviation from median yield strength range for outer lid (*WDZOLID*) |
| Early Failure Drip Shield | Expected dose resulting from early failure of drip shields over 20,000 years (2,000 years) | • Probability of early failure per drip shield (*PROBDSEF*)<br>• Uncertainty factor accounting for small-scale heterogeneity in fracture permeability (*SEEPUNC*)<br>• Logarithm of mean fracture permeability in lithophysal rock units (*SEEPRM*) |
| Early Failure Waste Package | Expected dose resulting from early failure of waste packages over 20,000 years (12,000 years) | • Probability of early failure per waste package (*PROBWPEF*)<br>• Pointer variable for infiltration scenario (*INFIL*)<br>• Selector for host-rock thermal conductivity scenario (*THERMCON*) |
| Igneous Intrusive | Expected dose resulting from igneous intrusion over 20,000 years (20,000 years) | • Frequency of occurrence of igneous events (*IGRATE*)<br>• Logarithm of scale factor in ground water specific discharge (*SZGWSPDM*)<br>• Pointer variable for infiltration scenario (*INFIL*) |
| | Expected dose resulting from igneous intrusion over 1,000,000 years (1,000,000 years) | • Frequency of occurrence of igneous events (*IGRATE*)<br>• Logarithm of scale factor in ground water specific discharge (*SZGWSPDM*)<br>• Pointer variable for infiltration scenario (*INFIL*) |
| Igneous Eruptive | Expected dose resulting from volcanic eruption over 20,000 years (20,000 years) | • Frequency of occurrence of volcanic eruptions (*IGERATE*)<br>• Pointer variable for long-term inhalation dose conversation factors for exposure to volcanic ash (*INHLTPV*)<br>• Diffusivity of radionuclides in divides (*DDIVIDE*) |
| | Expected dose resulting from volcanic eruption over 1,000,000 years (1,000,000 years) | • Frequency of occurrence of volcanic eruptions (*IGERATE*)<br>• Depth of soil within which radionuclides affect the biosphere (*BTILLAGE*) |

Table K9-1[a]. Summary of Selected Sensitivity Analysis Results (Continued)

| Scenario Class | TSPA-LA Model Output (time of maximum mean value) | Key Uncertain Inputs[a] |
|---|---|---|
| Seismic Ground Motion | Expected dose resulting from seismic ground motion over 20,000 years (20,000 years) | • Residual stress threshold for SCC (*SCCTHRP*) |
| | Expected dose resulting from combination of seismic ground motion and corrosion processes over 1,000,000 years (1,000,000 years) | • General corrosion rate (Alloy 22) temperature dependence (*WDGCA22*)<br>• Residual stress threshold (*SCCTHRP*) |
| Seismic Fault Displacement | Expected dose resulting from fault displacement over 20,000 years (20,000 years) | • Groundwater biosphere dose conversion factor for $^{99}$Tc (*MICTC99*)<br>• Pointer variable for infiltration scenario (*INFIL*)<br>• Logarithm of scale factor in ground water specific discharge (*SZGWSPDM*)<br>• Selector variable determining the collapsed drift rubble thermal conductivity (*DTDRHUNC*) |
| | Expected dose resulting from fault displacement over 1,000,000 years (1,000,000 years) | • Pointer variable for infiltration scenario (*INFIL*)<br>• Logarithm of scale factor for uncertainty in plutonium solubility at ionic strength below 1 molal (*EP1LOWPU*)<br>• Logarithm of scale factor in ground water specific discharge (*SZGWSPDM*)<br>• Waste package flux splitting factor (*WPFLUX*) |

[a] Name (in parentheses) is the variable name used in the sensitivity analyses (see Table K3-1).

## K10[a] HUMAN INTRUSION SCENARIO

Uncertainty and sensitivity analysis results for human intrusion at 200,000 yr are presented in two sets. The first set is for expected dose to the RMEI **(***EXPDOSE*, mrem/yr**)** over the time period [200,000, 220,000 yr] (Figures K10-1[a] and K10-2[a]); the second set is for expected dose to the RMEI **(***EXPDOSE*, mrem/yr**)** over the time period [220,000, 1,000,000 yr] (Figures K10-3[a] and K10-4[a]). This division is made because of the rapid changes in *EXPDOSE* that occur in the first 20,000 yr after a drilling intrusion. This analysis is reported separately from the other scenario classes because the human intrusion results are calculated for comparison with the human intrusion standard. In contrast, the preceding analyses for expected dose to the RMEI are calculated for comparison with the individual protection standard.

As examination of Figure K10-1a,b[a] shows, *EXPDOSE* increases rapidly for the first 1000 to 2000 yr after a drilling intrusion at 200,000 yr and then decreases monotonically out to 220,000 yr. The individual sample elements produce peak values for *EXPDOSE* between approximately 0.003 and 0.1 mrem/yr; at 220,000 yr the values for *EXPDOSE* are between 0.00006 and 0.02 mrem/yr. The monotonic decrease in *EXPDOSE* can be seen in Figure K10-3a,b[a] to continue out to approximately 400,000 yr; beyond 400,000 yr, *EXPDOSE* remains approximately constant with a slight tendency to increase.

For the time period [200,000, 300,000 yr], $^{99}$Tc and $^{129}$I are the dominant radionuclides contributing to *EXPDOSE*; for the time period [300,000, 1,000,000 yr], $^{242}$Pu is the dominant radionuclide contributing to *EXPDOSE* (Figure 8.1-17[a]).

Sensitivity analysis results for the [200,000, 220,000 yr] time period are presented in Figures K10-1c[a] and K10-2b,c,d,e,f,g[a]. As indicated by the PRCCs in Figure K10-1c[a], the most important variables affecting *EXPDOSE* for the first 5000 yr after the intrusion are *INFIL* (infiltration level), *CSSPECSA* (effective specific surface area of CSNF waste, $m^2$/mg; as sampled, *CSSPECSA* is actually the logarithm of the indicated surface area), *SZGWSPDM* (groundwater specific discharge multiplier*;* as sampled, *SZGWSPDM* is actually the logarithm of the indicated multiplier), *SZFIPOVO* (flowing interval porosity in the volcanic unit of the SZ), *MICTC99* (dose conversion factor for $^{99}$Tc for modern interglacial climate, (rem/yr)/(pCi/L)), and *EBSDIFCF* (scale factor used to represent uncertainty in EBS diffusion coefficient; as sampled, *EBSDIFCF* is actually the logarithm of the indicated scale factor). For the first 5000 yr after the intrusion, *INFIL*, *CSSPECSA*, *SZGWSPDM*, *MICTC99* and *EBSDIFCF* have positive effects on *EXPDOSE*, and *SZFIPOVO* has a negative effect on *EXPDOSE*. These effects result because (1) increasing *INFIL* increases water flow in the EBS and UZ, (2) increasing *CSSPECSA* increases the release of radionuclides from degrading CSNF waste, (3) increasing *SZGWSPDM* increases water movement in the SZ, (4) increasing *MICTC99* increases the dose received from a unit concentration of $^{99}$Tc in groundwater, and (5) increasing *EBSDIFCF* increases the release of radionuclides from the EBS. In contrast, increasing *SZFIPOVO* has an early negative effect on *EXPDOSE* as a result of increasing the volume of water involved in radionuclide transport in the SZ; however, this dilution effect is short lived and quickly ceases as more radionuclides enter the SZ.

After approximately 5000 yr, *INFIL*, *CSSPECSA*, *SZGWSPDM* and *EBSDIFCF* have a negative effect on *EXPDOSE* (Figure K10-1c[a]). This reversal in effects results from the high mobility

of $^{99}$Tc and $^{129}$I, which are the dominant radionuclides contributing to *EXPDOSE* prior to 300,000 yr. Because of this mobility, variables that increase the release of $^{99}$Tc and $^{129}$I at early times (i.e., in the first 5000 yr after intrusion) also decrease the releases of $^{99}$Tc and $^{129}$I at later times. As a result, *INFIL*, *CSSPECSA*, *SZGWSPDM* and *EBSDIFCF* have a positive effect on *EXPDOSE* in the first 5000 yr after intrusion and a negative effect on *EXPDOSE* at later times. In contrast, *MICTC99* continues to have a positive effect on *EXPDOSE* with increasing time.

More detailed analyses for *EXPDOSE* for the time period [200,000, 205,000 yr] are provided by the stepwise regression analyses and scatterplots in Figure K10-2[a]. As examination of the regression analyses and associated scatterplots shows, many individual variables affect *EXPDOSE* with no single variable having a dominant effect on the uncertainty in *EXPDOSE*. Further, many variables having small effects and possibly some complex interactions between variables and the radionuclides that they affect, results in regression models with small $R^2$ values (i.e., 0.75, 0.53 and 0.41).

As indicated by the PRCCS in Figure K10-3c[a], the most important variables affecting *EXPDOSE* after approximately 300,000 yr are *SZGWSPDM*, *GOESITED* (density of sorption sites on goethite, sites/nm$^2$), *COLFEOSS* (iron oxide colloid concentration when degraded stainless steel is present but no degrading carbon steel is present, mg/L), *EP1LOWPU* (scale factor used to incorporate uncertainty into plutonium solubility under low ionic strength conditions; as sampled, *EP1LOWPU* is actually the logarithm of the indicated scale factor), and *SZFISPVO* (flowing interval spacing in volcanic unit of SZ, m). The variables *SZGWSPDM*, *COLFEOSS*, *EP1LOWPU* and *SZFISPVO* have positive effects on *EXPDOSE*; in contrast, *GOESITED* has a negative effect. The positive effects associated with *SZGWSPDM*, *COLFEOSS*, *EP1LOWPU* and *SZFISPVO* result because (1) increasing *SZGWSPDM* increases water flow in the SZ, (2) increasing *COLFEOSS* increases the attachment of radionuclides to mobile colloids, (3) increasing *EP1LOWPU* increases the solubility of plutonium, and (4) increasing *SZFISPVO* decreases the diffusion of radionuclides from fractures in the volcanic unit of the SZ into the surrounding rock matrix. The negative effect associated with *GOESITED* results from increasing the sorption of radionuclides onto corrosion products in the EBS.

More detailed analyses for *EXPDOSE* for the time period [220,000, 1,000,000 yr] are provided by the stepwise regression analyses and scatterplots in Figure K10-4[a]. As examination of the regression analyses and associated scatterplots shows, many individual variables affect *EXPDOSE* with no single variable having a dominant effect on the uncertainty in *EXPDOSE*. Further, many variables having small effects and possibly some complex interactions between variables and the radionuclides that they affect is resulting in regression models with small $R^2$ values (i.e., 0.50, 0.55, and 0.63).

Comparisons of results for *EXPDOSE* resulting from human intrusion at 200,000 yr obtained with versions 5.000 and 5.005 of the TSPA-LA Model are presented in Figures K10-5[a] and K10-6[a].

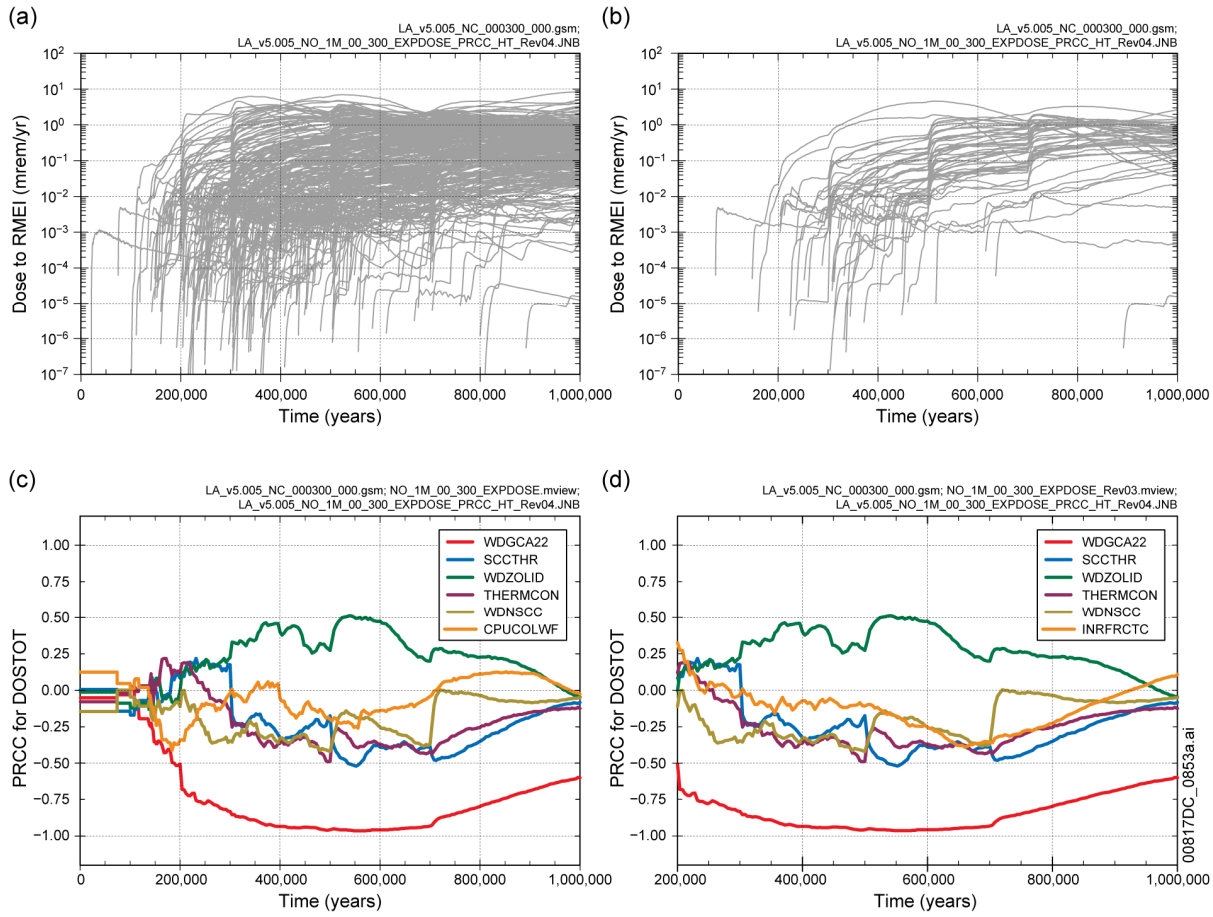


Source: Output DTNs: MO0710ADTSPAWO.000 [DIRS 183752]; and MO0710PLOTSFIG.000 [DIRS 185207].

Figure K4.5-1[a]. Dose to RMEI (*DOSTOT*, mrem/yr) for all radioactive species under nominal conditions obtained with version 5.005 of the TSPA-LA Model: (a) *DOSTOT* for all (i.e., 300) sample elements, (b) *DOSTOT* for first 50 sample elements, (c) PRCCs for *DOSTOT* for [0; 1,000,000 yr], and (d) PRCCs for *DOSTOT* for [200,000; 1,000,000 yr]

(a)

| | DOSTOT: 400,000 Years | | | DOSTOT: 600,000 Years | | | DOSTOT: 800,000 Years | | |
|---|---|---|---|---|---|---|---|---|---|
| Step[a] | Variable[b] | $R^{2c}$ | SRRC[d] | Variable | $R^2$ | SRRC | Variable | $R^2$ | SRRC |
| 1 | WDGCA22 | 0.78 | −0.90 | WDGCA22 | 0.85 | −0.94 | WDGCA22 | 0.63 | −0.80 |
| 2 | WDZOLID | 0.81 | 0.16 | WDZOLID | 0.87 | 0.14 | WDZOLID | 0.65 | 0.16 |
| 3 | WDNSCC | 0.82 | −0.12 | THERMCON | 0.88 | −0.10 | MICI129 | 0.67 | 0.13 |
| 4 | THERMCON | 0.83 | −0.13 | INFIL | 0.89 | −0.10 | SCCTHR | 0.68 | −0.10 |
| 5 | INFIL | 0.84 | −0.10 | SCCTHR | 0.90 | −0.09 | | | |
| 6 | SCCTHR | 0.85 | −0.09 | WDNSCC | 0.91 | −0.08 | | | |
| 7 | WDGCUA22 | 0.85 | 0.07 | CORRATSS | 0.91 | −0.07 | | | |
| 8 | WDLCRATE | 0.86 | 0.06 | WDGCUA22 | 0.92 | 0.08 | | | |
| 9 | | | | MICTC99 | 0.92 | 0.07 | | | |
| 10 | | | | DTDRHUNC | 0.92 | 0.04 | | | |
| 11 | | | | CSNFMASS | 0.92 | 0.04 | | | |

a: Steps in stepwise rank regression analysis
b: Variables listed in order of selection in stepwise regression
c: Cumulative $R^2$ value with entry of each variable into regression model
d: Standardized rank regression coefficients (SRRCs) in final regression model

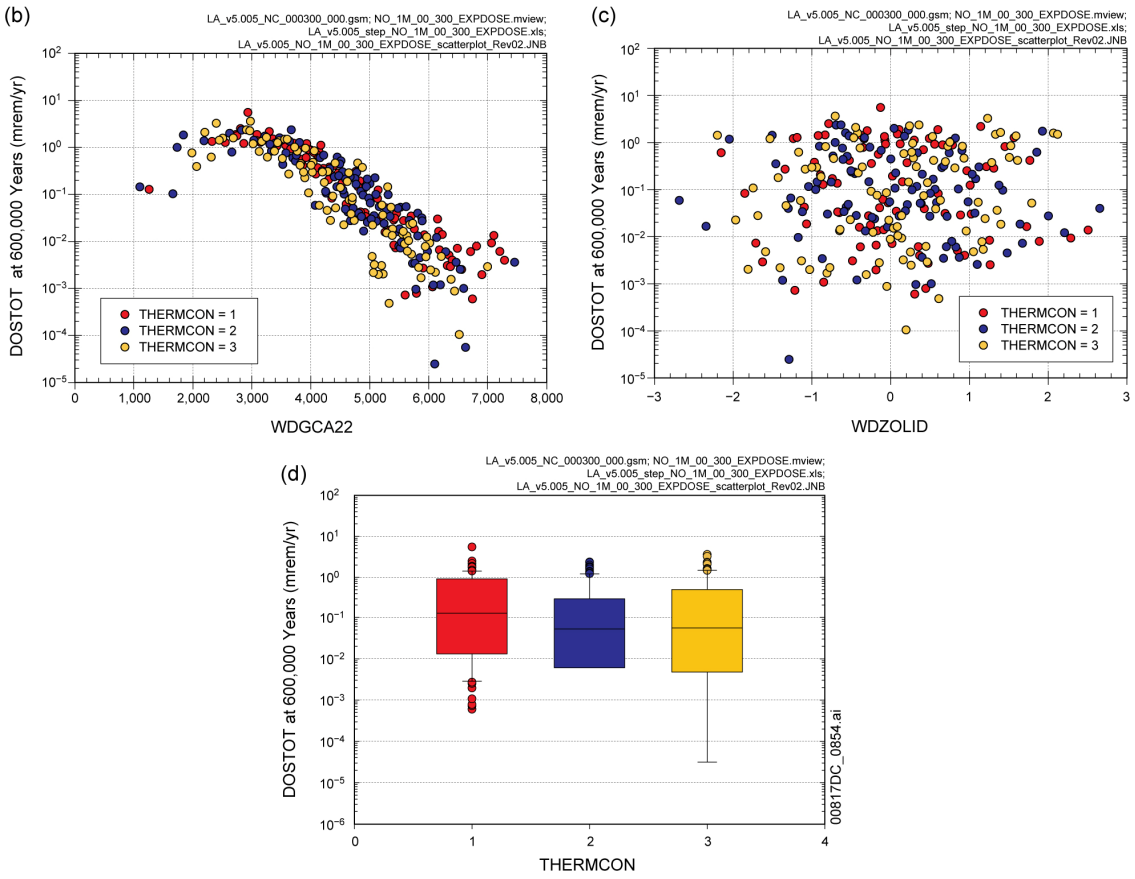


Source: Output DTNs: MO0710ADTSPAWO.000 [DIRS 183752]; and MO0710PLOTSFIG.000 [DIRS 185207].

NOTE: In (d), the box extends from 0.25 to 0.75 quantile; lower and upper bar and whisker extend to 0.1 and 0.9 quantile, respectively; dots represent values outside 0.1 to 0.9 quantile range; median indicated by light horizontal line.

Figure K4.5-2[a]. Stepwise rank regression analyses and selected scatterplots for dose to RMEI (*DOSTOT*, mrem/yr) for all radioactive species under nominal conditions obtained with version 5.005 of the TSPA-LA Model: (a) regressions for *DOSTOT* at 400,000, 600,000, and 800,000 years, and (b,c,d) scatterplots for *DOSTOT* at 600,000 years

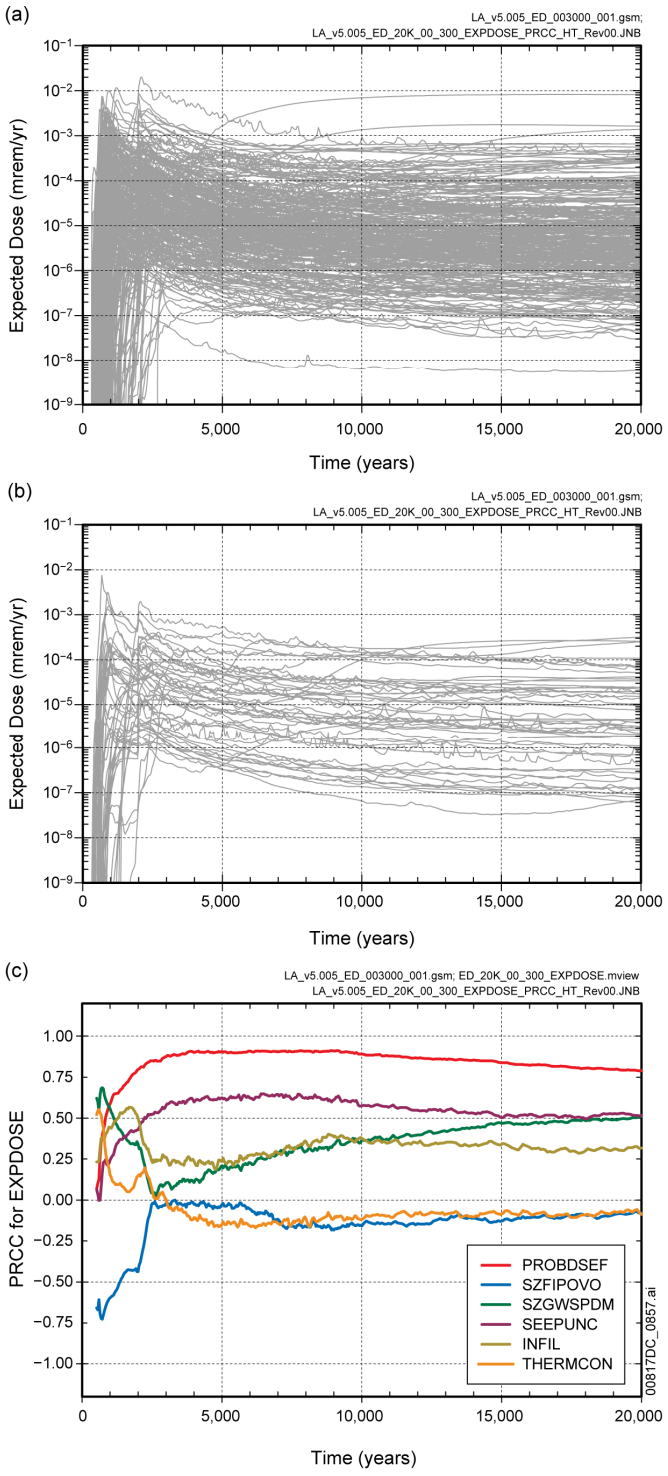


Source: Output DTNs: MO0710ADTSPAWO.000 [DIRS 183752]; and MO0710PLOTSFIG.000 [DIRS 185207].

Figure K5.7.1-1[a]. Expected dose to RMEI (*EXPDOSE*, mrem/yr) over [0, 20,000 yr] for all radioactive species resulting from early DS failure obtained with version 5.005 of the TSPA-LA Model: (a) *EXPDOSE* for all (i.e., 300) sample elements, (b) *EXPDOSE* for first 50 sample elements, and (c) PRCCs for *EXPDOSE*

(a)

| | EXPDOSE: 3,000 Years | | | EXPDOSE: 5,000 Years | | | EXPDOSE: 10,000 Years | | |
|---|---|---|---|---|---|---|---|---|---|
| Step[a] | Variable[b] | $R^{2c}$ | SRRC[d] | Variable | $R^2$ | SRRC | Variable | $R^2$ | SRRC |
| 1 | PROBDSEF | 0.70 | 0.80 | PROBDSEF | 0.71 | 0.81 | PROBDSEF | 0.63 | 0.79 |
| 2 | SEEPUNC | 0.77 | 0.24 | SEEPUNC | 0.78 | 0.24 | INFIL | 0.69 | 0.23 |
| 3 | SEEPPRM | 0.81 | −0.22 | SEEPPRM | 0.81 | −0.19 | SEEPUNC | 0.73 | 0.23 |
| 4 | MICTC99 | 0.83 | 0.15 | INFIL | 0.83 | 0.13 | SEEPPRM | 0.77 | −0.21 |
| 5 | INFIL | 0.85 | 0.12 | MICTC99 | 0.84 | 0.09 | ALPHAL | 0.79 | −0.13 |
| 6 | ALPHAL | 0.86 | −0.08 | ALPHAL | 0.85 | −0.11 | SZCOLRAL | 0.80 | −0.12 |
| 7 | MICNP237 | 0.87 | 0.07 | MICNP237 | 0.86 | 0.09 | MICPU239 | 0.81 | 0.09 |
| 8 | CSNFMASS | 0.87 | 0.07 | | | | CPUCOLWF | 0.82 | 0.08 |
| 9 | GP4NO3 | 0.87 | 0.07 | | | | SEEPPRMN | 0.82 | −0.08 |
| 10 | | | | | | | RHMU0 | 0.83 | 0.08 |
| 11 | | | | | | | SMECSA | 0.83 | 0.08 |
| 12 | | | | | | | SZGWSPDM | 0.84 | 0.07 |
| 13 | | | | | | | UZFAG4 | 0.84 | −0.07 |
| 14 | | | | | | | EP1LOWPU | 0.85 | 0.06 |

a: Steps in stepwise rank regression analysis
b: Variables listed in order of selection in stepwise regression
c: Cumulative $R^2$ value with entry of each variable into regression model
d: Standardized rank regression coefficients (SRRCs) in final regression model

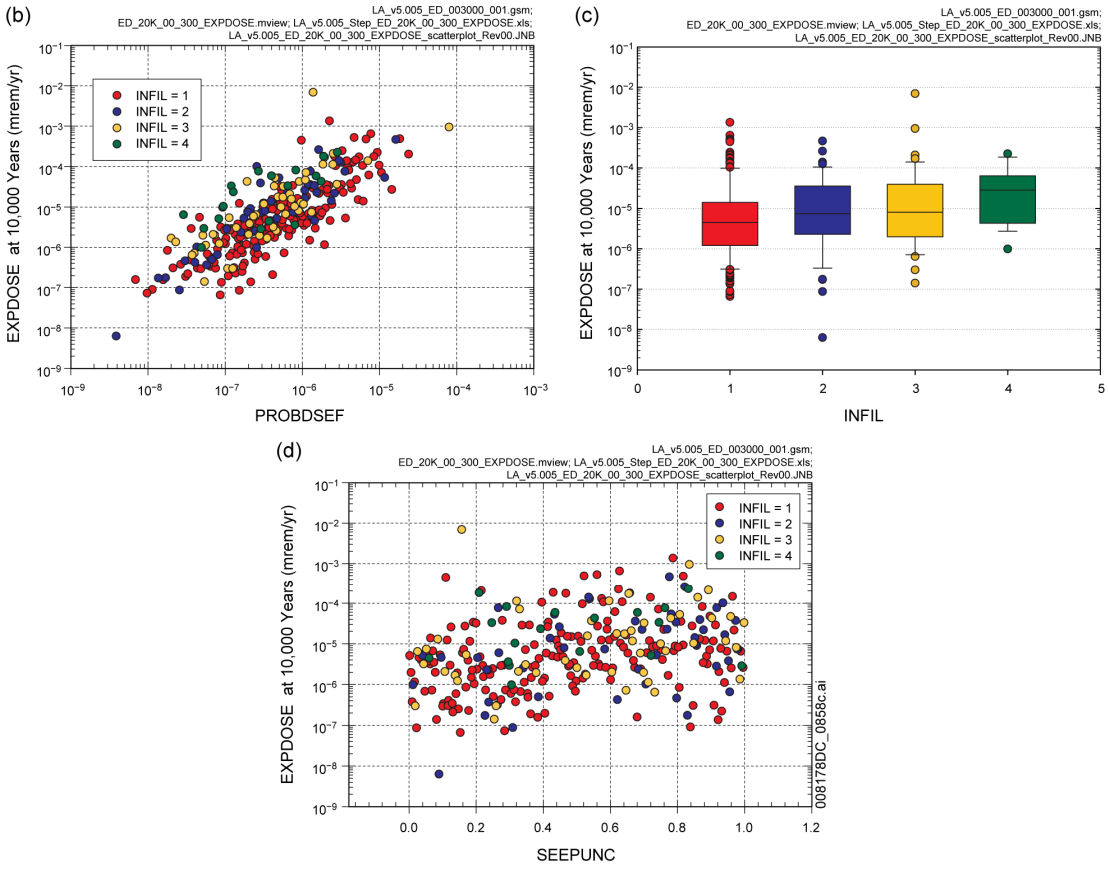


Source: Output DTNs: MO0710ADTSPAWO.000 [DIRS 183752]; and MO0710PLOTSFIG.000 [DIRS 185207].

NOTE: In (c), the box extends from 0.25 to 0.75 quantile; lower and upper bar and whisker extend to 0.1 and 0.9 quantile, respectively; dots represent values outside 0.1 to 0.9 quantile range; median indicated by light horizontal line.

Figure K5.7.1-2[a]. Stepwise rank regression analyses and selected scatterplots for expected dose to RMEI (*EXPDOSE*, mrem/yr) over [0, 20,000 yr] for all radioactive species resulting from early DS failure obtained with version 5.005 of the TSPA-LA Model: (a) regressions for *EXPDOSE* at 3,000, 5,000, and 10,000 years, and (b,c,d) scatterplots for *EXPDOSE* at 10,000 years

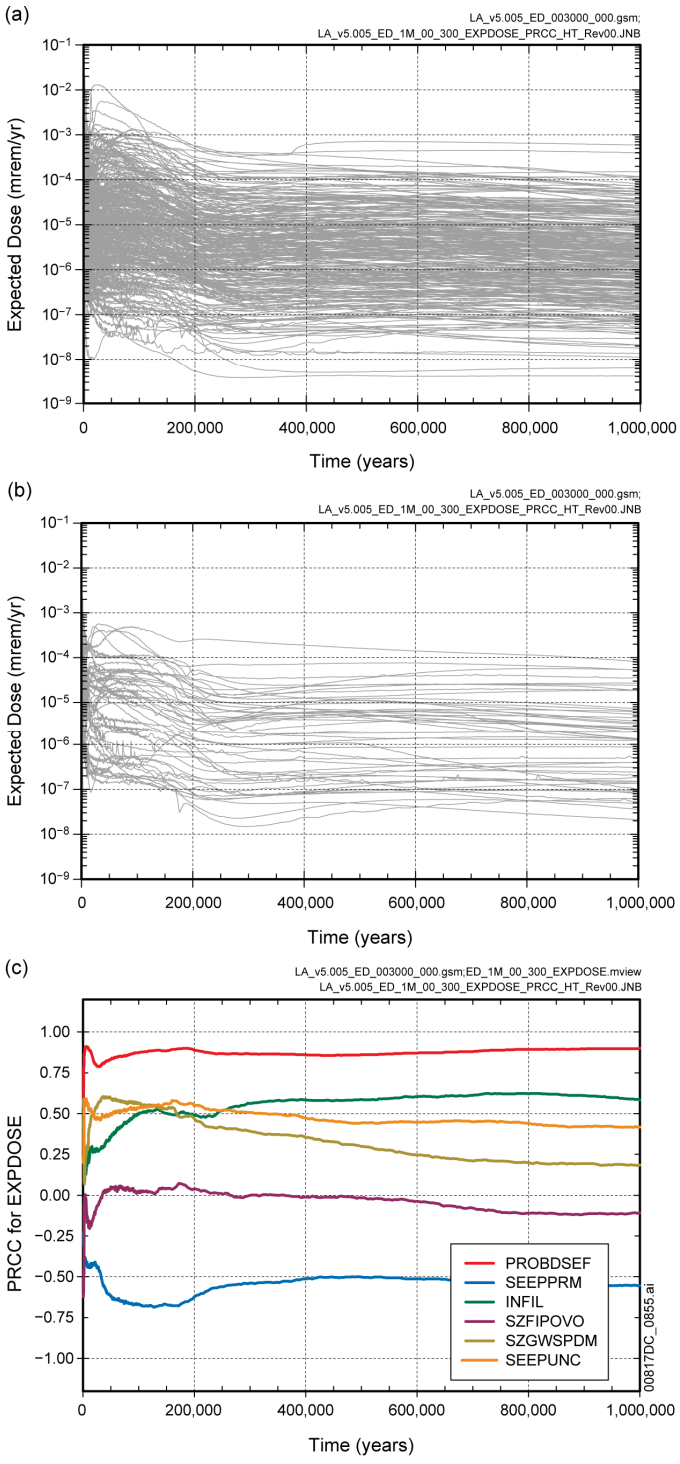


Source: Output DTNs: MO0710ADTSPAWO.000 [DIRS 183752]; and MO0710PLOTSFIG.000 [DIRS 185207].

Figure K5.7.1-3[a]. Expected dose to RMEI (*EXPDOSE*, mrem/yr) over [0, 1,000,000 yr] for all radioactive species resulting from early DS failure obtained with version 5.005 of the TSPA-LA Model: (a) *EXPDOSE* for all (i.e., 300) sample elements, (b) *EXPDOSE* for first 50 sample elements, and (c) PRCCs for *EXPDOSE*

(a)

| | EXPDOSE: 50,000 Years | | | EXPDOSE: 200,000 Years | | | EXPDOSE: 500,000 Years | | |
|---|---|---|---|---|---|---|---|---|---|
| Step[a] | Variable[b] | $R^{2c}$ | SRRC[d] | Variable | $R^2$ | SRRC | Variable | $R^2$ | SRRC |
| 1 | PROBDSEF | 0.47 | 0.71 | PROBDSEF | 0.55 | 0.76 | PROBDSEF | 0.52 | 0.73 |
| 2 | SZGWSPDM | 0.55 | 0.29 | INFIL | 0.63 | 0.26 | INFIL | 0.63 | 0.31 |
| 3 | INFIL | 0.64 | 0.28 | SEEPPRM | 0.68 | −0.23 | SEEPPRM | 0.68 | −0.21 |
| 4 | SEEPPRM | 0.69 | −0.26 | SZGWSPDM | 0.72 | 0.21 | EP1LOWPU | 0.71 | 0.18 |
| 5 | EP1LOWPU | 0.73 | 0.20 | SEEPUNC | 0.77 | 0.23 | SEEPUNC | 0.75 | 0.20 |
| 6 | SEEPUNC | 0.77 | 0.20 | EP1LOWPU | 0.79 | 0.15 | SZGWSPDM | 0.78 | 0.15 |
| 7 | MICPU239 | 0.78 | 0.10 | MICPU239 | 0.80 | 0.13 | GOESITED | 0.79 | −0.12 |
| 8 | SEEPPRMN | 0.78 | −0.08 | GOESITED | 0.82 | −0.11 | MICPU239 | 0.81 | 0.11 |
| 9 | SZCOLRAL | 0.79 | −0.10 | SEEPPRMN | 0.82 | −0.07 | PHCSS | 0.82 | 0.11 |
| 10 | PHCSS | 0.80 | −0.08 | HFOSA | 0.83 | −0.09 | SEEPPRMN | 0.82 | −0.08 |
| 11 | SZDIFCVO | 0.81 | −0.10 | SZFISPVO | 0.84 | 0.10 | EP1LOWNU | 0.83 | 0.11 |
| 12 | SZFISPVO | 0.81 | 0.10 | SZDIFCVO | 0.84 | −0.09 | ALPHAL | 0.84 | −0.10 |
| 13 | ALPHAL | 0.82 | −0.07 | ALPHAL | 0.85 | −0.09 | UZFAG4 | 0.85 | −0.07 |
| 14 | | | | EP1LOWNU | 0.85 | 0.08 | SZFISPVO | 0.85 | 0.10 |
| 15 | | | | SZCONCOL | 0.86 | 0.07 | SZDIFCVO | 0.86 | −0.09 |
| 16 | | | | SZCOLRVO | 0.86 | 0.06 | HFOSA | 0.87 | −0.08 |

a: Steps in stepwise rank regression analysis
b: Variables listed in order of selection in stepwise regression
c: Cumulative $R^2$ value with entry of each variable into regression model
d: Standardized rank regression coefficients (SRRCs) in final regression model

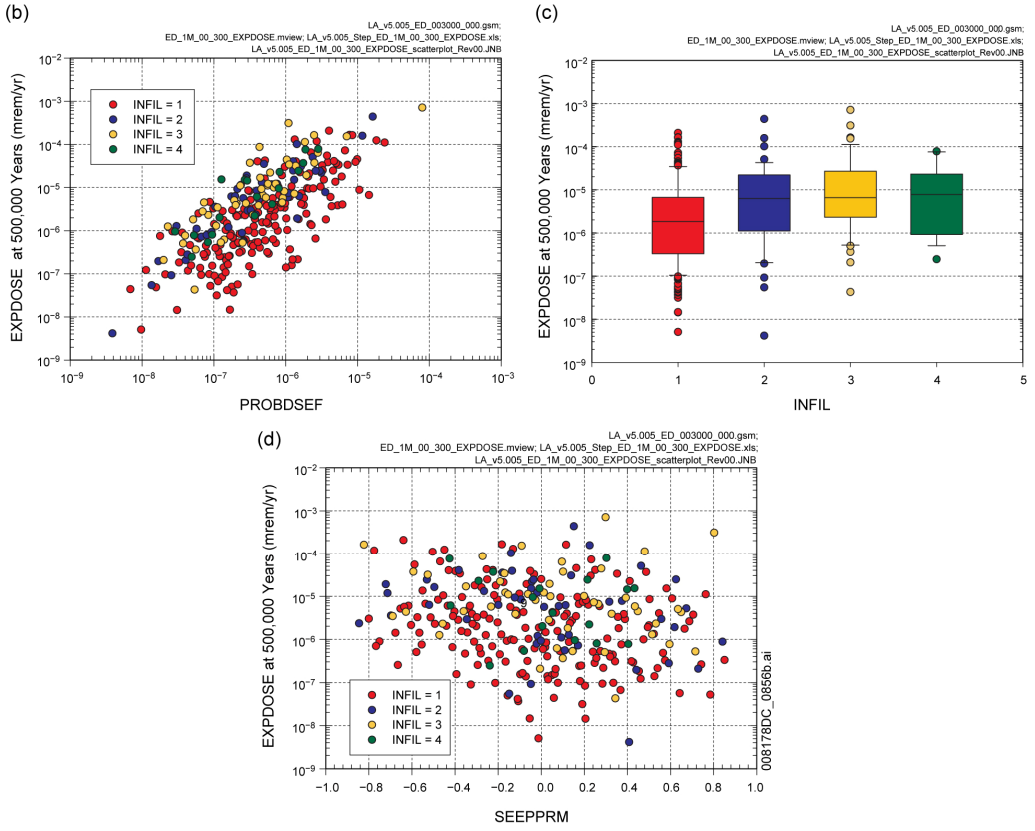


Source: Output DTNs: MO0710ADTSPAWO.000 [DIRS 183752]; and MO0710PLOTSFIG.000 [DIRS 185207].

NOTE: In (c), the box extends from 0.25 to 0.75 quantile; lower and upper bar and whisker extend to 0.1 and 0.9 quantile, respectively; dots represent values outside 0.1 to 0.9 quantile range; median indicated by light horizontal line.

Figure K5.7.1-4[a]. Stepwise rank regression analyses and selected scatterplots for expected dose to RMEI (*EXPDOSE*, mrem/yr) over [0, 1,000,000 yr] for all radioactive species resulting from early DS failure obtained with version 5.005 of the TSPA-LA Model: (a) regressions for *EXPDOSE* at 50,000, 200,000, and 500,000 years, and (b,c,d) scatterplots for *EXPDOSE* at 500,000 years

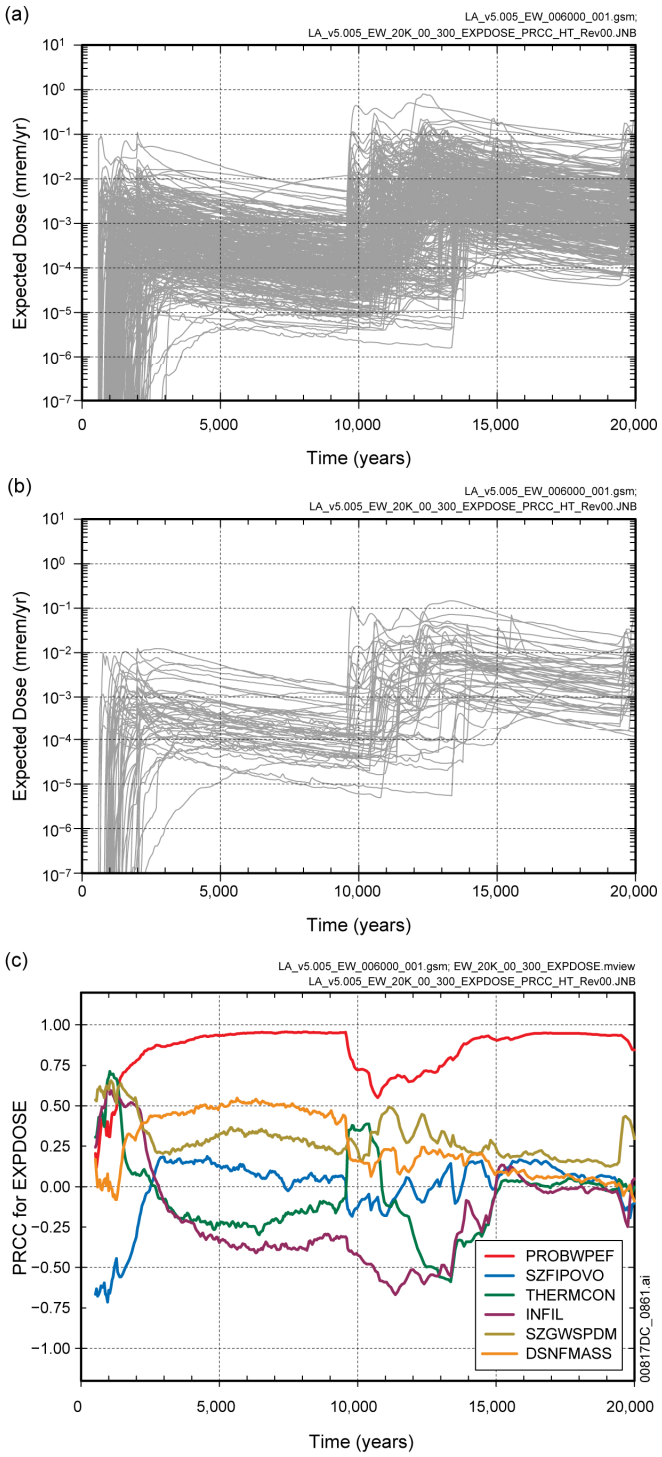


Source: Output DTNs: MO0710ADTSPAWO.000 [DIRS 183752]; and MO0710PLOTSFIG.000 [DIRS 185207].

Figure K5.7.2-1[a]. Expected dose to RMEI (*EXPDOSE*, mrem/yr) over [0, 20,000 yr] for all radioactive species resulting from early WP failure obtained with version 5.005 of the TSPA-LA Model: (a) *EXPDOSE* for all (i.e., 300) sample elements, (b) *EXPDOSE* for first 50 sample elements, and (c) PRCCs for *EXPDOSE*

(a)

| | EXPDOSE: 3,000 Years | | | EXPDOSE: 5,000 Years | | | EXPDOSE: 10,000 Years | | |
|---|---|---|---|---|---|---|---|---|---|
| Step[a] | Variable[b] | $R^{2c}$ | SRRC[d] | Variable | $R^2$ | SRRC | Variable | $R^2$ | SRRC |
| 1 | PROBWPEF | 0.62 | 0.76 | PROBWPEF | 0.77 | 0.86 | PROBWPEF | 0.47 | 0.69 |
| 2 | MICTC99 | 0.67 | 0.22 | MICTC99 | 0.81 | 0.16 | INFIL | 0.57 | −0.30 |
| 3 | MICC14 | 0.70 | 0.16 | DSNFMASS | 0.83 | 0.18 | THERMCON | 0.64 | 0.26 |
| 4 | DSNFMASS | 0.72 | 0.17 | MICC14 | 0.85 | 0.14 | MICCI36 | 0.66 | 0.10 |
| 5 | UZFAG8 | 0.74 | −0.13 | UZFAG8 | 0.86 | −0.10 | EP1LOWPU | 0.67 | 0.10 |
| 6 | SZFISPVO | 0.75 | 0.13 | HLWDRACD | 0.87 | 0.08 | MICTC99 | 0.68 | 0.12 |
| 7 | HLWDRACD | 0.76 | 0.09 | INFIL | 0.87 | −0.09 | SZSREG1Y | 0.69 | −0.10 |
| 8 | UZTORRG3 | 0.77 | 0.11 | HLWDRALK | 0.88 | 0.06 | DSNFMASS | 0.69 | 0.09 |
| 9 | SZGWSPDM | 0.78 | 0.10 | MICNP237 | 0.88 | 0.07 | SEEPPRM | 0.70 | 0.09 |
| 10 | SZDIFCVO | 0.79 | −0.08 | THERMCON | 0.88 | −0.06 | KDSNCOL | 0.71 | 0.09 |
| 11 | UZGAM | 0.80 | −0.08 | PH2DHLNS | 0.89 | −0.06 | | | |
| 12 | | | | UZGAM | 0.89 | −0.06 | | | |
| 13 | | | | RHMUN65 | 0.89 | −0.05 | | | |

a: Steps in stepwise rank regression analysis
b: Variables listed in order of selection in stepwise regression
c: Cumulative $R^2$ value with entry of each variable into regression model
d: Standardized rank regression coefficients (SRRCs) in final regression model

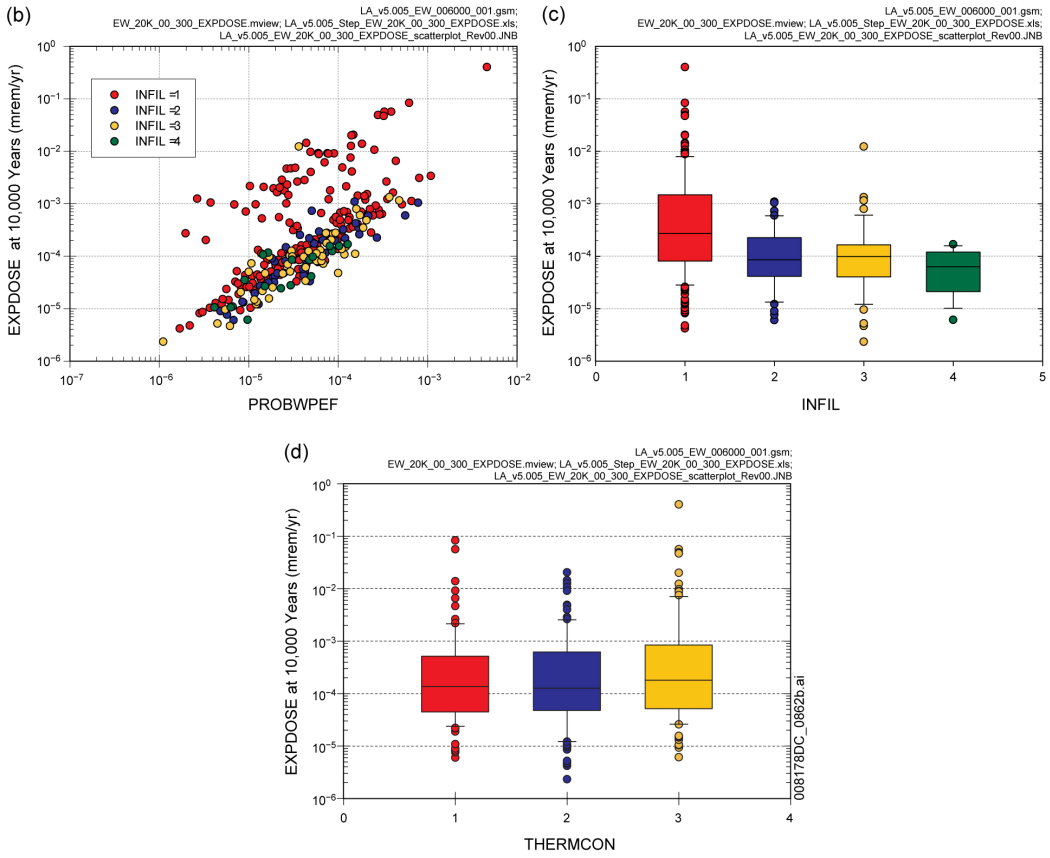


Source: Output DTNs: MO0710ADTSPAWO.000 [DIRS 183752]; and MO0710PLOTSFIG.000 [DIRS 185207].

NOTE: In (c,d), the box extends from 0.25 to 0.75 quantile; lower and upper bar and whisker extend to 0.1 and 0.9 quantile, respectively; dots represent values outside 0.1 to 0.9 quantile range; median indicated by light horizontal line.

Figure K5.7.2-2[a]. Stepwise rank regression analyses and selected scatterplots for expected dose to RMEI (*EXPDOSE*, mrem/yr) over [0, 20,000 yr] for all radioactive species resulting from early WP failure obtained with version 5.005 of the TSPA-LA Model: (a) regressions for *EXPDOSE* at 3,000, 5,000, and 10,000 years, and (b,c,d) scatterplots for *EXPDOSE* at 10,000 years

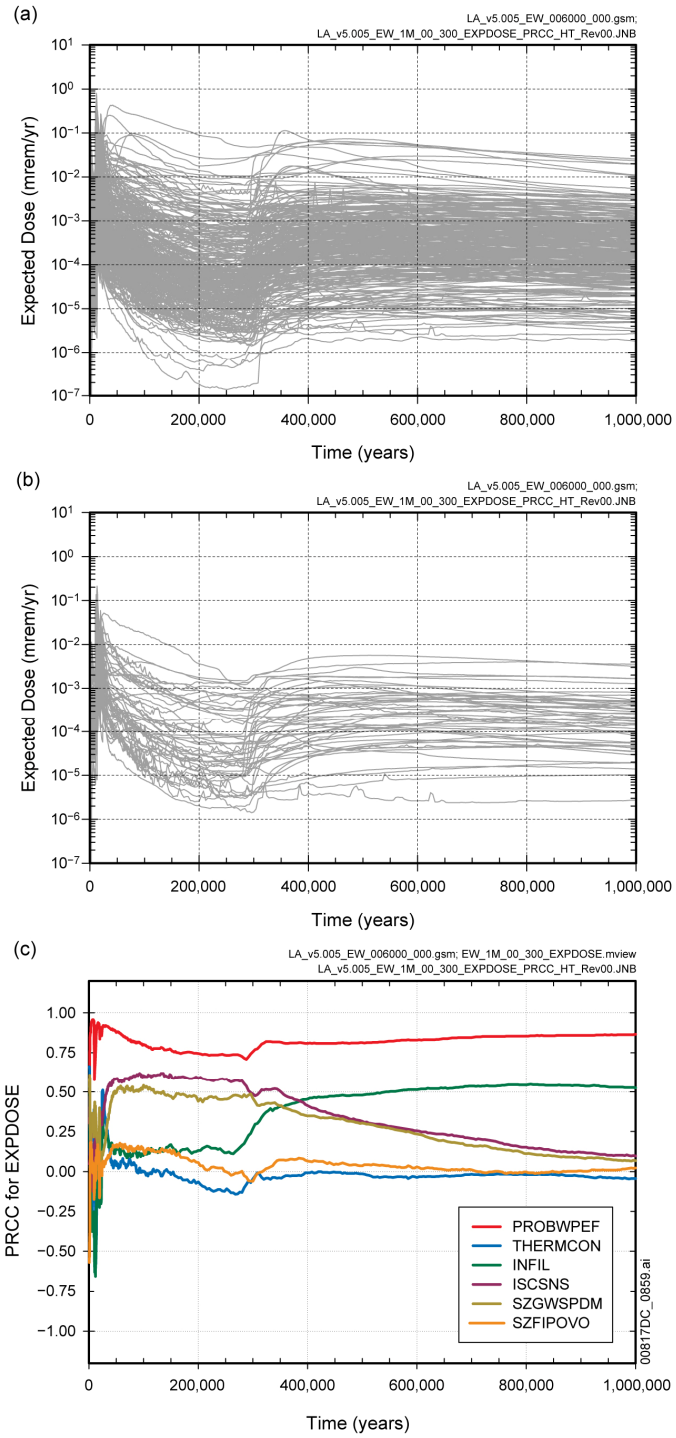


Source: Output DTNs: MO0710ADTSPAWO.000 [DIRS 183752]; and MO0710PLOTSFIG.000 [DIRS 185207].

Figure K5.7.2-3[a]. Expected dose to RMEI (*EXPDOSE*, mrem/yr) over [0, 1,000,000 yr] for all radioactive species resulting from early WP failure obtained with version 5.005 of the TSPA-LA Model: (a) *EXPDOSE* for all (i.e., 300) sample elements, (b) *EXPDOSE* for first 50 sample elements, and (c) PRCCs for *EXPDOSE*

(a)

| | EXPDOSE: 50,000 Years | | | EXPDOSE: 200,000 Years | | | EXPDOSE: 500,000 Years | | |
|---|---|---|---|---|---|---|---|---|---|
| Step[a] | Variable[b] | $R^{2c}$ | SRRC[d] | Variable | $R^2$ | SRRC | Variable | $R^2$ | SRRC |
| 1 | PROBWPEF | 0.60 | 0.79 | PROBWPEF | 0.37 | 0.62 | PROBWPEF | 0.39 | 0.70 |
| 2 | ISCSNS | 0.66 | 0.25 | ISCSNS | 0.50 | 0.38 | INFIL | 0.51 | 0.31 |
| 3 | SZGWSPDM | 0.72 | 0.22 | SZGWSPDM | 0.56 | 0.24 | EP1LOWPU | 0.55 | 0.20 |
| 4 | EP1LOWPU | 0.74 | 0.14 | EP1LOWPU | 0.58 | 0.15 | SEEPPRM | 0.59 | −0.22 |
| 5 | MICNP237 | 0.75 | 0.10 | SZFISPVO | 0.60 | 0.17 | SZGWSPDM | 0.62 | 0.17 |
| 6 | SZFISPVO | 0.75 | 0.08 | SZDIFCVO | 0.61 | −0.14 | SEEPUNC | 0.65 | 0.19 |
| 7 | SZKDSRAL | 0.76 | 0.09 | IGRATE | 0.63 | 0.10 | EP1LOWNU | 0.67 | 0.17 |
| 8 | COLU | 0.77 | 0.08 | SEEPPRM | 0.64 | −0.11 | ALPHAL | 0.69 | −0.14 |
| 9 | | | | SEEPUNC | 0.65 | 0.10 | SZFISPVO | 0.71 | 0.15 |
| 10 | | | | RHMU20 | 0.66 | 0.10 | GOESITED | 0.73 | −0.14 |
| 11 | | | | | | | HFOSA | 0.74 | −0.12 |
| 12 | | | | | | | MICPU239 | 0.75 | 0.11 |
| 13 | | | | | | | SZDIFCVO | 0.76 | −0.10 |
| 14 | | | | | | | SEEPPRMN | 0.77 | −0.09 |
| 15 | | | | | | | ISCSNS | 0.77 | 0.09 |
| 16 | | | | | | | HFOSITED | 0.78 | −0.08 |

a: Steps in stepwise rank regression analysis
b: Variables listed in order of selection in stepwise regression
c: Cumulative $R^2$ value with entry of each variable into regression model
d: Standardized rank regression coefficients (SRRCs) in final regression model

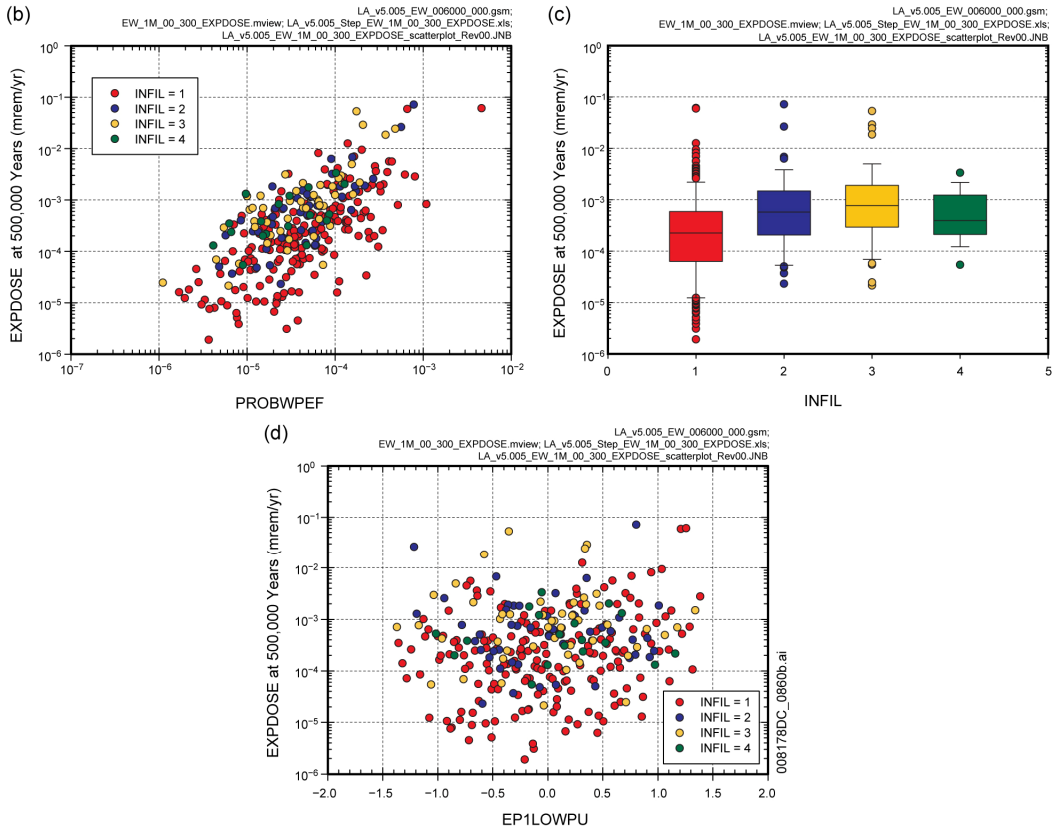


Source: Output DTNs: MO0710ADTSPAWO.000 [DIRS 183752]; and MO0710PLOTSFIG.000 [DIRS 185207].

NOTE: In (c), the box extends from 0.25 to 0.75 quantile; lower and upper bar and whisker extend to 0.1 and 0.9 quantile, respectively; dots represent values outside 0.1 to 0.9 quantile range; median indicated by light horizontal line.

Figure K5.7.2-4[a]. Stepwise rank regression analyses and selected scatterplots for expected dose to RMEI (*EXPDOSE*, mrem/yr) over [0, 1,000,000 yr] for all radioactive species resulting from early WP failure obtained with version 5.005 of the TSPA-LA Model: (a) regressions for *EXPDOSE* at 50,000, 200,000, and 500,000 years, and (b,c,d) scatterplots for *EXPDOSE* at 500,000 years

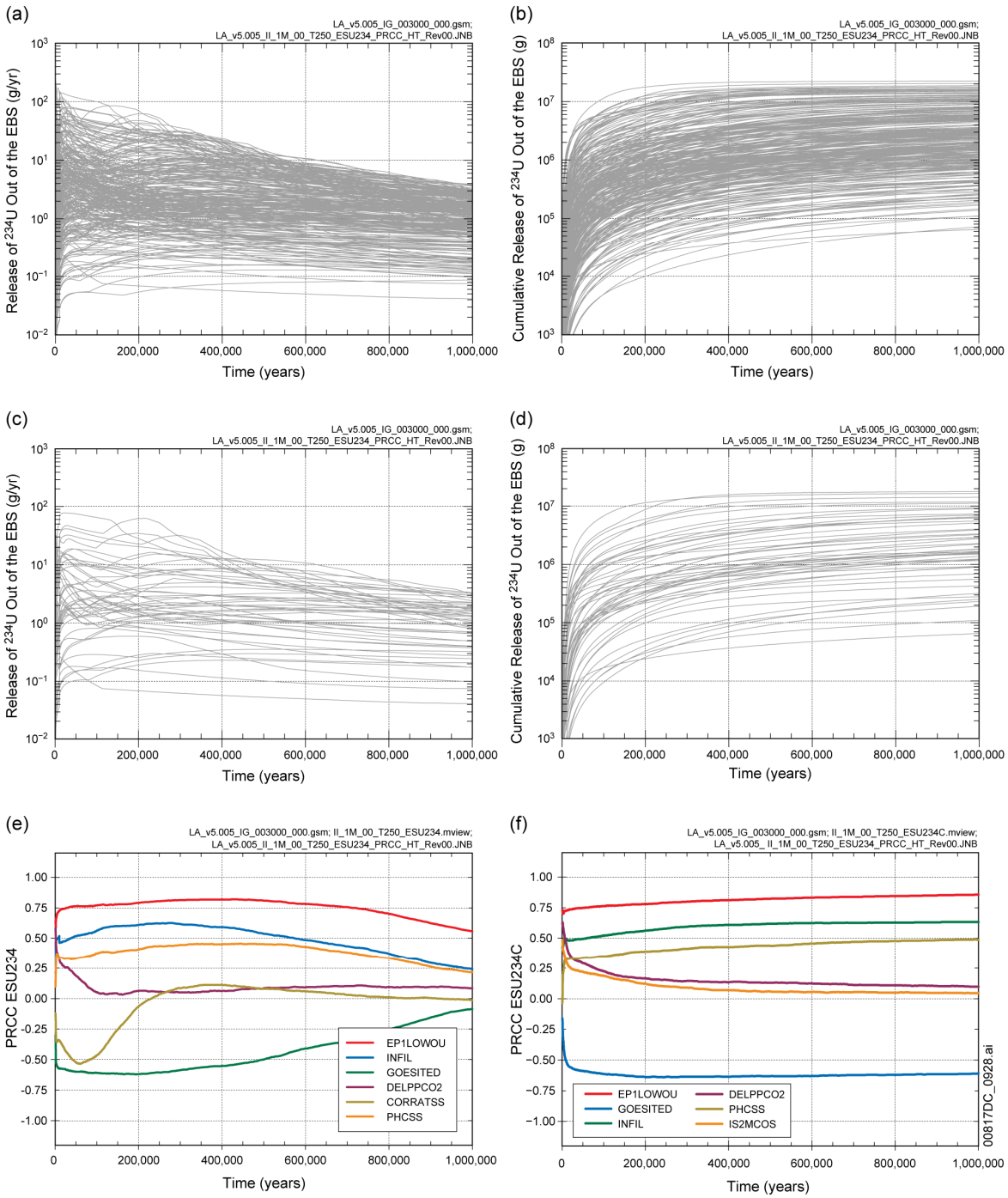


Source: Output DTNs: MO0801TSPAPRSA.000 [DIRS 184620]; and MO0710PLOTSFIG.000 [DIRS 185207].

Figure K6.3.2-5[a]. Time-dependent release rates (*ESU234*, g/yr) and cumulative (i.e., integrated) releases (*ESU234C*, g) over 1,000,000 years for the movement of dissolved $^{234}U$ from the EBS to the UZ resulting from an igneous intrusive event at 250 years that destroys all WPs in the repository obtained with version 5.005 of the TSPA-LA Model: (a,b) *ESU234* and *ESU234C* for all (i.e., 300) sample elements, (c,d) *ESU234* and *ESU234C* for first 50 sample elements, and (e,f) PRCCs for *ESU234* and *ESU234C*

(a)

| | ESU234: 50,000 Years | | | ESU234: 200,000 Years | | | ESU234: 500,000 Years | | |
|---|---|---|---|---|---|---|---|---|---|
| Step[a] | Variable[b] | $R^2$ [c] | SRRC[d] | Variable | $R^2$ | SRRC | Variable | $R^2$ | SRRC |
| 1 | EP1LOWOU | 0.38 | 0.56 | EP1LOWOU | 0.41 | 0.60 | EP1LOWOU | 0.49 | 0.68 |
| 2 | INFIL | 0.49 | 0.33 | INFIL | 0.58 | 0.39 | INFIL | 0.64 | 0.38 |
| 3 | GOESITED | 0.57 | −0.29 | GOESITED | 0.66 | −0.32 | PHCSS | 0.69 | 0.22 |
| 4 | CORRATSS | 0.64 | −0.30 | HFOSA | 0.70 | −0.20 | GOESITED | 0.73 | −0.23 |
| 5 | HFOSA | 0.67 | −0.19 | PHCSS | 0.73 | 0.19 | HFOSA | 0.75 | −0.14 |
| 6 | GOERELAB | 0.69 | 0.12 | DSNFMASS | 0.75 | 0.12 | CSNFMASS | 0.77 | 0.13 |
| 7 | DSNFMASS | 0.71 | 0.12 | GOERELAB | 0.76 | 0.13 | GOERELAB | 0.78 | 0.12 |
| 8 | PHCSS | 0.72 | 0.16 | GOESA | 0.77 | −0.09 | WDLCRATE | 0.79 | −0.11 |
| 9 | IS2MCOS | 0.74 | 0.13 | CSNFMASS | 0.77 | 0.08 | PROBWPEF | 0.80 | 0.09 |
| 10 | CSNFMASS | 0.75 | 0.12 | HFOSITED | 0.78 | −0.08 | | | |
| 11 | KDPUCOL | 0.76 | 0.09 | IS2MCONS | 0.79 | 0.07 | | | |
| 12 | GOESA | 0.77 | −0.08 | WDDSGC29 | 0.79 | 0.08 | | | |
| 13 | DELPPCO2 | 0.76 | 0.08 | | | | | | |

(b)

| | ESU234C: 50,000 Years | | | ESU234C: 200,000 Years | | | ESU234C: 500,000 Years | | |
|---|---|---|---|---|---|---|---|---|---|
| Step[a] | Variable[b] | $R^2$ [c] | SRRC[d] | Variable | $R^2$ | SRRC | Variable | $R^2$ | SRRC |
| 1 | EP1LOWOU | 0.37 | 0.56 | EP1LOWOU | 0.40 | 0.58 | EP1LOWOU | 0.45 | 0.62 |
| 2 | INFIL | 0.48 | 0.34 | INFIL | 0.53 | 0.36 | INFIL | 0.61 | 0.38 |
| 3 | GOESITED | 0.55 | −0.29 | GOESITED | 0.62 | −0.30 | GOESITED | 0.68 | −0.29 |
| 4 | CORRATSS | 0.60 | −0.25 | HFOSA | 0.65 | −0.19 | HFOSA | 0.72 | −0.20 |
| 5 | PHCSS | 0.63 | 0.19 | CORRATSS | 0.68 | −0.21 | PHCSS | 0.75 | 0.21 |
| 6 | IS2MCOS | 0.65 | 0.16 | PHCSS | 0.71 | 0.18 | GOERELAB | 0.77 | 0.13 |
| 7 | HFOSA | 0.67 | −0.17 | DSNFMASS | 0.73 | 0.12 | DSNFMASS | 0.78 | 0.10 |
| 8 | DELPPCO2 | 0.69 | 0.12 | GOERELAB | 0.74 | 0.13 | GOESA | 0.79 | −0.08 |
| 9 | CSNFMASS | 0.70 | 0.14 | GOESA | 0.75 | −0.09 | CSNFMASS | 0.80 | 0.11 |
| 10 | GOERELAB | 0.71 | 0.11 | KDPUCOL | 0.76 | 0.09 | KDPUCOL | 0.80 | 0.08 |
| 11 | GOESA | 0.72 | −0.09 | CSNFMASS | 0.77 | 0.10 | CORRATSS | 0.81 | −0.08 |
| 12 | DSNFMASS | 0.73 | 0.09 | IS2MCOS | 0.78 | 0.09 | HFOSITED | 0.81 | −0.07 |
| 13 | CPUPERCS | 0.74 | −0.08 | | | | | | |
| 14 | RHMUN40 | 0.75 | −0.08 | | | | | | |
| 15 | KDPUCOL | 0.75 | 0.08 | | | | | | |

a: Steps in stepwise rank regression analysis
b: Variables listed in order of selection in stepwise regression
c: Cumulative $R^2$ value with entry of each variable into regression model
d: Standardized rank regression coefficients (SRRCs) in final regression model

00817DC_0929a.ai

Source: Output DTNs: MO0801TSPAPRSA.000 [DIRS 184620]; and MO0710PLOTSFIG.000 [DIRS 185207].

Figure K6.3.2-6[a]. Stepwise rank regression analyses and selected scatterplots for time-dependent release rates (*ESU234*, g/yr) and cumulative (i.e., integrated) releases (*ESU234C*, g) for the movement of dissolved $^{234}U$ from the EBS to the UZ resulting from an igneous intrusive event at 250 years that destroys all WPs in the repository obtained with version 5.005 of the TSPA-LA Model: (a,b) regressions for *ESU234* and *ESU234C* at 50,000, 200,000, and 500,000 years, and (c-h) scatterplots for *ESU234* and *ESU234C* at 500,000 years

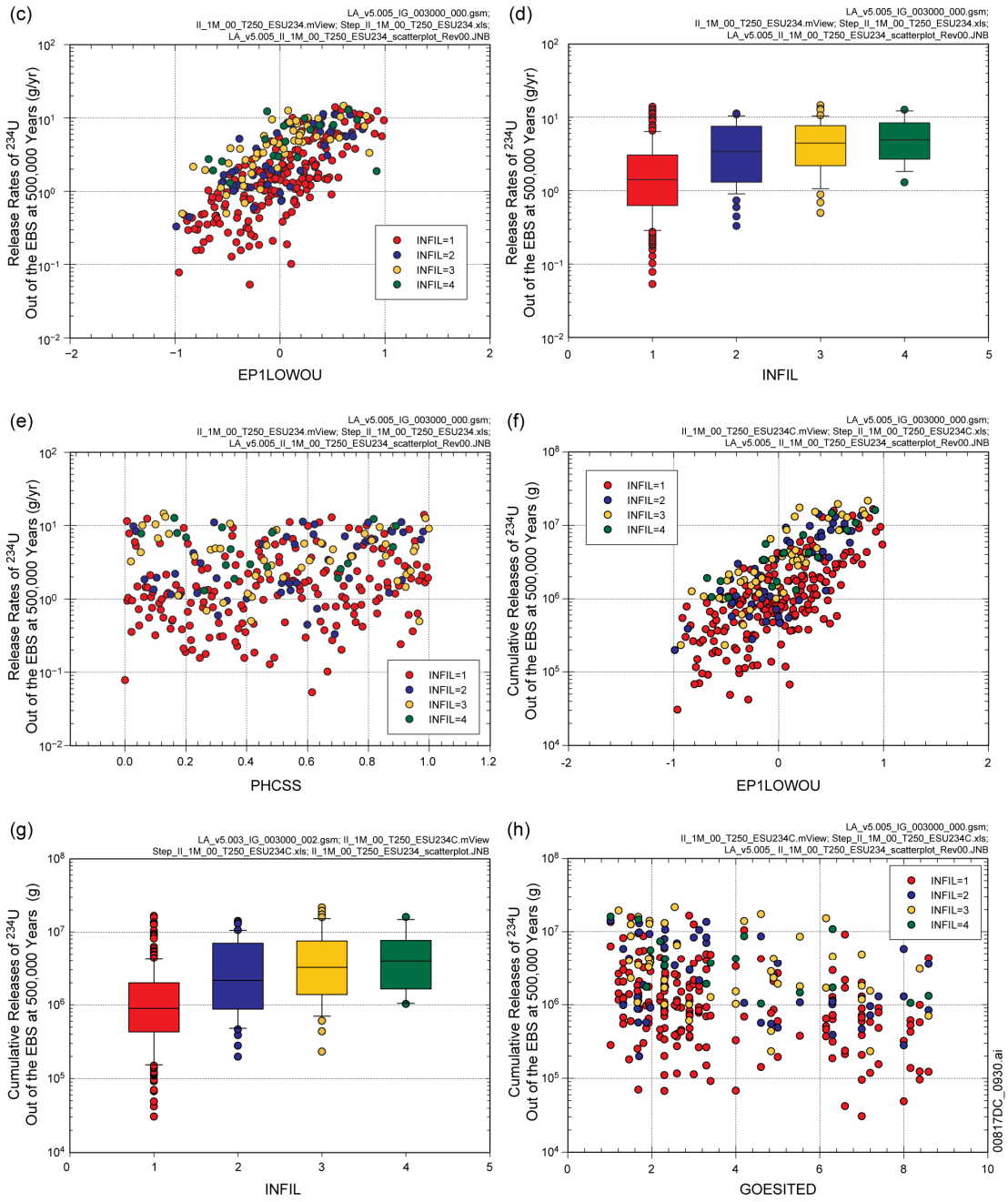


Source: Output DTNs: MO0801TSPAPRSA.000 [DIRS 184620]; and MO0710PLOTSFIG.000 [DIRS 185207].

NOTE: In (d,g), the box extends from 0.25 to 0.75 quantile; lower and upper bar and whisker extend to 0.1 and 0.9 quantile, respectively; dots represent values outside 0.1 to 0.9 quantile range; median indicated by light horizontal line.

Figure K6.3.2-6[a]. Stepwise rank regression analyses and selected scatterplots for time-dependent release rates (*ESU234*, g/yr) and cumulative (i.e., integrated) releases (*ESU234C*, g) for the movement of dissolved $^{234}$U from the EBS to the UZ resulting from an igneous intrusive event at 250 years that destroys all WPs in the repository obtained with version 5.005 of the TSPA-LA Model: (a,b) regressions for *ESU234* and *ESU234C* at 50,000, 200,000, and 500,000 years, and (c-h) scatterplots for *ESU234* and *ESU234C* at 500,000 years (continued)

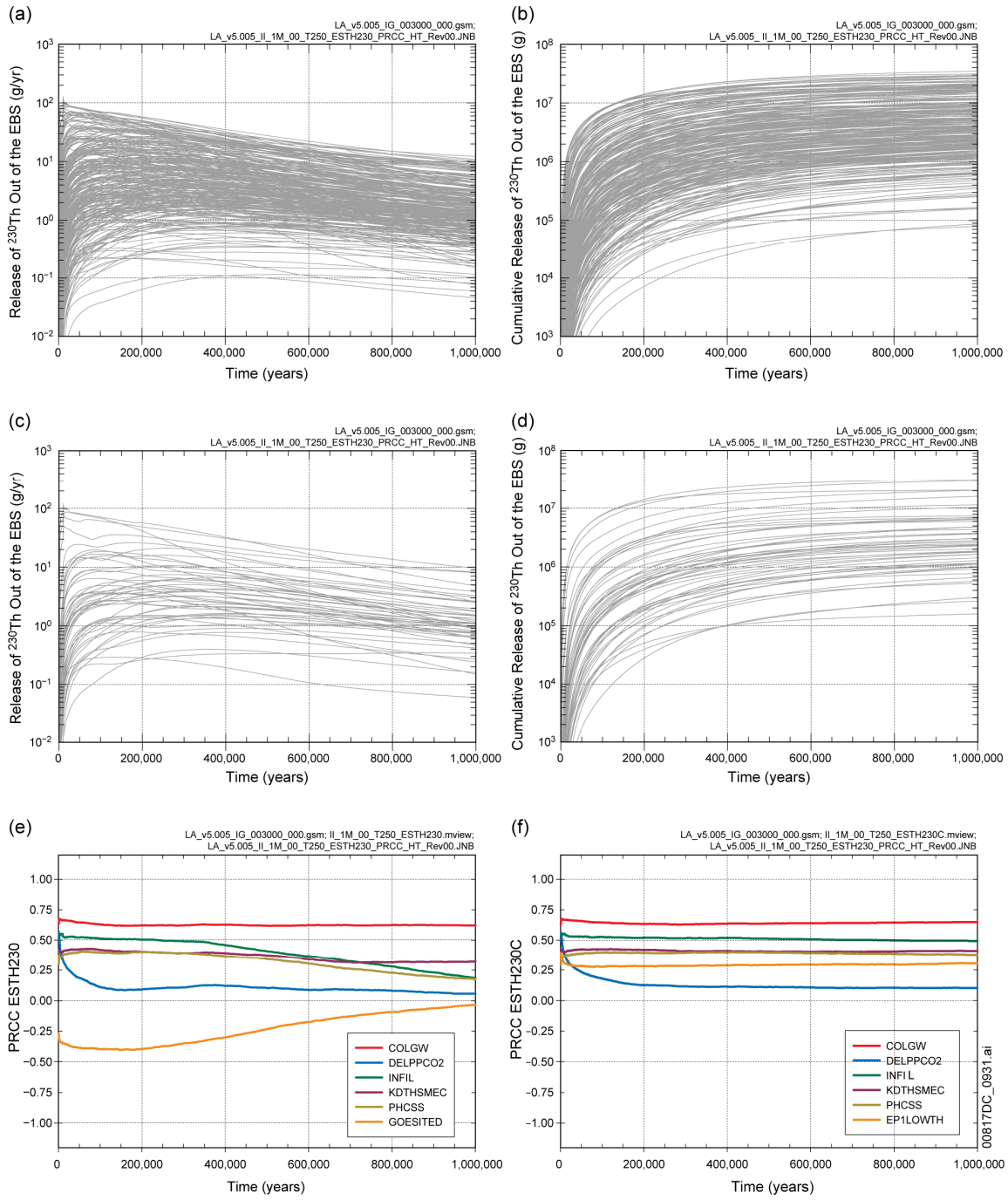


Source: Output DTNs: MO0801TSPAPRSA.000 [DIRS 184620]; and MO0710PLOTSFIG.000 [DIRS 185207].

Figure K6.3.2-7[a]. Time-dependent release rates (*ESTH230*, g/yr) and cumulative (i.e., integrated) releases (*ESTH230C*, g) over 1,000,000 years for the movement of dissolved $^{230}$Th from the EBS to the UZ resulting from an igneous intrusive event at 250 years that destroys all WPs in the repository obtained with version 5.005 of the TSPA-LA Model: (a,b) *ESTH230* and *ESTH230C* for all (i.e., 300) sample elements, (c,d) *ESTH230* and *ESTH230C* for first 50 sample elements, and (e,f) PRCCs for *ESTH230* and *ESTH230C*

(a)

| | ESTH230: 50,000 Years | | | ESTH230: 200,000 Years | | | ESTH230: 500,000 Years | | |
|---|---|---|---|---|---|---|---|---|---|
| Step[a] | Variable[b] | $R^{2\,c}$ | SRRC[d] | Variable | $R^2$ | SRRC | Variable | $R^2$ | SRRC |
| 1 | INFIL | 0.24 | 0.43 | INFIL | 0.25 | 0.43 | COLGW | 0.23 | 0.45 |
| 2 | COLGW | 0.42 | 0.43 | COLGW | 0.41 | 0.42 | INFIL | 0.38 | 0.36 |
| 3 | KDTHSMEC | 0.51 | 0.27 | KDTHSMEC | 0.51 | 0.29 | KDTHSMEC | 0.49 | 0.30 |
| 4 | PHCSS | 0.55 | 0.24 | PHCSS | 0.56 | 0.24 | PHCSS | 0.52 | 0.21 |
| 5 | EP1LOWTH | 0.59 | 0.22 | EP1LOWTH | 0.59 | 0.21 | EP1LOWTH | 0.56 | 0.21 |
| 6 | UZKDTHDT | 0.62 | −0.20 | EP1LOWOU | 0.62 | 0.15 | UZKDTHDT | 0.59 | −0.17 |
| 7 | CORRATSS | 0.66 | −0.17 | UZKDTHDT | 0.65 | −0.17 | CSNFMASS | 0.61 | 0.15 |
| 8 | GOESITED | 0.68 | −0.13 | GOESITED | 0.67 | −0.17 | HFOSA | 0.62 | −0.11 |
| 9 | EP1LOWOU | 0.69 | 0.12 | HFOSA | 0.68 | −0.12 | FHHISSCP | 0.63 | 0.10 |
| 10 | HLWMASS | 0.70 | 0.10 | GOESA | 0.69 | −0.09 | GOESITED | 0.64 | −0.10 |
| 11 | | | | | | | RUBMAXL | 0.65 | 0.09 |

(b)

| | ESTH230C: 50,000 Years | | | ESTH230C: 200,000 Years | | | ESTH230C: 500,000 Years | | |
|---|---|---|---|---|---|---|---|---|---|
| Step[a] | Variable[b] | $R^{2\,c}$ | SRRC[d] | Variable | $R^2$ | SRRC | Variable | $R^2$ | SRRC |
| 1 | INFIL | 0.24 | 0.43 | INFIL | 0.25 | 0.44 | INFIL | 0.25 | 0.43 |
| 2 | COLGW | 0.43 | 0.45 | COLGW | 0.42 | 0.43 | COLGW | 0.43 | 0.43 |
| 3 | KDTHSMEC | 0.51 | 0.27 | KDTHSMEC | 0.51 | 0.29 | KDTHSMEC | 0.52 | 0.28 |
| 4 | PHCSS | 0.56 | 0.24 | PHCSS | 0.56 | 0.23 | PHCSS | 0.57 | 0.22 |
| 5 | EP1LOWTH | 0.60 | 0.22 | EP1LOWTH | 0.60 | 0.22 | EP1LOWTH | 0.61 | 0.21 |
| 6 | UZKDTHDT | 0.63 | −0.22 | UZKDTHDT | 0.62 | −0.18 | UZKDTHDT | 0.63 | −0.17 |
| 7 | CORRATSS | 0.66 | −0.16 | EP1LOWOU | 0.65 | 0.14 | EP1LOWOU | 0.66 | 0.14 |
| 8 | GOESITED | 0.68 | −0.13 | CORRATSS | 0.67 | −0.13 | GOESITED | 0.67 | −0.15 |
| 9 | EP1LOWOU | 0.69 | 0.12 | GOESITED | 0.69 | −0.15 | HFOSA | 0.69 | −0.12 |
| 10 | DELPPCO2 | 0.70 | 0.12 | HFOSA | 0.69 | −0.10 | | | |
| 11 | HLWMASS | 0.71 | 0.10 | HLWMASS | 0.70 | 0.09 | | | |
| 12 | HFOSA | 0.72 | −0.09 | | | | | | |

00817DC_0932a.ai

a: Steps in stepwise rank regression analysis
b: Variables listed in order of selection in stepwise regression
c: Cumulative $R^2$ value with entry of each variable into regression model
d: Standardized rank regression coefficients (SRRCs) in final regression model

Source: Output DTNs: MO0801TSPAPRSA.000 [DIRS 184620]; and MO0710PLOTSFIG.000 [DIRS 185207].

Figure K6.3.2-8[a]. Stepwise rank regression analyses and selected scatterplots for time-dependent release rates (*ESTH230*, g/yr) and cumulative (i.e., integrated) releases (*ESTH230C*, g) for the movement of dissolved $^{230}$Th from the EBS to the UZ resulting from an igneous intrusive event at 250 years that destroys all WPs in the repository obtained with version 5.005 of the TSPA-LA Model: (a,b) regressions for *ESTH230* and *ESTH230C* at 50,000, 200,000, and 500,000 years, and (c-h) scatterplots for *ESTH230* and *ESTH230C* at 200,000 years

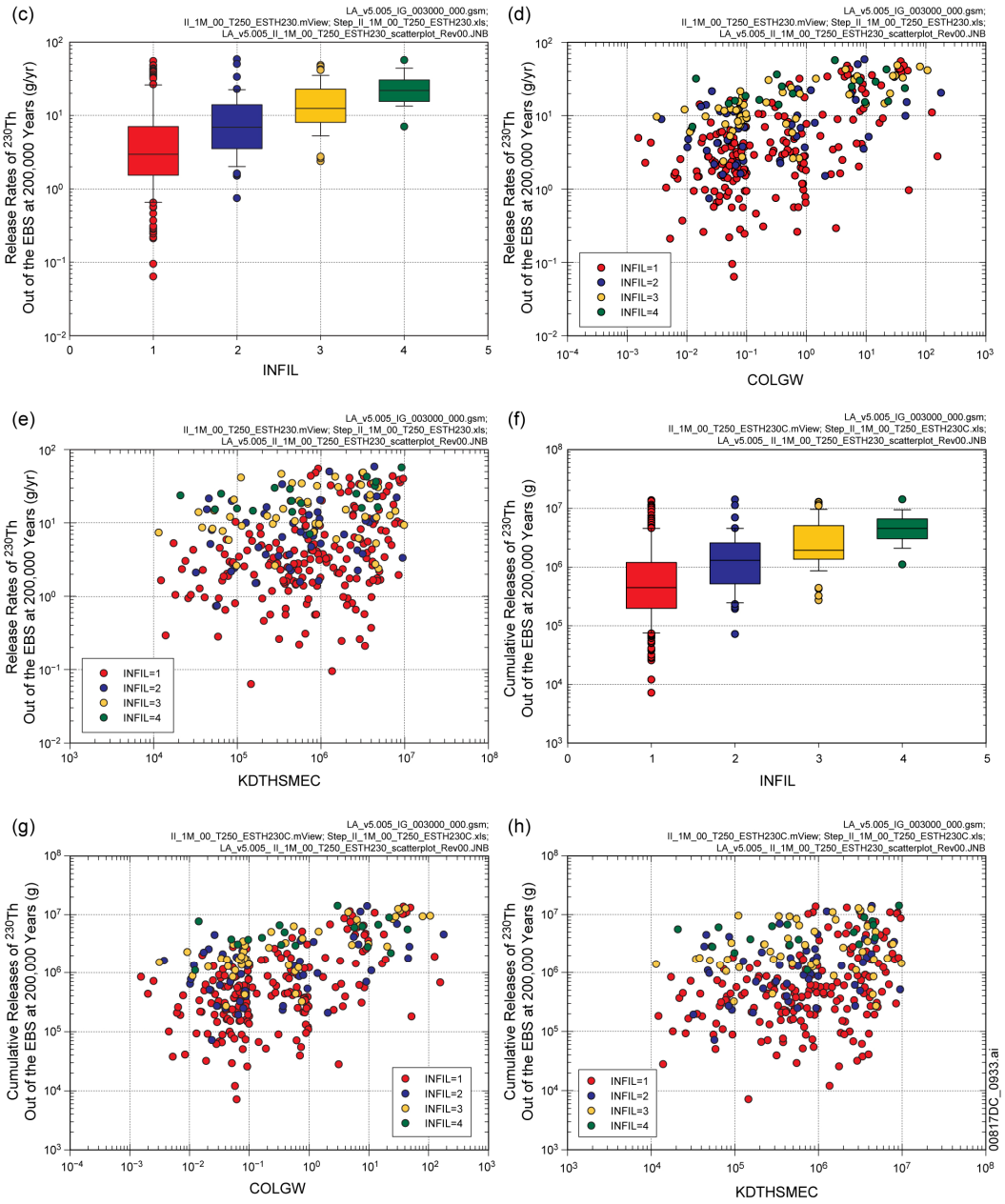


Source: Output DTNs: MO0801TSPAPRSA.000 [DIRS 184620]; and MO0710PLOTSFIG.000 [DIRS 185207].

NOTE: In (c,f), the box extends from 0.25 to 0.75 quantile; lower and upper bar and whisker extend to 0.1 and 0.9 quantile, respectively; dots represent values outside 0.1 to 0.9 quantile range; median indicated by light horizontal line.

Figure K6.3.2-8[a]. Stepwise rank regression analyses and selected scatterplots for time-dependent release rates (*ESTH230*, g/yr) and cumulative (i.e., integrated) releases (*ESTH230C*, g) for the movement of dissolved $^{230}$Th from the EBS to the UZ resulting from an igneous intrusive event at 250 years that destroys all WPs in the repository obtained with version 5.005 of the TSPA-LA Model: (a,b) regressions for *ESTH230* and *ESTH230C* at 50,000, 200,000, and 500,000 years, and (c-h) scatterplots for *ESTH230* and *ESTH230C* at 200,000 years (continued)

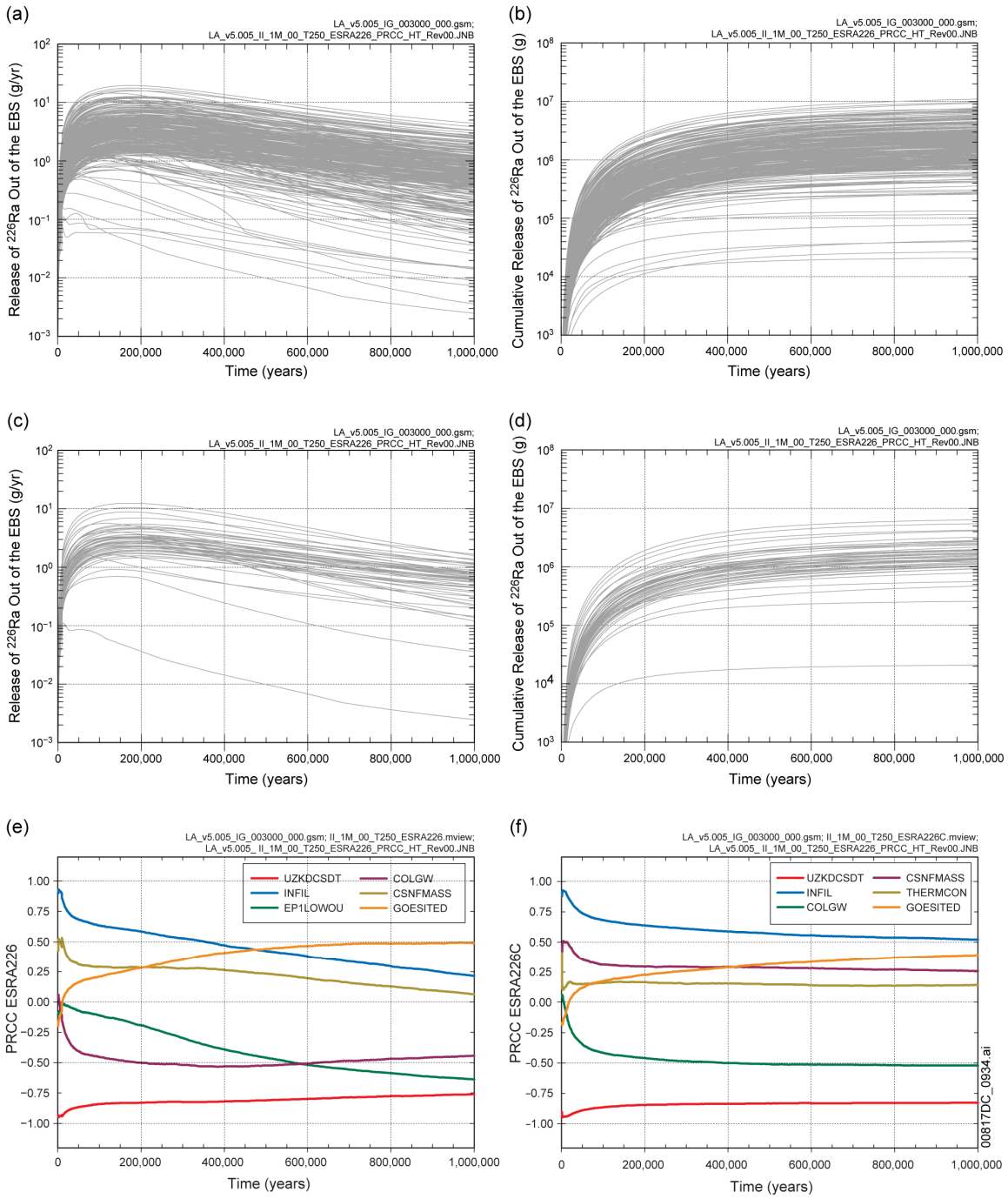


Source: Output DTNs: MO0801TSPAPRSA.000 [DIRS 184620]; and MO0710PLOTSFIG.000 [DIRS 185207].

Figure K6.3.2-9[a] Time-dependent release rates (*ESRA226*, g/yr) and cumulative (i.e., integrated) releases (*ESRA226C*, g) over 1,000,000 years for the movement of dissolved $^{226}$Ra from the EBS to the UZ resulting from an igneous intrusive event at 250 years that destroys all WPs in the repository obtained with version 5.005 of the TSPA-LA Model: (a,b) *ESRA226* and *ESRA226C* for all (i.e., 300) sample elements, (c,d) *ESRA226* and *ESRA226C* for first 50 sample elements, and (e,f) PRCCs for *ESRA226* and *ESRA226C*

(a)

| | ESRA226: 50,000 Years | | | ESRA226: 200,000 Years | | | ESRA226: 500,000 Years | | |
|---|---|---|---|---|---|---|---|---|---|
| Step[a] | Variable[b] | $R^{2c}$ | SRRC[d] | Variable | $R^2$ | SRRC | Variable | $R^2$ | SRRC |
| 1 | UZKDCSDT | 0.54 | −0.76 | UZKDCSDT | 0.50 | −0.73 | UZKDCSDT | 0.46 | −0.68 |
| 2 | INFIL | 0.71 | 0.42 | INFIL | 0.59 | 0.30 | EP1LOWOU | 0.53 | −0.29 |
| 3 | COLGW | 0.75 | −0.21 | COLGW | 0.66 | −0.27 | COLGW | 0.59 | −0.28 |
| 4 | CSNFMASS | 0.78 | 0.17 | CSNFMASS | 0.68 | 0.16 | KDTHSMEC | 0.62 | −0.16 |
| 5 | KDTHSMEC | 0.79 | −0.12 | EP1LOWOU | 0.70 | −0.16 | INFIL | 0.64 | 0.15 |
| 6 | EP1LOWOU | 0.80 | −0.09 | KDTHSMEC | 0.72 | −0.16 | PHCSS | 0.67 | −0.13 |
| 7 | KDNPSMEC | 0.80 | 0.09 | PHCSS | 0.73 | −0.09 | GOESITED | 0.69 | 0.14 |
| 8 | DSNFMASS | 0.81 | 0.09 | DSNFMASS | 0.73 | 0.09 | CSNFMASS | 0.70 | 0.13 |
| 9 | | | | KDNPSMEC | 0.74 | 0.09 | | | |

(b)

| | ESRA226C: 50,000 Years | | | ESRA226C: 200,000 Years | | | ESRA226C: 500,000 Years | | |
|---|---|---|---|---|---|---|---|---|---|
| Step[a] | Variable[b] | $R^{2c}$ | SRRC[d] | Variable | $R^2$ | SRRC | Variable | $R^2$ | SRRC |
| 1 | UZKDCSDT | 0.56 | −0.78 | UZKDCSDT | 0.52 | −0.75 | UZKDCSDT | 0.51 | −0.73 |
| 2 | INFIL | 0.77 | 0.45 | INFIL | 0.65 | 0.36 | INFIL | 0.58 | 0.28 |
| 3 | COLGW | 0.80 | −0.18 | COLGW | 0.70 | −0.25 | COLGW | 0.65 | −0.27 |
| 4 | CSNFMASS | 0.82 | 0.17 | CSNFMASS | 0.73 | 0.17 | EP1LOWOU | 0.67 | −0.18 |
| 5 | KDTHSMEC | 0.83 | −0.10 | KDTHSMEC | 0.74 | −0.14 | CSNFMASS | 0.70 | 0.16 |
| 6 | DSNFMASS | 0.84 | 0.08 | EP1LOWOU | 0.75 | −0.12 | KDTHSMEC | 0.72 | −0.15 |
| 7 | KDNPSMEC | 0.84 | 0.08 | KDNPSMEC | 0.76 | 0.10 | PHCSS | 0.73 | −0.09 |
| 8 | EP1LOWOU | 0.85 | −0.08 | DSNFMASS | 0.77 | 0.09 | GOESITED | 0.74 | 0.09 |
| 9 | CPUPERCS | 0.85 | 0.06 | | | | KDNPSMEC | 0.74 | 0.09 |
| 10 | | | | | | | DSNFMASS | 0.75 | 0.08 |

00817DC_0936a.ai

a: Steps in stepwise rank regression analysis
b: Variables listed in order of selection in stepwise regression
c: Cumulative $R^2$ value with entry of each variable into regression model
d: Standardized rank regression coefficients (SRRCs) in final regression model

Source: Output DTNs: MO0801TSPAPRSA.000 [DIRS 184620]; and MO0710PLOTSFIG.000 [DIRS 185207].

Figure K6.3.2-10[a]. Stepwise rank regression analyses and selected scatterplots for time-dependent release rates (*ESRA226*, g/yr) and cumulative (i.e., integrated) releases (*ESRA226C*, g) for the movement of dissolved $^{226}$Ra from the EBS to the UZ resulting from an igneous intrusive event at 250 years that destroys all WPs in the repository obtained with version 5.005 of the TSPA-LA Model: (a,b) regressions for *ESRA226* and *ESRA226C* at 50,000, 200,000, and 500,000 years, and (c-h) scatterplots for *ESRA226* and *ESRA226C* at 50,000 years

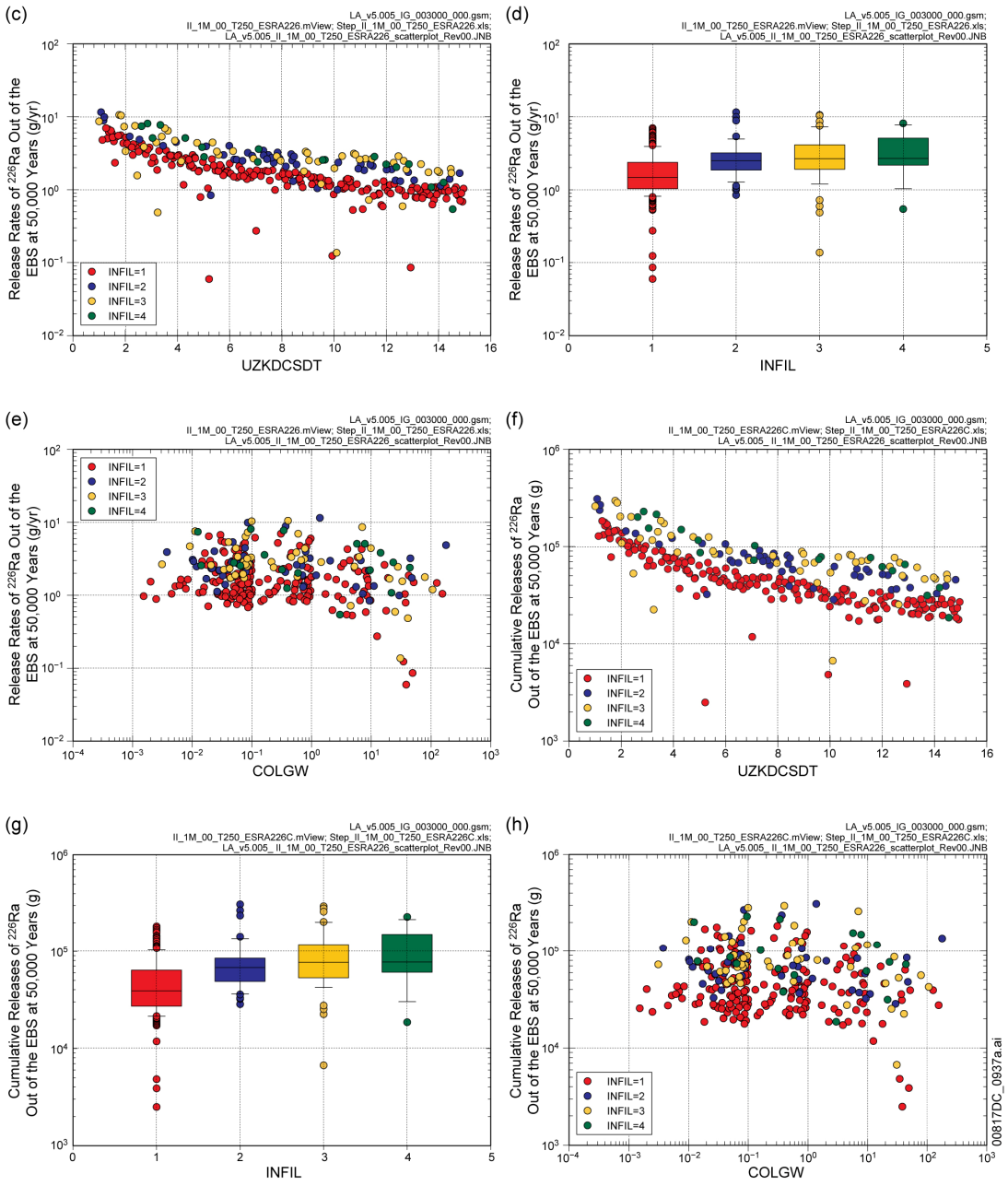


Source: Output DTNs: MO0801TSPAPRSA.000 [DIRS 184620]; and MO0710PLOTSFIG.000 [DIRS 185207].

NOTE: In (d,g), the box extends from 0.25 to 0.75 quantile; lower and upper bar and whisker extend to 0.1 and 0.9 quantile, respectively; dots represent values outside 0.1 to 0.9 quantile range; median indicated by light horizontal line.

Figure K6.3.2-10[a]. Stepwise rank regression analyses and selected scatterplots for time-dependent release rates (*ESRA226*, g/yr) and cumulative (i.e., integrated) releases (*ESRA226C*, g) for the movement of dissolved $^{226}$Ra from the EBS to the UZ resulting from an igneous intrusive event at 250 years that destroys all WPs in the repository obtained with version 5.005 of the TSPA-LA Model: (a,b) regressions for *ESRA226* and *ESRA226C* at 50,000, 200,000, and 500,000 years, and (c-h) scatterplots for *ESRA226* and *ESRA226C* at 50,000 years (continued)

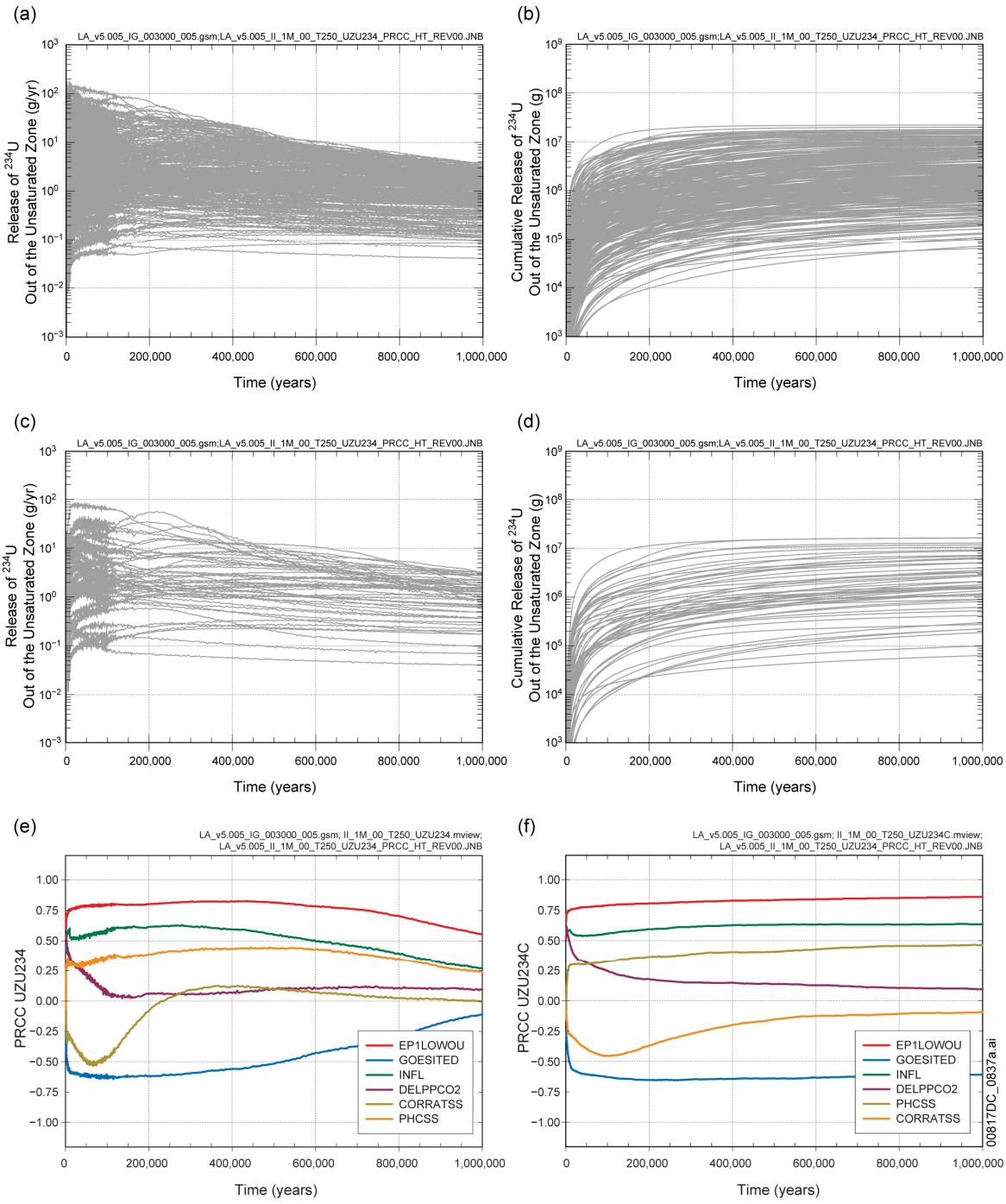


Source: Output DTNs: MO0801TSPAPRSA.000 [DIRS 184620]; and MO0710PLOTSFIG.000 [DIRS 185207].

Figure K6.4.2-1[a]. Time-dependent release rates (*UZU234*, g/yr) and cumulative (i.e., integrated) releases (*UZU234C*, g) over 1,000,000 years for the movement of dissolved $^{234}U$ from the UZ to the SZ resulting from an igneous intrusive event at 250 years that destroys all WPs in the repository obtained with version 5.005 of the TSPA-LA Model: (a,b) *UZU234* and *UZU234C* for all (i.e., 300) sample elements, (c,d) *UZU234* and *UZU234C* for first 50 sample elements, and (e,f) PRCCs for *UZU234* and *UZU234C*

(a)

| Step[a] | UZU234: 50,000 Years Variable[b] | $R^{2c}$ | SRRC[d] | UZU234: 200,000 Years Variable | $R^2$ | SRRC | UZU234: 500,000 Years Variable | $R^2$ | SRRC |
|---|---|---|---|---|---|---|---|---|---|
| 1 | EP1LOWOU | 0.38 | 0.57 | EP1LOWOU | 0.41 | 0.60 | EP1LOWOU | 0.49 | 0.68 |
| 2 | INFIL | 0.49 | 0.34 | INFIL | 0.58 | 0.40 | INFIL | 0.64 | 0.38 |
| 3 | GOESITED | 0.58 | -0.29 | GOESITED | 0.66 | -0.31 | PHCSS | 0.69 | 0.22 |
| 4 | CORRATSS | 0.65 | -0.29 | HFOSA | 0.70 | -0.21 | GOESITED | 0.73 | -0.23 |
| 5 | HFOSA | 0.67 | -0.18 | PHCSS | 0.73 | 0.20 | HFOSA | 0.75 | -0.14 |
| 6 | GORELAB | 0.70 | 0.13 | DSNFMASS | 0.75 | 0.12 | GORELAB | 0.77 | 0.12 |
| 7 | DSNFMASS | 0.71 | 0.12 | GORELAB | 0.76 | 0.13 | CSNFMASS | 0.78 | 0.13 |
| 8 | PHCSS | 0.73 | 0.16 | GOESA | 0.77 | -0.09 | WDLCRATE | 0.79 | -0.11 |
| 9 | IS2MCOS | 0.74 | 0.12 | CSNFMASS | 0.77 | 0.08 | PROBWPEF | 0.80 | 0.09 |
| 10 | CSNFMASS | 0.75 | 0.11 | HFOSITED | 0.78 | -0.08 | | | |
| 11 | KDPUCOL | 0.76 | 0.10 | KDPUCOL | 0.78 | 0.08 | | | |
| 12 | DELPPCO2 | 0.77 | 0.09 | UZFAG4 | 0.79 | -0.08 | | | |
| 13 | GOESA | 0.77 | -0.08 | | | | | | |
| 14 | UZFAG4 | 0.78 | -0.07 | | | | | | |

(b)

| Step[a] | UZU234C: 50,000 Years Variable[b] | $R^{2c}$ | SRRC[d] | UZU234C: 200,000 Years Variable | $R^2$ | SRRC | UZU234C: 500,000 Years Variable | $R^2$ | SRRC |
|---|---|---|---|---|---|---|---|---|---|
| 1 | EP1LOWOU | 0.36 | 0.56 | EP1LOWOU | 0.39 | 0.59 | EP1LOWOU | 0.45 | 0.62 |
| 2 | INFIL | 0.48 | 0.36 | INFIL | 0.54 | 0.37 | INFIL | 0.61 | 0.39 |
| 3 | GOESITED | 0.56 | -0.28 | GOESITED | 0.62 | -0.30 | GOESITED | 0.69 | -0.29 |
| 4 | CORRATSS | 0.61 | -0.24 | CORRATSS | 0.66 | -0.21 | HFOSA | 0.72 | -0.20 |
| 5 | PHCSS | 0.63 | 0.19 | HFOSA | 0.69 | -0.20 | PHCSS | 0.75 | 0.21 |
| 6 | IS2MCOS | 0.65 | 0.15 | PHCSS | 0.71 | 0.19 | GORELAB | 0.77 | 0.14 |
| 7 | HFOSA | 0.68 | -0.17 | DSNFMASS | 0.73 | 0.12 | DSNFMASS | 0.78 | 0.10 |
| 8 | DELPPCO2 | 0.69 | 0.13 | GORELAB | 0.75 | 0.13 | GOESA | 0.79 | -0.08 |
| 9 | GORELAB | 0.71 | 0.12 | GOESA | 0.76 | -0.09 | CSNFMASS | 0.80 | 0.10 |
| 10 | CSNFMASS | 0.72 | 0.13 | IS2MCOS | 0.77 | 0.09 | CORRATSS | 0.80 | -0.08 |
| 11 | GOESA | 0.73 | -0.08 | CSNFMASS | 0.77 | 0.10 | KDPUCOL | 0.81 | 0.09 |
| 12 | DSNFMASS | 0.74 | 0.09 | KDPUCOL | 0.78 | 0.09 | UZFAG4 | 0.81 | -0.08 |
| 13 | CPUPERCS | 0.75 | -0.08 | UZFAG4 | 0.79 | -0.08 | HFOSITED | 0.82 | -0.07 |
| 14 | RHMUN40 | 0.75 | -0.10 | DELPPCO2 | 0.79 | 0.07 | | | |
| 15 | UZFAG4 | 0.76 | -0.09 | | | | | | |
| 16 | KDPUCOL | 0.77 | 0.09 | | | | | | |

00817DC_0838c.ai

a: Steps in stepwise rank regression analysis
b: Variables listed in order of selection in stepwise regression
c: Cumulative $R^2$ value with entry of each variable into regression model
d: Standardized rank regression coefficients (SRRCs) in final regression model

Source: Output DTNs: MO0801TSPAPRSA.000 [DIRS 184620]; and MO0710PLOTSFIG.000 [DIRS 185207].

Figure K6.4.2-2[a]. Stepwise rank regression analyses and selected scatterplots for time-dependent release rates (*UZU234*, g/yr) and cumulative (i.e., integrated) releases (*UZU234C*, g) for the movement of dissolved $^{234}U$ from the UZ to the SZ resulting from an igneous intrusive event at 250 years that destroys all WPs in the repository obtained with version 5.005 of the TSPA-LA Model: (a,b) regressions for *UZU234* and *UZU234C* at 50,000, 200,000, and 500,000 years, and (c-h) scatterplots for *UZU234* and *UZU234C* at 500,000 years

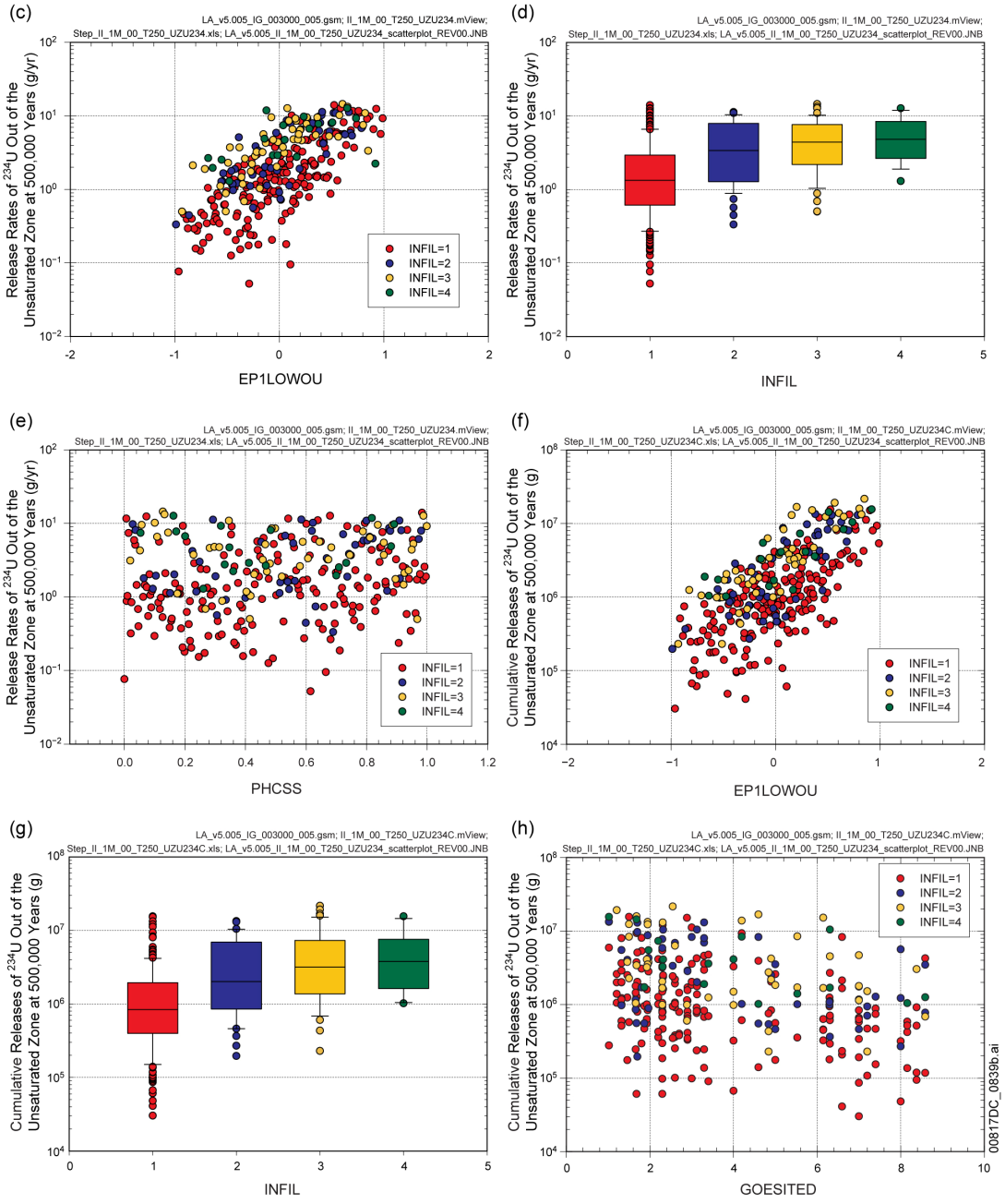


Source: Output DTNs: MO0801TSPAPRSA.000 [DIRS 184620]; and MO0710PLOTSFIG.000 [DIRS 185207].

NOTE: In (d,g), the box extends from 0.25 to 0.75 quantile; lower and upper bar and whisker extend to 0.1 and 0.9 quantile, respectively; dots represent values outside 0.1 to 0.9 quantile range; median indicated by light horizontal line.

Figure K6.4.2-2[a]. Stepwise rank regression analyses and selected scatterplots for time-dependent release rates (*UZU234*, g/yr) and cumulative (i.e., integrated) releases (*UZU234C*, g) for the movement of dissolved $^{234}U$ from the UZ to the SZ resulting from an igneous intrusive event at 250 years that destroys all WPs in the repository obtained with version 5.005 of the TSPA-LA Model: (a,b) regressions for *UZU234* and *UZU234C* at 50,000, 200,000, and 500,000 years, and (c-h) scatterplots for *UZU234* and *UZU234C* at 500,000 years (continued)

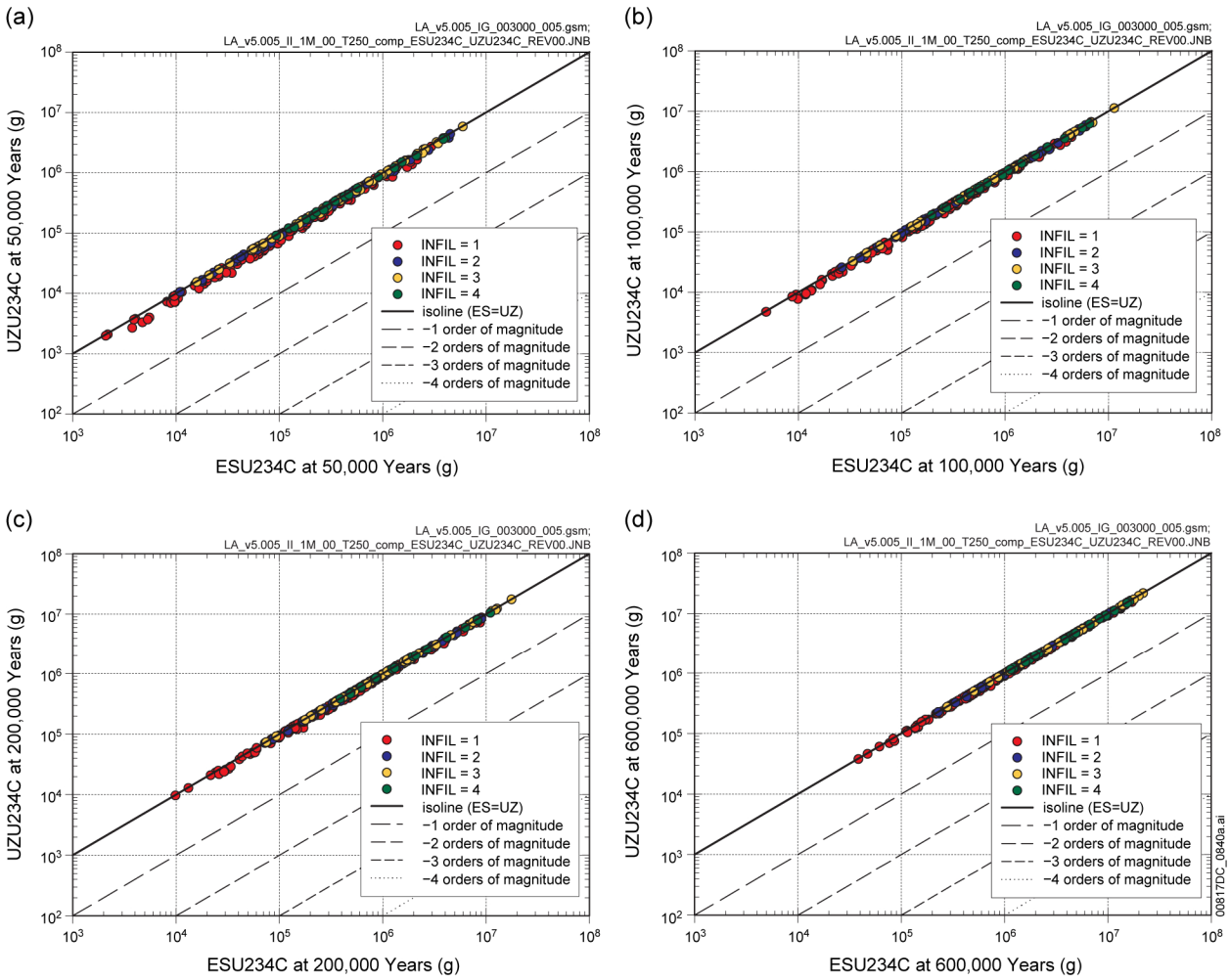


Source: Output DTNs: MO0801TSPAPRSA.000 [DIRS 184620]; and MO0710PLOTSFIG.000 [DIRS 185207].

Figure K.6.4.2-3[a]. Comparison of cumulative releases of dissolved $^{234}U$ into the UZ (*ESU234C*, g) and out of the UZ (*UZU234C*, g) obtained with version 5.005 of the TSPA-LA Model at (a) 50,000, (b) 100,000, (c) 200,000, and (d) 600,000 years for an igneous intrusive event at 250 years that destroys all WPs in the repository

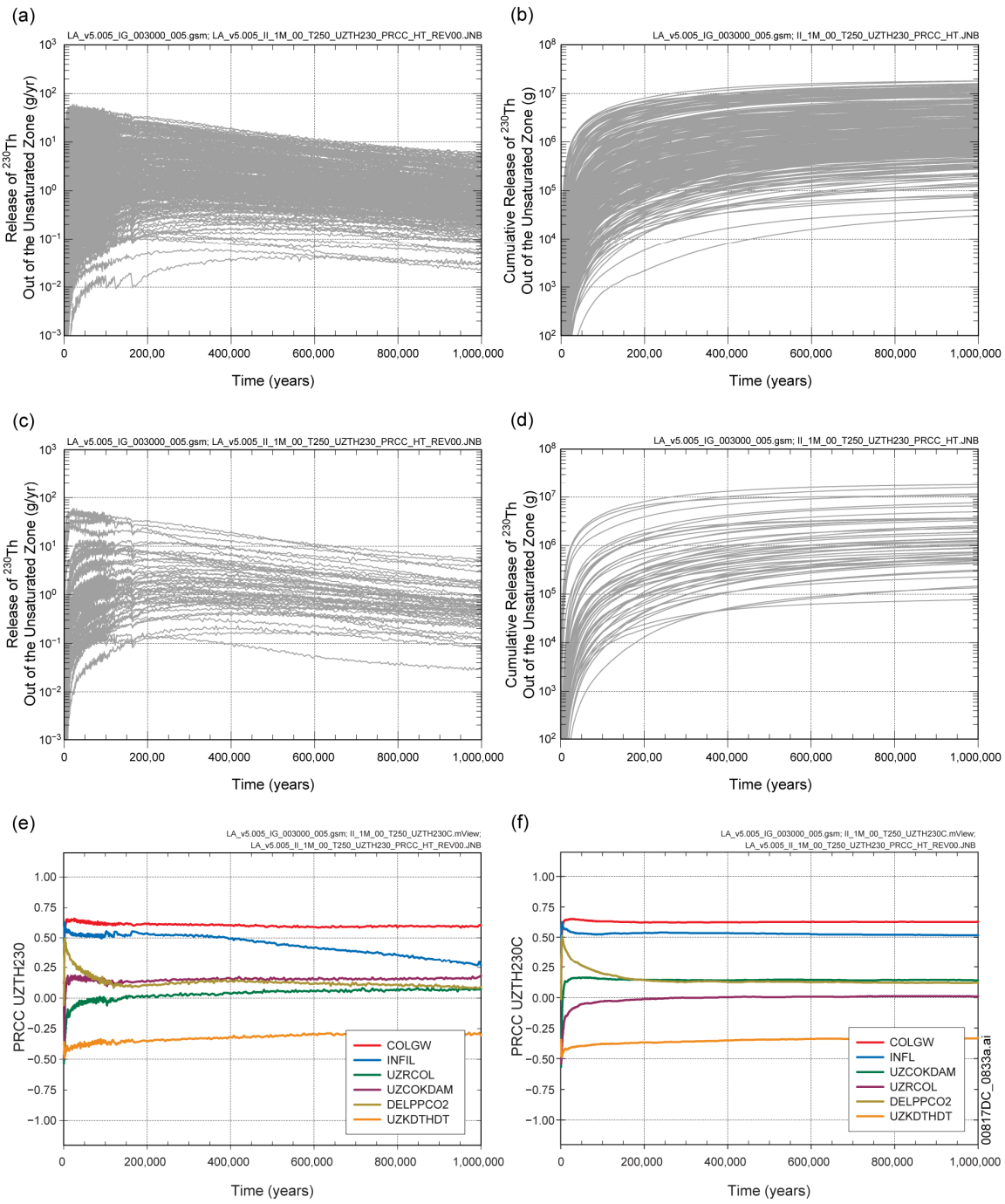


Source: Output DTNs: MO0801TSPAPRSA.000 [DIRS 184620]; and MO0710PLOTSFIG.000 [DIRS 185207].

Figure K6.4.2-4[a]. Time-dependent release rates (*UZTH230*, g/yr) and cumulative (i.e., integrated) releases (*UZTH230C*, g) over 1,000,000 years for the movement of dissolved $^{230}$Th from the UZ to the SZ resulting from an igneous intrusive event at 250 years that destroys all WPs in the repository obtained with version 5.005 of the TSPA-LA Model: (a,b) *UZTH230* and *UZTH230C* for all (i.e., 300) sample elements, (c,d) *UZTH230* and *UZTH230C* for first 50 sample elements, and (e,f) PRCCs for *UZTH230* and *UZTH230C*

(a)

| | UZTH230: 50,000 Years | | | UZTH230: 200,000 Years | | | UZTH230: 500,000 Years | | |
|---|---|---|---|---|---|---|---|---|---|
| Step[a] | Variable[b] | $R^{2}$ [c] | SRRC[d] | Variable | $R^2$ | SRRC | Variable | $R^2$ | SRRC |
| 1 | INFIL | 0.25 | 0.44 | INFIL | 0.27 | 0.46 | COLGW | 0.22 | 0.43 |
| 2 | COLGW | 0.42 | 0.44 | COLGW | 0.43 | 0.41 | INFIL | 0.40 | 0.39 |
| 3 | KDTHSMEC | 0.51 | 0.28 | KDTHSMEC | 0.52 | 0.29 | KDTHSMEC | 0.50 | 0.29 |
| 4 | PHCSS | 0.55 | 0.24 | PHCSS | 0.57 | 0.23 | UZKDTHDT | 0.54 | -0.20 |
| 5 | UZKDTHDT | 0.60 | -0.23 | EP1LOWTH | 0.60 | 0.21 | PHCSS | 0.58 | 0.20 |
| 6 | EP1LOWTH | 0.63 | 0.22 | UZKDTHDT | 0.63 | -0.19 | EP1LOWTH | 0.61 | 0.20 |
| 7 | CORRATSS | 0.66 | -0.15 | EP1LOWOU | 0.66 | 0.15 | CSNFMASS | 0.63 | 0.12 |
| 8 | EP1LOWOU | 0.68 | 0.13 | GOESITED | 0.68 | -0.17 | HFOSA | 0.64 | -0.12 |
| 9 | GOESITED | 0.69 | -0.14 | HFOSA | 0.70 | -0.13 | GOESITED | 0.65 | -0.12 |
| 10 | HLWMASS | 0.70 | 0.10 | GOESA | 0.70 | -0.09 | UZFAG1 | 0.66 | -0.09 |
| 11 | DELPPCO2 | 0.71 | 0.10 | HLWMASS | 0.71 | 0.09 | EP2HICAM | 0.67 | 0.09 |

(b)

| | UZTH230C: 50,000 Years | | | UZTH230C: 200,000 Years | | | UZTH230C: 500,000 Years | | |
|---|---|---|---|---|---|---|---|---|---|
| Step[a] | Variable[b] | $R^{2}$ [c] | SRRC[d] | Variable | $R^2$ | SRRC | Variable | $R^2$ | SRRC |
| 1 | INFIL | 0.25 | 0.44 | INFIL | 0.27 | 0.46 | INFIL | 0.27 | 0.46 |
| 2 | COLGW | 0.44 | 0.45 | COLGW | 0.43 | 0.42 | COLGW | 0.44 | 0.43 |
| 3 | KDTHSMEC | 0.52 | 0.27 | KDTHSMEC | 0.52 | 0.28 | KDTHSMEC | 0.53 | 0.30 |
| 4 | UZKDTHDT | 0.57 | -0.24 | PHCSS | 0.57 | 0.22 | PHCSS | 0.58 | 0.22 |
| 5 | PHCSS | 0.61 | 0.23 | EP1LOWTH | 0.60 | 0.21 | EP1LOWTH | 0.61 | 0.21 |
| 6 | EP1LOWTH | 0.65 | 0.22 | UZKDTHDT | 0.64 | -0.20 | UZKDTHDT | 0.65 | -0.20 |
| 7 | CORRATSS | 0.67 | -0.15 | GOESITED | 0.66 | -0.15 | EP1LOWOU | 0.67 | 0.14 |
| 8 | GOESITED | 0.69 | -0.13 | EP1LOWOU | 0.68 | 0.13 | GOESITED | 0.69 | -0.15 |
| 9 | EP1LOWOU | 0.70 | 0.11 | CORRATSS | 0.70 | -0.13 | HFOSA | 0.70 | -0.12 |
| 10 | DELPPCO2 | 0.71 | 0.13 | HFOSA | 0.71 | -0.10 | HLWMASS | 0.71 | 0.09 |
| 11 | HLWMASS | 0.72 | 0.10 | HLWMASS | 0.71 | 0.09 | GOESA | 0.72 | -0.09 |
| 12 | HFOSA | 0.73 | -0.10 | | | | DSCRACKA | 0.72 | -0.08 |

00817DC_0834c.ai

a: Steps in stepwise rank regression analysis
b: Variables listed in order of selection in stepwise regression
c: Cumulative $R^2$ value with entry of each variable into regression model
d: Standardized rank regression coefficients (SRRCs) in final regression model

Source: Output DTNs: MO0801TSPAPRSA.000 [DIRS 184620]; and MO0710PLOTSFIG.000 [DIRS 185207].

Figure K6.4.2-5[a]. Stepwise rank regression analyses and selected scatterplots for time-dependent release rates (*UZTH230*, g/yr) and cumulative (i.e., integrated) releases (*UZTH230C*, g) for the movement of dissolved $^{230}$Th from the UZ to the SZ resulting from an igneous intrusive event at 250 years that destroys all WPs in the repository obtained with version 5.005 of the TSPA-LA Model: (a,b) regressions for *UZTH230* and *UZTH230C* at 50,000, 200,000, and 500,000 years, and (c-h) scatterplots for *UZTH230* and *UZTH230C* at 200,000 years

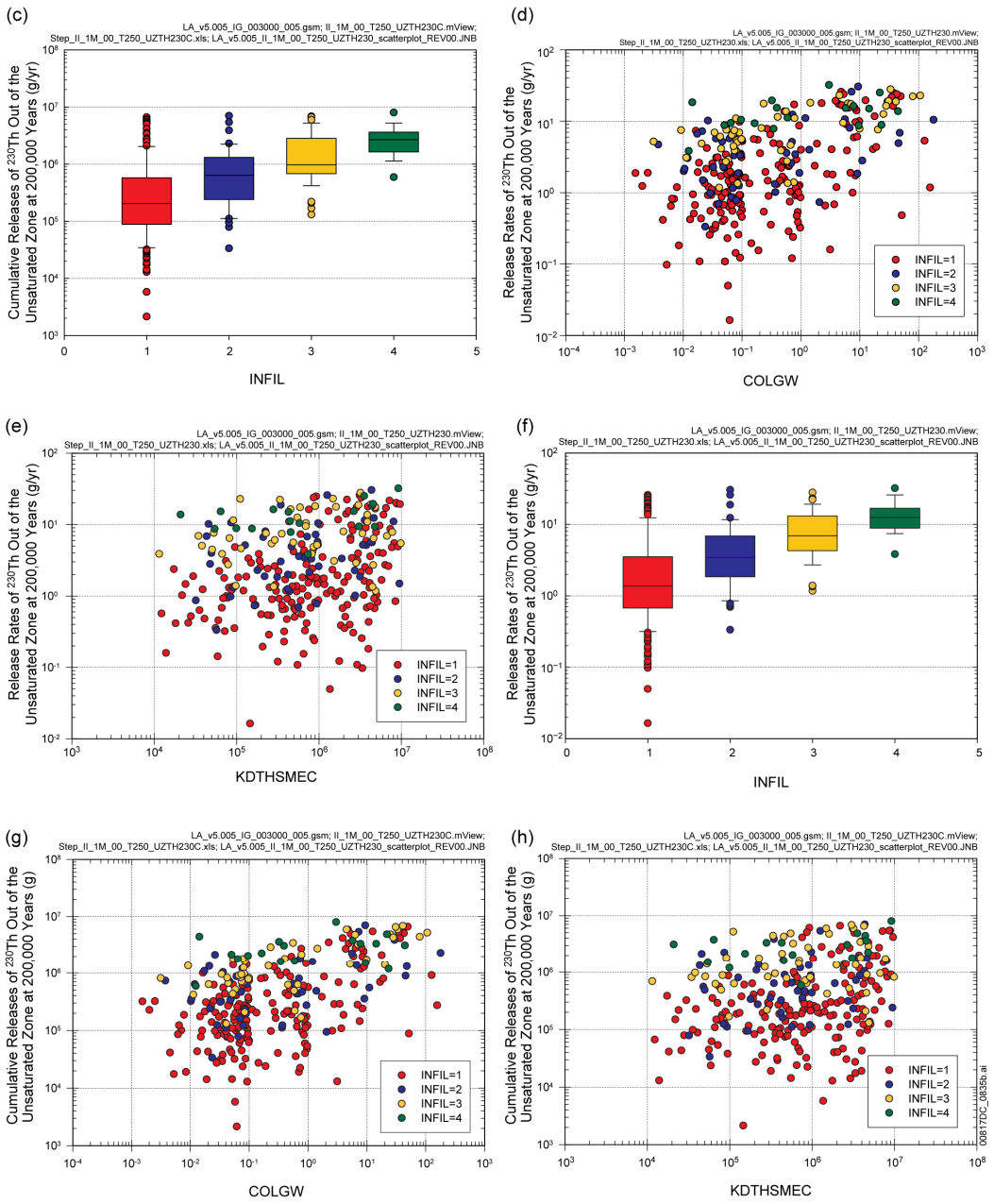


Source: Output DTNs: MO0801TSPAPRSA.000 [DIRS 184620]; and MO0710PLOTSFIG.000 [DIRS 185207].

NOTE: In (c,f), the box extends from 0.25 to 0.75 quantile; lower and upper bar and whisker extend to 0.1 and 0.9 quantile, respectively; dots represent values outside 0.1 to 0.9 quantile range; median indicated by light horizontal line.

Figure K6.4.2-5[a]. Stepwise rank regression analyses and selected scatterplots for time-dependent release rates (*UZTH230*, g/yr) and cumulative (i.e., integrated) releases (*UZTH230C*, g) for the movement of dissolved $^{230}$Th from the UZ to the SZ resulting from an igneous intrusive event at 250 years that destroys all WPs in the repository obtained with version 5.005 of the TSPA-LA Model: (a,b) regressions for *UZTH230* and *UZTH230C* at 50,000, 200,000, and 500,000 years, and (c-h) scatterplots for *UZTH230* and *UZTH230C* at 200,000 years (continued)

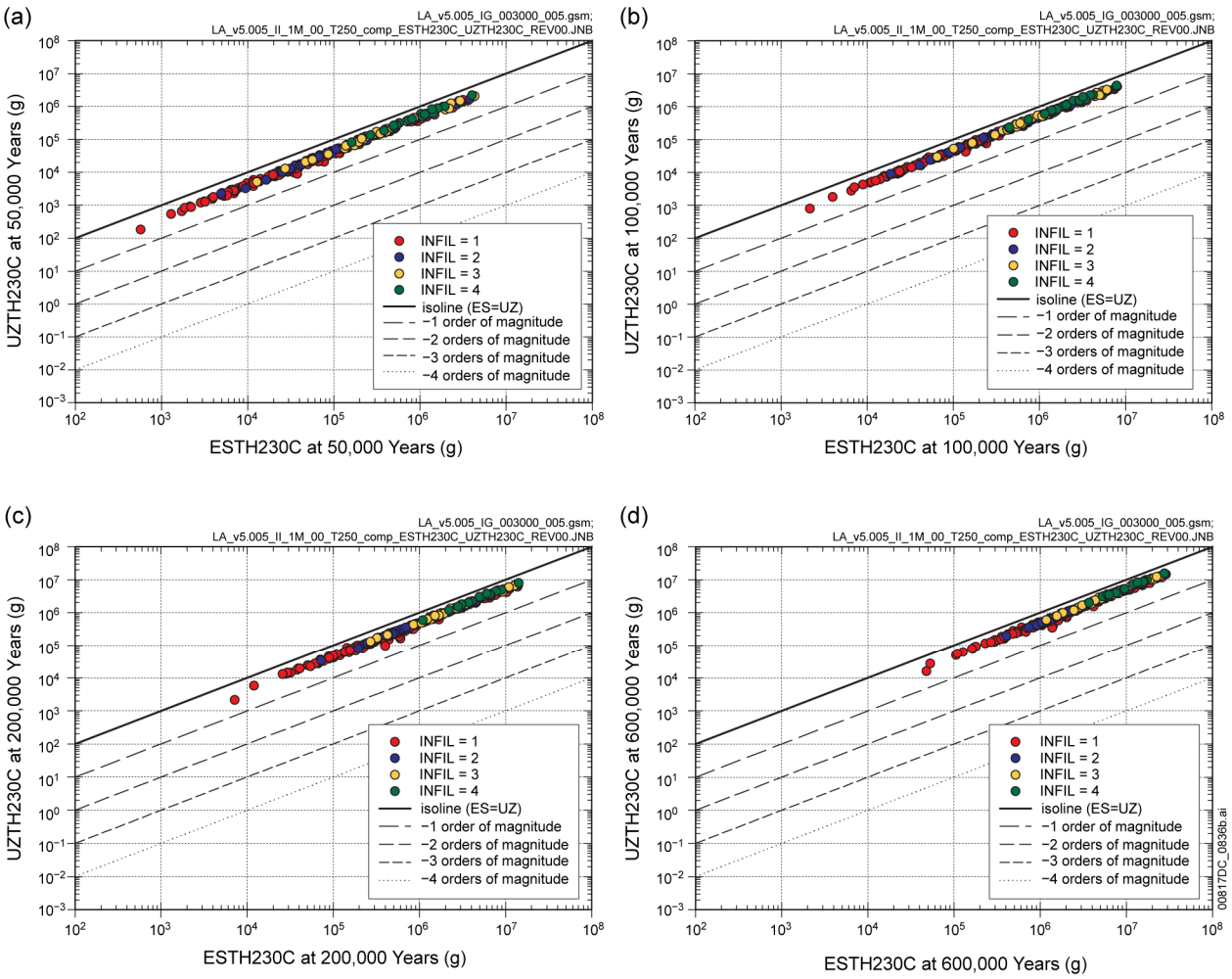


Source: Output DTNs: MO0801TSPAPRSA.000 [DIRS 184620]; and MO0710PLOTSFIG.000 [DIRS 185207].

Figure K.6.4.2-6[a]. Comparison of cumulative releases of dissolved $^{230}$Th into the UZ (*ESTH230C*, g) and out of the UZ (*UZTH230C*, g) obtained with version 5.005 of the TSPA-LA Model at (a) 50,000, (b) 100,000, (c) 200,000, and (d) 600,000 years for an igneous intrusive event at 250 years that destroys all WPs in the repository

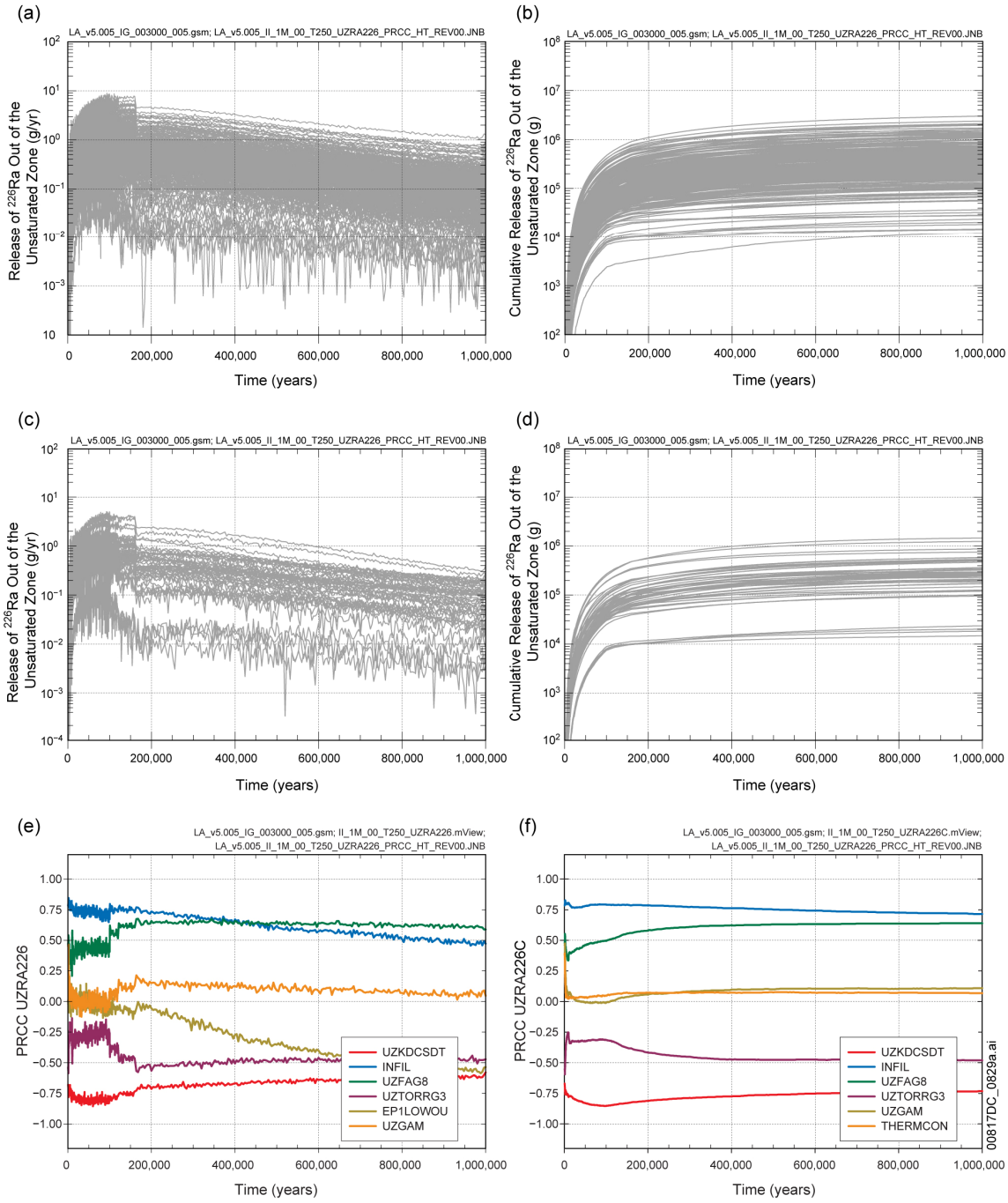


Source: Output DTNs: MO0801TSPAPRSA.000 [DIRS 184620]; and MO0710PLOTSFIG.000 [DIRS 185207].

Figure K6.4.2-7[a]. Time-dependent release rates (*UZRA226*, g/yr) and cumulative (i.e., integrated) releases (*UZRA226C*, g) over 1,000,000 years for the movement of dissolved $^{226}$Ra from the UZ to the SZ resulting from an igneous intrusive event at 250 years that destroys all WPs in the repository obtained with version 5.005 of the TSPA-LA Model: (a,b) *UZRA226* and *UZRA226C* for all (i.e., 300) sample elements, (c,d) *UZRA226* and *UZRA226C* for first 50 sample elements, and (e,f) PRCCs for *UZRA226* and *UZRA226C*

(a)

| Step[a] | UZRA226: 50,000 Years Variable[b] | $R^2$ [c] | SRRC[d] | UZRA226: 200,000 Years Variable | $R^2$ | SRRC | UZRA226: 500,000 Years Variable | $R^2$ | SRRC |
|---|---|---|---|---|---|---|---|---|---|
| 1 | UZKDCSDT | 0.41 | −0.64 | INFIL | 0.27 | 0.52 | UZKDCSDT | 0.24 | −0.47 |
| 2 | INFIL | 0.72 | 0.54 | UZKDCSDT | 0.52 | −0.48 | UZFAG8 | 0.41 | 0.42 |
| 3 | UZFAG8 | 0.76 | 0.20 | UZFAG8 | 0.67 | 0.38 | INFIL | 0.56 | 0.39 |
| 4 | CSNFMASS | 0.78 | 0.15 | UZTORRG3 | 0.77 | −0.33 | UZTORRG3 | 0.64 | −0.32 |
| 5 | UZTORRG3 | 0.80 | −0.14 | CSNFMASS | 0.78 | 0.13 | EP1LOWOU | 0.68 | −0.22 |
| 6 | KDNPSMEC | 0.80 | 0.08 | COLGW | 0.79 | 0.09 | CSNFMASS | 0.70 | 0.13 |
| 7 | KDAMSMEC | 0.81 | −0.08 | UZGAM | 0.80 | 0.07 | UZKDTHDT | 0.71 | 0.11 |
| 8 | KDNPCOL | 0.81 | 0.07 | UZKDTHDT | 0.80 | 0.08 | | | |
| 9 | | | | EP1LOWOU | 0.81 | −0.07 | | | |

(b)

| Step[a] | UZRA226C: 50,000 Years Variable[b] | $R^2$ [c] | SRRC[d] | UZRA226C: 200,000 Years Variable | $R^2$ | SRRC | UZRA226C: 500,000 Years Variable | $R^2$ | SRRC |
|---|---|---|---|---|---|---|---|---|---|
| 1 | UZKDCSDT | 0.40 | −0.63 | UZKDCSDT | 0.38 | −0.61 | UZKDCSDT | 0.31 | −0.55 |
| 2 | INFIL | 0.73 | 0.56 | INFIL | 0.69 | 0.55 | INFIL | 0.59 | 0.53 |
| 3 | UZFAG8 | 0.77 | 0.18 | UZFAG8 | 0.77 | 0.28 | UZFAG8 | 0.71 | 0.35 |
| 4 | UZTORRG3 | 0.79 | −0.16 | UZTORRG3 | 0.81 | −0.22 | UZTORRG3 | 0.77 | −0.27 |
| 5 | CSNFMASS | 0.81 | 0.15 | CSNFMASS | 0.83 | 0.14 | CSNFMASS | 0.79 | 0.15 |
| 6 | COLGW | 0.83 | 0.13 | UZKDTHDT | 0.83 | 0.06 | EP1LOWOU | 0.80 | −0.10 |
| 7 | KDTHSMEC | 0.84 | 0.09 | | | | UZKDTHDT | 0.81 | 0.08 |
| 8 | GOESITED | 0.84 | −0.06 | | | | | | |

00817DC_0830b.ai

a: Steps in stepwise rank regression analysis
b: Variables listed in order of selection in stepwise regression
c: Cumulative $R^2$ value with entry of each variable into regression model
d: Standardized rank regression coefficients (SRRCs) in final regression model

Source: Output DTNs: MO0801TSPAPRSA.000 [DIRS 184620]; and MO0710PLOTSFIG.000 [DIRS 185207].

Figure K6.4.2-8[a]. Stepwise rank regression analyses and selected scatterplots for time-dependent release rates (*UZRA226*, g/yr) and cumulative (i.e., integrated) releases (*UZRA226C*, g) for the movement of dissolved $^{226}$Ra from the UZ to the SZ resulting from an igneous intrusive event at 250 years that destroys all WPs in the repository obtained with version 5.005 of the TSPA-LA Model: (a,b) regressions for *UZRA226* and *UZRA226C* at 50,000, 200,000, and 500,000 years, and (c-h) scatterplots for *UZRA226* and *UZRA226C* at 50,000 years

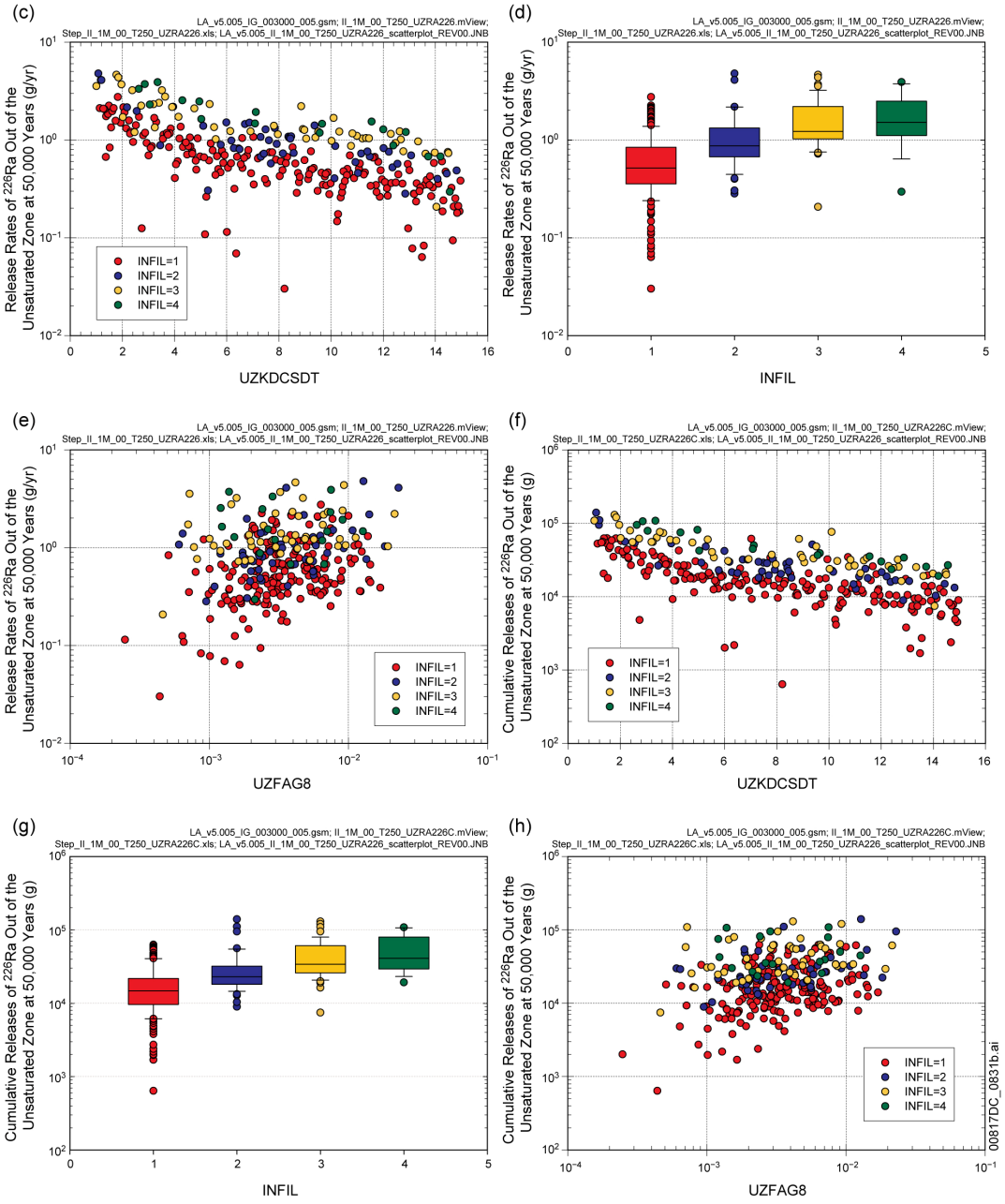


Source: Output DTNs: MO0801TSPAPRSA.000 [DIRS 184620]; and MO0710PLOTSFIG.000 [DIRS 185207].

NOTE: In (d,g), the box extends from 0.25 to 0.75 quantile; lower and upper bar and whisker extend to 0.1 and 0.9 quantile, respectively; dots represent values outside 0.1 to 0.9 quantile range; median indicated by light horizontal line.

Figure K6.4.2-8[a]. Stepwise rank regression analyses and selected scatterplots for time-dependent release rates (*UZRA226*, g/yr) and cumulative (i.e., integrated) releases (*UZRA226C*, g) for the movement of dissolved $^{226}$Ra from the UZ to the SZ resulting from an igneous intrusive event at 250 years that destroys all WPs in the repository obtained with version 5.005 of the TSPA-LA Model: (a,b) regressions for *UZRA226* and *UZRA226C* at 50,000, 200,000, and 500,000 years, and (c-h) scatterplots for *UZRA226* and *UZRA226C* at 50,000 years (continued)

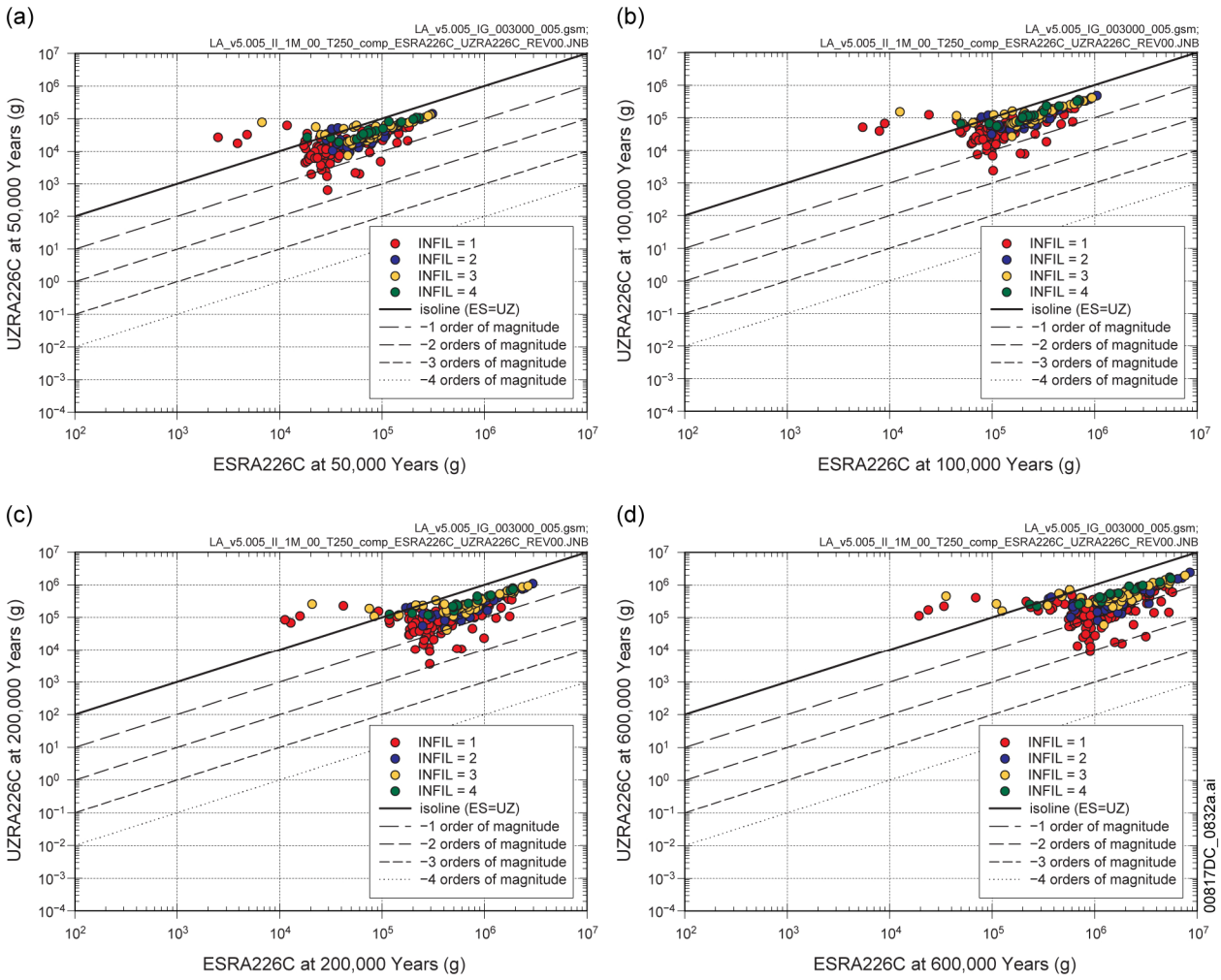


Source: Output DTNs: MO0801TSPAPRSA.000 [DIRS 184620]; and MO0710PLOTSFIG.000 [DIRS 185207].

Figure K.6.4.2-9[a]. Comparison of cumulative releases of dissolved $^{226}Ra$ into the UZ (*UZRA226C*, g) and out of the UZ (*UZRA226C*, g) obtained with version 5.005 of the TSPA-LA Model at (a) 50,000, (b) 100,000, (c) 200,000, and (d) 600,000 years for an igneous intrusive event at 250 years that destroys all WPs in the repository

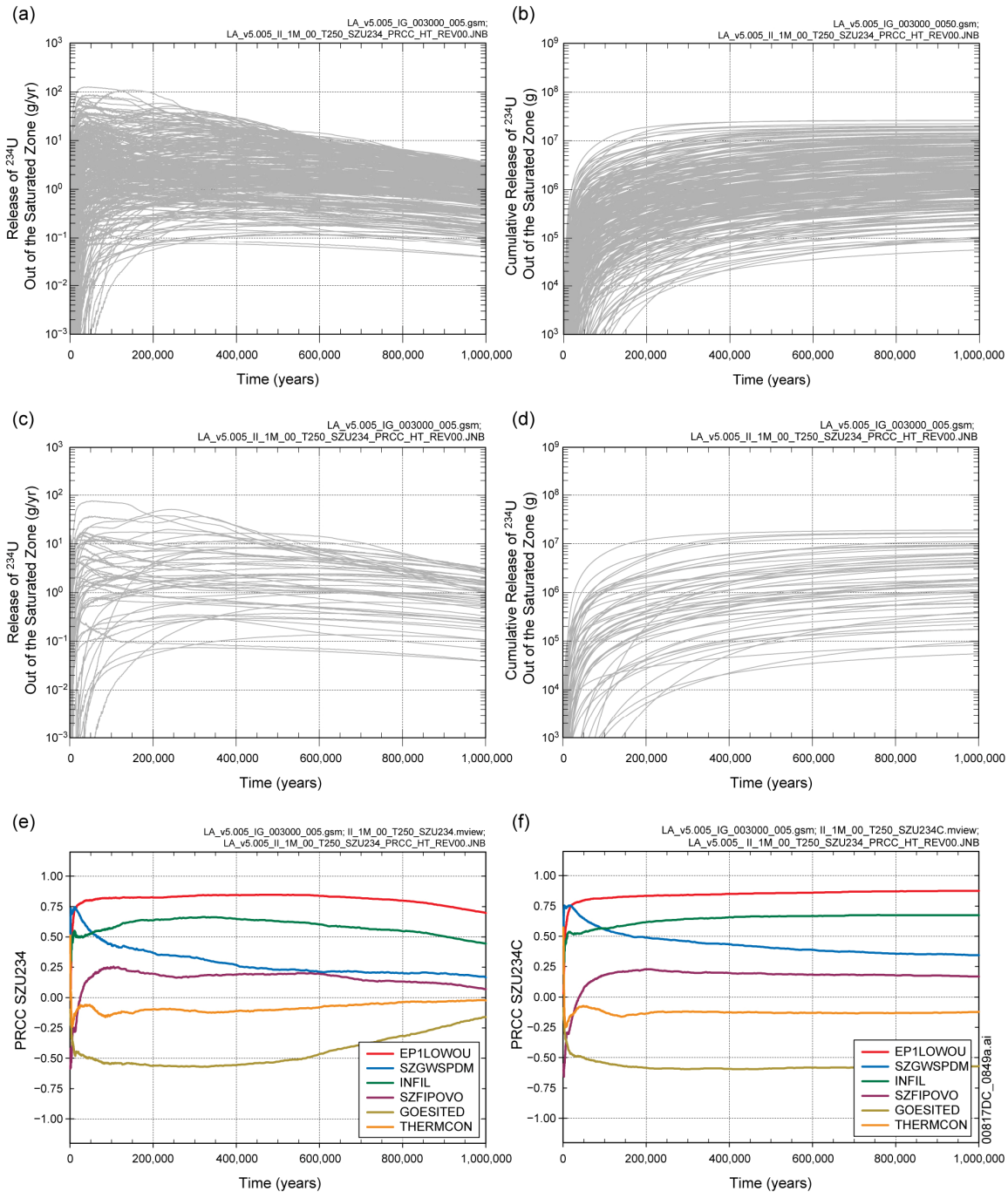


Source: Output DTNs: MO0801TSPAPRSA.000 [DIRS 184620]; and MO0710PLOTSFIG.000 [DIRS 185207].

Figure K6.5.2-5[a]. Time-dependent release rates (*SZU234*, g/yr) and cumulative (i.e., integrated) releases (*SZU234C*, g) over 1,000,000 years for the movement of dissolved $^{234}U$ across a subsurface plane at the location of the RMEI resulting from an igneous intrusive event at 250 years that destroys all WPs in the repository obtained with version 5.005 of the TSPA-LA Model: (a,b) *SZU234* and *SZU234C* for all (i.e., 300) sample elements, (c,d) *SZU234* and *SZU234C* for first 50 sample elements, and (e,f) PRCCs for *SZU234* and *SZU234C*

(a)

| | SZU234: 50,000 Years | | | SZU234: 200,000 Years | | | SZU234: 500,000 Years | | |
|---|---|---|---|---|---|---|---|---|---|
| Step[a] | Variable[b] | $R^{2c}$ | SRRC[d] | Variable | $R^2$ | SRRC | Variable | $R^2$ | SRRC |
| 1 | EP1LOWOU | 0.30 | 0.53 | EP1LOWOU | 0.37 | 0.58 | EP1LOWOU | 0.46 | 0.65 |
| 2 | INFIL | 0.42 | 0.36 | INFIL | 0.54 | 0.41 | INFIL | 0.64 | 0.41 |
| 3 | SZGWSPDM | 0.49 | 0.29 | GOESITED | 0.62 | −0.27 | PHCSS | 0.69 | 0.21 |
| 4 | GOESITED | 0.55 | −0.22 | PHCSS | 0.65 | 0.20 | GOESITED | 0.73 | −0.25 |
| 5 | CORRATSS | 0.59 | −0.22 | SZGWSPDM | 0.68 | 0.19 | HFOSA | 0.75 | −0.13 |
| 6 | PHCSS | 0.62 | 0.17 | HFOSA | 0.71 | −0.17 | SZGWSPDM | 0.77 | 0.12 |
| 7 | IS2MCOS | 0.64 | 0.15 | GORELAB | 0.72 | 0.12 | CSNFMASS | 0.78 | 0.13 |
| 8 | CSNFMASS | 0.66 | 0.14 | CORRATSS | 0.73 | −0.11 | GOERELAB | 0.79 | 0.11 |
| 9 | SZDIFCVO | 0.68 | −0.15 | CSNFMASS | 0.74 | 0.12 | WDLCRATE | 0.80 | −0.10 |
| 10 | SZFISPVO | 0.70 | 0.13 | KDPUSMEC | 0.75 | 0.10 | SZLODISP | 0.81 | −0.08 |
| 11 | KDPUSMEC | 0.71 | 0.12 | CSCORRAT | 0.76 | 0.09 | UZFAG1 | 0.81 | −0.07 |
| 12 | GOERELAB | 0.72 | 0.11 | KDPUCOL | 0.77 | 0.09 | SZSREG2X | 0.82 | 0.07 |
| 13 | HFOSA | 0.73 | −0.12 | UZFAG4 | 0.77 | −0.08 | | | |
| 14 | CSWFA4AC | 0.73 | −0.10 | WDDEFCNT | 0.78 | −0.08 | | | |
| 15 | DELPPCO2 | 0.74 | 0.09 | | | | | | |
| 16 | SZSREG1X | 0.75 | −0.09 | | | | | | |

(b)

| | SZU234C: 50,000 Years | | | SZU234C: 200,000 Years | | | SZU234C: 500,000 Years | | |
|---|---|---|---|---|---|---|---|---|---|
| Step[a] | Variable[b] | $R^{2c}$ | SRRC[d] | Variable | $R^2$ | SRRC | Variable | $R^2$ | SRRC |
| 1 | EP1LOWOU | 0.26 | 0.51 | EP1LOWOU | 0.34 | 0.56 | EP1LOWOU | 0.41 | 0.61 |
| 2 | INFIL | 0.38 | 0.35 | INFIL | 0.48 | 0.37 | INFIL | 0.58 | 0.39 |
| 3 | SZGWSPDM | 0.49 | 0.35 | GOESITED | 0.56 | −0.26 | GOESITED | 0.65 | −0.26 |
| 4 | GOESITED | 0.55 | −0.20 | SZGWSPDM | 0.61 | 0.24 | PHCSS | 0.69 | 0.21 |
| 5 | SZDIFCVO | 0.58 | −0.18 | CORRATSS | 0.64 | −0.21 | SZGWSPDM | 0.72 | 0.19 |
| 6 | SZFISPVO | 0.61 | 0.17 | PHCSS | 0.67 | 0.18 | HFOSA | 0.74 | −0.16 |
| 7 | CORRATSS | 0.64 | −0.19 | HFOSA | 0.69 | −0.14 | GOERELAB | 0.75 | 0.12 |
| 8 | PHCSS | 0.66 | 0.16 | GOERELAB | 0.70 | 0.11 | CSNFMASS | 0.76 | 0.11 |
| 9 | IS2MCOS | 0.68 | 0.17 | SZFISPVO | 0.72 | 0.13 | CORRATSS | 0.77 | −0.10 |
| 10 | CSNFMASS | 0.70 | 0.12 | SZDIFCVO | 0.73 | −0.13 | KDPUSMEC | 0.78 | 0.09 |
| 11 | KDPUSMEC | 0.71 | 0.11 | CSNFMASS | 0.74 | 0.11 | CSCORRAT | 0.79 | 0.08 |
| 12 | DELPPCO2 | 0.72 | 0.11 | IS2MCOS | 0.76 | 0.09 | KDPUCOL | 0.80 | 0.09 |
| 13 | HFOSA | 0.72 | −0.10 | KDPUSMEC | 0.77 | 0.10 | SZDIFCVO | 0.80 | −0.09 |
| 14 | DSCRACKA | 0.73 | −0.10 | KDPUCOL | 0.77 | 0.09 | SZFISPVO | 0.81 | 0.10 |
| 15 | CSWFA4AC | 0.74 | −0.09 | UZFAG4 | 0.78 | −0.09 | UZFAG4 | 0.81 | −0.07 |
| 16 | GOERELAB | 0.75 | 0.09 | DSNFMASS | 0.79 | 0.08 | DSNFMASS | 0.82 | 0.07 |

00817DC_0850a.ai

a: Steps in stepwise rank regression analysis
b: Variables listed in order of selection in stepwise regression
c: Cumulative $R^2$ value with entry of each variable into regression model
d: Standardized rank regression coefficients (SRRCs) in final regression model

Source: Output DTNs: MO0801TSPAPRSA.000 [DIRS 184620]; and MO0710PLOTSFIG.000 [DIRS 185207].

Figure K6.5.2-6[a]. Stepwise rank regression analyses and selected scatterplots for time-dependent release rates (*SZU234*, g/yr) and cumulative (i.e., integrated) releases (*SZU234C*, g) for the movement of dissolved $^{234}U$ across a subsurface plane at the location of the RMEI resulting from an igneous intrusive event at 250 years that destroys all WPs in the repository obtained with version 5.005 of the TSPA-LA Model: (a,b) regressions for *SZU234* and *SZU234C* at 50,000, 200,000, and 500,000 years, and (c-h) scatterplots for *SZU234* and *SZU234C* at 500,000 years

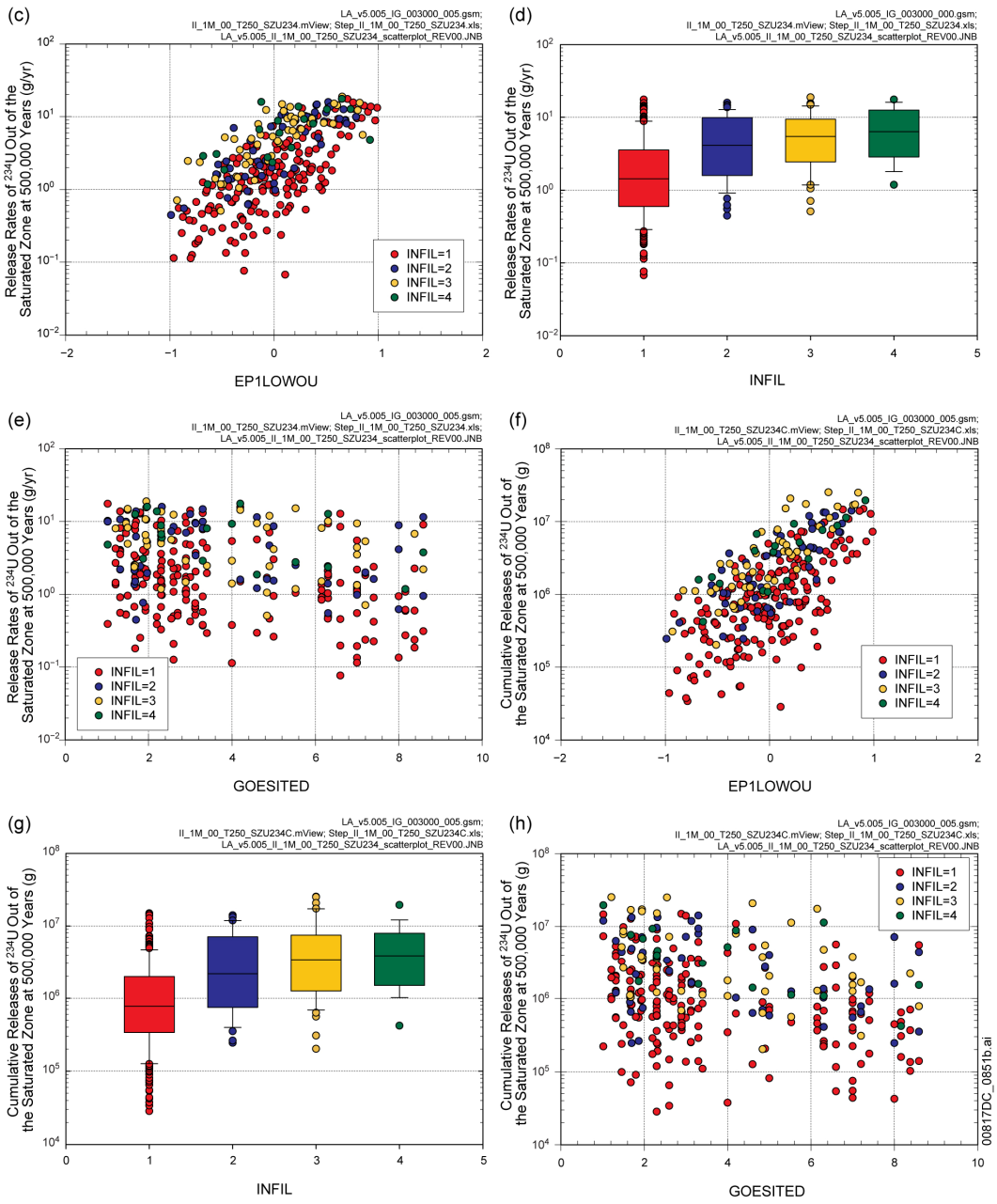


Source: Output DTNs: MO0801TSPAPRSA.000 [DIRS 184620]; and MO0710PLOTSFIG.000 [DIRS 185207].

NOTE: In (d,g), the box extends from 0.25 to 0.75 quantile; lower and upper bar and whisker extend to 0.1 and 0.9 quantile, respectively; dots represent values outside 0.1 to 0.9 quantile range; median indicated by light horizontal line.

Figure K6.5.2-6[a]. Stepwise rank regression analyses and selected scatterplots for time-dependent release rates (*SZU234*, g/yr) and cumulative (i.e., integrated) releases (*SZU234C*, g) for the movement of dissolved $^{234}$U across a subsurface plane at the location of the RMEI resulting from an igneous intrusive event at 250 years that destroys all WPs in the repository obtained with version 5.005 of the TSPA-LA Model: (a,b) regressions for *SZU234* and *SZU234C* at 50,000, 200,000, and 500,000 years, and (c-h) scatterplots for *SZU234* and *SZU234C* at 500,000 years (continued)

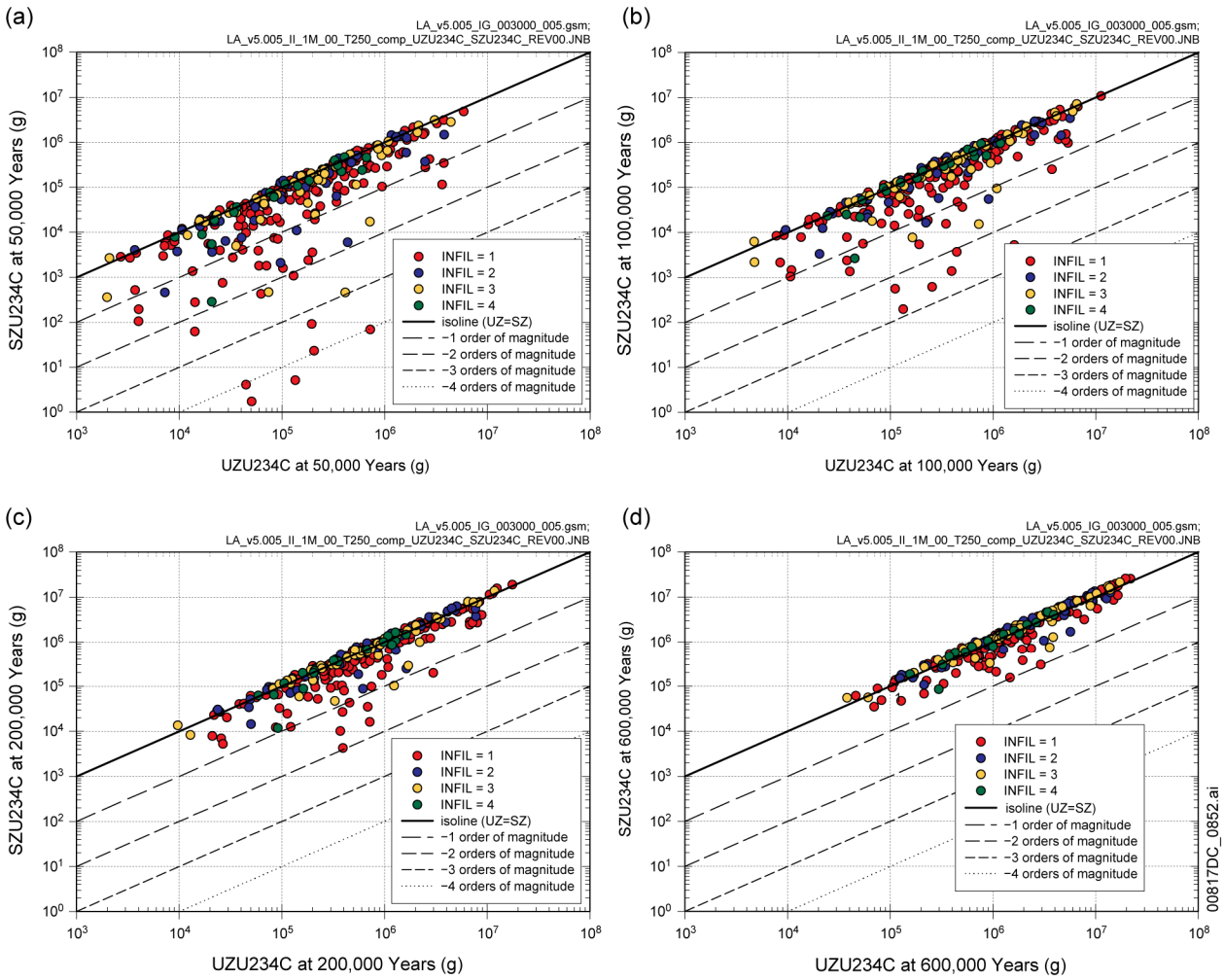


Source: Output DTNs: MO0801TSPAPRSA.000 [DIRS 184620]; and MO0710PLOTSFIG.000 [DIRS 185207].

Figure K.6.5.2-7[a]. Comparison of cumulative releases of dissolved $^{234}U$ into the SZ (*UZU234C*, g) and across a subsurface plane at the location of the RMEI (*SZU234C*, g) obtained with version 5.005 of the TSPA-LA Model at (a) 50,000, (b) 100,000, (c) 200,000, and (d) 600,000 years for an igneous intrusive event at 250 years that destroys all WPs in the repository

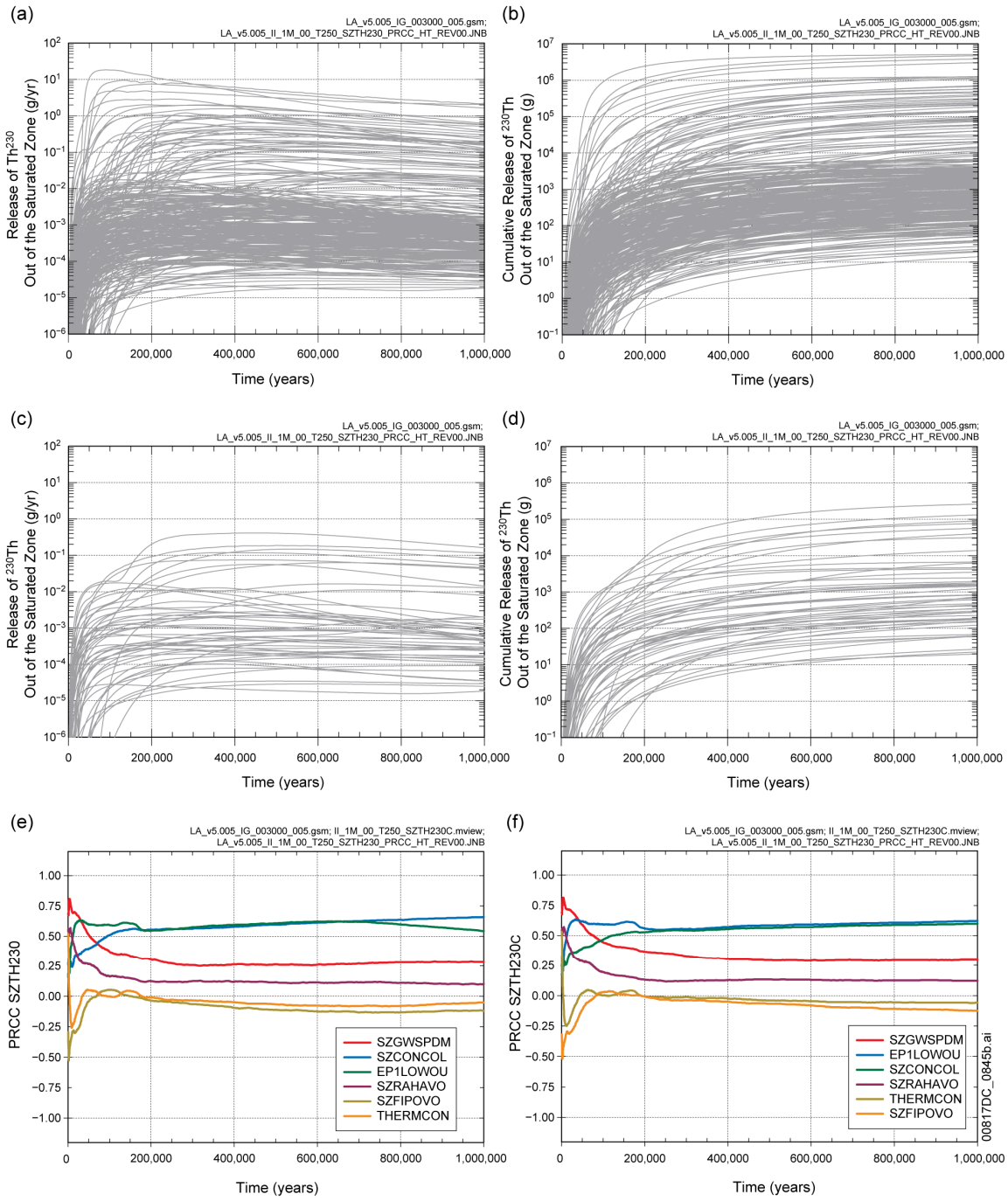


Source: Output DTNs: MO0801TSPAPRSA.000 [DIRS 184620]; and MO0710PLOTSFIG.000 [DIRS 185207].

Figure K6.5.2-8[a]. Time-dependent release rates (*SZTH230*, g/yr) and cumulative (i.e., integrated) releases (*SZTH230C*, g) over 1,000,000 years for the movement of dissolved $^{230}$Th across a subsurface plane at the location of the RMEI resulting from an igneous intrusive event at 250 years that destroys all WPs in the repository obtained with version 5.005 of the TSPA-LA Model: (a,b) *SZTH230* and *SZTH230C* for all (i.e., 300) sample elements, (c,d) *SZTH230* and *SZTH230C* for first 50 sample elements, and (e,f) PRCCs for *SZTH230* and *SZTH230C*

(a)

| | SZTH230: 50,000 Years | | | SZTH230: 200,000 Years | | | SZTH230: 500,000 Years | | |
|---|---|---|---|---|---|---|---|---|---|
| Step[a] | Variable[b] | $R^2$ [c] | SRRC[d] | Variable | $R^2$ | SRRC | Variable | $R^2$ | SRRC |
| 1 | EP1LOWOU | 0.17 | 0.40 | SZCONCOL | 0.19 | 0.45 | SZCONCOL | 0.20 | 0.46 |
| 2 | SZCONCOL | 0.33 | 0.39 | EP1LOWOU | 0.37 | 0.38 | EP1LOWOU | 0.40 | 0.40 |
| 3 | SZGWSPDM | 0.45 | 0.36 | SZKDAMCO | 0.43 | 0.23 | SZKDAMCO | 0.48 | 0.26 |
| 4 | INFIL | 0.52 | 0.29 | INFIL | 0.49 | 0.27 | INFIL | 0.54 | 0.24 |
| 5 | GOESITED | 0.57 | −0.20 | GOESITED | 0.54 | −0.23 | SZGWSPDM | 0.57 | 0.20 |
| 6 | SZKDAMCO | 0.60 | 0.17 | SZGWSPDM | 0.58 | 0.23 | GOESITED | 0.60 | −0.19 |
| 7 | SZDIFCVO | 0.62 | −0.12 | KDPUSMEC | 0.60 | 0.14 | SZKDAMAL | 0.61 | −0.13 |
| 8 | CSWFA4AC | 0.63 | −0.11 | CORRATSS | 0.62 | −0.15 | SZKDUAL | 0.63 | 0.13 |
| 9 | KDPUSMEC | 0.64 | 0.11 | RHMUNO65 | 0.63 | −0.11 | HFOSA | 0.65 | −0.11 |
| 10 | CORRATSS | 0.65 | −0.13 | HFOSA | 0.65 | −0.14 | PHCSS | 0.66 | 0.10 |
| 11 | CSNFMASS | 0.66 | 0.13 | SZKDSNAL | 0.66 | −0.15 | CSNFMASS | 0.67 | 0.10 |
| 12 | IS2MCOS | 0.67 | 0.12 | SZKDSEAL | 0.67 | 0.11 | KDPUSMEC | 0.67 | 0.10 |
| 13 | PHCSS | 0.68 | 0.12 | SZSREG2X | 0.68 | 0.10 | WDGCUA22 | 0.68 | 0.09 |
| 14 | | | | RHMU20 | 0.69 | 0.10 | | | |
| 15 | | | | HLWDRALK | 0.70 | 0.09 | | | |
| 16 | | | | IS2MCONS | 0.70 | 0.09 | | | |

(b)

| | SZTH230C: 50,000 Years | | | SZTH230C: 200,000 Years | | | SZTH230C: 500,000 Years | | |
|---|---|---|---|---|---|---|---|---|---|
| Step[a] | Variable[b] | $R^2$ [c] | SRRC[d] | Variable | $R^2$ | SRRC | Variable | $R^2$ | SRRC |
| 1 | EP1LOWOU | 0.16 | 0.40 | SZCONCOL | 0.19 | 0.44 | SZCONCOL | 0.19 | 0.46 |
| 2 | SZCONCOL | 0.30 | 0.34 | EP1LOWOU | 0.37 | 0.39 | EP1LOWOU | 0.39 | 0.40 |
| 3 | SZGWSPDM | 0.46 | 0.41 | SZGWSPDM | 0.44 | 0.28 | SZKDAMCO | 0.46 | 0.27 |
| 4 | INFIL | 0.53 | 0.29 | INFIL | 0.50 | 0.27 | INFIL | 0.52 | 0.24 |
| 5 | GOESITED | 0.58 | −0.19 | SZKDAMCO | 0.55 | 0.24 | SZGWSPDM | 0.57 | 0.22 |
| 6 | SZKDAMCO | 0.60 | 0.15 | GOESITED | 0.60 | −0.20 | GOESITED | 0.61 | −0.21 |
| 7 | SZDIFCVO | 0.62 | −0.16 | CORRATSS | 0.62 | −0.20 | KDPUSMEC | 0.62 | 0.12 |
| 8 | SZFISPVO | 0.64 | 0.10 | KDPUSMEC | 0.64 | 0.12 | HFOSA | 0.64 | −0.12 |
| 9 | CSWFA4AC | 0.65 | −0.11 | RHMUNO65 | 0.65 | −0.09 | SZKDSNAL | 0.65 | −0.16 |
| 10 | DSCRACKA | 0.66 | −0.09 | CSWFA4AC | 0.66 | −0.09 | SZKDNPAL | 0.66 | 0.11 |
| 11 | PHCSS | 0.67 | 0.12 | PHCSS | 0.68 | 0.13 | PHCSS | 0.67 | 0.11 |
| 12 | CORRATSS | 0.68 | −0.12 | PROBWPEF | 0.69 | 0.10 | CSNFMASS | 0.68 | 0.11 |
| 13 | IS2MCOS | 0.69 | 0.12 | CSCORRAT | 0.70 | 0.11 | CORRATSS | 0.69 | −0.10 |
| 14 | CSNFMASS | 0.70 | 0.11 | CSNFMASS | 0.70 | 0.12 | | | |
| 15 | KDPUSMEC | 0.71 | 0.10 | SZKDSNAL | 0.71 | −0.10 | | | |
| 16 | SZFIPOVO | 0.72 | −0.09 | | | | | | |

00817DC_0846b.ai

a: Steps in stepwise rank regression analysis
b: Variables listed in order of selection in stepwise regression
c: Cumulative $R^2$ value with entry of each variable into regression model
d: Standardized rank regression coefficients (SRRCs) in final regression model

Source: Output DTNs: MO0801TSPAPRSA.000 [DIRS 184620]; and MO0710PLOTSFIG.000 [DIRS 185207].

Figure K6.5.2-9[a]. Stepwise rank regression analyses and selected scatterplots for time-dependent release rates (*SZTH230*, g/yr) and cumulative (i.e., integrated) releases (*SZTH230C*, g) for the movement of dissolved $^{230}$Th across a subsurface plane at the location of the RMEI resulting from an igneous intrusive event at 250 years that destroys all WPs in the repository obtained with version 5.005 of the TSPA-LA Model: (a,b) regressions for *SZTH230* and *SZTH230C* at 50,000, 200,000, and 500,000 years, and (c-h) scatterplots for *SZTH230* and *SZTH230C* at 500,000 years

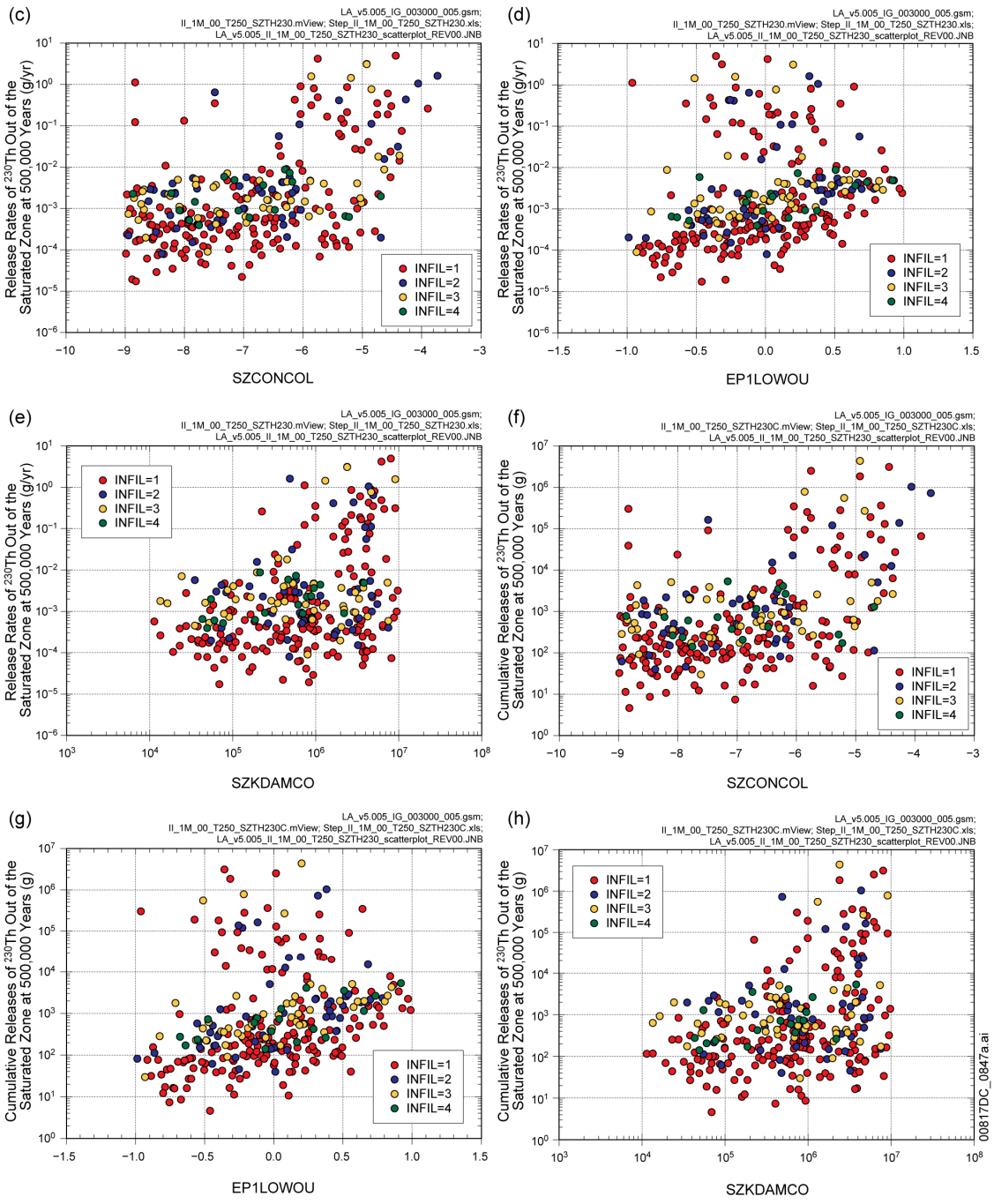


Source: Output DTNs: MO0801TSPAPRSA.000 [DIRS 184620]; and MO0710PLOTSFIG.000 [DIRS 185207].

Figure K6.5.2-9[a]. Stepwise rank regression analyses and selected scatterplots for time-dependent release rates (*SZTH230*, g/yr) and cumulative (i.e., integrated) releases (*SZTH230C*, g) for the movement of dissolved $^{230}$Th across a subsurface plane at the location of the RMEI resulting from an igneous intrusive event at 250 years that destroys all WPs in the repository obtained with version 5.005 of the TSPA-LA Model: (a,b) regressions for *SZTH230* and *SZTH230C* at 50,000, 200,000, and 500,000 years, and (c-h) scatterplots for *SZTH230* and *SZTH230C* at 500,000 years (continued)

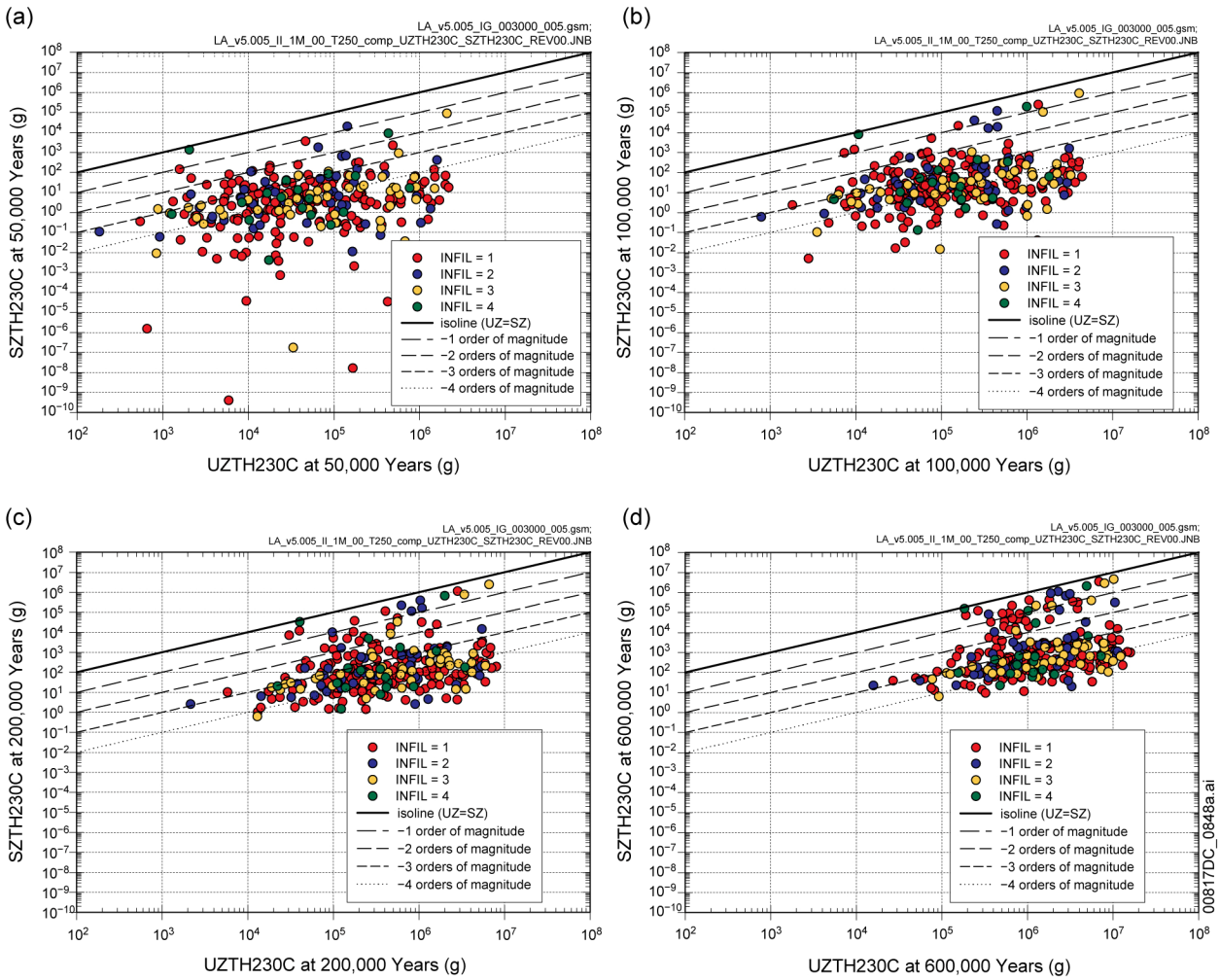


Source: Output DTNs: MO0801TSPAPRSA.000 [DIRS 184620]; and MO0710PLOTSFIG.000 [DIRS 185207].

Figure K.6.5.2-10[a]. Comparison of cumulative releases of dissolved $^{230}$Th into the SZ (*UZTH230C*, g) and across a subsurface plane at the location of the RMEI (*SZTH230C*, g) obtained with version 5.005 of the TSPA-LA Model at (a) 50,000, (b) 100,000, (c) 200,000, and (d) 600,000 years for an igneous intrusive event at 250 years that destroys all WPs in the repository

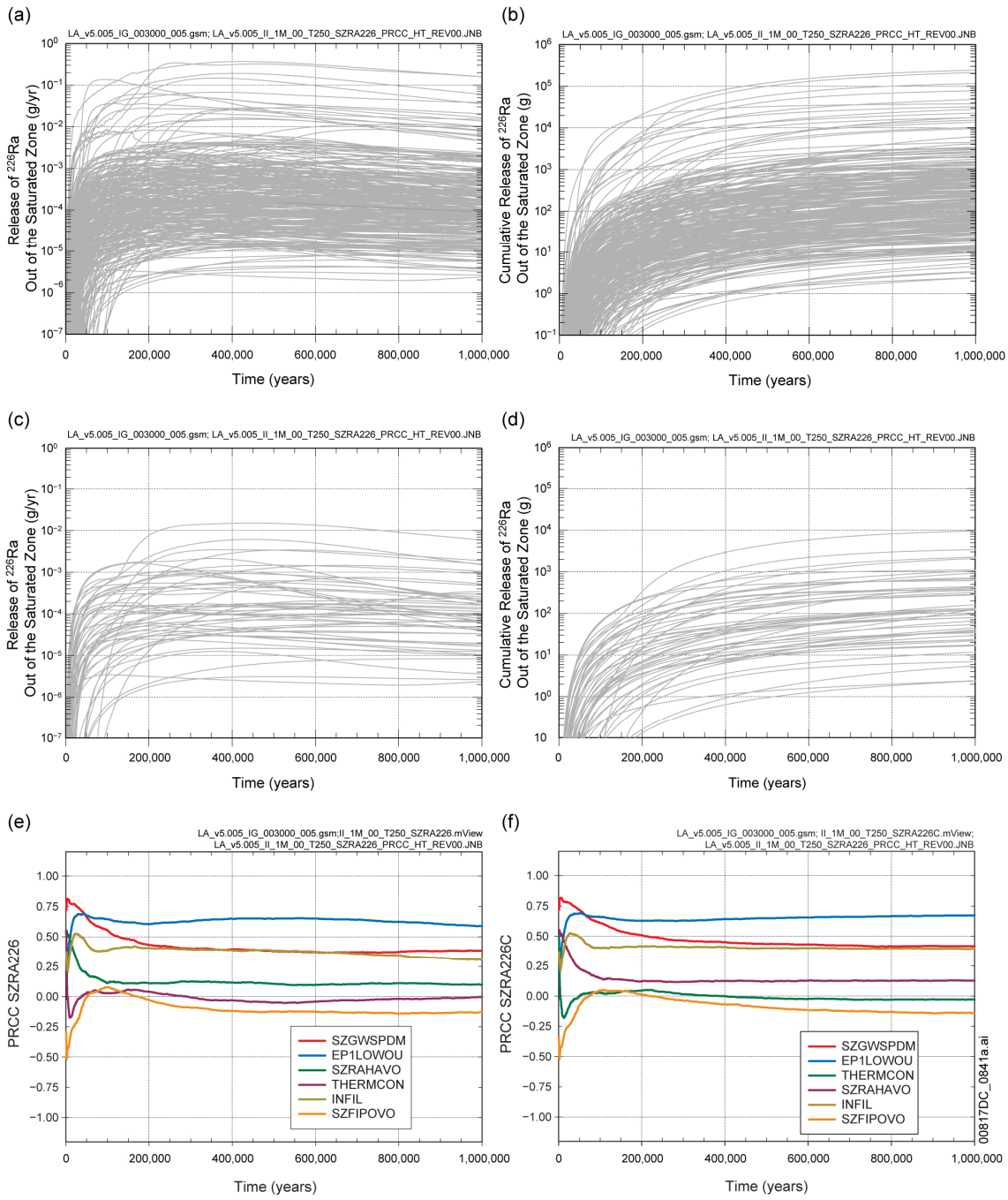


Source: Output DTNs: MO0801TSPAPRSA.000 [DIRS 184620]; and MO0710PLOTSFIG.000 [DIRS 185207].

Figure K6.5.2-11[a]. Time-dependent release rates (*SZRA226*, g/yr) and cumulative (i.e., integrated) releases (*SZRA226C*, g) over 1,000,000 years for the movement of dissolved $^{226}$Ra across a subsurface plane at the location of the RMEI resulting from an igneous intrusive event at 250 years that destroys all WPs in the repository obtained with version 5.005 of the TSPA-LA Model: (a,b) *SZRA226* and *SZRA226C* for all (i.e., 300) sample elements, (c,d) *SZRA226* and *SZRA226C* for first 50 sample elements, and (e,f) PRCCs for *SZRA226* and *SZRA226C*

(a)

| | SZRA226: 50,000 Years | | | SZRA226: 200,000 Years | | | SZRA226: 500,000 Years | | |
|---|---|---|---|---|---|---|---|---|---|
| Step[a] | Variable[b] | $R^2$ [c] | SRRC[d] | Variable | $R^2$ | SRRC | Variable | $R^2$ | SRRC |
| 1 | SZGWSPDM | 0.22 | 0.48 | EP1LOWOU | 0.19 | 0.43 | EP1LOWOU | 0.21 | 0.45 |
| 2 | EP1LOWOU | 0.40 | 0.43 | SZGWSPDM | 0.28 | 0.34 | SZCONCOL | 0.37 | 0.27 |
| 3 | INFIL | 0.48 | 0.32 | INFIL | 0.41 | 0.26 | SZGWSPDM | 0.45 | 0.27 |
| 4 | GOESITED | 0.52 | −0.20 | GOESITED | 0.47 | −0.26 | INFIL | 0.49 | 0.22 |
| 5 | SZKDRAAL | 0.56 | −0.21 | SZCONCOL | 0.52 | 0.20 | SZKDAMCO | 0.53 | 0.20 |
| 6 | CORRATSS | 0.58 | −0.15 | HFOSA | 0.55 | −0.16 | GOESITED | 0.56 | −0.21 |
| 7 | PHCSS | 0.60 | 0.13 | SZKDAMCO | 0.57 | 0.13 | PHCSS | 0.59 | 0.14 |
| 8 | IS2MCOS | 0.61 | 0.13 | PHCSS | 0.59 | 0.15 | HFOSA | 0.61 | −0.15 |
| 9 | CSNFMASS | 0.63 | 0.12 | CORRATSS | 0.61 | −0.15 | SZKDUAL | 0.62 | 0.13 |
| 10 | KDPUSMEC | 0.65 | 0.16 | KDPUSMEC | 0.63 | 0.12 | SZKDRAAL | 0.63 | −0.28 |
| 11 | UZFAG4 | 0.66 | −0.10 | UZFAG4 | 0.64 | −0.12 | | | |
| 12 | THERMCON | 0.67 | 0.11 | HLWDRALK | 0.65 | 0.11 | | | |
| 13 | HFOSA | 0.67 | −0.09 | SZKDRAAL | 0.66 | −0.27 | | | |
| 14 | SZRAHAVO | 0.68 | 0.11 | | | | | | |
| 15 | DSCRACKA | 0.69 | −0.09 | | | | | | |
| 16 | SZDIFCVO | 0.70 | −0.09 | | | | | | |

(b)

| | SZRA226C: 50,000 Years | | | SZRA226C: 200,000 Years | | | SZRA226C: 500,000 Years | | |
|---|---|---|---|---|---|---|---|---|---|
| Step[a] | Variable[b] | $R^2$ [c] | SRRC[d] | Variable | $R^2$ | SRRC | Variable | $R^2$ | SRRC |
| 1 | SZGWSPDM | 0.25 | 0.50 | EP1LOWOU | 0.19 | 0.43 | EP1LOWOU | 0.21 | 0.46 |
| 2 | EP1LOWOU | 0.42 | 0.40 | SZGWSPDM | 0.31 | 0.39 | SZGWSPDM | 0.31 | 0.29 |
| 3 | INFIL | 0.51 | 0.32 | INFIL | 0.37 | 0.26 | SZKDCSAL | 0.37 | −0.25 |
| 4 | GOESITED | 0.54 | −0.16 | GOESITED | 0.43 | −0.25 | SZCONCOL | 0.45 | 0.23 |
| 5 | SZKDRAAL | 0.58 | −0.20 | SZKDRAAL | 0.50 | −0.25 | INFIL | 0.50 | 0.23 |
| 6 | KDPUSMEC | 0.59 | 0.13 | SZCONCOL | 0.54 | 0.19 | GOESITED | 0.54 | −0.22 |
| 7 | SZDIFCVO | 0.61 | −0.15 | CORRATSS | 0.58 | −0.19 | SZKDAMCO | 0.58 | 0.18 |
| 8 | SZRAHAVO | 0.63 | 0.13 | PHCSS | 0.60 | 0.16 | HFOSA | 0.60 | −0.16 |
| 9 | SZFISPVO | 0.64 | 0.13 | HFOSA | 0.62 | −0.14 | PHCSS | 0.62 | 0.15 |
| 10 | CORRATSS | 0.66 | −0.16 | KDPUSMEC | 0.64 | 0.13 | SZRAHAVO | 0.64 | 0.10 |
| 11 | IS2MCOS | 0.67 | 0.13 | UZFAG4 | 0.65 | −0.12 | KDPUSMEC | 0.65 | 0.10 |
| 12 | PHCSS | 0.69 | 0.12 | HLWDRALK | 0.66 | 0.10 | UZFAG4 | 0.65 | −0.11 |
| 13 | CSNFMASS | 0.70 | 0.11 | SZKDAMCO | 0.67 | 0.11 | UZCOKDPU | 0.66 | 0.09 |
| 14 | SZFIPOVO | 0.71 | −0.10 | CSCORRAT | 0.68 | 0.09 | | | |
| 15 | DSCRACKA | 0.72 | −0.10 | | | | | | |
| 16 | THERMCON | 0.73 | 0.10 | | | | | | |

008178DC_0842a.ai

a: Steps in stepwise rank regression analysis
b: Variables listed in order of selection in stepwise regression
c: Cumulative $R^2$ value with entry of each variable into regression model
d: Standardized rank regression coefficients (SRRCs) in final regression model

Source: Output DTNs: MO0801TSPAPRSA.000 [DIRS 184620]; and MO0710PLOTSFIG.000 [DIRS 185207].

Figure K6.5.2-12[a]. Stepwise rank regression analyses and selected scatterplots for time-dependent release rates (*SZRA226*, g/yr) and cumulative (i.e., integrated) releases (*SZRA226C*, g) for the movement of dissolved $^{226}$Ra across a subsurface plane at the location of the RMEI resulting from an igneous intrusive event at 250 years that destroys all WPs in the repository obtained with version 5.005 of the TSPA-LA Model: (a,b) regressions for *SZRA226* and *SZRA226C* at 50,000, 200,000, and 500,000 years, and (c-h) scatterplots for *SZRA226* and *SZRA226C* at 50,000 years

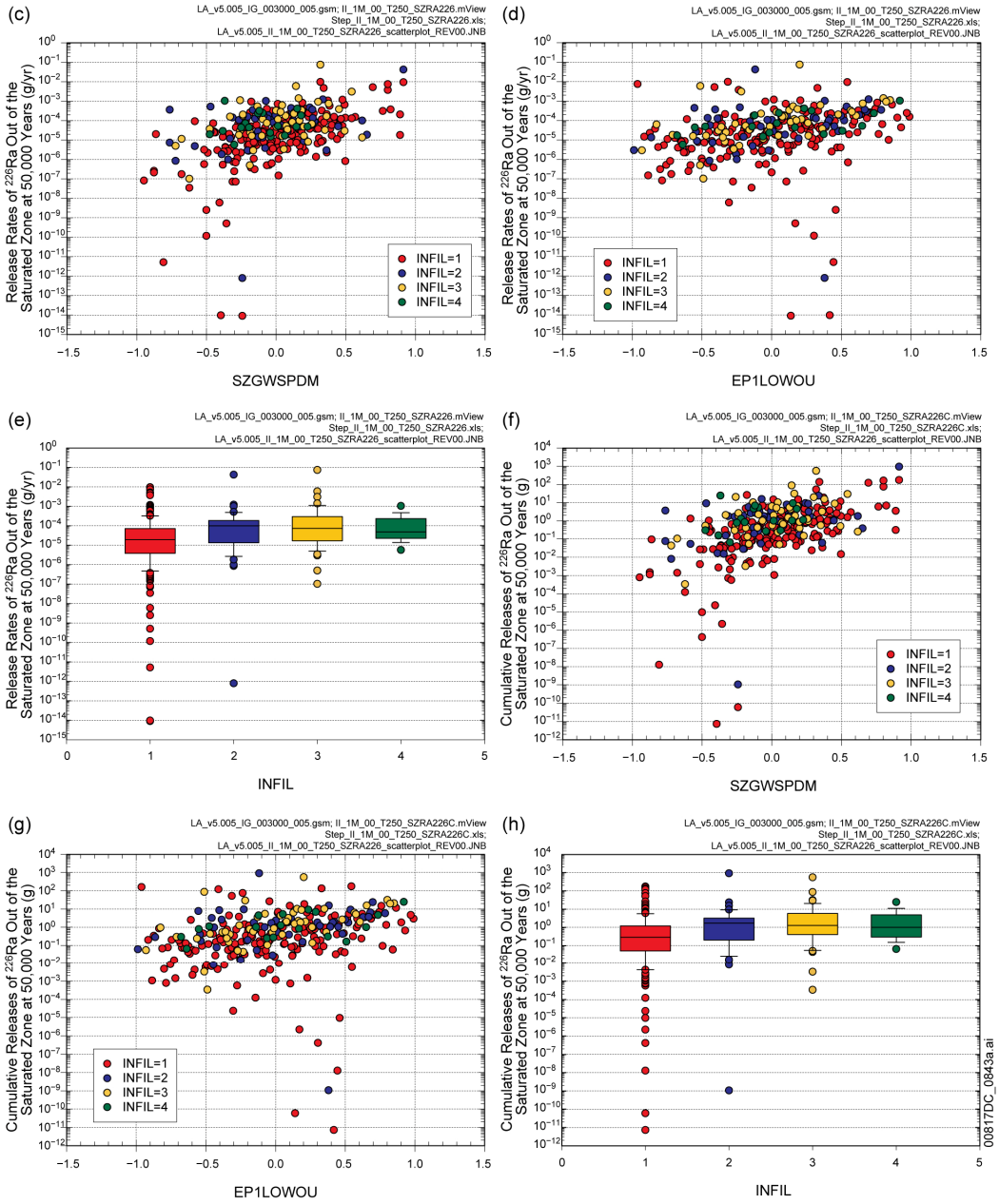


Source: Output DTNs: MO0801TSPAPRSA.000 [DIRS 184620]; and MO0710PLOTSFIG.000 [DIRS 185207].

NOTE: In (e,h), the box extends from 0.25 to 0.75 quantile; lower and upper bar and whisker extend to 0.1 and 0.9 quantile, respectively; dots represent values outside 0.1 to 0.9 quantile range; median indicated by light horizontal line.

Figure K6.5.2-12[a]. Stepwise rank regression analyses and selected scatterplots for time-dependent release rates (*SZRA226*, g/yr) and cumulative (i.e., integrated) releases (*SZRA226C*, g) for the movement of dissolved $^{226}$Ra across a subsurface plane at the location of the RMEI resulting from an igneous intrusive event at 250 years that destroys all WPs in the repository obtained with version 5.005 of the TSPA-LA Model: (a,b) regressions for *SZRA226* and *SZRA226C* at 50,000, 200,000, and 500,000 years, and (c-h) scatterplots for *SZRA226* and *SZRA226C* at 50,000 years (continued)

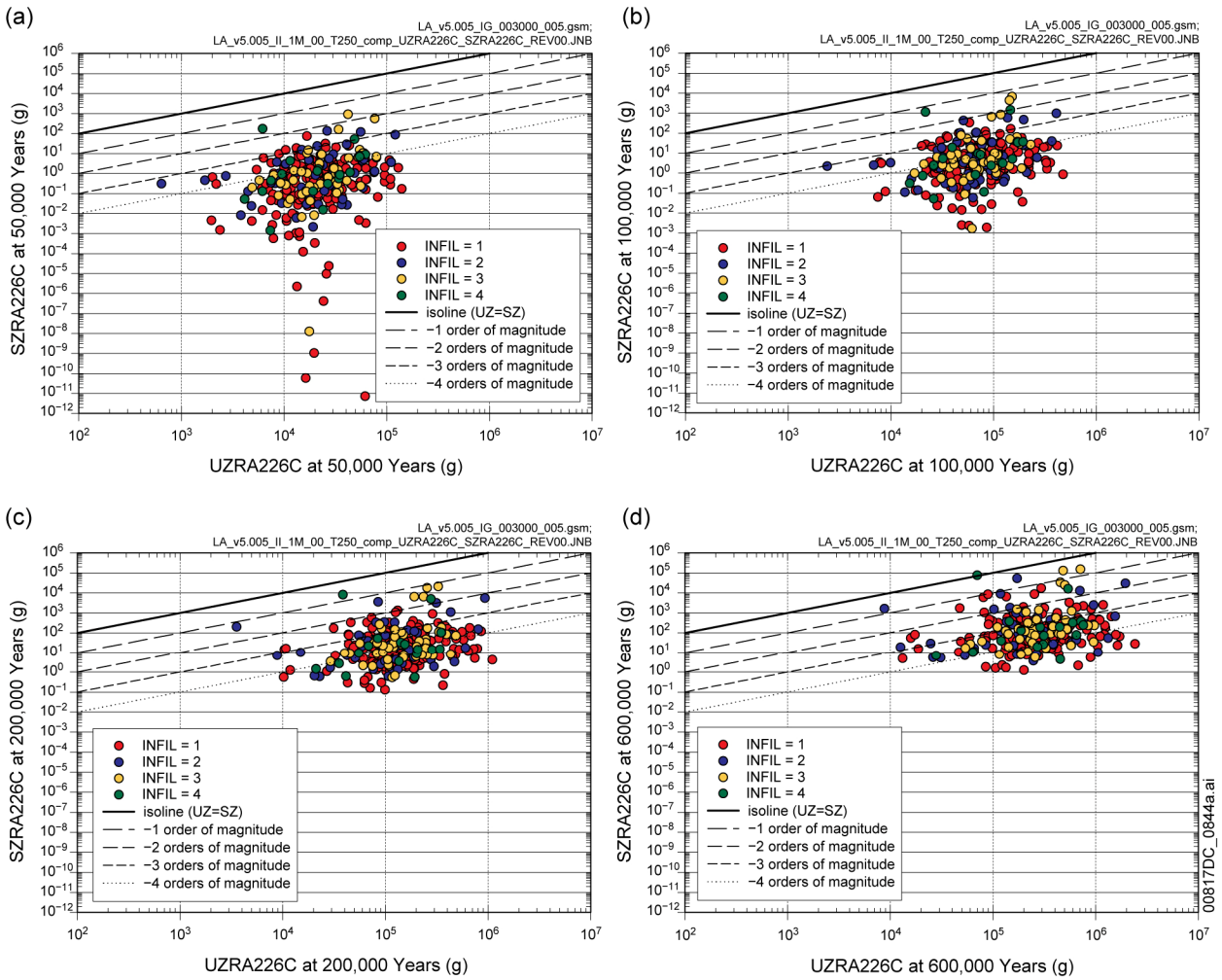


Source: Output DTNs: MO0801TSPAPRSA.000 [DIRS 184620]; and MO0710PLOTSFIG.000 [DIRS 185207].

Figure K.6.5.2-13[a]. Comparison of cumulative releases of dissolved $^{226}Ra$ into the SZ (*UZRA226C*, g) and across a subsurface plane at the location of the RMEI (*SZRA226C*, g) obtained with version 5.005 of the TSPA-LA Model at (a) 50,000, (b) 100,000, (c) 200,000, and (d) 600,000 years for an igneous intrusive event at 250 years that destroys all WPs in the repository

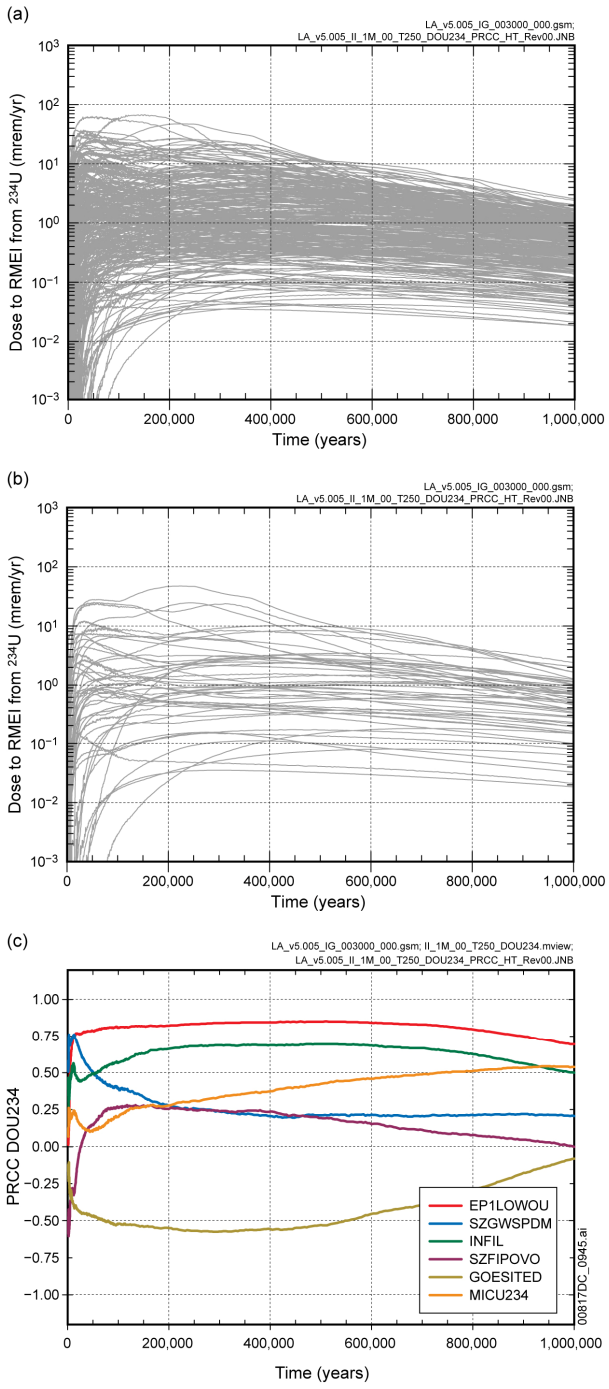


Source: Output DTNs: MO0801TSPAPRSA.000 [DIRS 184620]; and MO0710PLOTSFIG.000 [DIRS 185207].

Figure K.6.6.2-5[a]. Time-dependent dose to the RMEI (*DOU234*, mrem/yr) over 1,000,000 years for the movement of dissolved $^{234}U$ across a subsurface plane at the location of the RMEI resulting from an igneous intrusive event at 250 years that destroys all WPs in the repository obtained with version 5.005 of the TSPA-LA Model: (a) *DOU234* for all (i.e., 300) sample elements, (b) *DOU234* for first 50 sample elements, and (c) PRCCs for *DOU234*

(a)

| | DOU234: 50,000 Years | | | DOU234: 200,000 Years | | | DOU234: 500,000 Years | | |
|---|---|---|---|---|---|---|---|---|---|
| Step[a] | Variable[b] | $R^{2c}$ | SRRC[d] | Variable | $R^2$ | SRRC | Variable | $R^2$ | SRRC |
| 1 | EP1LOWOU | 0.27 | 0.49 | EP1LOWOU | 0.35 | 0.57 | EP1LOWOU | 0.42 | 0.64 |
| 2 | INFIL | 0.40 | 0.36 | INFIL | 0.54 | 0.41 | INFIL | 0.61 | 0.40 |
| 3 | SZGWSPDM | 0.48 | 0.28 | GOESITED | 0.61 | −0.26 | MICU234 | 0.66 | 0.25 |
| 4 | GOESITED | 0.55 | −0.21 | MICU234 | 0.65 | 0.17 | GOESITED | 0.71 | −0.24 |
| 5 | CORRATSS | 0.59 | −0.23 | PHCSS | 0.68 | 0.19 | PHCSS | 0.75 | 0.19 |
| 6 | PHCSS | 0.61 | 0.16 | SZGWSPDM | 0.70 | 0.18 | HFOSA | 0.77 | −0.13 |
| 7 | IS2MCOS | 0.64 | 0.12 | HFOSA | 0.72 | −0.15 | SZGWSPDM | 0.78 | 0.12 |
| 8 | CSNFMASS | 0.66 | 0.14 | GOERELAB | 0.74 | 0.11 | GOERELAB | 0.79 | 0.11 |
| 9 | SZDIFCVO | 0.67 | −0.15 | KDPUSMEC | 0.75 | 0.10 | CSNFMASS | 0.80 | 0.10 |
| 10 | SZFISPVO | 0.69 | 0.12 | UZFAG4 | 0.75 | −0.09 | MICTC99 | 0.81 | −0.08 |
| 11 | MICU234 | 0.70 | 0.11 | CORRATSS | 0.76 | −0.10 | WDLCRATE | 0.81 | −0.09 |
| 12 | KDPUSMEC | 0.71 | 0.10 | CSCORRAT | 0.77 | 0.09 | SZSREG2X | | |
| 13 | GOERELAB | 0.72 | 0.10 | DSNFMASS | 0.78 | 0.07 | | | |
| 14 | WDDEFCNT | 0.73 | −0.09 | CSNFMASS | 0.78 | 0.10 | | | |
| 15 | INRFRCCS | 0.73 | −0.09 | KDPUCOL | 0.79 | 0.09 | | | |
| 16 | KDPUCOL | 0.74 | 0.09 | WDDEFCNT | 0.80 | −0.08 | | | |

a: Steps in stepwise rank regression analysis
b: Variables listed in order of selection in stepwise regression
c: Cumulative $R^2$ value with entry of each variable into regression model
d: Standardized rank regression coefficients (SRRCs) in final regression model

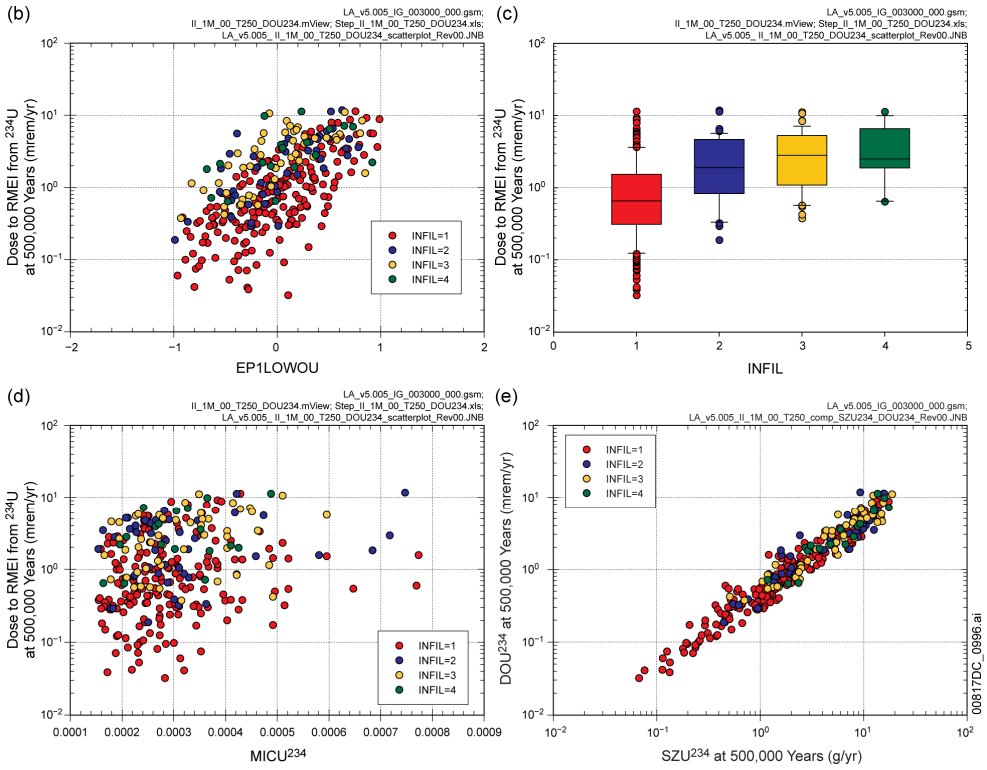


Source: Output DTNs: MO0801TSPAPRSA.000 [DIRS 184620]; and MO0710PLOTSFIG.000 [DIRS 185207].

NOTE: In (c), the box extends from 0.25 to 0.75 quantile; lower and upper bar and whisker extend to 0.1 and 0.9 quantile, respectively; dots represent values outside 0.1 to 0.9 quantile range; median indicated by light horizontal line.

Figure K.6.6.2-6[a]. Stepwise rank regression analyses and selected scatterplots for time-dependent dose to the RMEI (*DOU234*, mrem/yr) for the movement of dissolved $^{234}U$ across a subsurface plane at the location of the RMEI (*SZU234*, g/yr) resulting from an igneous intrusive event at 250 years that destroys all WPs in the repository obtained with version 5.005 of the TSPA-LA Model: (a) regressions for *DOU234* at 50,000, 200,000, and 500,000 years, (b,c,d) scatterplots for *DOU234* at 500,000 years, and (e) scatterplot comparing *SZU234* and *DOU234* at 500,000 years

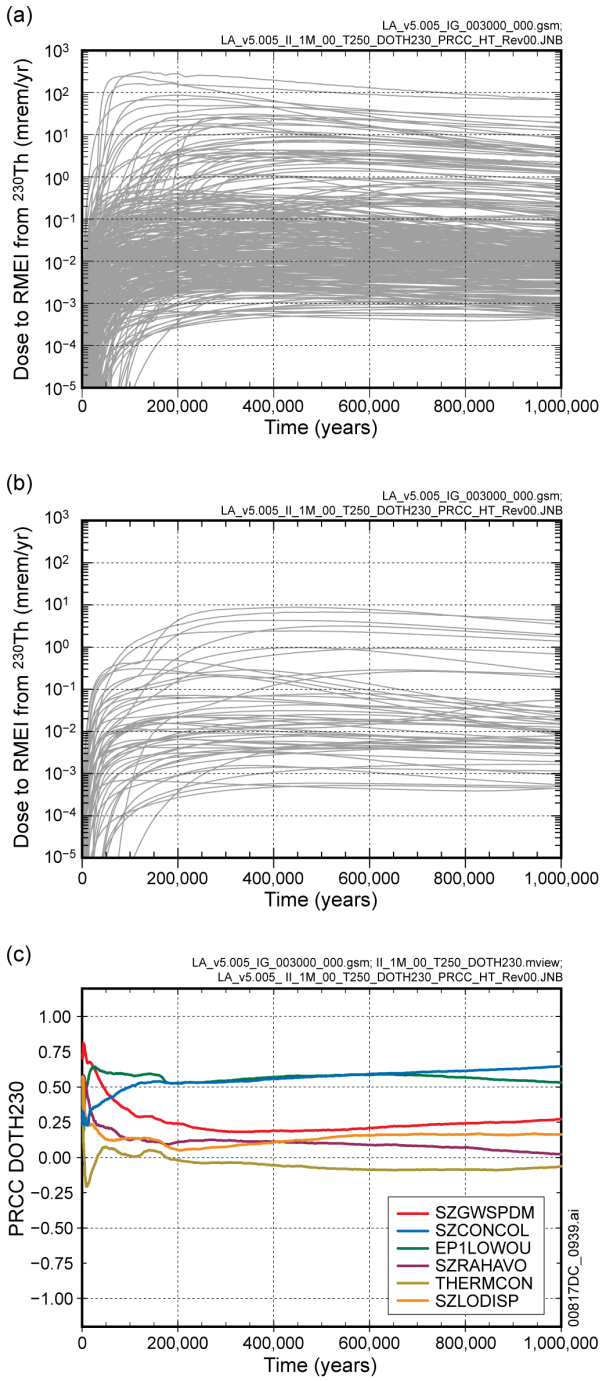


Source: Output DTNs: MO0801TSPAPRSA.000 [DIRS 184620]; and MO0710PLOTSFIG.000 [DIRS 185207].

Figure K.6.6.2-7[a]. Time-dependent dose to the RMEI (*DOTH230*, mrem/yr) over 1,000,000 years for the movement of dissolved $^{230}$Th across a subsurface plane at the location of the RMEI resulting from an igneous intrusive event at 250 years that destroys all WPs in the repository obtained with version 5.005 of the TSPA-LA Model: a) *DOTH230* for all (i.e., 300) sample elements, (b) *DOTH230* for first 50 sample elements, and (c) PRCCs for *DOTH230*

(a)

| | DOTH230: 50,000 Years | | | DOTH230: 200,000 Years | | | DOTH230: 500,000 Years | | |
|---|---|---|---|---|---|---|---|---|---|
| Step[a] | Variable[b] | $R^{2c}$ | SRRC[d] | Variable | $R^2$ | SRRC | Variable | $R^2$ | SRRC |
| 1 | EP1LOWOU | 0.16 | 0.41 | SZCONCOL | 0.19 | 0.45 | SZCONCOL | 0.20 | 0.46 |
| 2 | SZCONCOL | 0.31 | 0.38 | EP1LOWOU | 0.36 | 0.37 | EP1LOWOU | 0.39 | 0.39 |
| 3 | SZGWSPDM | 0.42 | 0.35 | SZKDAMCO | 0.42 | 0.25 | SZKDAMCO | 0.46 | 0.26 |
| 4 | INFIL | 0.50 | 0.29 | INFIL | 0.48 | 0.26 | INFIL | 0.52 | 0.22 |
| 5 | GOESITED | 0.55 | −0.20 | GOESITED | 0.52 | −0.21 | SZGWSPDM | 0.55 | 0.19 |
| 6 | MICTH229 | 0.59 | 0.17 | SZGWSPDM | 0.56 | 0.21 | GOESITED | 0.58 | −0.17 |
| 7 | SZKDAMCO | 0.61 | 0.17 | MICTH229 | 0.59 | 0.16 | MICTH229 | 0.60 | 0.17 |
| 8 | SZDIFCVO | 0.63 | −0.12 | CORRATSS | 0.61 | −0.16 | PHCSS | 0.62 | 0.12 |
| 9 | CSWFA4AC | 0.64 | −0.11 | KDPUSMEC | 0.63 | 0.13 | SZKDAMAL | 0.63 | −0.15 |
| 10 | KDPUSMEC | 0.65 | 0.11 | PHCSS | 0.64 | 0.11 | HFOSA | 0.64 | −0.10 |
| 11 | PHCSS | 0.66 | 0.13 | CSNFMASS | 0.65 | 0.11 | SZKDUAL | 0.65 | 0.12 |
| 12 | CORRATSS | 0.67 | −0.13 | SZKDSNAL | 0.66 | −0.16 | CSNFMASS | 0.66 | 0.10 |
| 13 | CSNFMASS | 0.69 | 0.13 | HFOSA | 0.67 | −0.11 | WDGCUA22 | 0.67 | 0.09 |
| 14 | IS2MCOS | 0.70 | 0.12 | SZKDNPAL | 0.68 | 0.11 | | | |
| 15 | | | | SZSREG2X | 0.69 | 0.09 | | | |

a: Steps in stepwise rank regression analysis
b: Variables listed in order of selection in stepwise regression
c: Cumulative $R^2$ value with entry of each variable into regression model
d: Standardized rank regression coefficients (SRRCs) in final regression model

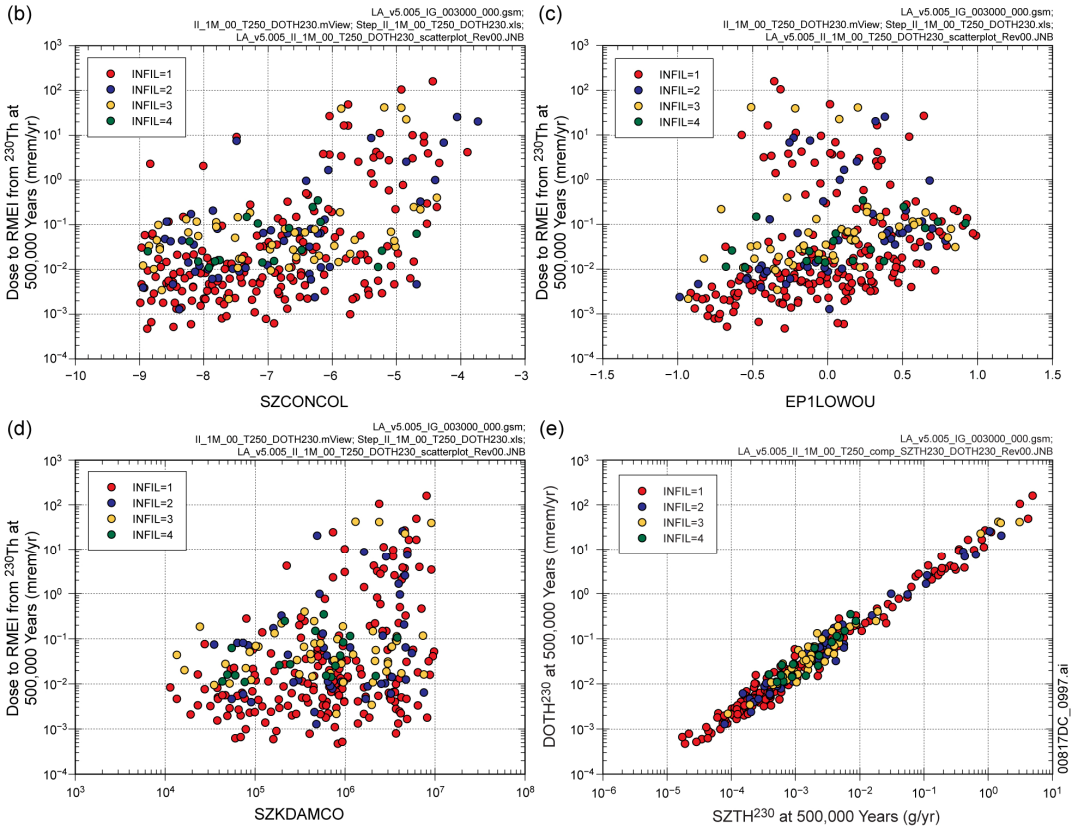


Source: Output DTNs: MO0801TSPAPRSA.000 [DIRS 184620]; and MO0710PLOTSFIG.000 [DIRS 185207].

Figure K.6.6.2-8[a]. Stepwise rank regression analyses and selected scatterplots for time-dependent dose to the RMEI (*DOTH230*, mrem/yr) for the movement of dissolved $^{230}$Th across a subsurface plane at the location of the RMEI (*SZTH230*, g/yr) resulting from an igneous intrusive event at 250 years that destroys all WPs in the repository obtained with version 5.005 of the TSPA-LA Model: (a) regressions for *DOTH230* at 50,000, 200,000, and 500,000 years, (b,c,d) scatterplots for *DOTH230* at 500,000 years, and (e) scatterplot comparing *SZTH230* and *DOTH230* at 500,000 years

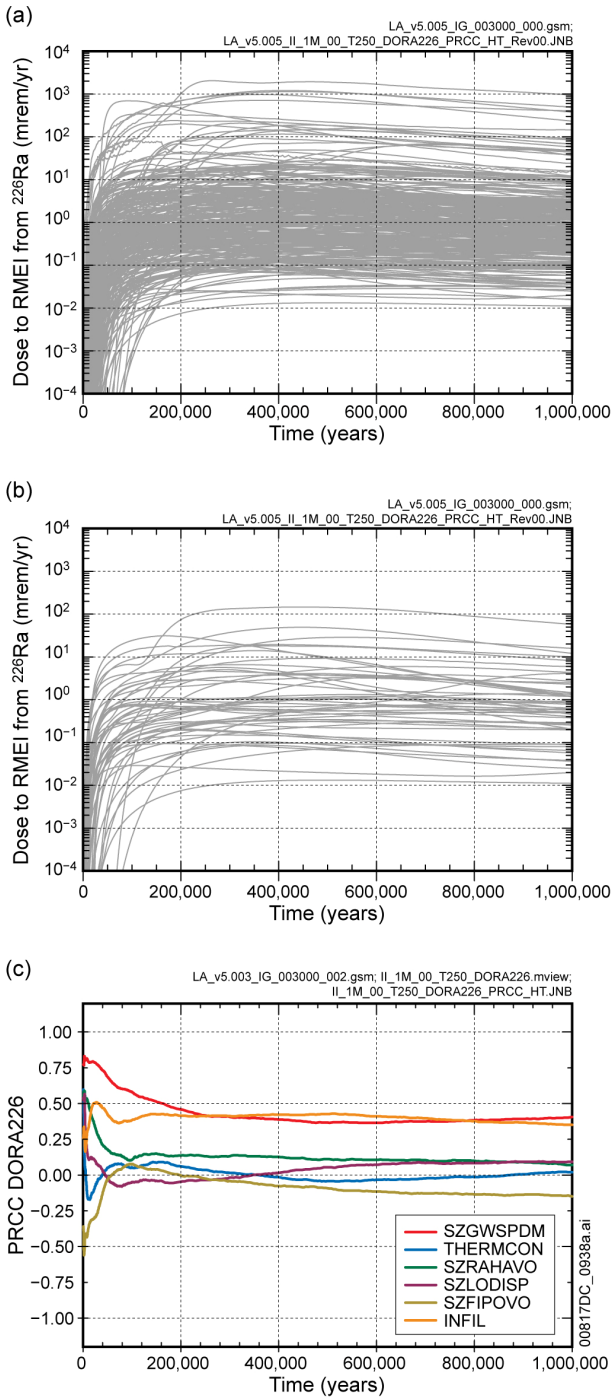


Source: Output DTNs: MO0801TSPAPRSA.000 [DIRS 184620]; and MO0710PLOTSFIG.000 [DIRS 185207].

Figure K.6.6.2-9[a]. Time-dependent dose to the RMEI (*DORA226*, mrem/yr) over 1,000,000 years for the movement of dissolved $^{226}$Ra across a subsurface plane at the location of the RMEI resulting from an igneous intrusive event at 250 years that destroys all WPs in the repository obtained with version 5.005 of the TSPA-LA Model: (a) *DORA226* for all (i.e., 300) sample elements, (b) *DORA226* for first 50 sample elements, and (c) PRCCs for *DORA226*

(a)

| | DORA226: 50,000 Years | | | DORA226: 200,000 Years | | | DORA226: 500,000 Years | | |
|---|---|---|---|---|---|---|---|---|---|
| Step[a] | Variable[b] | $R^2$ [c] | SRRC[d] | Variable | $R^2$ | SRRC | Variable | $R^2$ | SRRC |
| 1 | SZGWSPDM | 0.21 | 0.50 | EP1LOWOU | 0.19 | 0.43 | EP1LOWOU | 0.21 | 0.44 |
| 2 | EP1LOWOU | 0.39 | 0.43 | SZKDCSAL | 0.28 | −0.24 | SZKDCSAL | 0.30 | −0.26 |
| 3 | INFIL | 0.47 | 0.32 | SZGWSPDM | 0.34 | 0.32 | SZCONCOL | 0.36 | 0.25 |
| 4 | GOESITED | 0.51 | −0.19 | INFIL | 0.40 | 0.25 | SZGWSPDM | 0.43 | 0.24 |
| 5 | SZKDRAAL | 0.55 | −0.20 | MICRA226 | 0.45 | 0.24 | INFIL | 0.47 | 0.22 |
| 6 | MICRA226 | 0.58 | 0.17 | GOESITED | 0.51 | −0.23 | MICRA226 | 0.51 | 0.20 |
| 7 | KDPUSMEC | 0.60 | 0.16 | SZCONCOL | 0.55 | 0.20 | SZKDAMCO | 0.55 | 0.19 |
| 8 | UZFAG4 | 0.62 | −0.11 | HFOSA | 0.58 | −0.15 | GOESITED | 0.57 | −0.19 |
| 9 | PHCSS | 0.64 | 0.14 | PHCSS | 0.60 | 0.16 | PHCSS | 0.60 | 0.14 |
| 10 | CORRATSS | 0.65 | −0.15 | SZKDAMCO | 0.62 | 0.13 | HFOSA | 0.62 | −0.15 |
| 11 | IS2MCOS | 0.66 | 0.14 | CORRATSS | 0.64 | −0.12 | SZKDUAL | 0.63 | 0.10 |
| 12 | CSNFMASS | 0.68 | 0.11 | KDPUSMEC | 0.65 | 0.11 | SZRAHAVO | 0.64 | 0.10 |
| 13 | SZCONCOL | 0.69 | 0.09 | UZFAG4 | 0.66 | −0.12 | | | |
| 14 | HFOSA | 0.70 | −0.09 | HLWDRALK | 0.67 | 0.11 | | | |
| 15 | THERMCON | 0.70 | 0.09 | SZKDSNAL | 0.68 | −0.10 | | | |
| 16 | | | | SZDENAL | 0.68 | −0.09 | | | |

a: Steps in stepwise rank regression analysis
b: Variables listed in order of selection in stepwise regression
c: Cumulative $R^2$ value with entry of each variable into regression model
d: Standardized rank regression coefficients (SRRCs) in final regression model

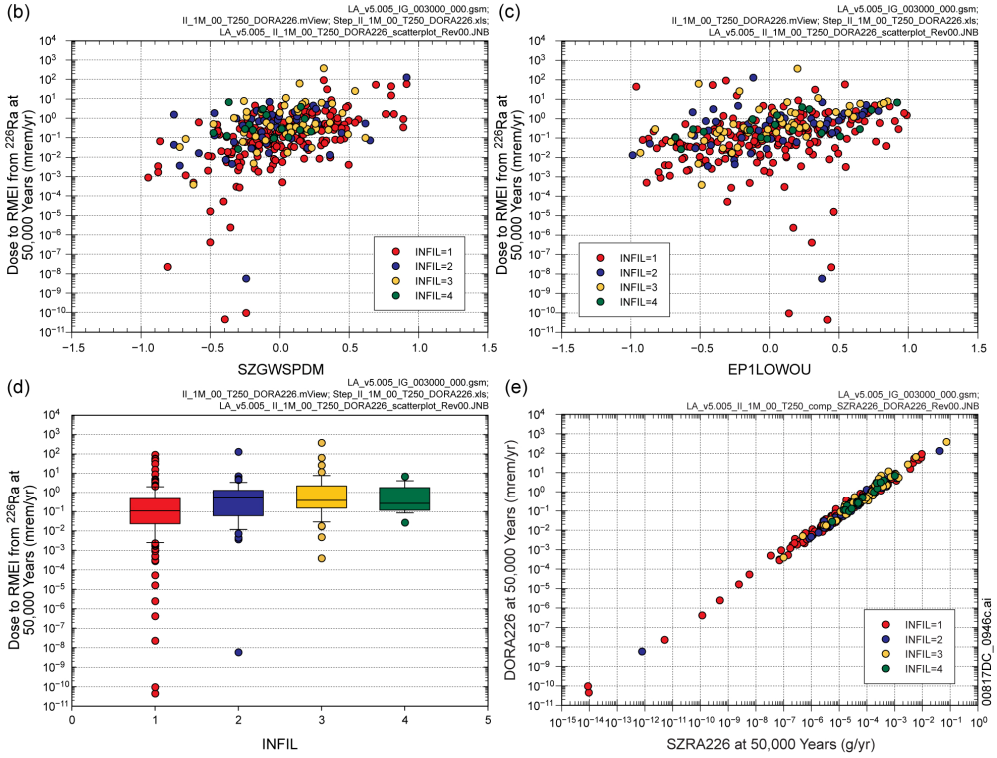


Source: Output DTNs: MO0801TSPAPRSA.000 [DIRS 184620]; and MO0710PLOTSFIG.000 [DIRS 185207].

NOTE: In (d), the box extends from 0.25 to 0.75 quantile; lower and upper bar and whisker extend to 0.1 and 0.9 quantile, respectively; dots represent values outside 0.1 to 0.9 quantile range; median indicated by light horizontal line.

Figure K.6.6.2-10[a]. Stepwise rank regression analyses and selected scatterplots for time-dependent dose to the RMEI (*DORA226*, mrem/yr) for the movement of dissolved $^{226}$Ra across a subsurface plane at the location of the RMEI (*SZRA226*, g/yr) resulting from an igneous intrusive event at 250 years that destroys all WPs in the repository obtained with version 5.005 of the TSPA-LA Model: (a) regressions for *DORA226* at 50,000, 200,000, and 500,000 years, (b,c,d) scatterplots for *DORA226* at 50,000 years, and (e) scatterplot comparing *SZRA226* and *DORA226* at 50,000 years

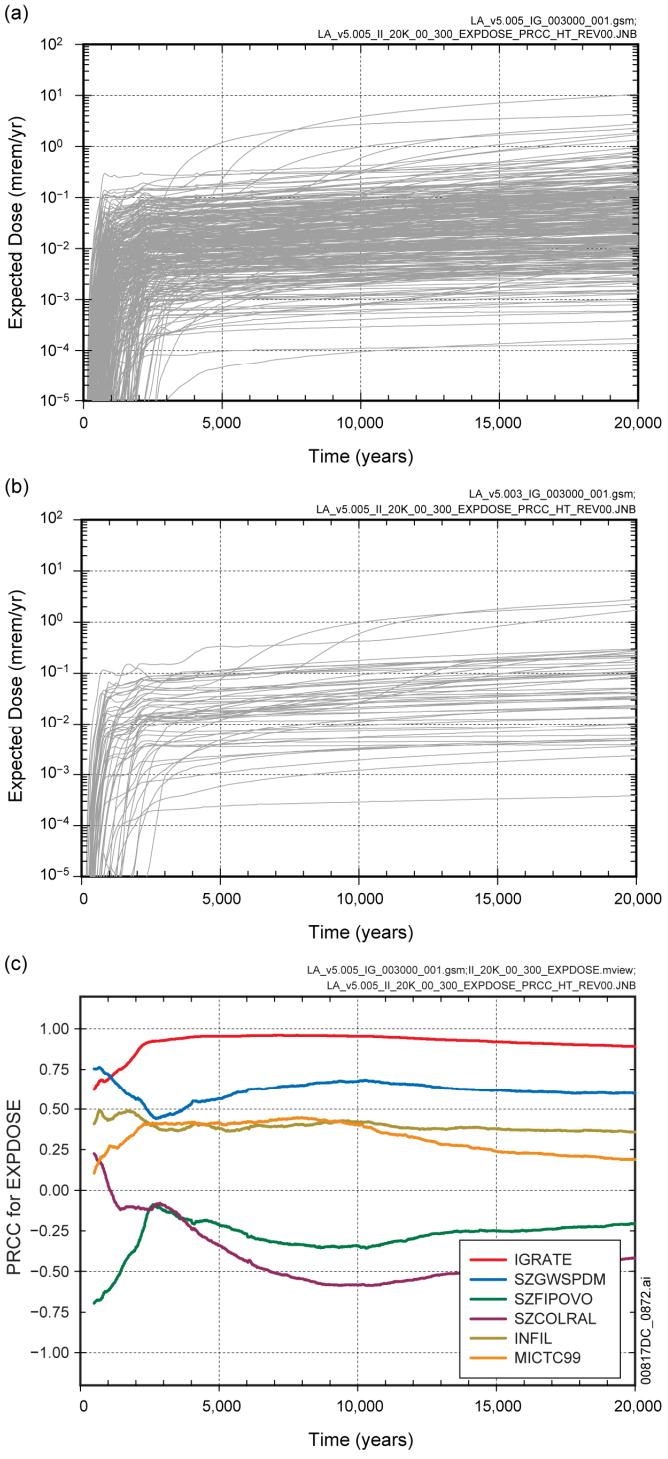


Source: Output DTNs: MO0710ADTSPAWO.000 [DIRS 183752]; and MO0710PLOTSFIG.000 [DIRS 185207].

Figure K6.7.1-1[a]. Expected dose to RMEI (*EXPDOSE*, mrem/yr) over [0, 20,000 yr] for all radioactive species resulting from igneous intrusion obtained with version 5.005 of the TSPA-LA Model: (a) *EXPDOSE* for all (i.e., 300) sample elements, (b) *EXPDOSE* for first 50 sample elements, and (c) PRCCs for *EXPDOSE*

(a)

| | 3,000 Years | | | 5,000 Years | | | 10,000 Years | | |
|---|---|---|---|---|---|---|---|---|---|
| Step[a] | Variable[b] | $R^2$ [c] | SRRC[d] | Variable | $R^2$ | SRRC | Variable | $R^2$ | SRRC |
| 1 | IGRATE | 0.74 | 0.88 | IGRATE | 0.80 | 0.90 | IGRATE | 0.76 | 0.87 |
| 2 | SZGWSPDM | 0.79 | 0.22 | SZGWSPDM | 0.84 | 0.19 | SZGWSPDM | 0.81 | 0.22 |
| 3 | INFIL | 0.82 | 0.16 | MICTC99 | 0.86 | 0.13 | INFIL | 0.83 | 0.15 |
| 4 | MICTC99 | 0.85 | 0.15 | INFIL | 0.89 | 0.16 | MICTC99 | 0.85 | 0.09 |
| 5 | SZFISPVO | 0.87 | 0.13 | SZFISPVO | 0.90 | 0.07 | SZCOLRAL | 0.86 | −0.13 |
| 6 | CSNFMASS | 0.87 | 0.09 | MICC14 | 0.90 | 0.09 | CPUCOLWF | 0.87 | 0.10 |
| 7 | SZDIFCVO | 0.88 | −0.09 | CSNFMASS | 0.91 | 0.08 | SZFIPOVO | 0.88 | −0.08 |
| 8 | MICC14 | 0.89 | 0.08 | MICNP237 | 0.91 | 0.08 | MICNP237 | 0.89 | 0.10 |
| 9 | MICNP237 | 0.89 | 0.08 | SZFIPOVO | 0.92 | −0.07 | SZFISPVO | 0.89 | 0.08 |
| 10 | SZCOLRVO | 0.89 | −0.06 | SZCOLRAL | 0.92 | −0.06 | ISCSS | 0.90 | −0.06 |
| 11 | SZFIPOVO | 0.90 | −0.06 | SZCOLRVO | 0.92 | −0.06 | SZDENAL | 0.90 | −0.06 |
| 12 | SZSREG3Y | 0.90 | −0.06 | SMECSA | 0.92 | 0.05 | EP1LOWNU | 0.90 | 0.06 |
| 13 | ISCSNS | 0.90 | 0.05 | PHCSNS | 0.93 | −0.04 | KDRASMEC | 0.91 | 0.07 |
| 14 | | | | | | | EP1NPO2 | 0.91 | 0.06 |
| 15 | | | | | | | WPFLUX | 0.91 | 0.05 |

a: Steps in stepwise rank regression analysis
b: Variables listed in order of selection in stepwise regression
c: Cumulative $R^2$ value with entry of each variable into regression model
d: Standardized rank regression coefficients (SRRCs) in final regression model

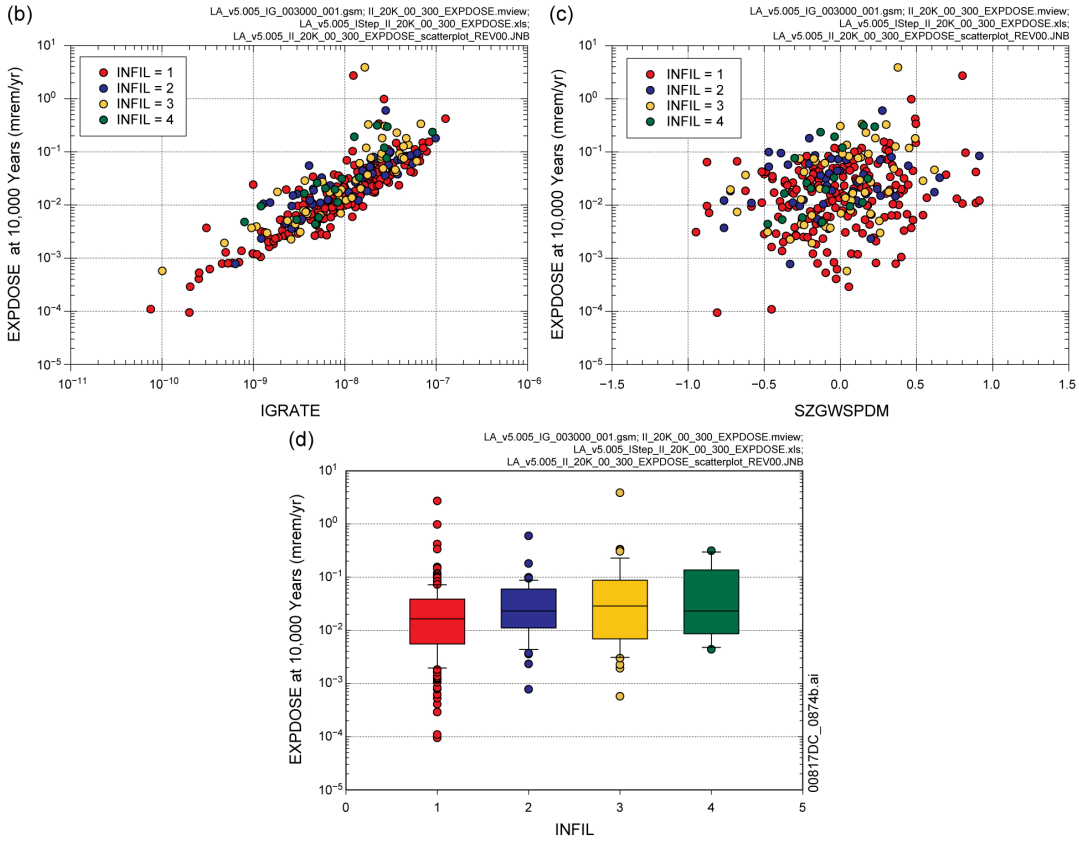


Source: Output DTNs: MO0710ADTSPAWO.000 [DIRS 183752]; and MO0710PLOTSFIG.000 [DIRS 185207].

NOTE: In (d), the box extends from 0.25 to 0.75 quantile; lower and upper bar and whisker extend to 0.1 and 0.9 quantile, respectively; dots represent values outside 0.1 to 0.9 quantile range; median indicated by light horizontal line.

Figure K6.7.1-2[a]. Stepwise rank regression analyses and selected scatterplots for expected dose to RMEI (*EXPDOSE*, mrem/yr) over [0, 20,000 yr] for all radioactive species resulting from igneous intrusion obtained with version 5.005 of the TSPA-LA Model: (a) regressions for *EXPDOSE* at 3,000, 5,000, and 10,000 years, and (b,c,d) scatterplots for *EXPDOSE* at 10,000 years

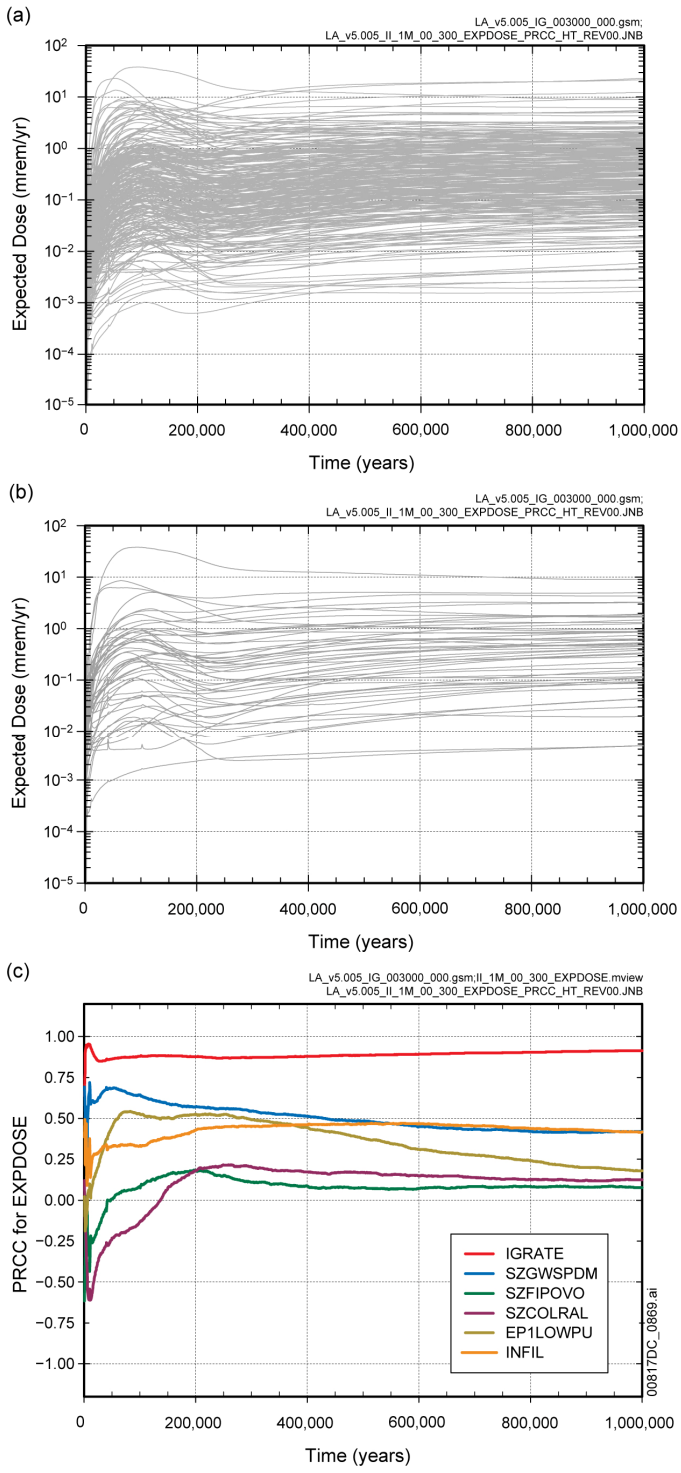


Source: Output DTNs: MO0710ADTSPAWO.000 [DIRS 183752]; and MO0710PLOTSFIG.000 [DIRS 185207].

Figure K.6.7.2-1[a]. Expected dose to RMEI (*EXPDOSE*, mrem/yr) over [0, 1,000,000 yr] for all radioactive species resulting from igneous intrusion obtained with version 5.005 of the TSPA-LA Model: (a) *EXPDOSE* for all (i.e., 300) sample elements, (b) *EXPDOSE* for first 50 sample elements, and (c) PRCCs for *EXPDOSE*

(a)

| | EXPDOSE: 50,000 Years | | | EXPDOSE: 200,000 Years | | | EXPDOSE: 500,000 Years | | |
|---|---|---|---|---|---|---|---|---|---|
| Step[a] | Variable[b] | $R^{2}$ [c] | SRRC[d] | Variable | $R^{2}$ | SRRC | Variable | $R^{2}$ | SRRC |
| 1 | IGRATE | 0.53 | 0.72 | IGRATE | 0.57 | 0.75 | IGRATE | 0.62 | 0.79 |
| 2 | SZGWSPDM | 0.69 | 0.39 | SZGWSPDM | 0.67 | 0.30 | SZGWSPDM | 0.68 | 0.25 |
| 3 | EP1LOWPU | 0.74 | 0.20 | EP1LOWPU | 0.72 | 0.20 | INFIL | 0.73 | 0.19 |
| 4 | INFIL | 0.77 | 0.16 | INFIL | 0.75 | 0.19 | EP1LOWPU | 0.75 | 0.16 |
| 5 | EP1NPO2 | 0.78 | 0.11 | SZFISPVO | 0.77 | 0.16 | GOESITED | 0.78 | −0.15 |
| 6 | MICNP237 | 0.79 | 0.11 | GOESITED | 0.79 | −0.12 | EP1LOWNU | 0.79 | 0.14 |
| 7 | CPUCOLWF | 0.80 | 0.13 | EP1NPO2 | 0.81 | 0.11 | SZFISPVO | 0.80 | 0.13 |
| 8 | SZFISPVO | 0.81 | 0.11 | CORRATSS | 0.82 | −0.06 | MICPU239 | 0.82 | 0.13 |
| 9 | SZCOLRAL | 0.82 | −0.10 | HFOSA | 0.83 | −0.09 | SZCONCOL | 0.83 | 0.10 |
| 10 | KDRASMEC | 0.83 | 0.08 | EP1LOWNU | 0.83 | 0.09 | HFOSA | 0.84 | −0.08 |
| 11 | | | | SZDIFCVO | 0.84 | −0.09 | UZFAG4 | 0.84 | −0.08 |
| 12 | | | | SZCONCOL | 0.85 | 0.08 | SZDIFCVO | 0.85 | −0.07 |
| 13 | | | | PHCSS | 0.85 | −0.07 | CSWFA0AK | 0.85 | −0.07 |
| 14 | | | | SZKDAMCO | 0.85 | 0.06 | SZKDAMCO | 0.85 | 0.07 |
| 15 | | | | SCHOBOLT | 0.86 | 0.07 | SZSREG1X | 0.86 | 0.07 |
| 16 | | | | MICNP237 | 0.86 | 0.11 | | | |

a: Steps in stepwise rank regression analysis
b: Variables listed in order of selection in stepwise regression
c: Cumulative $R^2$ value with entry of each variable into regression model
d: Standardized rank regression coefficients (SRRCs) in final regression model

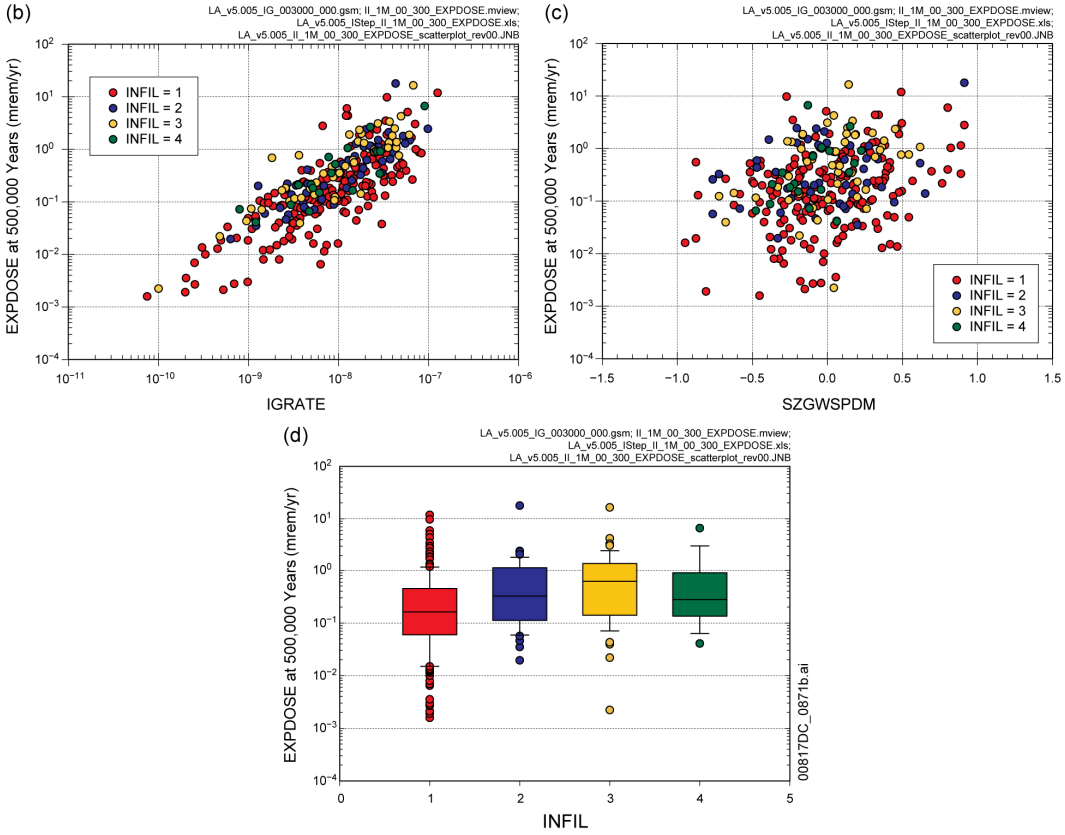


Source: Output DTNs: MO0710ADTSPAWO.000 [DIRS 183752]; and MO0710PLOTSFIG.000 [DIRS 185207].

NOTE: In (d), the box extends from 0.25 to 0.75 quantile; lower and upper bar and whisker extend to 0.1 and 0.9 quantile, respectively; dots represent values outside 0.1 to 0.9 quantile range; median indicated by light horizontal line.

Figure K.6.7.2-2[a]. Stepwise rank regression analyses and selected scatterplots for expected dose to RMEI (*EXPDOSE*, mrem/yr) over [0, 1,000,000 yr] for all radioactive species resulting from igneous intrusion obtained with version 5.005 of the TSPA-LA Model: (a) regressions for *EXPDOSE* at 50,000, 200,000, and 500,000 years, and (b,c,d) scatterplots for *EXPDOSE* at 500,000 years

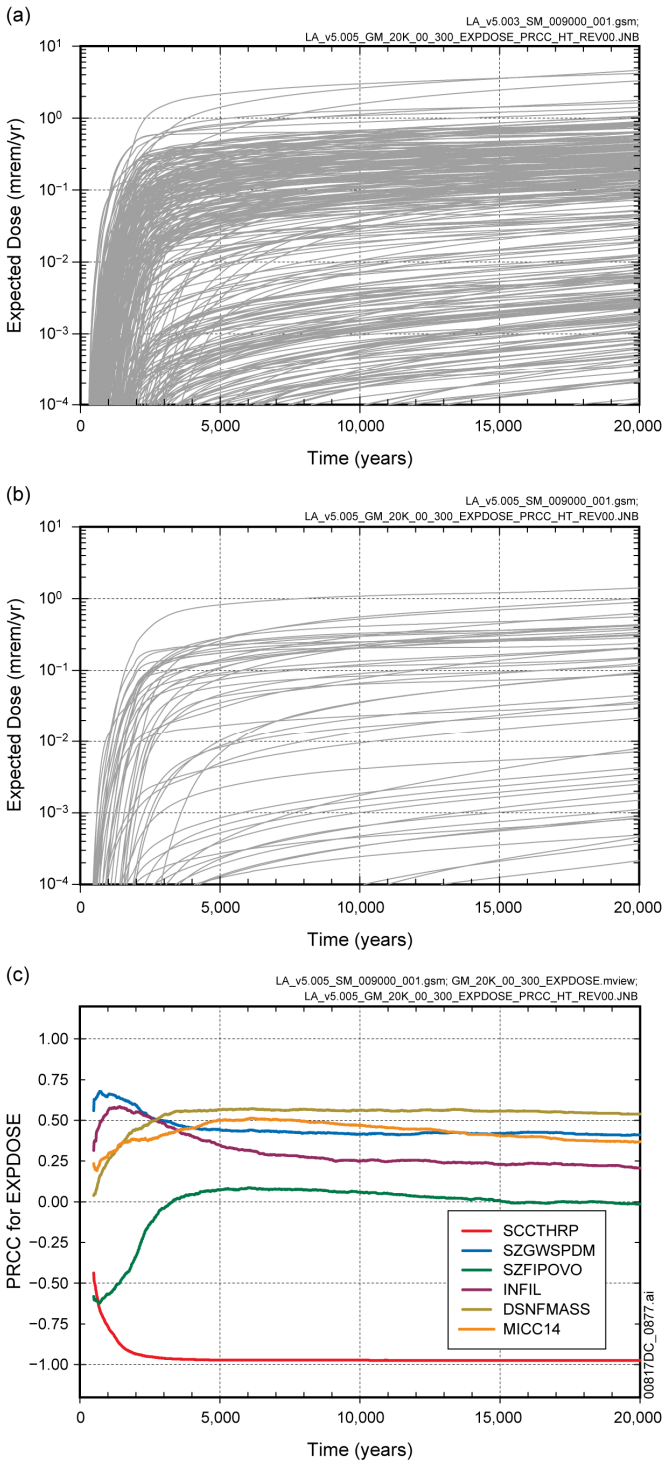


Source: Output DTNs: MO0710ADTSPAWO.000 [DIRS 183752]; and MO0710PLOTSFIG.000 [DIRS 185207].

Figure K7.7.1-1[a]. Expected dose to RMEI (*EXPDOSE*, mrem/yr) over [0, 20,000 yr] for all radioactive species resulting from seismic ground motion obtained with version 5.005 of the TSPA-LA Model: (a) *EXPDOSE* for all (i.e., 300) sample elements, (b) *EXPDOSE* for first 50 sample elements, and (c) PRCCs for *EXPDOSE*

(a)

| | 3,000 Years | | | 5,000 Years | | | 10,000 Years | | |
|---|---|---|---|---|---|---|---|---|---|
| Step[a] | Variable[b] | $R^{2}$ [c] | SRRC[d] | Variable | $R^{2}$ | SRRC | Variable | $R^{2}$ | SRRC |
| 1 | SCCTHRP | 0.81 | −0.87 | SCCTHRP | 0.86 | −0.91 | SCCTHRP | 0.88 | −0.93 |
| 2 | SZGWSPDM | 0.83 | 0.16 | MICTC99 | 0.88 | 0.10 | MICTC99 | 0.90 | 0.12 |
| 3 | INFIL | 0.85 | 0.13 | DSNFMASS | 0.89 | 0.14 | DSNFMASS | 0.91 | 0.14 |
| 4 | MICTC99 | 0.87 | 0.10 | SZGWSPDM | 0.90 | 0.11 | HLWDRACD | 0.91 | 0.08 |
| 5 | DSNFMASS | 0.88 | 0.13 | MICC14 | 0.90 | 0.10 | MICC14 | 0.92 | 0.08 |
| 6 | SZFISPVO | 0.88 | 0.10 | INFIL | 0.91 | 0.07 | WDCRCDEN | 0.93 | 0.09 |
| 7 | MICC14 | 0.89 | 0.10 | WDCRCDEN | 0.92 | 0.09 | SZGWSPDM | 0.93 | 0.07 |
| 8 | WDCRCDEN | 0.90 | 0.08 | HLWDRACD | 0.92 | 0.06 | PH2DHLNS | 0.93 | −0.06 |
| 9 | SZDIFCVO | 0.90 | −0.06 | SZFISPVO | 0.93 | 0.06 | WFDEGEXF | 0.94 | 0.07 |
| 10 | UZFAG8 | 0.91 | −0.06 | UZFAG8 | 0.93 | −0.07 | INFIL | 0.94 | 0.04 |
| 11 | SEEPUNC | 0.91 | 0.07 | SEEPUNC | 0.93 | 0.05 | UZFAG8 | 0.94 | −0.06 |
| 12 | UZTORRG3 | 0.91 | 0.05 | UZTORRG3 | 0.94 | 0.05 | HLWDRALK | 0.94 | 0.04 |
| 13 | HLWDRACD | 0.91 | 0.05 | KDUSMEC | 0.94 | 0.04 | SZFISPVO | 0.94 | 0.04 |
| 14 | KDUSMEC | 0.92 | 0.05 | HLWDRALK | 0.94 | 0.05 | WDGCUA22 | 0.95 | −0.04 |
| 15 | GOESA | 0.92 | 0.05 | WFDEGEXF | 0.94 | 0.05 | UZGAM | 0.95 | −0.04 |
| 16 | SZSREG4X | 0.92 | −0.05 | | | | SEEPUNC | 0.95 | 0.04 |

a: Steps in stepwise rank regression analysis
b: Variables listed in order of selection in stepwise regression
c: Cumulative $R^2$ value with entry of each variable into regression model
d: Standardized rank regression coefficients (SRRCs) in final regression model

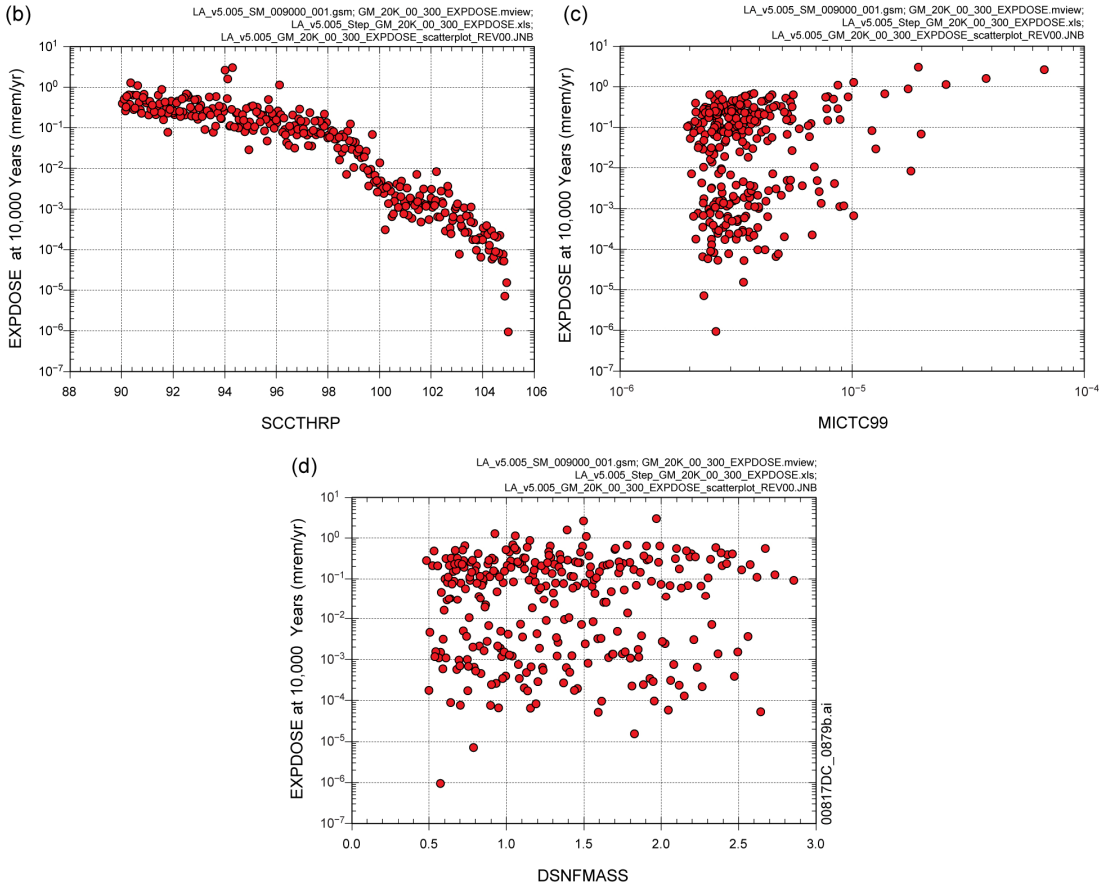


Source: Output DTNs: MO0710ADTSPAWO.000 [DIRS 183752]; and MO0710PLOTSFIG.000 [DIRS 185207].

Figure K7.7.1-2[a]. Stepwise rank regression analyses and selected scatterplots for expected dose to RMEI (*EXPDOSE*, mrem/yr) over [0, 20,000 yr] for all radioactive species resulting from seismic ground motion obtained with version 5.005 of the TSPA-LA Model: (a) regressions for *EXPDOSE* at 3,000, 5,000, and 10,000 years, and (b,c,d) scatterplots for *EXPDOSE* at 10,000 years

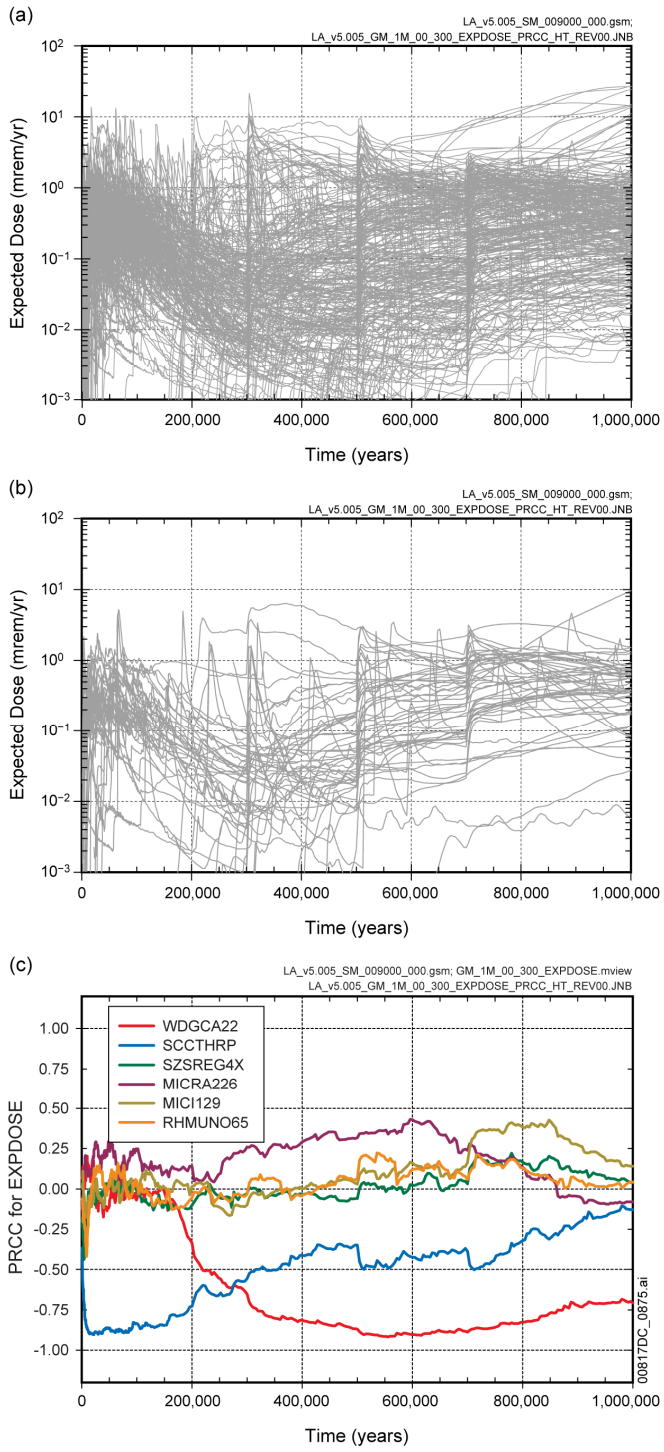


Source: Output DTNs: MO0710ADTSPAWO.000 [DIRS 183752]; and MO0710PLOTSFIG.000 [DIRS 185207].

Figure K7.7.2-1[a]. Expected dose to RMEI (*EXPDOSE*, mrem/yr) over [0, 1,000,000 yr] for all radioactive species resulting from seismic ground motion obtained with version 5.005 of the TSPA-LA Model: (a) *EXPDOSE* for all (i.e., 300) sample elements, (b) *EXPDOSE* for first 50 sample elements, and (c) PRCCs for *EXPDOSE*

(a)

| | 50,000 Years | | | 200,000 Years | | | 500,000 Years | | |
|---|---|---|---|---|---|---|---|---|---|
| Step[a] | Variable[b] | $R^{2}$ [c] | SRRC[d] | Variable | $R^2$ | SRRC | Variable | $R^2$ | SRRC |
| 1 | SCCTHRP | 0.71 | −0.85 | SCCTHRP | 0.54 | −0.72 | WDGCA22 | 0.62 | −0.77 |
| 2 | MICTC99 | 0.72 | 0.09 | WDDSGC29 | 0.58 | −0.18 | SCCTHRP | 0.71 | −0.28 |
| 3 | HLWDRACD | 0.73 | 0.10 | WDGCA22 | 0.60 | −0.14 | WDNSCC | 0.72 | −0.12 |
| 4 | DSNFMASS | 0.74 | 0.11 | DSNFMASS | 0.61 | 0.11 | SZPORSAL | 0.73 | 0.08 |
| 5 | SZLODISP | 0.75 | −0.10 | CSNFMASS | 0.62 | 0.10 | SZGWSPDM | 0.73 | 0.11 |
| 6 | SZKDSEVO | 0.76 | −0.09 | | | | SZCONCOL | 0.74 | 0.09 |
| 7 | CPUPERCS | 0.77 | 0.09 | | | | EP1LOWNU | 0.75 | 0.10 |
| 8 | | | | | | | UZFAG4 | 0.76 | −0.08 |

a: Steps in stepwise rank regression analysis
b: Variables listed in order of selection in stepwise regression
c: Cumulative $R^2$ value with entry of each variable into regression model
d: Standardized rank regression coefficients (SRRCs) in final regression model

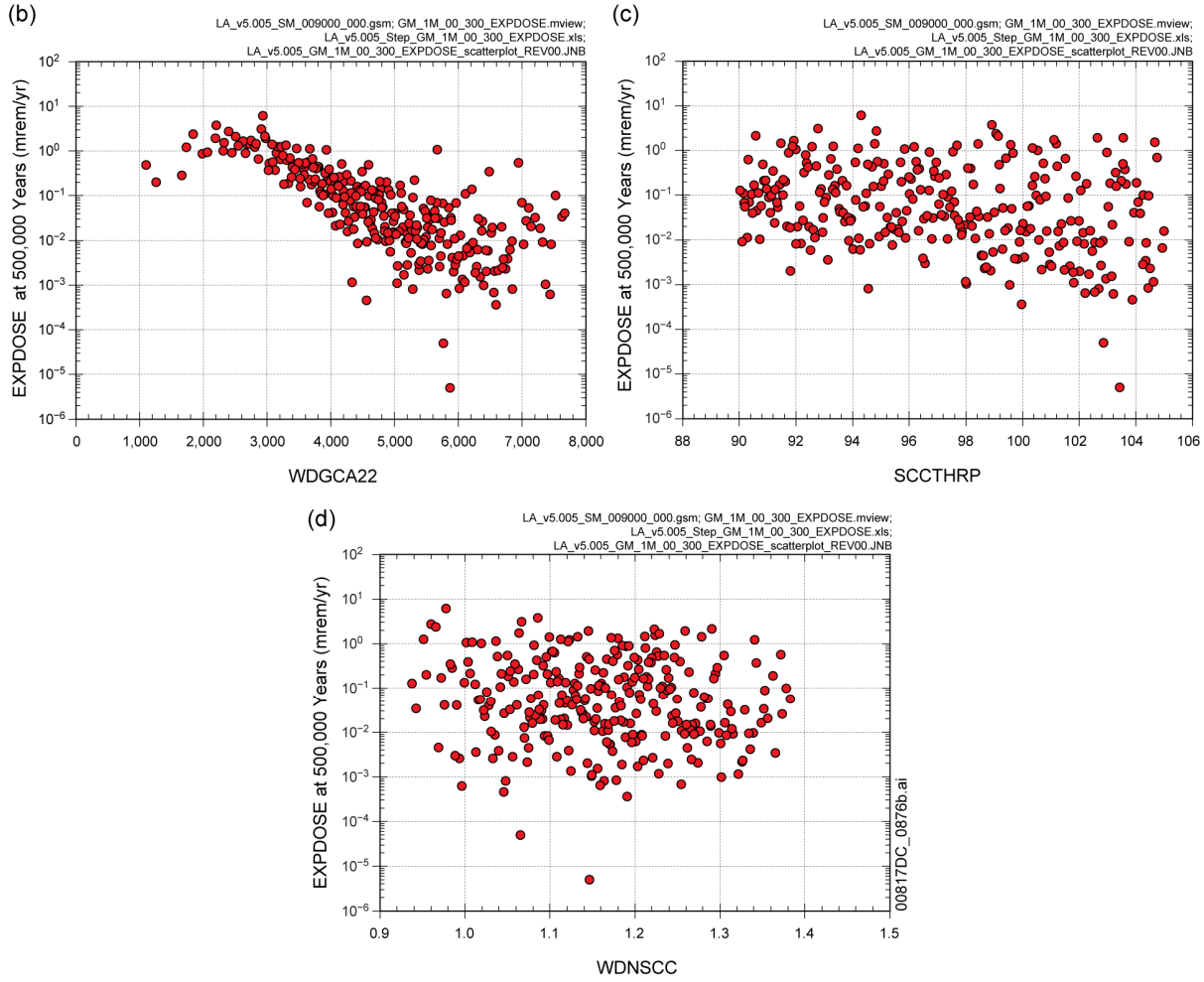


Source: Output DTNs: MO0710ADTSPAWO.000 [DIRS 183752]; and MO0710PLOTSFIG.000 [DIRS 185207].

Figure K7.7.2-2[a]. Stepwise rank regression analyses and selected scatterplots for expected dose to RMEI (*EXPDOSE*, mrem/yr) over [0, 1,000,000 yr] for all radioactive species resulting from seismic ground motion obtained with version 5.005 of the TSPA-LA Model: (a) regressions for *EXPDOSE* at 50,000, 200,000, and 500,000 years, and (b,c,d) scatterplots for *EXPDOSE* at 500,000 years

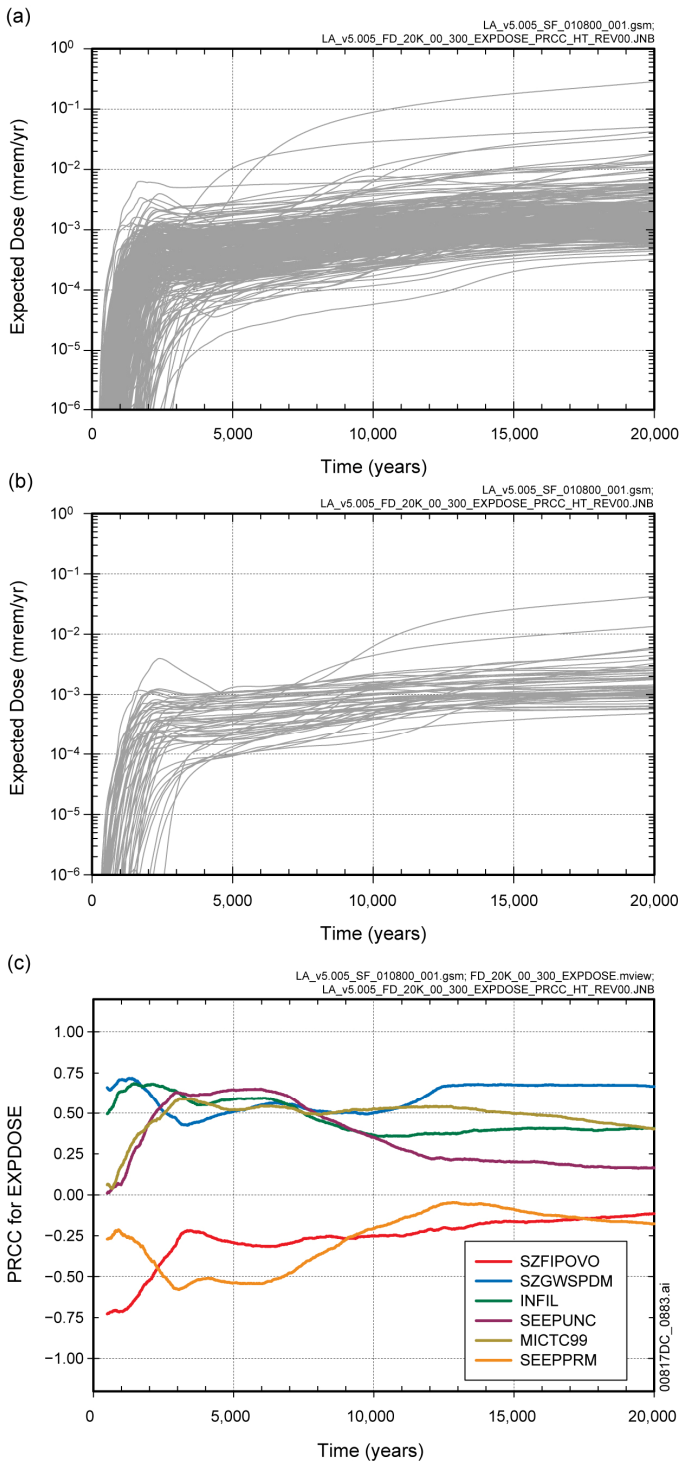


Source: Output DTNs: MO0710ADTSPAWO.000 [DIRS 183752]; and MO0710PLOTSFIG.000 [DIRS 185207].

Figure K7.8.1-1[a]. Expected dose to RMEI (*EXPDOSE*, mrem/yr) over [0, 20,000 yr] for all radioactive species resulting from seismic fault displacement: (a) *EXPDOSE* for all (i.e., 300) sample elements, (b) *EXPDOSE* for first 50 sample elements, and (c) PRCCs for *EXPDOS*

(a)

| | 3,000 years | | | 5,000 years | | | 10,000 years | | |
|---|---|---|---|---|---|---|---|---|---|
| Step[a] | Variable[b] | $R^{2c}$ | SRRC[d] | Variable | $R^2$ | SRRC | Variable | $R^2$ | SRRC |
| 1 | INFIL | 0.18 | 0.45 | INFIL | 0.19 | 0.44 | MICTC99 | 0.15 | 0.36 |
| 2 | MICTC99 | 0.31 | 0.32 | MICTC99 | 0.32 | 0.34 | INFIL | 0.27 | 0.35 |
| 3 | SZGWSPDM | 0.40 | 0.31 | SEEPPRM | 0.42 | -0.31 | SZGWSPDM | 0.37 | 0.33 |
| 4 | SEEPPRM | 0.49 | -0.29 | SZGWSPDM | 0.49 | 0.29 | DTDRHUNC | 0.45 | 0.26 |
| 5 | SEEPUNC | 0.57 | 0.30 | SEEPUNC | 0.57 | 0.31 | SEEPPRM | 0.49 | -0.16 |
| 6 | CSSPECSA | 0.62 | 0.22 | CSSPECSA | 0.62 | 0.21 | SZCOLRAL | 0.52 | -0.19 |
| 7 | SZFISPVO | 0.66 | 0.22 | SZFISPVO | 0.65 | 0.18 | SZFISPVO | 0.55 | 0.18 |
| 8 | CSNFMASS | 0.68 | 0.15 | ALPHAL | 0.67 | -0.16 | SZFIPOVO | 0.56 | -0.14 |
| 9 | MICC14 | 0.69 | 0.14 | CSNFMASS | 0.68 | 0.18 | CSNFMASS | 0.58 | 0.13 |
| 10 | SZDIFCVO | 0.71 | -0.14 | MICC14 | 0.70 | 0.12 | SZDIFCVO | 0.59 | -0.13 |
| 11 | ALPHAL | 0.73 | -0.14 | SZCOLRAL | 0.71 | -0.14 | MICAM243 | 0.61 | 0.13 |
| 12 | MICSE79 | 0.74 | 0.09 | SZFIPOVO | 0.72 | -0.12 | CSSPECSA | 0.62 | 0.13 |
| 13 | SZFIPOVO | 0.74 | -0.10 | SZCOLRVO | 0.73 | -0.12 | CSWFA4AC | 0.63 | 0.12 |
| 14 | SZCOLRVO | 0.75 | -0.08 | MICSN126 | 0.74 | 0.10 | KDUSMEC | 0.64 | 0.11 |
| 15 | THERMCON | 0.76 | -0.08 | SZDIFCVO | 0.75 | -0.10 | | | |
| 16 | | | | CSWFA4AC | 0.76 | 0.09 | | | |

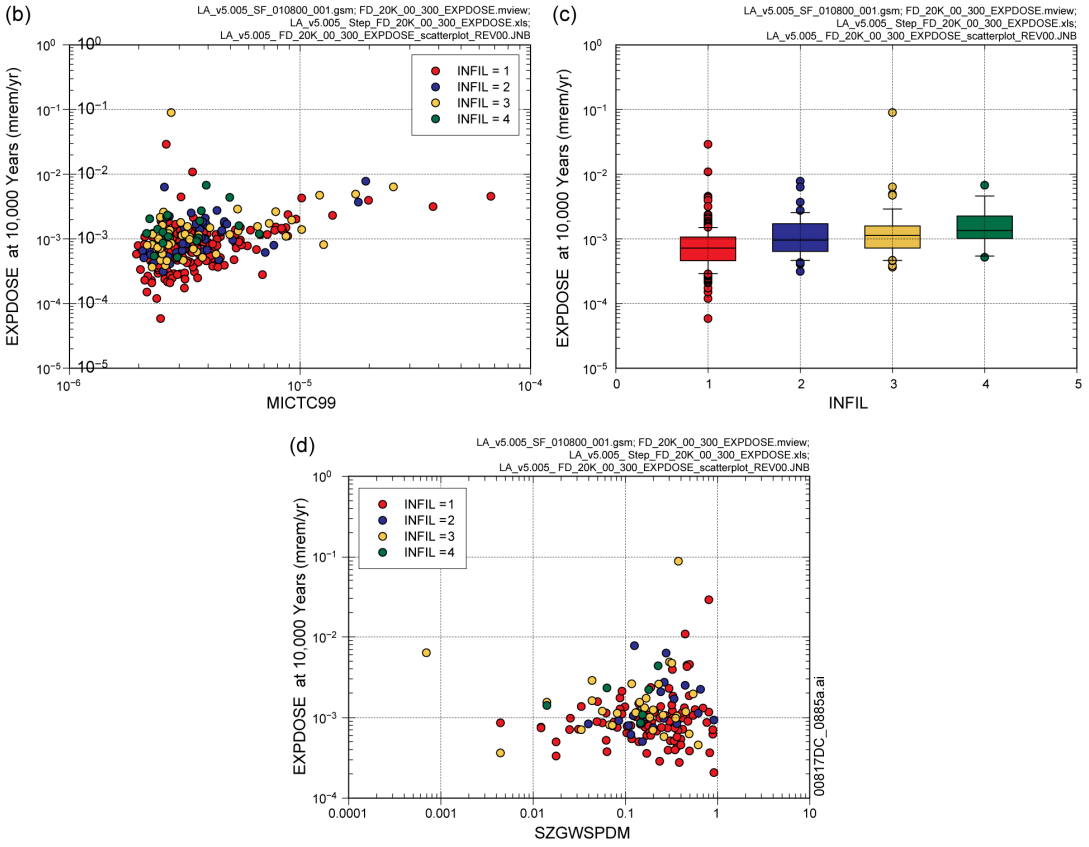


Source: Output DTNs: MO0710ADTSPAWO.000 [DIRS 183752]; and MO0710PLOTSFIG.000 [DIRS 185207].

NOTE: In (c), the box extends from 0.25 to 0.75 quantile; lower and upper bar and whisker extend to 0.1 and 0.9 quantile, respectively; dots represent values outside 0.1 to 0.9 quantile range; median indicated by light horizontal line.

Figure K7.8.1-2[a]. Stepwise rank regression analyses and selected scatterplots for expected dose to RMEI (*EXPDOSE*, mrem/yr) over [0, 20,000 yr] for all radioactive species resulting from seismic fault displacement: (a) regressions for *EXPDOSE* at 3,000, 5,000, and 10,000 years, and (b,c,d) scatterplots for *EXPDOSE* at 10,000 years

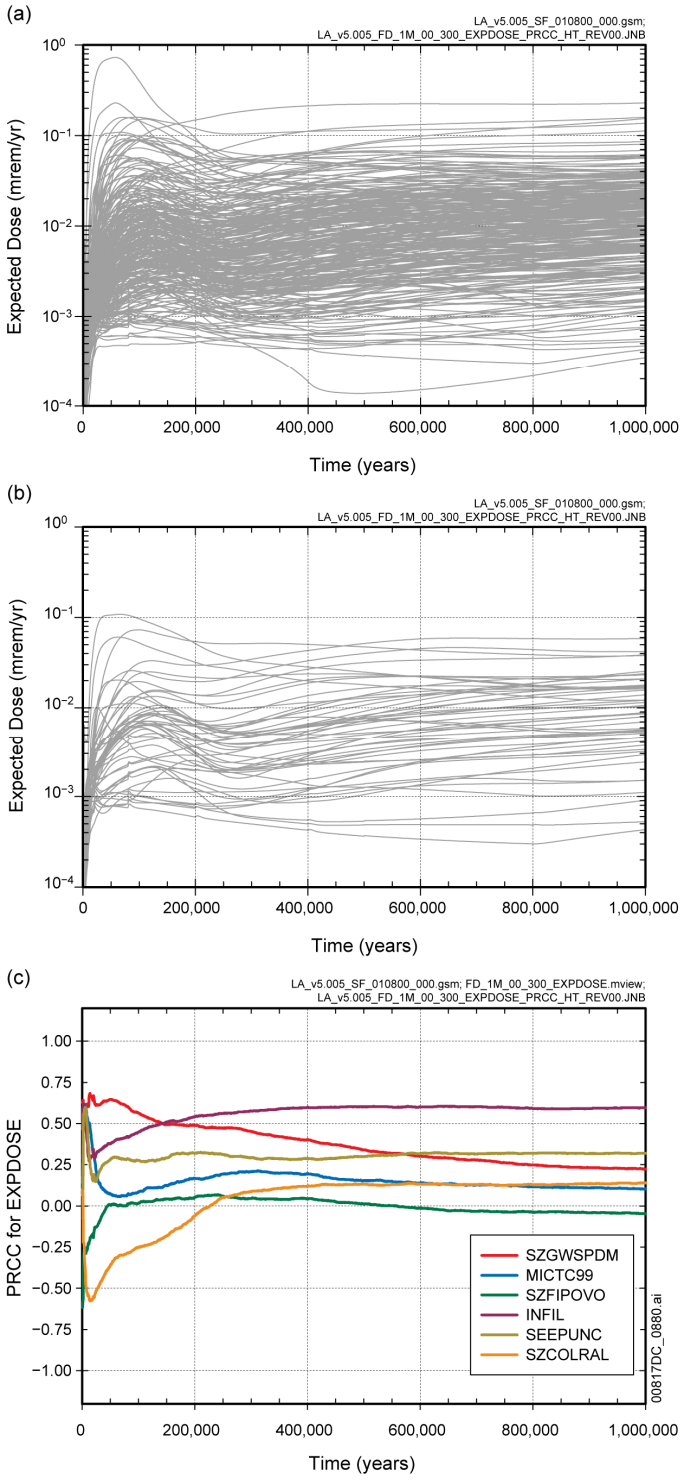


Source: Output DTNs: MO0710ADTSPAWO.000 [DIRS 183752]; and MO0710PLOTSFIG.000 [DIRS 185207].

Figure K7.8.2-1[a]. Expected dose to RMEI (*EXPDOSE*, mrem/yr) over [0, 1,000,000 yr] for all radioactive species resulting from seismic fault displacement: (a) *EXPDOSE* for all (i.e., 300) sample elements, (b) *EXPDOSE* for first 50 sample elements, and (c) PRCCs for *EXPDOS*

(a)

| | 50,000 years | | | 200,000 years | | | 500,000 years | | |
|---|---|---|---|---|---|---|---|---|---|
| Step[a] | Variable[b] | $R^{2c}$ | SRRC[d] | Variable | $R^2$ | SRRC | Variable | $R^2$ | SRRC |
| 1 | SZGWSPDM | 0.25 | 0.51 | INFIL | 0.15 | 0.37 | INFIL | 0.18 | 0.40 |
| 2 | INFIL | 0.37 | 0.31 | SZGWSPDM | 0.29 | 0.40 | EP1LOWPU | 0.29 | 0.33 |
| 3 | WPFLUX | 0.43 | 0.22 | WPFLUX | 0.37 | 0.28 | SZGWSPDM | 0.38 | 0.36 |
| 4 | EP1LOWPU | 0.48 | 0.21 | EP1LOWPU | 0.44 | 0.28 | WPFLUX | 0.43 | 0.25 |
| 5 | SEEPPRM | 0.52 | −0.19 | SEEPPRM | 0.48 | −0.22 | GOESITED | 0.48 | −0.18 |
| 6 | MICNP237 | 0.55 | 0.18 | SZFISPVO | 0.55 | 0.19 | SEEPPRM | 0.52 | −0.20 |
| 7 | CPUCOLWF | 0.57 | 0.17 | SEEPUNC | 0.57 | 0.17 | MICPU239 | 0.54 | 0.19 |
| 8 | SZCOLRAL | 0.60 | −0.15 | CORRATSS | 0.59 | −0.10 | SEEPUNC | 0.57 | 0.17 |
| 9 | SZFISPVO | 0.62 | 0.16 | EP1NPO2 | 0.60 | 0.11 | SZFISPVO | 0.60 | 0.17 |
| 10 | SEEPUNC | 0.63 | 0.12 | SZCONCOL | 0.62 | 0.11 | SZCONCOL | 0.62 | 0.14 |
| 11 | PHCSS | 0.65 | −0.12 | EP1LOWNU | 0.63 | 0.12 | EP1LOWNU | 0.64 | 0.18 |
| 12 | HFOSA | 0.66 | −0.11 | SZDIFCVO | 0.64 | −0.11 | UZFAG4 | 0.67 | −0.15 |
| 13 | RUBMAXL | 0.67 | −0.10 | SZKDAMCO | 0.65 | 0.10 | HFOSA | 0.68 | −0.11 |
| 14 | PH2MCONS | 0.67 | −0.09 | GOESITED | 0.66 | −0.11 | SZDIFCVO | 0.69 | −0.12 |
| 15 | | | | MICPU239 | 0.67 | 0.19 | KDPUSMEC | 0.70 | 0.10 |
| 16 | | | | UZFAG4 | 0.68 | −0.11 | SZWBNDAL | 0.71 | −0.10 |

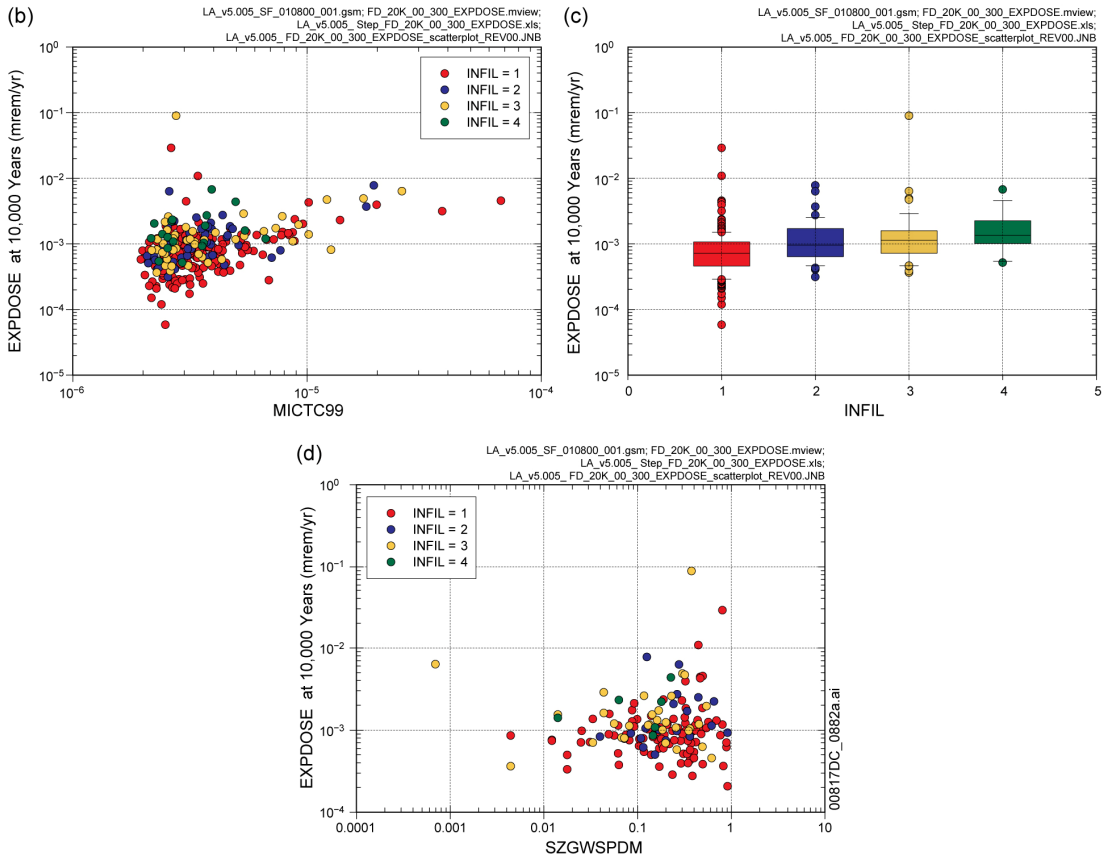


Source: Output DTNs: MO0710ADTSPAWO.000 [DIRS 183752]; and MO0710PLOTSFIG.000 [DIRS 185207].

NOTE: In (c), the box extends from 0.25 to 0.75 quantile; lower and upper bar and whisker extend to 0.1 and 0.9 quantile, respectively; dots represent values outside 0.1 to 0.9 quantile range; median indicated by light horizontal line.

Figure K7.8.2-2[a]. Stepwise rank regression analyses and selected scatterplots for expected dose to RMEI (*EXPDOSE*, mrem/yr) over [0, 1,000,000 yr] for all radioactive species resulting from seismic fault displacement: (a) regressions for *EXPDOSE* at 50,000, 200,000, and 500,000 years, and (b,c,d) scatterplots for *EXPDOSE* at 500,000 years

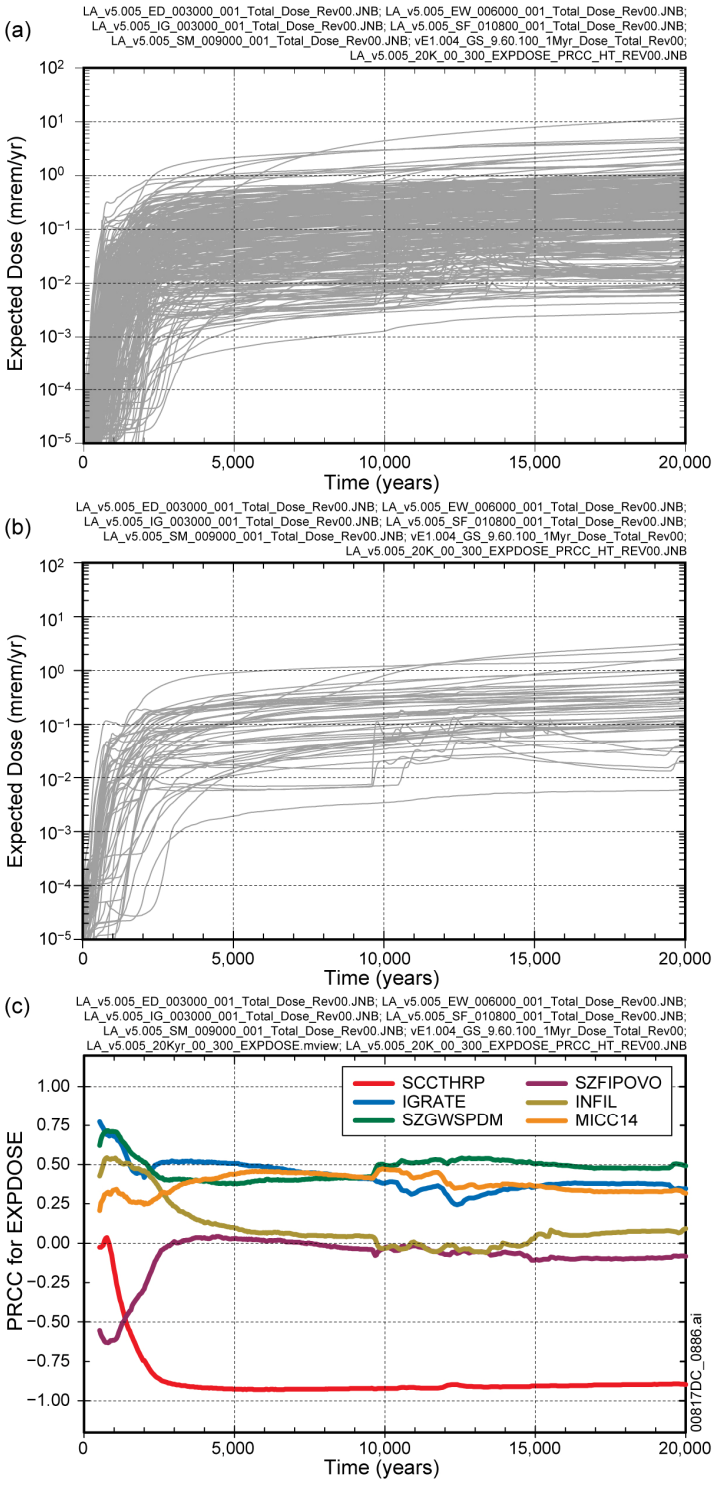


Source: Output DTNs: MO0710ADTSPAWO.000 [DIRS 183752]; and MO0710PLOTSFIG.000 [DIRS 185207].

Figure K8.1-1[a]. Expected dose to RMEI (*EXPDOSE*, mrem/yr) over [0, 20,000 yr] for all scenario classes obtained with version 5.005 of the TSPA-LA Model: (a) *EXPDOSE* for all (i.e., 300) sample elements, (b) *EXPDOSE* for first 50 sample elements, and (c) PRCCs for *EXPDOSE*

(a)

| | 3,000 Years | | | 5,000 Years | | | 10,000 Years | | |
|---|---|---|---|---|---|---|---|---|---|
| Step[a] | Variable[b] | $R^{2c}$ | SRRC[d] | Variable | $R^2$ | SRRC | Variable | $R^2$ | SRRC |
| 1 | SCCTHRP | 0.55 | −0.72 | SCCTHRP | 0.66 | −0.79 | SCCTHRP | 0.69 | −0.83 |
| 2 | IGRATE | 0.62 | 0.28 | IGRATE | 0.71 | 0.24 | IGRATE | 0.73 | 0.22 |
| 3 | SZGWSPDM | 0.67 | 0.21 | SZGWSPDM | 0.74 | 0.15 | SZGWSPDM | 0.76 | 0.16 |
| 4 | INFIL | 0.71 | 0.19 | MICTC99 | 0.76 | 0.14 | MICTC99 | 0.77 | 0.14 |
| 5 | MICTC99 | 0.73 | 0.15 | MICC14 | 0.78 | 0.12 | WFDEGEXF | 0.78 | 0.10 |
| 6 | SZFISPVO | 0.75 | 0.14 | INFIL | 0.79 | 0.11 | MICC14 | 0.79 | 0.11 |
| 7 | MICC14 | 0.76 | 0.12 | DSNFMASS | 0.80 | 0.11 | UZGAM | 0.80 | −0.09 |
| 8 | DSNFMASS | 0.77 | 0.10 | SZFISPVO | 0.81 | 0.09 | INFIL | 0.81 | 0.09 |
| 9 | UZFAG8 | 0.78 | −0.10 | UZFAG8 | 0.82 | −0.10 | CSWFA0AC | 0.81 | −0.07 |
| 10 | UZGAM | 0.79 | −0.09 | UZGAM | 0.82 | −0.10 | UZKDSRDT | 0.82 | 0.07 |
| 11 | SZDIFCVO | 0.79 | −0.08 | WFDEGEXF | 0.83 | 0.10 | | | |
| 12 | WFDEGEXF | 0.80 | 0.08 | WDCRCDEN | 0.83 | 0.08 | | | |
| 13 | KDUSMEC | 0.80 | 0.08 | WDZOLID | 0.84 | −0.07 | | | |
| 14 | MICPA231 | 0.81 | −0.08 | WDGCUA22 | 0.84 | 0.07 | | | |
| 15 | | | | BCKRA226 | 0.85 | −0.06 | | | |

a: Steps in stepwise rank regression analysis
b: Variables listed in order of selection in stepwise regression
c: Cumulative $R^2$ value with entry of each variable into regression model
d: Standardized rank regression coefficients (SRRCs) in final regression model

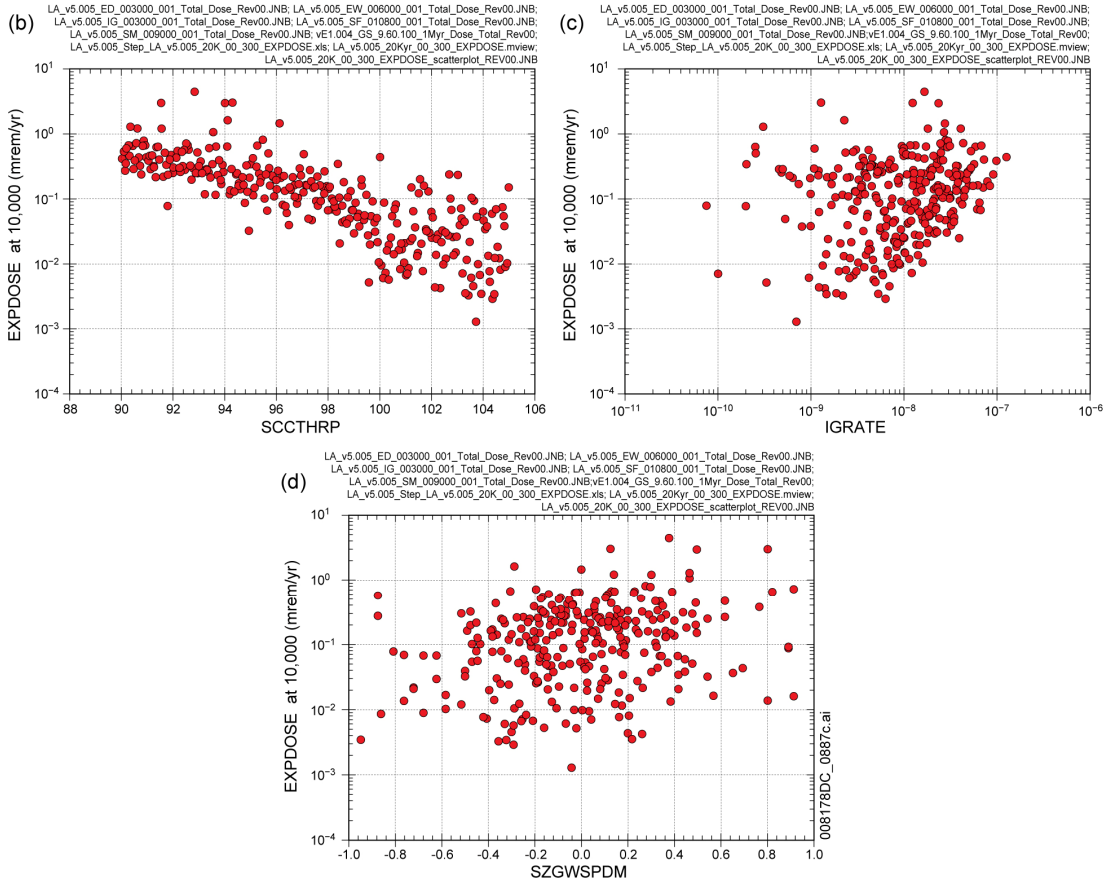


Source: Output DTNs: MO0710ADTSPAWO.000 [DIRS 183752]; and MO0710PLOTSFIG.000 [DIRS 185207].

Figure K8.1-2[a]. Stepwise rank regression analyses and selected scatterplots for expected dose to RMEI (*EXPDOSE*, mrem/yr) over [0, 20,000 yr] for all scenario classes obtained with version 5.005 of the TSPA-LA Model: (a) regressions for *EXPDOSE* at 3,000, 5,000, and 10,000 years, and (b,c,d) scatterplots for *EXPDOSE* at 10,000 years

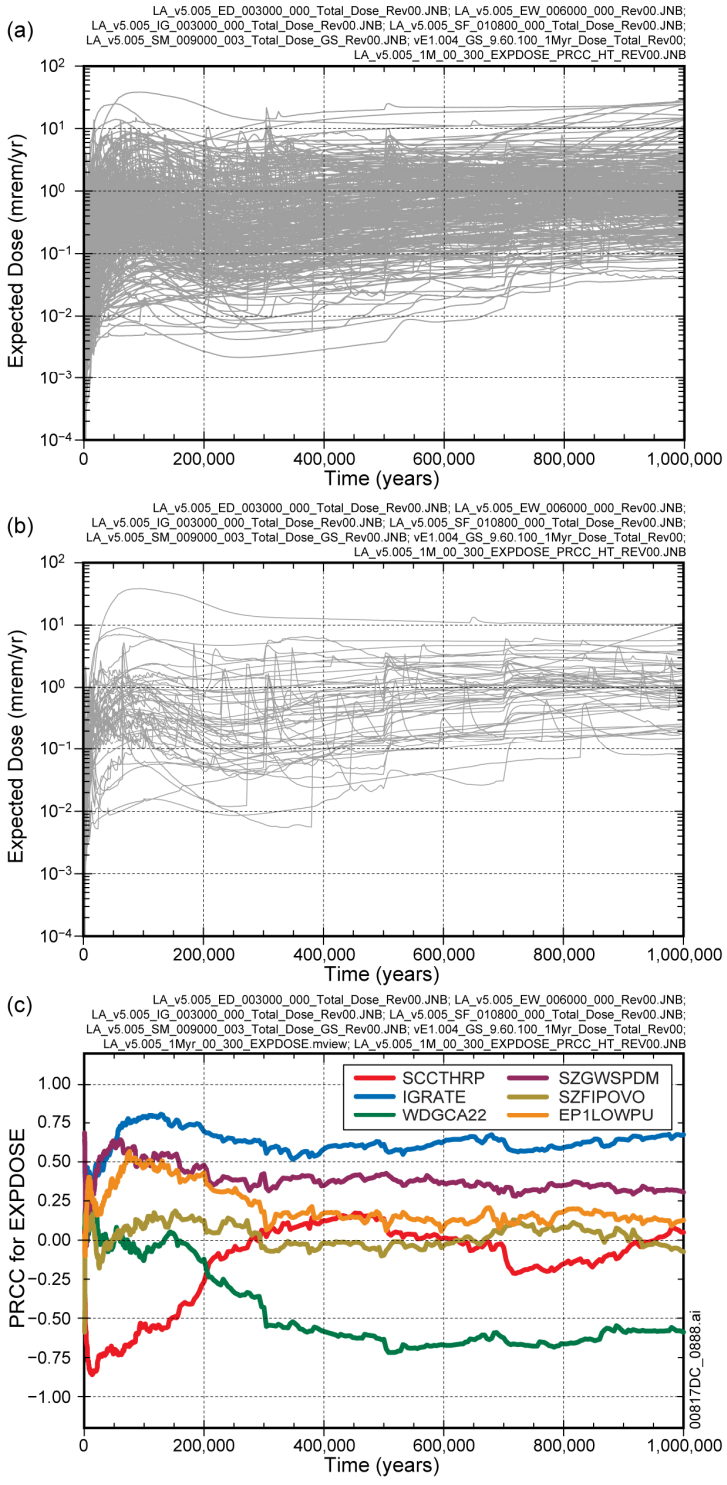


Source: Output DTNs: MO0710ADTSPAWO.000 [DIRS 183752]; and MO0710PLOTSFIG.000 [DIRS 185207].

Figure K8.2-1[a]. Expected dose to RMEI (*EXPDOSE*, mrem/yr) over [0, 1,000,000 yr] for all scenario classes obtained with version 5.005 of the TSPA-LA Model: (a) *EXPDOSE* for all (i.e., 300) sample elements, (b) *EXPDOSE* for first 50 sample elements, and (c) PRCCs for *EXPDOSE*

(a)

| | EXPDOSE: 50,000 Years | | | EXPDOSE: 200,000 Years | | | EXPDOSE: 500,000 Years | | |
|---|---|---|---|---|---|---|---|---|---|
| Step[a] | Variable[b] | $R^2$[c] | SRRC[d] | Variable | $R^2$ | SRRC | Variable | $R^2$ | SRRC |
| 1 | SCCTHRP | 0.27 | −0.48 | IGRATE | 0.38 | 0.61 | IGRATE | 0.29 | 0.54 |
| 2 | IGRATE | 0.43 | 0.41 | SZGWSPDM | 0.48 | 0.28 | WDGCA22 | 0.46 | −0.38 |
| 3 | SZGWSPDM | 0.55 | 0.33 | EP1LOWPU | 0.53 | 0.23 | SZGWSPDM | 0.53 | 0.24 |
| 4 | EP1LOWPU | 0.60 | 0.20 | SCCTHRP | 0.57 | −0.21 | EP1LOWNU | 0.56 | 0.19 |
| 5 | MICNP237 | 0.62 | 0.11 | SZFISPVO | 0.60 | 0.15 | MICNP237 | 0.59 | 0.16 |
| 6 | INFIL | 0.63 | 0.13 | INFIL | 0.62 | 0.16 | EP1L0WPU | 0.61 | 0.17 |
| 7 | EP1NPO2 | 0.65 | 0.13 | EP1NPO2 | 0.64 | 0.14 | SZCONCOL | 0.64 | 0.15 |
| 8 | MICTC99 | 0.66 | 0.11 | GOESITED | 0.66 | −0.14 | SZFISPVO | 0.66 | 0.15 |
| 9 | ALPHAL | 0.67 | 0.10 | MICSE79 | 0.68 | 0.09 | INFIL | 0.67 | 0.11 |
| 10 | | | | MICNP237 | 0.69 | 0.14 | GOESITED | 0.68 | −0.10 |
| 11 | | | | EP1LOWNU | 0.70 | 0.11 | SZKDCSVO | 0.69 | −0.10 |
| 12 | | | | SZCONCOL | 0.71 | 0.11 | HFOSITED | 0.69 | −0.09 |
| 13 | | | | PHCSS | 0.72 | −0.11 | SZDIFCVO | 0.70 | −0.09 |
| 14 | | | | HFOSA | 0.73 | −0.09 | | | |
| 15 | | | | SZDIFCVO | 0.73 | −0.09 | | | |
| 16 | | | | SEEPCOND | 0.74 | −0.09 | | | |

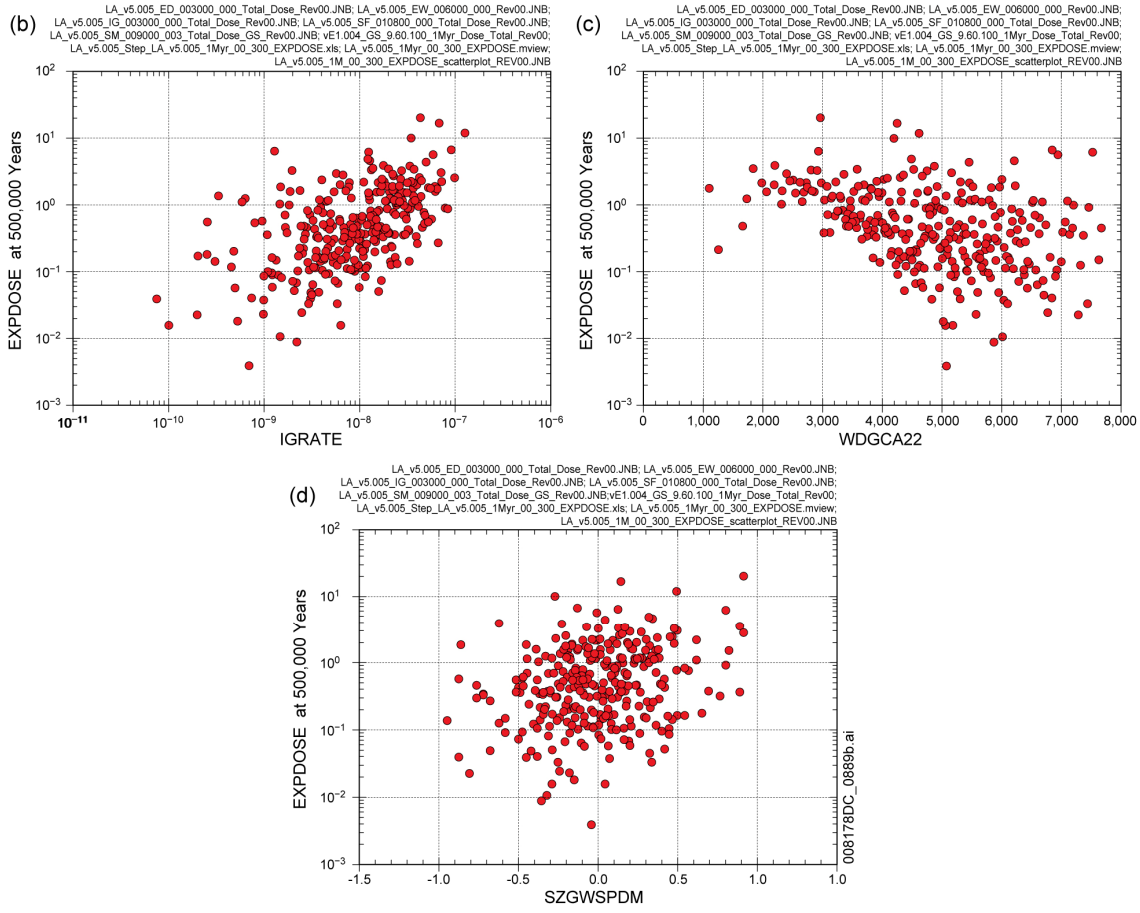


Source: Output DTNs: MO0710ADTSPAWO.000 [DIRS 183752]; and MO0710PLOTSFIG.000 [DIRS 185207].

Figure K8.2-2[a]. Stepwise rank regression analyses and selected scatterplots for expected dose to RMEI (*EXPDOSE*, mrem/yr) over [0, 1,000,000 yr] for all scenario classes obtained with version 5.005 of the TSPA-LA Model: (a) regressions for *EXPDOSE* at 50,000, 200,000, and 500,000 years, and (b,c,d) scatterplots for *EXPDOSE* at 500,000 years

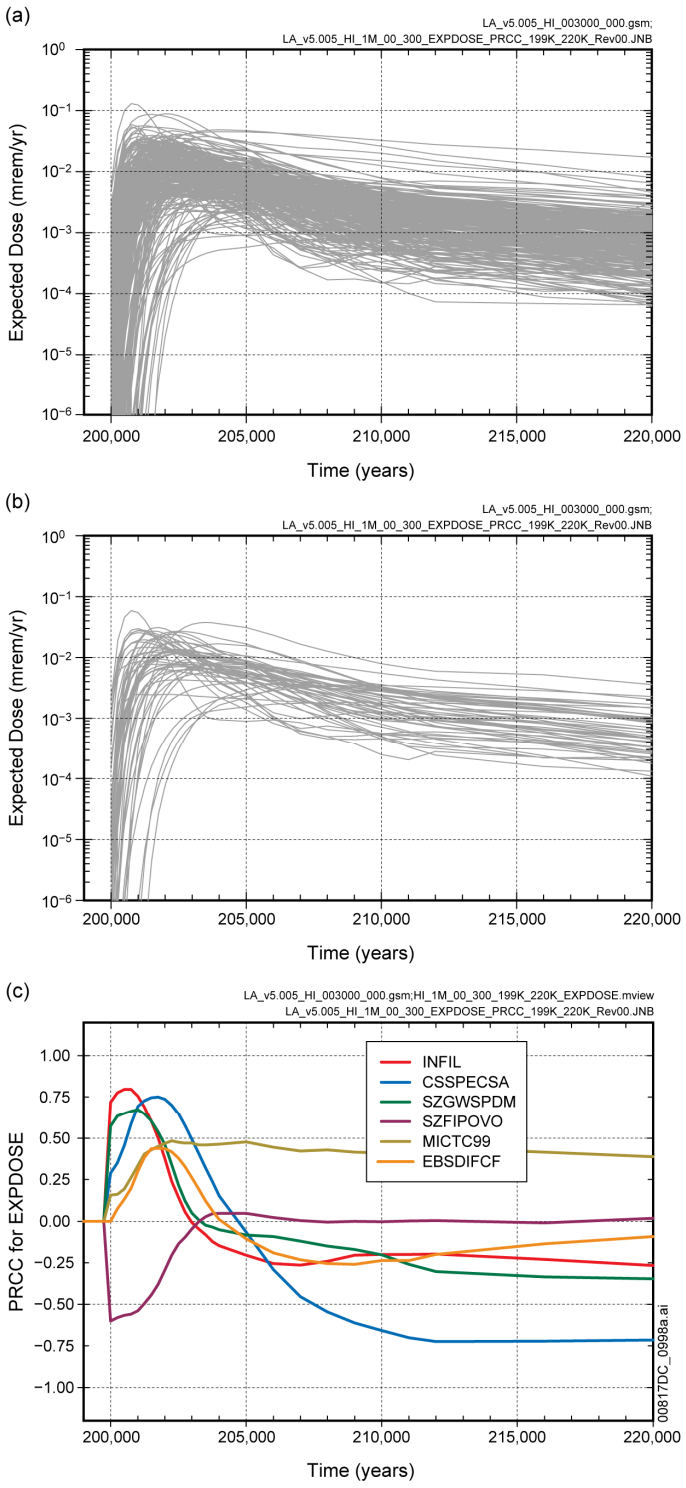


Source: Output DTNs: MO0710ADTSPAWO.000 [DIRS 183752]; and MO0710PLOTSFIG.000 [DIRS 185207].

Figure K10-1[a]. Expected dose to RMEI (*EXPDOSE*, mrem/yr) over [200,000, 220,000 yr] resulting from human intrusion at 200,000 years obtained with version 5.005 of the TSPA-LA Model: (a) *EXPDOSE* for all (i.e., 300) sample elements, (b) *EXPDOSE* for first 50 sample elements, and (c) PRCCs for *EXPDOSE*

| | EXPDOSE: 201,000 Year | | | EXPDOSE: 203,000 Year | | | EXPDOSE: 205,000 Year | | |
|---|---|---|---|---|---|---|---|---|---|
| Step[a] | Variable[b] | $R^{2c}$ | SRRC[d] | Variable | $R^2$ | SRRC | Variable | $R^2$ | SRRC |
| 1 | SZGWSPDM | 0.20 | 0.45 | MICTC99 | 0.15 | 0.44 | MICTC99 | 0.33 | 0.58 |
| 2 | INFIL | 0.40 | 0.48 | CSSPECSA | 0.33 | 0.44 | CSNFMASS | 0.38 | 0.22 |
| 3 | CSSPECSA | 0.54 | 0.41 | SZFISPVO | 0.40 | 0.26 | INFIL | 0.41 | −0.18 |
| 4 | SZFISPVO | 0.61 | 0.28 | SZGWSPDM | 0.43 | 0.18 | | | |
| 5 | SZFIPOVO | 0.65 | −0.20 | CSNFMASS | 0.47 | 0.19 | | | |
| 6 | SZDIFCVO | 0.68 | −0.18 | SZDIFCVO | 0.50 | −0.19 | | | |
| 7 | MICTC99 | 0.70 | 0.14 | INFIL | 0.51 | −0.13 | | | |
| 8 | CSWFA4AC | 0.71 | 0.11 | CSRINDPO | 0.53 | −0.11 | | | |
| 9 | PHCSS | 0.72 | −0.11 | | | | | | |
| 10 | EP1NP2O5 | 0.73 | −0.10 | | | | | | |
| 11 | CSNFMASS | 0.73 | 0.10 | | | | | | |
| 12 | SZPORSAL | 0.74 | 0.09 | | | | | | |
| 13 | DIAMCOLL | 0.75 | 0.08 | | | | | | |

00817DC_0999.ai

a: Steps in stepwise rank regression analysis
b: Variables listed in order of selection in stepwise regression
c: Cumulative $R^2$ value with entry of each variable into regression model
d: Standardized rank regression coefficients (SRRCs) in final regression model

Source: Output DTNs: MO0710ADTSPAWO.000 [DIRS 183752]; and MO0710PLOTSFIG.000 [DIRS 185207].

Figure K10-2[a]. Stepwise rank regression analyses and selected scatterplots for expected dose to RMEI (*EXPDOSE*, mrem/yr) over [200,000, 220,000 yr] resulting from human intrusion at 200,000 years obtained with version 5.005 of the TSPA-LA Model: (a) regressions for *EXPDOSE* at 201,000, 203,000, and 205,000 years, (b,c,d) scatterplots for *EXPDOSE* at 201,000 years, and (e,f,g) scatterplots for *EXPDOSE* at 205,000 years

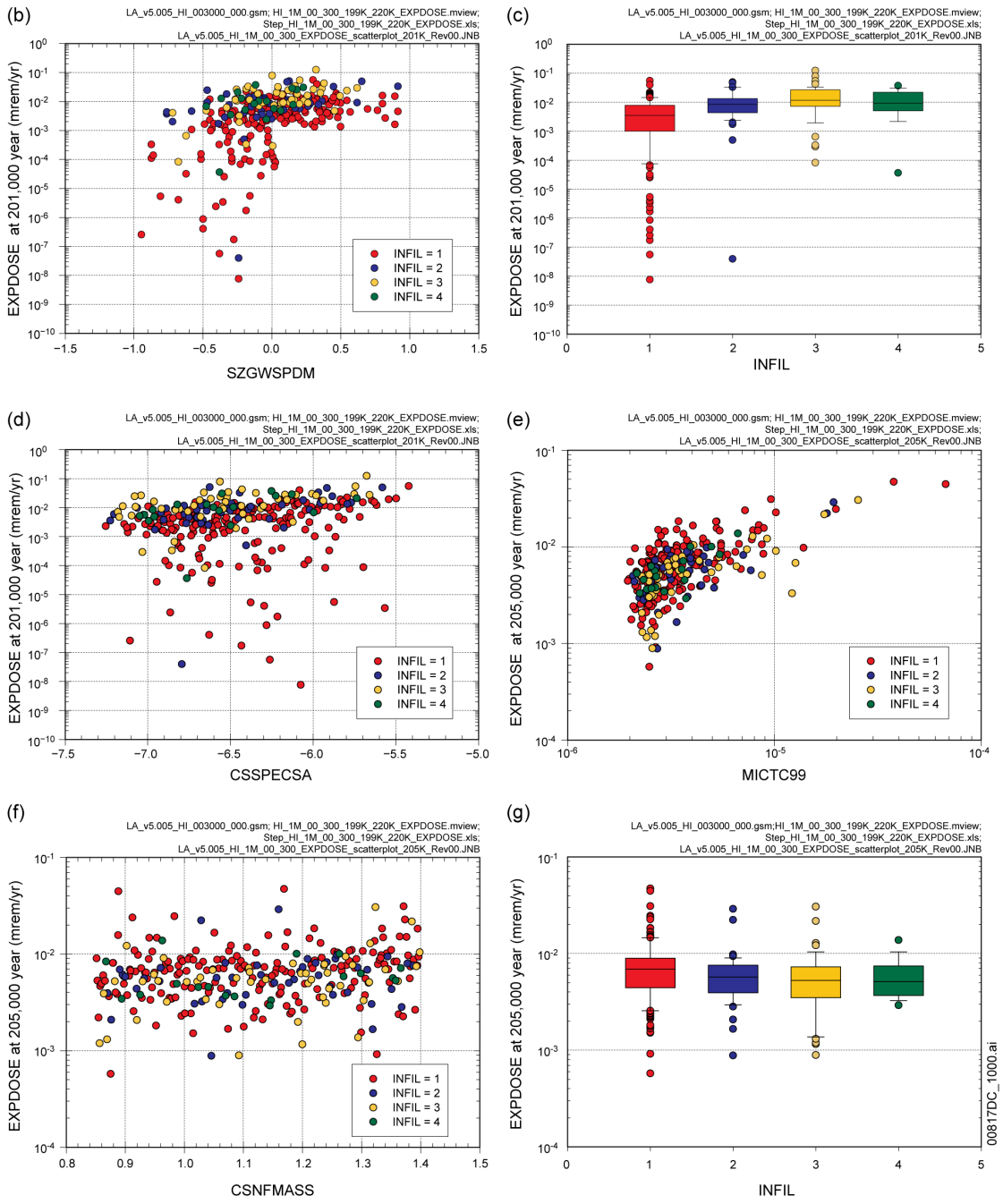


Source: Output DTNs: MO0710ADTSPAWO.000 [DIRS 183752]; and MO0710PLOTSFIG.000 [DIRS 185207].

NOTE: In (c, g), the box extends from 0.25 to 0.75 quantile; lower and upper bar and whisker extend to 0.1 and 0.9 quantile, respectively; dots represent values outside 0.1 to 0.9 quantile range; median indicated by light horizontal line.

Figure K10-2[a]. Stepwise rank regression analyses and selected scatterplots for expected dose to RMEI (*EXPDOSE*, mrem/yr) over [200,000, 220,000 yr] resulting from human intrusion at 200,000 years obtained with version 5.005 of the TSPA-LA Model: (a) regressions for *EXPDOSE* at 201,000, 203,000, and 205,000 years, (b,c,d) scatterplots for *EXPDOSE* at 201,000 years, and (e,f,g) scatterplots for *EXPDOSE* at 205,000 years (continued)

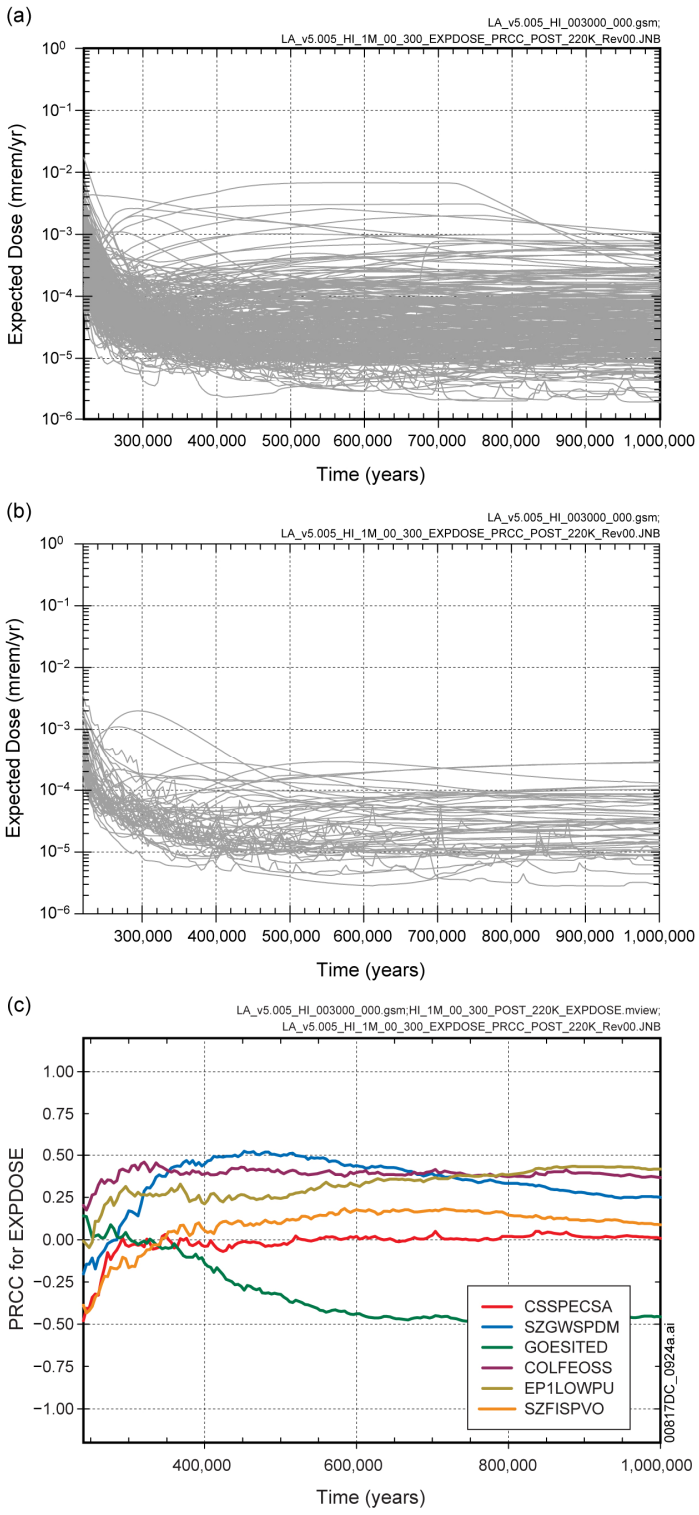


Source: Output DTNs: MO0710ADTSPAWO.000 [DIRS 183752]; and MO0710PLOTSFIG.000 [DIRS 185207].

Figure K10-3[a]. Expected dose to RMEI (*EXPDOSE*, mrem/yr) over [220,000, 1,000,000 yr] resulting from human intrusion at 200,000 years obtained with version 5.005 of the TSPA-LA Model: (a) *EXPDOSE* for all (i.e., 300) sample elements, (b) *EXPDOSE* for first 50 sample elements, and (c) PRCCs for *EXPDOSE*

(a)

| | EXPDOSE: 240,000 Years | | | EXPDOSE: 500,000 Years | | | EXPDOSE: 760,000 Years | | |
|---|---|---|---|---|---|---|---|---|---|
| Step[a] | Variable[b] | $R^{2\,c}$ | SRRC[d] | Variable | $R^2$ | SRRC | Variable | $R^2$ | SRRC |
| 1 | CSSPECSA | 0.20 | −0.44 | SZGWSPDM | 0.15 | 0.37 | GOESITED | 0.10 | −0.33 |
| 2 | SZGWSPDM | 0.29 | −0.29 | GOESITED | 0.23 | −0.27 | SZGWSPDM | 0.20 | 0.27 |
| 3 | SZFISPVO | 0.36 | −0.34 | ISCSS | 0.29 | −0.26 | COLFEOSS | 0.27 | 0.29 |
| 4 | MICTC99 | 0.42 | 0.22 | COLFEOSS | 0.34 | 0.22 | EP1LOWPU | 0.34 | 0.23 |
| 5 | SZDIFCVO | 0.45 | 0.19 | EP1LOWPU | 0.39 | 0.22 | ISCSS | 0.39 | −0.23 |
| 6 | MICI129 | 0.46 | 0.14 | HFOSA | 0.43 | −0.20 | EP1LOWNU | 0.44 | 0.18 |
| 7 | UZKDCSDT | 0.48 | −0.12 | EP1LOWNU | 0.46 | 0.17 | HFOSA | 0.48 | −0.20 |
| 8 | CSNFMASS | 0.49 | 0.12 | MICCS135 | 0.48 | 0.14 | MICCS135 | 0.51 | 0.17 |
| 9 | ISCSS | 0.50 | −0.11 | SZDIFCVO | 0.49 | −0.16 | MICPU239 | 0.54 | 0.16 |
| 10 | | | | SZFISPVO | 0.51 | 0.17 | SZDIFCVO | 0.55 | −0.17 |
| 11 | | | | SZCOLRAL | 0.53 | −0.14 | SZFISPVO | 0.57 | 0.14 |
| 12 | | | | UZRCOL | 0.54 | 0.12 | HFOSITED | 0.59 | −0.15 |
| 13 | | | | HFOSITED | 0.55 | −0.11 | WDGCUA22 | 0.60 | 0.12 |
| 14 | | | | | | | SZSREG2Y | 0.61 | 0.13 |
| 15 | | | | | | | SZKDSRVO | 0.62 | −0.11 |
| 16 | | | | | | | SZLODISP | 0.63 | −0.10 |

a: Steps in stepwise rank regression analysis
b: Variables listed in order of selection in stepwise regression
c: Cumulative $R^2$ value with entry of each variable into regression model
d: Standardized rank regression coefficients (SRRCs) in final regression model

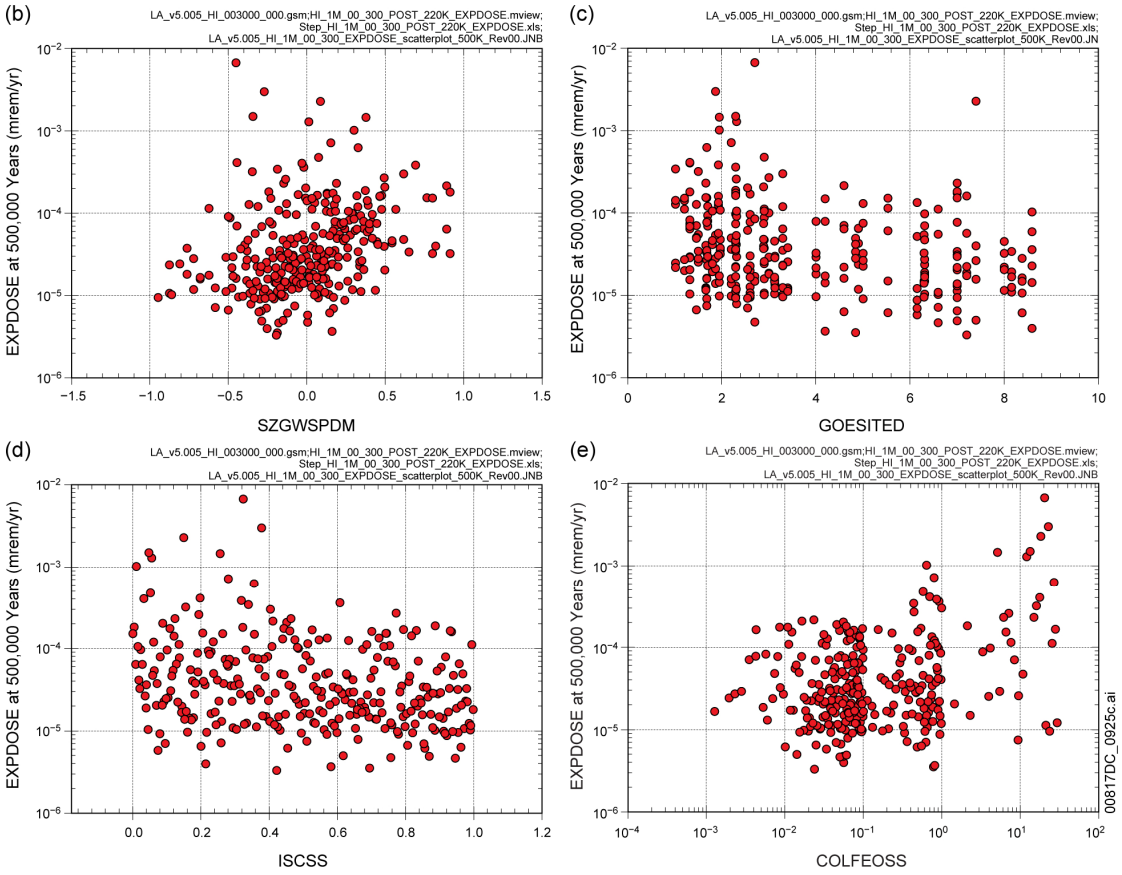


Source: Output DTNs: MO0710ADTSPAWO.000 [DIRS 183752]; and MO0710PLOTSFIG.000 [DIRS 185207].

Figure K10-4[a]. Stepwise rank regression analyses and selected scatterplots for expected dose to RMEI (*EXPDOSE*, mrem/yr) over [220,000, 1,000,000 yr] resulting from human intrusion at 200,000 years obtained with version 5.005 of the TSPA-LA Model: (a) regressions for *EXPDOSE* at 240,000, 500,000, and 760,000 years, and (b,c,d,e) scatterplots for *EXPDOSE* at 500,000 years

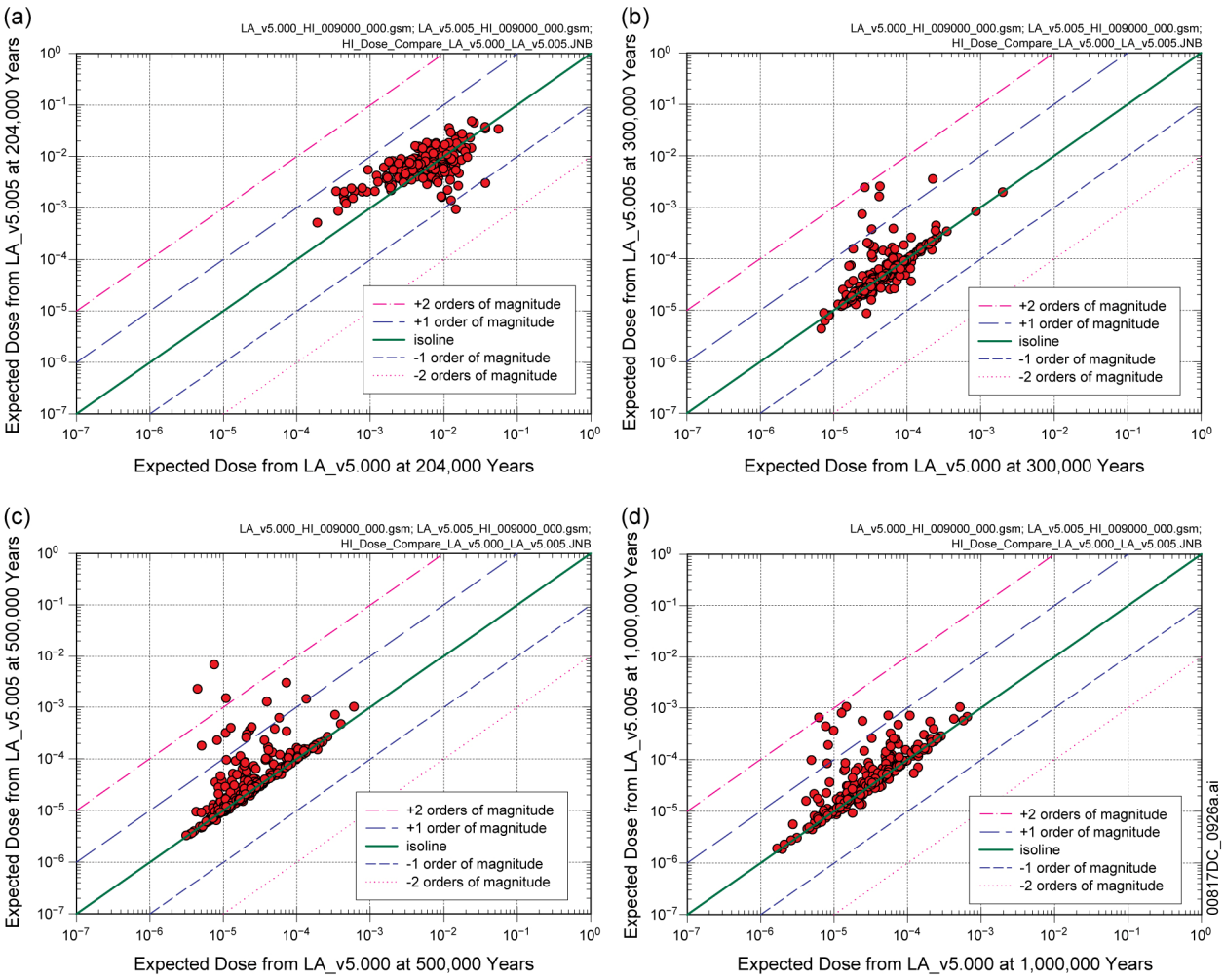


Source: Output DTNs: MO0710ADTSPAWO.000 [DIRS 183752]; and MO0710PLOTSFIG.000 [DIRS 185207].

Figure K10-5[a]. Comparison of expected dose to RMEI (*EXPDOSE*, mrem/yr) over [200,000, 1,000,000 yr] resulting from human intrusion at 200,000 years obtained with versions 5.000 and 5.005 of the TSPA-LA Model at (a) 201,000, (b) 205,000, (c) 500,000, and (d) 1,000,000 years

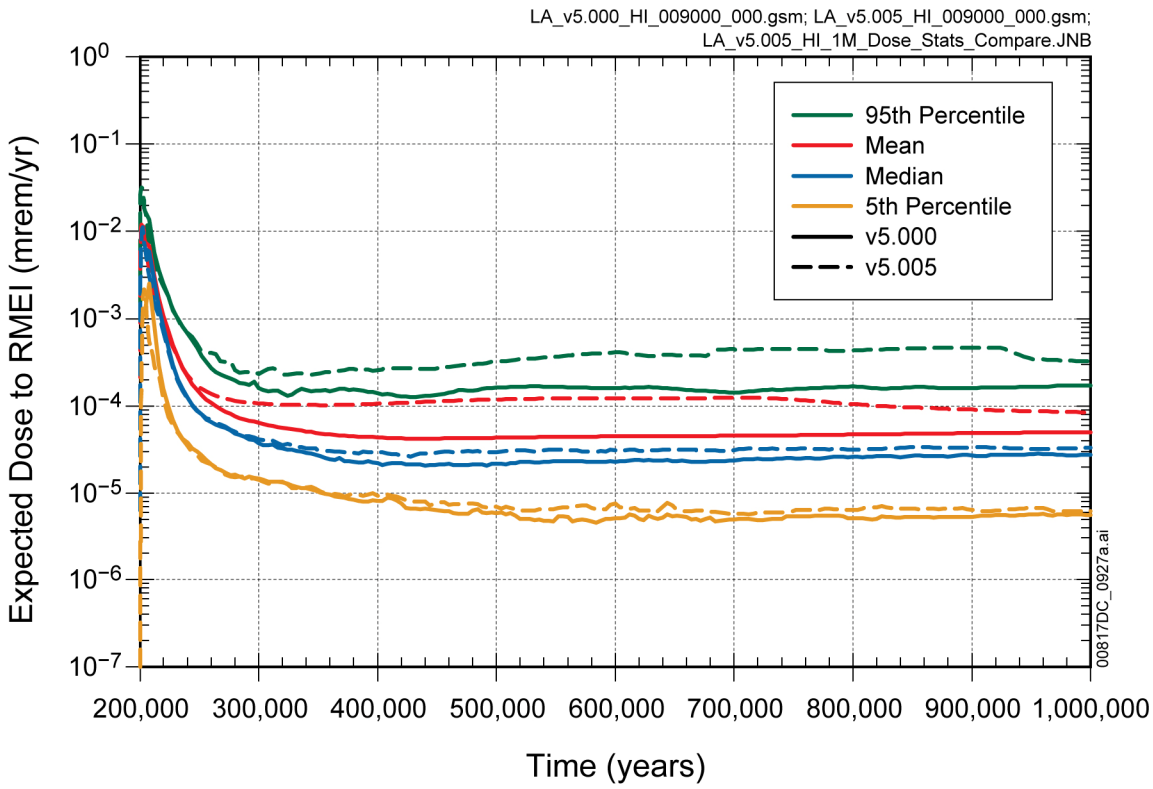


Source: Output DTNs: MO0710ADTSPAWO.000 [DIRS 183752]; and MO0710PLOTSFIG.000 [DIRS 185207].

Figure K10-6[a]. Comparison of summary curves (i.e., mean and 0.05, 0.5, and 0.95 quantile) for expected dose to RMEI (*EXPDOSE*, mrem/yr) over [200,000, 1,000,000 yr] resulting from human intrusion at 200,000 years obtained with versions 5.000 and 5.005 of the TSPA-LA Model

# APPENDIX M[a]
# COMPARISON WITH ELECTRIC POWER RESEARCH INSTITUTE ANALYSIS

# M1[a] INTRODUCTION

Appendix M[a] contains a minor change from the parent document to correct a reference to supporting documentation. The last paragraph in Section M3.3 of the parent document has been updated to correct the reference and is included in Section M3.3[a] of this addendum. The corrected paragraph should be substituted into the discussion presented in Appendix M of the parent document.

# M2[a] TSPA CONCEPTUAL MODEL DESIGN

No change.

# M3[a] TSPA NOMINAL SCENARIO COMPARISON

No change.

## M3.1[a] UNSATURATED FLOW

No change.

## M3.2[a] ENGINEERED BARRIER SYSTEM ENVIRONMENT

No change.

## M3.3[a] WASTE PACKAGE AND DRIP SHIELD DEGRADATION

In the Electric Power Research Institute (EPRI) TSPA, the computed failure distributions curves for the nominal scenario for the WP are shown on Figure 5-7 in Apted and Ross (2005 [DIRS 182229]), indicating onset of WP failures before 100,000 years. The EPRI TSPA Analysis only considers 8,160 CSNF WPs, of which 5,304 WPs fail after one million years (Senger 2008 [DIRS 185124]). In the TSPA-LA Nominal Scenario Class, the probabilistic projections of WP breaches exhibit a few realizations with a stress corrosion cracking penetrating crack occurring before 100,000 years (Section 8.2.1[a]). However, as Figure 7.7.3-2[a] indicates the bulk of the WP failures occur after about 200,000 years with 6,256 WPs failed by one million years.

INTENTIONALLY LEFT BLANK

# APPENDIX P[a]
# IMPACT ASSESSMENTS

# P1[a] INTRODUCTION

The checking and review activities following the completion of the TSPA-LA Model (v5.000) identified several issues related to errors in implementation, identification of undocumented conservatisms, and updates to parameter values. A detailed discussion of these issues, including an evaluation of the expected impact to the mean annual dose, is included in Appendix P of the parent document. The impact assessment documented in Section P13.3 of the parent document has been updated and is included in Section P13[a] of this addendum. The remaining issue descriptions and impact analyses documented in the parent document are not repeated in this addendum.

The results described in this addendum were generated with TSPA-LA Model v5.005, an updated version of the TSPA-LA Model v5.000, unless otherwise indicated. TSPA-LA Model v5.005 addresses most of the items presented in Appendix P of the parent document; the items resolved in v5.005 are listed in Appendix P[a] of this addendum. The issues addressed in v5.005 are identified in two updated tables, Table P-6[a] and P-7[a]. These two tables comprise a summary of the changes between v5.000 and v5.005 of the TSPA-LA Model.

The discussion and impact assessment presented in Appendix P of the parent document for the remaining issues not addressed in v5.005 of the TSPA-LA Model, as indicated on Table P-7[a], are not repeated in this addendum, as the issue description and impact assessment (excluding Section P13, which is revised in this addendum) remain unchanged and apply equally to v5.005 of the TSPA-LA Model.

# P2[a] INVENTORY AND SEEPAGE FRACTION

## P2.1[a] ISSUE

Addressed in TSPA-LA Model v5.005.

## P2.2[a] ISSUE DESCRIPTION

No change.

## P2.3[a] IMPACT ASSESSMENT

No impact to TSPA-LA v5.005 results.

# P3[a] WASTE PACKAGE DAMAGE FROM SEISMIC EVENTS

## P3.1[a] ISSUE

Addressed in TSPA-LA Model v5.005.

## P3.2[a] ISSUE DESCRIPTION

No change.

**P3.3[a] IMPACT ASSESSMENT**

No impact to TSPA-LA v5.005 results.

## P4[a] OUTER BARRIER FAILURE FLAG IN SEISMIC MODEL

**P4.1[a] ISSUE**

Addressed in TSPA-LA Model v5.005.

**P4.2[a] ISSUE DESCRIPTION**

No change.

**P4.3[a] IMPACT ASSESSMENT**

No impact to TSPA-LA v5.005 results.

## P5[a] INVERT CHEMISTRY

**P5.1[a] ISSUE**

Addressed in TSPA-LA Model v5.005.

**P5.2[a] ISSUE DESCRIPTION**

No change.

**P5.3[a] IMPACT ASSESSMENT**

No impact to TSPA-LA v5.005 results.

## P6[a] WELD VOLUME

**P6.1[a] ISSUE**

Addressed in TSPA-LA Model v5.005.

**P6.2[a] ISSUE DESCRIPTION**

No change.

**P6.3[a] IMPACT ASSESSMENT**

No impact to TSPA-LA v5.005 results.

## P7[a] CRACK FAILURE OPENING

### P7.1[a] ISSUE

Addressed in TSPA-LA Model v5.005.

### P7.2[a] ISSUE DESCRIPTION

No change.

### P7.3[a] IMPACT ASSESSMENT

No impact to TSPA-LA v5.005 results.

## P8[a] DEGRADATION START TIME

### P8.1[a] ISSUE

Addressed in TSPA-LA Model v5.005.

### P8.2[a] ISSUE DESCRIPTION

No change.

### P8.3[a] IMPACT ASSESSMENT

No impact to TSPA-LA v5.005 results.

## P9[a] THRESHOLD RUBBLE VOLUME

### P9.1[a] ISSUE

Addressed in TSPA-LA Model v5.005.

### P9.2[a] ISSUE DESCRIPTION

No change.

### P9.3[a] IMPACT ASSESSMENT

No impact to TSPA-LA v5.005 results.

## P10[a] UNINTENDED CORRELATION OF UNCERTAIN PARAMETERS

### P10.1[a] ISSUE

Addressed in TSPA-LA Model v5.005.

### P10.2[a] ISSUE DESCRIPTION

No change.

### P10.3[a] IMPACT ASSESSMENT

No impact to TSPA-LA v5.005 results.

## P11[a] UNCERTAINTY IN URANIUM SOLUBILITY

### P11.1[a] ISSUE

Addressed in TSPA-LA Model v5.005.

### P11.2[a] ISSUE DESCRIPTION

No change.

### P11.3[a] IMPACT ASSESSMENT

No impact to TSPA-LA v5.005 results.

## P12[a] IONIC STRENGTH FOR HIGH-LEVEL WASTE GLASS DOMAIN

### P12.1[a] ISSUE

Addressed in TSPA-LA Model v5.005.

### P12.2[a] ISSUE DESCRIPTION

No change.

### P12.3[a] IMPACT ASSESSMENT

No impact to TSPA-LA v5.005 results.

## P13[a] EFFECT ON SEEPAGE FROM WASTE PACKAGE LENGTH CHANGE

The impact assessment documented in Section P13.3 of the parent document has been updated. Specifically, the last two paragraphs of the impact assessment have been revised, however, the entire section has been repeated and is included below in Section P13.3[a] of this addendum.

### P13.1[a] ISSUE

No change.

### P13.2[a] ISSUE DESCRIPTION

No change.

## P13.3[a] IMPACT ASSESSMENT

The Seepage Model for Performance Assessment provides the mean and standard deviation of the distribution of seepage rates (kg/WP/yr) over a large range of capillary strengths, permeabilities, and percolation fluxes. The seepage dynamically linked library (DLL) used in the TSPA-LA Model uses these rates, along with percolation fields, thermal histories at each WP location, and sampled values for mean capillary strength and mean permeability, to determine seepage rates (kg/WP/yr) at each location and time in each realization, and computes the seepage fraction (fraction of WP locations at which seepage occurs) at each time in each realization.

The Seepage Model for Performance Assessment is a three-dimensional continuum representation of a fractured rock system used to calculate drift seepage at Yucca Mountain. The three-dimensional calculational domain for the model is 10-m high, 4-m wide, and 2.4384-m long (BSC 2004 [DIRS 167652], Figure 6-1). This domain takes advantage of model symmetry and spatial correlation lengths to represent a system based on a drift diameter of 5.5 m and a WP length of 5.1 m with a smaller domain. Rock above and around the drift is also represented in the model. Because the model uses a no-flow vertical boundary along the drift axis, and also only represents a part of the WP length, seepage rates from the model are scaled up by a factor of 4.183, which represents the ratio between the considered drift area (5.5 m × 5.1 m) and the modeled drift area ((5.5 m / 2)*2.4384 m).

The seepage rates for an average WP length of 5.614 m can be estimated by scaling the Seepage Model for Performance Assessment results for an average WP length of 5.0 m. As noted in *Seepage Model for PA Including Drift Collapse* (BSC 2004 [DIRS 167652]), the limited size of the calculational domain was chosen to allow for the use of a fine mesh at the same resolution as the Software Configuration Management, while containing a reasonable number of cells that would not make the computational time too long. The cell dimensions in the vertical plane perpendicular to the drift axis are 0.1 m by 0.1 m and cell lengths parallel to the drift axes are about 0.3 m each (BSC 2004 [DIRS 167652], Section 6.3.1). The vertical boundaries, perpendicular to the drift axis and along the drift centerline are appropriate due to symmetry. The main issue for a heterogeneous system is the domain length versus spatial correlation length (BSC 2004 [DIRS 167652], Section 6.3.1). The lengths of the flow domain in the direction of the drift axis (2.4384 m) and normal to the drift axis (4 m) are 8 times and 13 times the spatial correlation length (0.3 m), respectively. Since the length of the flow domain in the direction of the drift axis is 8 times the correlation length, the no flow boundaries perpendicular to the drift axis are considered appropriate, and should not have a significant effect on flow results. Because the no-flow boundaries have little effect on flow results, the model adequately represents any WP length longer than the model dimensions along the drift axis, as long as the results are scaled by the ratio of the chosen WP length to the modeled WP length. Thus, seepage rates for an average WP length of 5.614 m can be estimated by scaling the Seepage Model for Performance Assessment results for an average WP length of 5.0 m. This scaling would increase the mean and standard deviation of the distribution proportionally (by a factor of 5.614 / 5.1 = 1.10).

The seepage fraction is computed in the Seepage DLL as the fraction of locations at which seepage exceeds the threshold of 0.1 kg/WP/yr. Since seepage rates increase when the average WP length is increased, the seepage fraction may also increase, because the seepage rate at some locations may increase from just less than the threshold to greater than the threshold. Current

TSPA-LA software does not support a numerical evaluation of the degree to which the seepage fraction may increase when average WP length increases. To evaluate the potential impact on total dose associated with an increase in seepage fraction due to an increased WP length, the correlation between seepage fraction and expected annual dose was examined for the 1,000,000-year Nominal Modeling Case, the 10,000-year Seismic Ground Motion (GM) Modeling Case, and the 1,000,000-year Seismic GM Modeling Case. The 10,000-year Igneous Intrusion Modeling Case and the 1,000,000-year Igneous Intrusion Modeling Case which are also major contributors to dose were not examined because after an igneous event occurs, all WPs are evaluated in a seeping environment. For the three cases, scatter plots of expected annual doses versus seepage fraction at 10,000 or 1,000,000 years are presented along with the rank correlations of expected annual dose and seepage fraction at those times. As shown in Figure P-20[a], for the 1,000,000-year Nominal Modeling Case, negligible correlation between expected annual dose and seepage fraction at 1,000,000 years is seen. The rank correlation between expected annual dose and seepage fraction is $2.4 \times 10^{-2}$. Similarly, for the 10,000-year Seismic GM Case, negligible correlation between expected annual dose and seepage fraction at 10,000 years is seen (Figure P-21(a)[a]). The rank correlation between expected annual dose and seepage fraction, for the 10,000-year Seismic GM Case, is $4.65 \times 10^{-2}$. For the 1,000,000-year Seismic Ground Motion Case, negligible correlation between expected annual dose and seepage fraction at 1,000,000 years is seen (Figure P-21(b)[a]). The rank correlation between expected annual dose and seepage fraction, for the 1,000,000-year Seismic GM Case, is $1.17 \times 10^{-2}$. Based on the negligible correlation between expected annual dose and seepage fraction shown in these analyses, it is assumed that change in seepage fractions, associated with an increase in the waste package length to 5.614 m, will have little impact on total dose.

Because seepage rates increase proportionally with increased WP length, and seepage fraction is not anticipated to have a large impact on dose, the net effect of increasing WP length on annual dose is to increase seepage rates in a percolation bin by approximately 10 percent. As demonstrated in Section P17, annual dose may increase in proportion to changes in seepage rates for cases where the major dose-controlling radionuclide is solubility-controlled in the EBS. For radionuclides that do not have solubility limits, the increased seepage flux would have negligible impact on the mass flux. Therefore, the overall effect of increasing the average WP length used in the seepage abstraction by 10 percent would be minor.

## P14[a] IGNEOUS EVENT PROBABILITY

### P14.1[a] ISSUE

No change.

### P14.2[a] ISSUE DESCRIPTION

No change.

### P14.3[a] IMPACT ASSESSMENT

No change.

## P15[a] LONGITUDINAL DISPERSIVITY IN 1-D SZ TRANSPORT MODEL

### P15.1[a] ISSUE

Addressed in TSPA-LA Model v5.005.

### P15.2[a] ISSUE DESCRIPTION

No change.

### P15.3[a] IMPACT ASSESSMENT

No impact to TSPA-LA v5.005 results.

## P16[a] GLASS DEGRADATION RATE

### P16.1[a] ISSUE

Addressed in TSPA-LA Model v5.005.

### P16.2[a] ISSUE DESCRIPTION

No change.

### P16.3[a] IMPACT ASSESSMENT

No impact to TSPA-LA v5.005 results.

## P17[a] SEEPAGE FLUX AFTER DRIFT COLLAPSE

### P17.1[a] ISSUE

No change.

### P17.2[a] ISSUE DESCRIPTION

No change.

### P17.3[a] IMPACT ASSESSMENT

No change.

## P18[a] UNSTABLE IRON OXYHYDROXIDE COLLOIDS

### P18.1[a] ISSUE

Addressed in TSPA-LA Model v5.005.

**P18.2[a] ISSUE DESCRIPTION**

No change.

**P18.3[a] IMPACT ASSESSMENT**

No impact to TSPA-LA v5.005 results.

## P19[a] DOE SPENT NUCLEAR FUEL MASS RELEASE

**P19.1[a] ISSUE**

Addressed in TSPA-LA Model v5.005.

**P19.2[a] ISSUE DESCRIPTION**

No change.

**P19.3[a] IMPACT ASSESSMENT**

No impact to TSPA-LA v5.005 results.

## P20[a] GOLDSIM SOFTWARE ERROR

**P20.1[a] ISSUE**

Addressed in TSPA-LA Model v5.005.

**P20.2[a] ISSUE DESCRIPTION**

No change.

**P20.3[a] IMPACT ASSESSMENT**

No impact to TSPA-LA v5.005 results.

## P21[a] UNSATURATED ZONE TRANSPORT THROUGH FAULT ZONE

**P21.1[a] ISSUE**

No change.

**P21.2[a] ISSUE DESCRIPTION**

No change.

**P21.3[a] IMPACT ASSESSMENT**

No change.

## P22[a] OTHER MINOR IMPLEMENTATION ERRORS

### P22.1[a] ISSUE

Addressed in Table P-6[a].

### P22.2[a] ISSUE DESCRIPTION

No change.

## P23[a] SUPERFICIAL CHANGES

### P23.1[a] ISSUE

No change.

### P23.2[a] ISSUE DESCRIPTION

No change.

### P23.3[a] IMPACT ASSESSMENT

No change.

## P24[a] SUMMARY

The issues addressed in TSPA-LA Model v5.005 which were presented in Appendix P of the parent document are summarized in Table P-7[a]. Since most of the issues evaluated had a negligible to small impact (except for the issue discussed in Section P3), the combined effect of correcting the issues was small for mean annual dose for all modeling cases (as documented in Section 7.3.1[a]). In none of the issues evaluated does the mean annual dose increase appreciably above the base-case results presented in Section 8 of the parent document, in fact, in most cases, it decreases (see Section 7[a] and Section 8[a] of this addendum). Thus, the impact assessments presented in Appendix P of the parent document were accurate and the validation activities performed on the results documented therein remain applicable.

INTENTIONALLY LEFT BLANK

Table P-6[a]. Discussion of Other Minor Implementation Errors

| | ISSUE DESCRIPTION | ANTICIPATED IMPACT (V5.000) | ADDRESSED V5.005 |
|---|---|---|---|
| 1 | Drift-wall condensation incorrectly turned off in the non-dripping environments. | This error should have negligible or no impact in all modeling cases. Because drift-wall condensation occurs for at most 2,000 years (Section 6.3.3.2.2) and because the DS remains intact throughout this period in all modeling cases except Drip Shield EF Modeling Case, the release from any failed WP should be negligibly impacted. In the Drip Shield EF Modeling Case since the WP is always modeled to be located in the dripping environment (Section 6.4.1.3), there should be no impact. | Yes – Drift wall condensation appropriately applied to the non-dripping environments. |
| 2 | Inconsistent half-lives especially for $^{79}$Se and $^{126}$Sn between those applied in GoldSim and those used by the UZ and SZ transport models implemented using DLLs. | The $^{79}$Se half-life in GoldSim is set at 290,000 years while that in the UZ and SZ transport model is set at 295,000 years. The $^{126}$Sn half-life in GoldSim is set at 230,000 years while that in the UZ and SZ transport model is set at 250,000 years.<br><br>These inconsistencies are minor, as they occur only in the second significant digit. Since the dose contribution from $^{79}$Se and $^{126}$Sn is at least an order of magnitude lower than some of the other radionuclides (see Figures P-1 to P-5), the impact on the mean annual dose would be negligible. | Yes – EBS, Unsaturated Zone, and Saturated Zone submodels use the same half-life values. |
| 3 | In the calculations to determine the time of first seismic damage to the WP, the abstraction for WP failure under intact DS is considered while the DS is intact. This calculation should not be used after either the DS plate or DS framework has failed. However, this calculation ignores the DS framework failure and only considers the DS plate failure to determine whether to use this abstraction or not. | It should be noted that this error only affects the 1,000,000-year Seismic GM Modeling Case because the DS remains intact in the 10,000-year modeling case.<br><br>Since the DS framework failure (average failure time of 100,000 years) occurs earlier than the DS plate failure (average failure time of 250,000 years), there is a possibility of predicting the WP failure time earlier than intended in the time duration where the DS framework has failed but the DS plate is intact.<br><br>This error may have an impact on estimating first failure time for only CDSP WPs as the probability of WP failure under intact DS is generally greater than the probability of failure under failed DS that is surrounded by rubble. Even here, the probability of occurrence of this error is small, as the DS framework lasts up to 100,000 years on an average, during which time CDSP WPs that are likely to fail from seismic damage would have failed in a majority of the realizations (~70%). For CSNF WPs there is no impact anticipated, as the probability of failure under intact DS is much smaller than the probability of failure under the failed DS that is surrounded by rubble. As a result, this error is likely to have only a negligible impact on the mean annual dose. | Yes – Corrected to consider both the DS plate and framework failures. |
| 4 | The calculation for the time of first seismic damage may be incorrect if the WP damage is from the first seismic event. | This error only appears when the first seismic event causes the damage to the WP or leads to rockfall. Since seismic events occur on an average of every 2,330 years (inverse of specified annual rate of $4.287 \times 10^{-4}$ yr$^{-1}$), only those realizations would be impacted where the WP damage or rockfall occurs within 2,330 years (on an average). There are only five such realizations in the 9,000 realization seismic ground motion base case where the damage should have occurred from the first seismic event but did not occur due to the error. The impact of this error is negligible. No other modeling cases are affected. | Yes – Calculation was corrected to accurately reflect the first seismic event. |

Table P-6[a]. Discussion of Other Minor Implementation Errors (Continued)

| | ISSUE DESCRIPTION | ANTICIPATED IMPACT (V5.000) | ADDRESSED V5.005 |
|---|---|---|---|
| 5 | The HLW glass derived waste form colloid concentrations are overestimated under conditions when the waste form colloids are unstable. | This error occurs only when the conditions are unstable for the generation of glass waste form colloids. Since the maximum concentration of HLW glass waste form colloids, under stable conditions, is itself small (maximum of 2 mg/L and a mean of 0.3 mg/L) the mass transported on colloids will be negligibly small compared to that transported in the dissolved phase. Thus, this overestimation would have negligible impact on the mean annual dose. Furthermore, the unstable conditions generally occur when the ionic strength is greater than 0.4 mol/kg, which is typical while there is no flow through the WP. Since the transport mechanism is diffusion when there is no flow and because the diffusion coefficient of colloids is much smaller compared to the dissolved species (by at least two orders) no appreciable mass can be carried by the colloids. | Yes – High-level radioactive waste glass colloid concentration calculation was corrected. |
| 6 | The element that integrates the mass released from the WP in the Human Intrusion Scenario integrates the mass flux rate computed for the previous timestep over the next timestep using the next timestep length. It should instead integrate the mass flux rate computed for the given timestep over that timestep length. | This error would only have an impact when the timestep length is changing as the integrated mass would change. Since the intrusion time is set at 200,000 years in the Human Intrusion Scenario and because there is no change made in the timestep length for the remaining simulation duration, the calculations are not affected. The only impact is one timestep delay in passing the mass to the UZ borehole pathway while the dose magnitudes remain unaffected. Since this is a highly stylized modeling case, with a selected intrusion time, the one timestep delay is not important to the overall system results and does not affect the dose values. | Yes – The calculation has been corrected to use the appropriate timestep length. |

Table P-6[a]. Discussion of Other Minor Implementation Errors (Continued)

| | ISSUE DESCRIPTION | ANTICIPATED IMPACT (V5.000) | ADDRESSED V5.005 |
|---|---|---|---|
| 7 | The implemented range of two uncertain parameters used in determining the number of monolayers of adsorbed water for corrosion products as part of the EBS Transport submodel is different from their intended ranges. | The stochastic elements FHH_Isotherm_k_CP_a and FHH_Isotherm_s_CP_a are sampled to determine the value for parameters *k* and *s* that are used in the water adsorption isotherm for corrosion products to determine the number of sorbed layers of water (SNL 2007 [DIRS 177407], Section 6.3.4.3.2), which is eventually used in computing the saturation under conditions when there is no flow through the WP. The uniform distribution ranges used from *EBS Radionuclide Transport Abstraction*, (SNL 2007 [DIRS 177407], Table 8.2-4) are:<br>FHH_Isotherm_k_CP_a: 1.048 – 1.370<br>FHH_Isotherm_s_CP_a: 1.525 – 1.852<br>The correct ranges, as intended in Section 6.3.4.3.2 of *EBS Radionuclide Transport Abstraction* (SNL 2007 [DIRS 177407]) are:<br>FHH_Isotherm_k_CP_a: 1.030 – 1.326<br>FHH_Isotherm_s_CP_a: 1.493 – 1.799<br>The difference in the two ranges is small compared to their uncertainty ranges and thus the effect on calculating the number of monolayers of adsorbed water and saturation of corrosion products is likely to be negligible, leading to negligible impact on the mean annual dose. | Yes – Uncertainty distributions have been corrected. |
| 8 | The $K_d$ range for sorption of Np on the Uranium mineral colloids in the EBS is not correct. | The $K_d$ range for sorption of Np on the uranium colloids is given by a log-uniform distribution ranging from 10 to 500 mL/g (Table 6.3.7-64). The lower bound value of 10 mL/g was incorrectly set to 1 mL/g during the implementation. The impact of this reduction in the lower bound is anticipated to be negligible as the Np mass carried by the uranium colloids is likely to be small (even with the corrected values) compared to the mass carried by other colloid types and in the dissolved phase. Considering the mean uranium colloid concentration of about 6 mg/l (based on cumulative distribution function given in Table 6.3.7-64) and the maximum Np $K_d$ of 500 mL/g, and multiplying the two would lead to a value of about $3 \times 10^{-3}$, which represents the ratio of Np mass on the uranium colloids to the mass in the dissolved phase in given water volume. This indicates that the predominant mechanism for Np transport is in the dissolved phase. The impact of this error is anticipated to be negligible, if any, on the mean annual dose. | Yes – $K_d$ range for sorption of Np on the uranium colloids has been corrected. |

Table P-6[a]. Discussion of Other Minor Implementation Errors (Continued)

| | ISSUE DESCRIPTION | ANTICIPATED IMPACT (V5.000) | ADDRESSED V5.005 |
|---|---|---|---|
| 9 | In the Human Intrusion Modeling Case, the mass irreversibly associated with colloids that is released to the SZ is not partitioned into the fast transport fraction and the slow transport fraction. | In the Human Intrusion Modeling Case, the mass irreversibly associated with the waste form colloids (referred as "Ic") and the iron oxyhydroxide colloids (referred as "If") from the WP and passed through the UZ borehole needs to be combined together and repartitioned based on the fast fraction, before passing the mass to the SZ. This needs to be done in such a way that only a small fraction (0.00168) travels unretarded (fast) while the rest of the mass travels with some retardation (slowly).<br>The impact of this error is anticipated to be small as the relative contribution from the fast and slow traveling mass fractions cannot be fully differentiated due to large timesteps employed in the TSPA-LA Model past 200,000 years (when the human intrusion is modeled). Thus, even though the relative contribution of Ic and If species could vary, the combined mass flux from the mass irreversibly associated with colloids is not anticipated to change. As a result, the impact on the mean annual dose is anticipated to be negligible. | Yes – Human Intrusion Scenario Modeling Case was corrected to include a partitioning of the mass released to the SZ between fast and slow colloid fractions. |
| 10 | In the UZ transport model, the correct minimum value for the selenium $K_d$ for vitric rock units was supposed to be 0 mL/g. However, the minimum value after natural log transformation was set to 0, which is equivalent to a $K_d$ of 1 mL/g. | The impact of this error is anticipated to be negligible as the mean $K_d$ value remains largely unchanged (reduced by 0.8%) when the minimum value is corrected. Furthermore, $^{79}Se$ is not a large contributor to dose. | Yes – The selenium $K_d$ for vitric rock has been corrected. |
| 11 | For the UZ transport model, the uranium $K_d$ for zeolitic rock unit has an error at probability level of 1. It was incorrectly set to 20 mL/g instead of 30 mL/g. | The impact of this error is anticipated to be negligible as the mean $K_d$ value would change from 5.25 mL/g to 7.75 mL/g. This small increase is unlikely to affect the transport of uranium through the UZ. Furthermore, the current error is conservative as it leads to lowering the uranium $K_d$ in the UZ matrix. | Yes – The uranium $K_d$ for zeolitic rock has been corrected. |
| 12 | The concentration limit for plutonium and americium mass irreversibly sorbed on the iron oxyhydroxide colloids in the invert is incorrectly based on the stability criteria for the waste form domain instead of the corrosion products domain. | The error would only have an impact if the irreversible colloid concentration in the invert is nearing the concentration limit in the invert, which is an unlikely condition due to fast transport rates out of the invert compared to the incoming transport rate. Even if the conditions conducive to error occur, they would remain for a short time period compared to the simulation time. The impact of this error is expected to be negligible on the mean annual dose. | Yes – The calculation has been corrected to use the stability criteria in the corrosion products domain. |

Table P-6[a]. Discussion of Other Minor Implementation Errors (Continued)

| | ISSUE DESCRIPTION | ANTICIPATED IMPACT (V5.000) | ADDRESSED V5.005 |
|---|---|---|---|
| 13 | The time-dependent increase in the diffusive area from nominal corrosion of the WP outer barrier should be removed from the stylized Human Intrusion Modeling Case. | Ignoring the time-dependent increase in diffusive area from nominal corrosion processes (by either SCC or general corrosion patches) on the WP for the Human Intrusion Modeling Case is unlikely to affect the diffusive release out of the WP as only about 5% of the realizations would have some SCC failures by 200,000 years, the time when the human intrusion event is modeled. Following the event, the patch area equal to the drill stem area is applied to the WP for both diffusive and advective release. The patch area applied is large enough to cause large diffusive releases. Since the general corrosion patches do not occur until very late times (>400,000 years), any small increases in diffusive area from SCCs is unlikely to affect the diffusive flux. The impact of this error is likely to be negligibly small on the mean annual dose. | Yes – The nominal corrosion processes have been removed from the diffusive area calculation in the Human Intrusion Scenario. |
| 14 | In calculating the first damage time for the WP due to seismic ground motion, the possibility of failure from puncture was not considered. | The first damage time calculations only evaluate the failures caused by seismic-induced SCCs or by nominal corrosion processes (nominal SCC or general corrosion). However, there is a small probability that punctures could occur earlier under certain conditions. The conditions for puncture failure require that the DSs have failed and the WPs are surrounded by rubble. Under these conditions the probability of puncture varies as a function of PGV, but the probabilities remain low even at high PGVs (Figure 6.6-17). First failures from puncture damage are only likely to occur late in time when the WP has a reduced thickness (Figure 7.3.2-15). The number of realizations where puncture occurs before seismic-induced SCCs would be small since there is a higher probability of damage from seismic-induced SCCs (Figure 6.6-15).<br><br>Note that this error only occurs in the Seismic GM Modeling Case run for 1,000,000 years. There is no effect on the Seismic GM Modeling Case run for 10,000 years as the conditions conducive to puncture do not occur.<br><br>Analysis of a stand-alone model for WP degradation that includes both nominal and seismic degradation processes (output DTN: MO0709TSPAWPDS.000 [DIRS 183170]; file v5.000_GS_9.60.100_StandAlone_9krlz.gsm in folder Seismic_9k_Rlz) showed that 63 out of 9,000 realizations could have first damage from punctures. The impact of this on the mean annual dose is likely to be negligible as only 0.7% of the realizations would be affected and the effects are likely to be late (after the DSs are failed and the WPs have thinned). | Yes – Corrected the first damage calculation to include puncture failures during a seismic event. |

Table P-6[a]. Discussion of Other Minor Implementation Errors (Continued)

| | ISSUE DESCRIPTION | ANTICIPATED IMPACT (V5.000) | ADDRESSED V5.005 |
|---|---|---|---|
| 15 | The temperature and relative humidity modifications may be incorrectly applied after rubble fills the drifts as a result of degradation due to seismic ground motion. | The percolation subregion representative temperature and relative humidity time histories under nominal conditions (from MSTHM abstraction) are modified once the drifts become filled with rubble as a result of drift degradation from seismic ground motion. These modifications (deltas) are applied by adding to or subtracting from the representative temperature and relative humidity datasets. Twelve possible delta combinations, from four infiltration scenarios over three host-rock thermal conductivity cases (Section 6.3.2.2), are considered in the TSPA-LA Model for each percolation subregion and for each fuel type. However, in order to limit the computational burden, only eight delta combinations are actually calculated: six delta combinations for CSNF and two delta combinations for HLW. The six delta combinations for CSNF are then mapped to 12 possible delta combinations for the CSNF fuel type in each percolation subregion. Similarly, the two delta combinations for HLW are then mapped to 12 possible delta combinations for the HLW fuel type (CDSP WP) for each percolation subregion.<br><br>Due to an implementation error, some of the combinations are incorrectly matched and the data are incorrectly read from the look-up tables. This could sometimes result in incorrect modifications of representative temperature and relative humidity time histories for the given percolation subregion and a given fuel type. In addition, some of the data sets used in the modification of temperatures (called temperature deltas) have been entered in a sequence that is different compared to the relative humidity deltas resulting in internal inconsistency once the modifications are made.<br><br>Note that the error is only possible in the two modeling cases in which rubble fills the drifts, the Seismic GM Modeling Case run for 1,000,000 years and the Seismic FD Modeling Case. The impact of this error on the mean annual dose for either modeling case is likely to be negligible as the variation in the delta among various combinations is small. Thus, even though incorrect values may be applied, they would not result in any appreciable deviations from the corrected time history profiles. Furthermore, the magnitude of the modification is itself small relative to the actual temperature and relative humidity values even at the maximum initial values (the magnitudes of the deltas decrease with time). As a result, the downstream models affecting radionuclide transport are unlikely to be appreciably impacted by this error.<br><br>The impact of the error on localized corrosion initiation is also evaluated based on the Localized Corrosion Initiation Uncertainty Analysis described in Appendix O. The five realizations (out of 300) that have early rubble fill times (within 12,000 years) all have conditions that are not conducive to localized corrosion initiation, even accounting for slightly incorrect temperature and relative humidity. One realization (realization 142), which has conditions favorable for localized corrosion until 12,000 years, has a rubble fill time greater than 100,000 years, by which time localized corrosion is not favored. It is concluded that there is no impact of this error on the localized corrosion initiation. | No – Impact summary as assessed for v5.000. |

Table P-6[a]. Discussion of Other Minor Implementation Errors (Continued)

| | ISSUE DESCRIPTION | ANTICIPATED IMPACT (V5.000) | ADDRESSED V5.005 |
|---|---|---|---|
| 16 | Drift-wall condensation flux is being applied even after the igneous intrusive event, when the drifts are all assumed to be filled with magma. | The drift-wall condensation model is applicable only under nominal conditions and does not apply once the drifts are degraded from seismic ground motion or filled with magma following the igneous intrusion. However, it is being incorrectly applied even after the igneous intrusion.<br>The impact of the error is restricted to the first 2,000 years only because the drift-wall condensation can only occur in the first 2,000 years (Section 6.3.3.2.2). As a result, the water flux through the WP could be higher than the percolation flux leading to increased advective mass flux of radionuclides for realizations when the igneous intrusion occurs within the first 2,000 years. But because the probability of having an igneous event in the first 2,000 years is negligibly small (mean value of $3.3 \times 10^{-5}$) the effect on expected dose of this additional mass flux is small. The impact of the error is evaluated to be negligible. | Yes – Drift wall condensation flux was turned off after an igneous intrusion event. |

Table P-6[a]. Discussion of Other Minor Implementation Errors (Continued)

| | ISSUE DESCRIPTION | ANTICIPATED IMPACT (V5.000) | ADDRESSED V5.005 |
|---|---|---|---|
| 17 | The WP temperatures could sometimes fall below the lower range of validity of the abstractions provided for computing in-package chemistry, HLW glass degradation rate, and dissolved concentration limits in the TSPA-LA Model. | An assessment of the range of validity shows that most of the validity ranges specified for the process models and abstractions included in the TSPA-LA Model are honored (see output DTN: MO0709TSPALAMO.000 [DIRS 182981]). However for three submodels (discussed below) that are included in the 1,000,000-year performance calculations the representative WP temperatures could fall below the lower limit specified by the abstractions; the minimum waste package temperature noted in the TSPA-LA Model is about 17°C for the 1,000,000-year simulation period.<br><br>The lower temperature limit for the range of applicability of the In-Package Chemistry Abstraction (SNL 2007 [DIRS 180506]) is 25°C. Without an alternate implementation for low temperature conditions, the TSPA-LA Model applies the In-Package Chemistry Abstraction at temperatures below 25°C. Given that the In-Package Chemistry Abstraction for pH and ionic strength includes uncertainty to account for higher temperatures, the application of abstraction at lower temperatures is anticipated to produce results that are within the range of uncertainty captured in the abstractions for pH and ionic strength.<br><br>The lower temperature limit for the range of applicability of the HLW Glass Waste Form Degradation Abstraction (BSC 2004 [DIRS 169988]) is 20°C. Without an alternate implementation for low temperature conditions, the TSPA-LA Model applies the HLW glass waste form degradation rate model at temperatures below 20°C. The lower temperature limit was determined by the ranges considered in the experimental results used to validate the rate model (BSC 2004 [DIRS 169988], Section 7.3) which showed that the Arrhenius relationship for glass degradation rate is maintained between 20°C and 90°C. This relationship is not anticipated to change between 17°C and 20°C and therefore unlikely to have any effect on mass transport calculations.<br><br>The lower temperature limit for the range of applicability of the Dissolved Concentration Limits Abstraction (SNL 2007 [DIRS 177418]) is 25°C. Without an alternate implementation for low temperature conditions, the TSPA-LA Model applies the Dissolved Concentration Limits Abstraction at temperatures below 25°C. Because actinides have retrograde solubility (SNL 2007 [DIRS 177418], Section 6.3.3.3), it is possible that dissolved concentration limits below 25°C could be higher than those implemented in the TSPA-LA Model. But because the Dissolved Concentration Limits Abstraction includes additional uncertainty to account for differences in temperature conditions (SNL 2007 [DIRS 177418], Section 6.3.3), it is anticipated that any small effects from extrapolation would produce results that are within the range of uncertainty captured in the abstractions for dissolved concentration limits.<br><br>For the 10,000 year simulations the temperatures remain within the range of validity. | No – Impact summary as assessed for v5.000. |

Table P-6[a]. Discussion of Other Minor Implementation Errors (Continued)

| | ISSUE DESCRIPTION | ANTICIPATED IMPACT (V5.000) | ADDRESSED V5.005 |
|---|---|---|---|
| 18 | Drift-wall condensation flow only occurs in the non-lithophysal regions of the repository. | The drift wall condensation abstraction states that drift wall condensation should cease after the drift has collapsed. Drift collapse is only modeled in the Seismic Scenario Class. In the Seismic Scenario Class, drift collapse occurs in the lithophysal regions of the repository; thus the fraction of WPs that are exposed to drift wall condensation is limited to the fraction of WPs in the non-lithophysal region. However, this limit was not properly implemented in the TSPA-LA Model. As a result, in all but the Igneous Intrusion modeling case, drift wall condensation was limited to the fraction of WPs in the nonlithophysal region and therefore was underestimated in the TSPA-LA Model.<br><br>Because drift wall condensation only increases the flux in the repository for the first 2,000 years, the dose impact can only occur in the modeling cases that fail WPs in the first 2,000 years and have radionuclide transport in the first 2,000 years. The implementation is correct for the Seismic Ground Motion and Seismic Fault Displacement modeling cases and the Igneous Intrusion Modeling Case. The Nominal Scenario Class and Human Intrusion Scenario do not have failures in the first 2,000 years and thus are not affected. The EF WP modeling case does have WP failures in the first 2,000 years, but the DS remains intact so any additional condensation flux is not anticipated to change transport out of the EF WP. The flux through a failed WP in the EF DS modeling case could be increased by drift wall condensation. As a result, WP releases could also be increased, leading to a higher expected dose in the EF DS modeling case. Contributing less than 2.5% to the total mean dose, the EF DS modeling case is not a significant contributor to the total dose from the repository. The impact of the error is evaluated to be negligible. | No – Impact summary as assessed for v5.000. |
| 19 | Mass of iron oxyhydroxide colloids computed for Cell 1 is used in the preliminary forward rate constant calculation for americium in Cell 2 of the EBS Transport Submodel for CSNF WP. | A preliminary calculation to determine the forward rate constant for implementing kinetic sorption of americium on iron oxyhydroxide colloids and stationary corrosion products for CSNF WP incorrectly uses the mass of iron oxyhydroxide colloids from Cell 1 of the EBS Transport Submodel. It should instead use the mass of iron oxyhydroxide colloids from Cell 2 because the sorption calculation is relevant to Cell 2 (corrosion products domain) of the EBS transport submodel.<br><br>The impact of this error is anticipated to be negligible because it is used only in the preliminary calculation of the forward rate constant for americium. It is considered a final value only if certain constraints are met based on the stability of iron oxyhydroxide colloids and flow rates. In no case can it result in forward rate constant value outside the experimentally determined range. Because the bulk forward reaction rates are generally large (compared to the time step size), any small changes in the forward rate constant are likely to have negligible impact on the bulk reaction rates and consequently on the mass kinetically sorbed. The overall impact of the error is anticipated to be negligible, if any. | No |

Table P-7[a]. Impact Assessment Summary Table

| Issue No. | Issue Description | Anticipated Impact | Addressed in v5.005 |
|---|---|---|---|
| P2. | Inventory for $^{36}Cl$, $^{79}Se$, and $^{126}Sn$ was omitted in the 10,000-year simulation modeling cases and the seepage fractions applied for the 10,000-year simulations are based on the post-10,000-year climate. | Negligible | Yes – Added $^{36}Cl$, $^{79}Se$, and $^{126}Sn$ (which was inadvertently omitted in the 10,000-year simulation modeling cases) and modified the seepage calculations (Section 6.3.3.1.3[a]). |
| P3. | Conservative treatment of WP damage from seismic events following the first breach due to nominal corrosion processes. | Significant between 200,000 and 300,000 years | Yes – Modified seismic damage submodel to remove conservatism (Section 6.6.1.3[a]). |
| P4. | WP outer barrier failure flag is triggered when the inside-out corrosion of the WP is initiated in the Seismic GM Modeling Case, which could be earlier than the actual breach time. | Negligible | Yes – corrected model implementation to more accurately match breach time. |
| P5. | In-package chemistry applied in the invert after the DS is failed without considering flow through the WP. | Negligible | Yes – corrected model implementation to include flow through the WP. |
| P6. | Incorrect weld volume is used in computing the probability of manufacturing defects. | Negligible | Yes – corrected weld volume. |
| P7. | Nominal crack failure opening area incorrectly calculated once the elapsed time is greater than the seismic damage time. | Negligible | Yes – corrected model implementation. |
| P8. | Degradation processes inside the WP could start before the breach from an igneous event under certain aleatory configuration of specified igneous event times. | Negligible | Yes – corrected model implementation. |
| P9. | Threshold rubble volume (per drift length) that is used for determining when the non-lithophysal drifts undergo collapse is incorrect. It is currently using the value of 5 $m^3/m$ while the correct value is 0.5 $m^3/m$. | Negligible | Yes –corrected value to 0.5 $m^3/m$. |
| P10. | Unintended perfect correlation between two uncertainty parameters: WRIP_beta_rand_a and PCE_Delta_pCO2_a. | Negligible | Yes – removed unintended correlation. |
| P11. | The uncertainty associated with fluoride concentration in calculating the uranium solubility for the CSNF WPs is incorrectly calculated in the Igneous Intrusion Modeling Case. | Negligible | Yes – corrected model implementation. |
| P12. | The ionic strength for the HLW glass domain for conditions where there is flow through the WP always chooses the ionic strength determined for flowing conditions. | Negligible | Yes – corrected model implementation to select ionic strength based on flow conditions. |
| P13. | The average WP length seepage abstraction uses an average WP length of 5.0 m. However, the average length of WPs should be 5.6 m. | Small (≤12%) | No – Small impact (≤12%) |
| P14. | Evaluate the mean annual dose from the Igneous Intrusion and Volcanic Eruption Modeling Cases with the probability of the igneous event set to $10^{-7}$ per year. Note that this is purely a sensitivity analysis and not due to any error in the implementation. | None | NA |
| P15. | The distribution for longitudinal dispersivity that is sampled produces unrealistically large values in the 1-D SZ flow and transport model. | Small (<30%) | Yes – changed the longitudinal dispersivity (Section 6.3.10[a]). |

Table P-7[a]. Impact Assessment Summary Table (Continued)

| Issue No. | Issue Description | Anticipated Impact | Addressed in v5.005 |
|---|---|---|---|
| P16. | The HLW glass degradation rate calculation for the Igneous Intrusion Modeling Case uses the degradation model that was developed for nominal conditions instead of applying an instantaneous degradation | Negligible | Yes – corrected model implementation to include instantaneous degradation for the Igneous Intrusion Modeling Case. |
| P17. | The seepage flux in the lithophysal zones following the drift collapse may be under predicted in some realizations due to an error in estimating the bounding values. | Small (~20%) | Yes – corrected model implementation to include the degraded drift diameter of 11 m for estimating bounding values following drift collapse. |
| P18. | Minimum iron oxyhydroxide colloid concentration is being applied even under stable conditions due to error in calculating the ionic strength threshold for colloid stability calculations. | Negligible | Yes – corrected model implementation. |
| P19. | In the Igneous Intrusion Modeling Case, the number of WPs assigned for computing the DSNF mass in the non-dripping environments are not correctly calculated following the igneous event. | Small (<6%) | Yes – corrected model implementation. |
| P20. | GoldSim software error where incorrect masses could be calculated by the Source and Pipe elements (special GoldSim elements) when decay chains have feedback loops. | Small (<5%) | Yes – No impact. |
| P21. | Delay in transport for some radionuclides through the fault zones in the UZ transport model. | Small (<5%) | No. Small (<5%) |
| P22. | Other minor implementation errors that have been discovered since running the compliance case are grouped and addressed (Table P-6). | Negligible | See Table P-6[a] |
| P23. | Several suggested changes to the model file structure are tracked in a model status log. | None | Yes. |

INTENTIONALLY LEFT BLANK

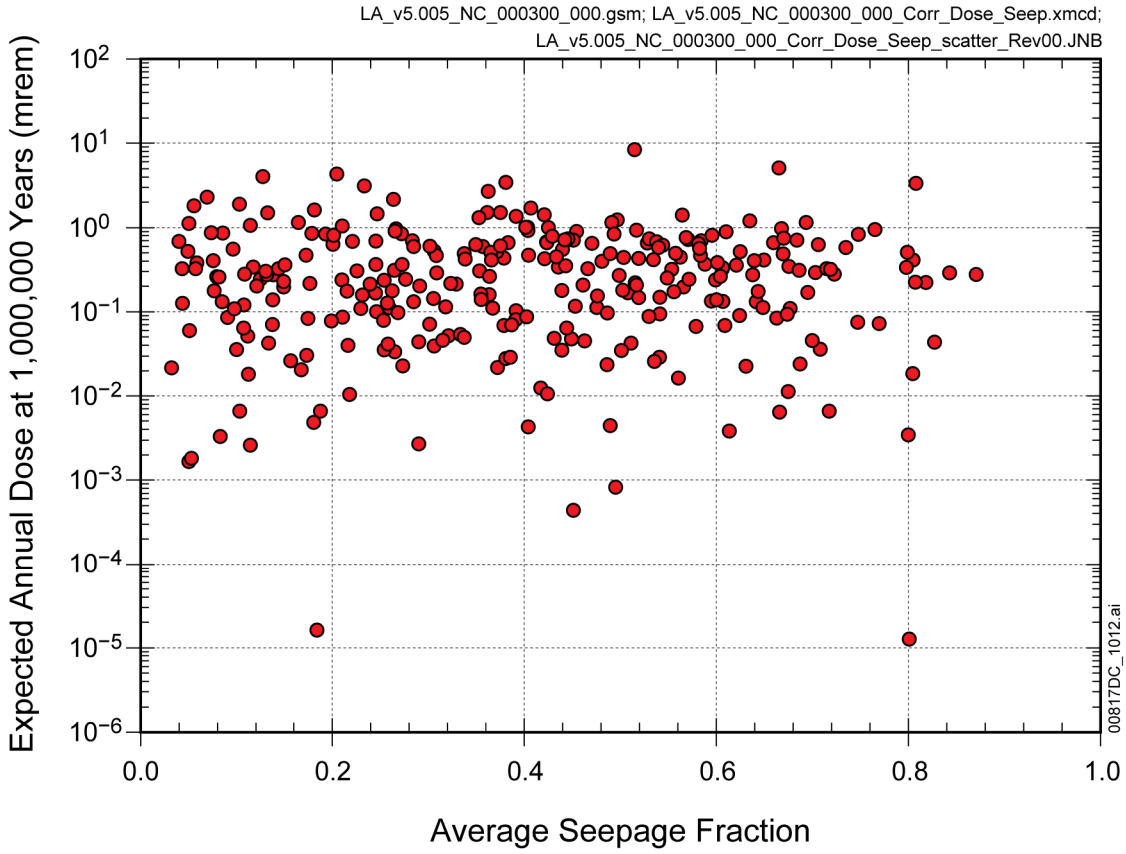


Source: Output DTN: MO0710ADTSPAWO.000 [DIRS 183752].

Figure P-20[a]. Expected Annual Dose versus Average Seepage Fraction for the Nominal Modeling Case for 1,000,000 Years after Repository Closure

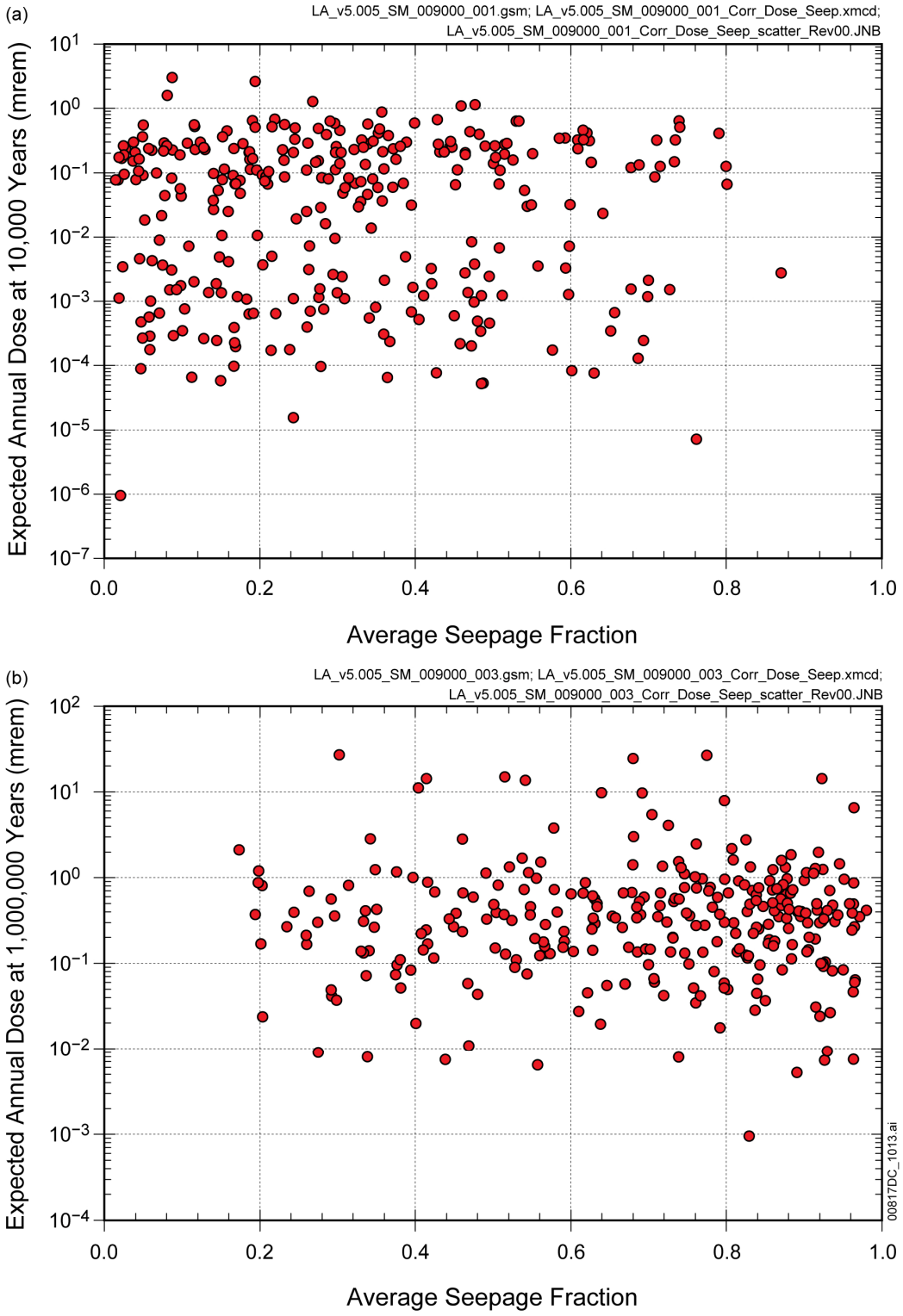


Source: Output DTN: MO0710ADTSPAWO.000 [DIRS 183752].

Figure P-21[a]. Expected Annual Dose versus Average Seepage Fraction for the Seismic Ground Motion Modeling Case for (a) 10,000 Years and (b) 1,000,000 Years after Repository Closure